



BRNO UNIVERSITY OF TECHNOLOGY

VYSOKÉ UČENÍ TECHNICKÉ V BRNĚ

FACULTY OF ELECTRICAL ENGINEERING AND COMMUNICATION

FAKULTA ELEKTROTECHNIKY
A KOMUNIKAČNÍCH TECHNOLOGIÍ

DEPARTMENT OF TELECOMMUNICATIONS

ÚSTAV TELEKOMUNIKACÍ

FULLY-DIFFERENTIAL FREQUENCY FILTERS WITH MODERN ACTIVE ELEMENTS

PLNĚ DIFERENČNÍ KMITOČTOVÉ FILTRY S MODERNÍMI AKTIVNÍMI PRVKY

DOCTORAL THESIS

DIZERTAČNÍ PRÁCE

AUTHOR

AUTOR PRÁCE

Ing. Lukáš Langhammer

SUPERVISOR

ŠKOLITEL

Ing. Jan Jeřábek, Ph.D.

BRNO 2016

ABSTRACT

This doctoral thesis focuses on research in the field of frequency filters. The main goal is to propose and analyze fully-differential current-mode frequency filters employing modern active elements. Presented filters are proposed using current followers, operational transconductance amplifiers, digitally adjustable current amplifiers and transresistance amplifiers. The proposal is focusing on ability to control some of the typical filter parameter or parameters using controllable active elements suitably placed in the circuit structure. Individual presented filters are proposed in their single-ended and fully-differential forms. Great emphasis is paid to a comparison of the fully-differential structures and their corresponding single-ended forms. The functionality of each proposal is verified by simulations and in some cases also by experimental measurements.

KEYWORDS

analogue filter, controllable filter, current follower, current mode, digitally adjustable amplifier, fractional-order filter, frequency filter, fully-differential filter, operational transconductance amplifier, transresistance amplifiers

ABSTRAKT

Tato disertační práce se zaměřuje na výzkum v oblasti frekvenčních filtrů. Hlavním cílem je navrhnout a analyzovat plně diferenční kmitočtové filtry pracující v proudovém módu a využívající moderní aktivní prvky. Prezentované filtry jsou navrženy za použití proudových sledovačů, operačních transkonduktančních zesilovačů, plně diferenčních proudových zesilovačů a transrezistančních zesilovačů. Návrh se zaměřuje na možnost řídit některý z typických parametrů filtru pomocí říditelných aktivních prvků, které jsou vhodně umístěny do obvodové struktury. Jednotlivé prezentované filtry jsou navrženy v nediferenční a diferenční verzi. Velký důraz je věnován srovnání plně diferenčních struktur s jejich odpovídajícími nediferenčními formami. Funkčnost jednotlivých návrhů je ověřena simulacemi a v některých případech i experimentálním měřením.

KLÍČOVÁ SLOVA

analogový filtr, říditelný filtr, proudový sledovač, proudový mód, plně diferenční říditelný zesilovač, filtr fraktálního řádu, kmitočtový filtr, plně diferenční filtr, operační transkonduktanční zesilovač, transrezistanční zesilovač

LANGHAMMER, L. *Plně diferenční kmitočtové filtry s moderními aktivními prvky*. Brno: Vysoké učení technické v Brně, Fakulta elektrotechniky a komunikačních technologií, 2016. 157 s. Vedoucí dizertační práce Ing. Jan Jeřábek, Ph.D..

DECLARATION

I declare that I have written my doctoral thesis on the theme of “Fully-Differential Frequency Filters with Modern Active Elements” independently under the supervision of a doctoral thesis supervisor and using the technical literature and other information sources which are all quoted in the thesis and detailed in the list of literature at the end of the thesis.

As the author of the doctoral thesis I furthermore declare that, as regards the creation of this doctoral thesis, I have not infringed any copyright. In particular, I have not unlawfully encroached on anyone’s personal and/or ownership rights and I am fully aware of the consequences in the case of breaking Regulation S 11 and the following of the Copyright Act No 121/2000 Sb., and of the rights related to intellectual property right and changes in some Acts (Intellectual Property Act) and formulated in later regulations, inclusive of the possible consequences resulting from the provisions of Criminal Act No 40/2009 Sb., Section 2, Head VI, Part 4.

Brno

.....

(author's signature)

ACKNOWLEDGMENTS

I would like to express my sincere gratitude to my supervisor *Ing. Jan Jeřábek, Ph.D.* for his guidance, professional help and invaluable remarks to the topics of this work.

My thanks also go to *doc. Ing. Jaroslav Koton, Ph.D.* and *Ing. Roman Šotner, Ph.D.* for useful hints and shared knowledge.

Last but not the least, I want to thank my parents for their never ending support during my whole study.

Brno

.....

(author's signature)

Research described in this doctoral thesis has been implemented in the laboratories supported by the SIX project; reg. no. CZ.1.05/2.1.00/03.0072, operational program Research and Development for Innovation.

Brno

.....
(author's signature)

List of Abbreviations

ACA	Adjustable Current Amplifier
AP	All Pass
BOTA	Balanced Operational Transconductance Amplifier
BP	Band Pass
BS	Band Stop
CC	Current Conveyor
CCII	Second Generation Current Conveyor
CCII+/-	Second Generation Current Conveyor with balanced output
CDBA	Current Differencing Buffered Amplifier
CDTA	Current Differencing Transconductance Amplifier
CF	Current Follower
CFTA	Current Follower Transconductance Amplifier
CITA	Current Inverter Transconductance Amplifier
CMOS	Complementary Metal Oxide Semiconductor
CTR	control
DACA	Digitally Adjustable Current Amplifier
DC	Direct Current
DO-CF	Double-Output Current Follower
DVCC	Differencing Voltage Current Conveyor
F-D	Fully-Differential
FDCC	Fully-Differential Current Conveyor
FD-CF	Fully-Differential Current Follower
FLF	Follow-the-Leader Feedback
FOE	Fractional-Order Element
HP	High Pass
IFLF	Inverse Follow-the-Leader Feedback
I/V	Current to Voltage
LP	Low Pass
M-C	Mason-Coates
MCDU	Modified Current Differencing Unit
MIMO	Multiple-Input Multiple-Output
MISO	Multiple-Input Single-Output
MO-CF	Multiple-Output Current Follower
MOTA	Multi-Output Transconductance Amplifier
OTA	Operational Transconductance Amplifier
OTRA	Operational Transresistance Amplifier
PCB	Printed Circuit Board
S-E	Single-Ended
SFGs	Signal-Flow Graphs
SIMO	Single-Input Multiple-Output
SISO	Single-Input Single-Output
SITO	Single-Input Triple-Output
SNAP	Symbolic Network Analysis Program
TISO	Triple-Input Single-Output
UCC	Universal Current Conveyor
UVC	Universal Voltage Conveyor
VCCS	Voltage-Controlled Current Source
V/I	Voltage to Current

List of Used Symbols

A	current gain
a_2, a_1, a_0	coefficients
α	fractional-order
A_{REAL}	actual obtained gain of the DACA element
A_{THEOR}	theoretical value of actual gain of the DACA element
B	current gain
b_2, b_1, b_0	terms of the denominator
C	capacitor
C	capacitance
D	denominator
Δ	determinant
E	voltage control current source
F	current control current source
f_0	pole frequency
G	conductance
g_m	transconductance
i, I	current
I	current (complex variable)
i_{CM}	common-mode signal (current)
$I_{\text{LP}}, I_{\text{HP}}, I_{\text{BP}}, I_{\text{BS}}, I_{\text{AP}}$	LP, HP, BP, BS, AP current responses
i_n	current of n input terminal of the OTRA
$i_{\text{IN DIF}}, i_{\text{ID}}$	differential input current
I_p	current of p input terminal of the OTRA
$i_{\text{OUT DIF}}, i_{\text{OD}}$	differential output current
$I_{\text{SET}}, I_{\text{setB}}$	bias DC current
K	transfer
k_1, k_2, k_3	coefficients
K_i	current transfer
L	inductor
L	inductance
N	numerator
n	controllable parameter
P_i	gain of i -th forward path
Q	quality factor
q_i	i -th parameter
R	resistor
R	resistance
R_T	transresistance
R_X	intrinsic resistance
S	relative sensitivity
s	Laplacian operator
τ	time constant
v, V	voltage
Y	admittance

Contents

Introduction.....	10
1 State of the Art Review	11
2 Thesis Goals	17
3 Definition of Single-Ended and Fully-Differential Current Transfers	18
3.1 Definition of Single-Ended Current Transfers	18
3.2 Definition of Fully-Differential Current Transfers	19
4 Signal-Flow Graphs Design Method.....	21
5 Description of Used Active Elements	25
5.1 Universal Current Conveyor.....	25
5.2 Current Followers.....	27
5.3 Operational Transconductance Amplifiers.....	29
5.4 Adjustable Current Amplifiers	31
5.5 Operational Transresistance Amplifiers	35
5.6 Concluding Summary of the Chapter	36
6 Newly Proposed Filtering Structures	37
6.1 General Conception of a Filter with Three CFs	39
6.2 Universal Filter with Three CFs and Two DACAs	40
6.2.1 Filter proposal	40
6.2.2 Simulation Results	43
6.2.3 Sensitivity Analysis.....	46
6.3 Universal Filter with Three CFs and Three DACAs	50
6.3.1 Filter proposal	50
6.3.2 Simulation Results	53
6.4 Universal Filter with Three CFs and Two DACAs	56
6.4.1 Filter proposal	56
6.4.2 Simulation Results	59
6.4.3 Parasitic Analysis	61
6.5 Universal Filter with Two CFs and Two DACAs	67
6.5.1 Filter proposal	67

6.5.2	Simulation Results	70
6.5.3	Sensitivity Analysis.....	72
6.6	Universal Filter with Three CFs and Two DACAs	78
6.6.1	Filter proposal	78
6.6.2	Simulation and Experimental Results	80
6.7	General Conception of a Filter with Two OTAs and One CF.....	84
6.8	Universal Filter with Two OTAs, One CF and One DACA	86
6.8.1	Filter proposal	86
6.8.2	Simulation and Experimental Results	89
6.9	Multifunctional Filter with Three OTAs and One OTRA.....	96
6.9.1	Filter proposal	96
6.9.2	Simulation and Experimental Results	99
6.9.3	Parasitic Analysis	106
6.10	Universal Filter with Three OTAs, One CF and One OTRA	109
6.10.1	Filter proposal	109
6.10.2	Simulation and Experimental Results	112
6.11	Concluding Summary of the Chapter	115
7	Proposal of Fractional-Order Filters	118
7.1	$(1+\alpha)$ -Order Low-Pass Filter with Three MO-CFs and Five ACAs	118
7.1.1	Filter proposal	118
7.1.2	Simulation results.....	122
7.2	$(1+\alpha)$ -Order Low-Pass Filter with Three OTAs Two ACAs and One CF	125
7.2.1	Filter proposal	125
7.2.2	Simulation results.....	127
7.3	Concluding Summary of the Chapter	130
8	Modified Design Method	131
9	Conclusion.....	138
	References.....	141

Introduction

Despite the fact that the technology is working with digital signals these days, analog frequency filters are a vital part of electronic circuits which we can encounter in a broad range of industry such as measurement technology, radio-technology, telecommunication, electro-acoustics etc. Analog frequency filters are required in cases when digital filters cannot be used e. g. the preprocessing of the analog signals before the digital signal processing. Digital filters also have some drawbacks such as the fact that the signals must be converted to digital form which always entails loss of information, bandwidth limitations, causes quantizing noise. The conversion process consists of sampling quantization and encoding. Each this task requires significant amount of time in comparison to analogue filters. Analogue frequency filters can be divided into passive and active ones depending on whether the structure contains active elements. By active element we understand for example a classical operational amplifier which is a typical voltage-mode active element. In case that the processed signal is represented by the voltage amplitude, the filter operates in the voltage mode. Lately, we can experience tendency of reducing the size of integrated circuits in order to decrease their requirements of power supply voltage and energy consumption which decreases the level of processed signals. This subsequently results in a reduction of signal-to-noise ratio and limits the dynamic range of the circuit. Therefore, the design of electrical circuits is currently focused on active elements operating in the current mode due to its advantages which can be in particular cases achieved. The advantages which can be achieved when we use the current amplitude to represent information of processed signals are mentioned in chapter 1. The design of frequency filters is also more and more focused on the design of these filters in the fully-differential form because of the advantages that the differential signal processing brings in comparison to single-ended structures as further on described in chapter 1. Furthermore, we can mention controllable active elements which allow us to adjust the characteristic frequency filter parameters, such as the pole frequency, quality factor, bandwidth and gain in the pass band area of any filter, or sometimes only of particular type of the filter. Fractional-order frequency filters are another interesting topic related to analogue frequency filters that is getting to the forefront of interest of many scientific teams lately. The fractional-order circuits can find practical use in precision measurement and modeling of various biological signals. Another use may be in control and electrical engineering, telecommunication and also agriculture.

1 State of the Art Review

The ever-increasing demands on the properties of electronic circuits lead to the development of new non-standard active elements with properties permitting signal processing in a wider frequency range and requiring a lower supply voltage than in case of standard operational amplifiers. Despite the proposal of voltage-mode frequency filters [1-10], the development is more and more focused on the design of either mixed-mode frequency filters [11-13], or current-mode frequency filters [14-91]. Circuits operating in the current mode can provide better signal-to-noise ratio, greater dynamic range, wider frequency bandwidth and lower power consumption in particular cases [92].

In case of the proposal of frequency filters, there are two basic trends. The first one is the proposal of more complex filtering structures using simpler active elements. Among the filters that use simpler active elements, we can mention filters employing Current Followers (CFs) [14-21], Fully-Differential Current Followers (FD-CFs) [22-25], a variety of Current Conveyors (CCs) [12], [13], [26-38], Differencing Voltage Current Conveyors (DVCCs) [2], [39-41] and Fully-Differential Current Conveyors (FDCCs) [1], [6], [42-46], Digitally Adjustable Current Amplifiers (DACAs) [14], [17], [22], [23], [45], [47] and basic Operational Transconductance Amplifiers (OTAs) [10], [11], [19], [25], [48-52]. A Current Conveyor operates in the mixed mode(it has both voltage and current terminals). It was firstly introduced in 1968. In retrospect, it was the first-generation current conveyor. There are totally three generations of current conveyors. Individual generations are, from the outside, only distinguished by orientation and derivation of the currents at the Y gate of this element. The second-generation is the most frequently used. Slightly different variants of the current conveyor such as current conveyors with various amount and orientation of the input and output terminals e.g. [12], [13], [27], [30], [38], inverting versions [28], [29] and current controlled versions [26], [31], [32], [35], [36] etc gradually emerged. Current follower is the simplest current-mode active element. Filters employing current followers can have a large bandwidth range thanks to a simple internal structure of these elements. Active elements with a higher number of outputs can reduce the number of used active elements in the circuit structure (in case of circuits working in the current mode). Therefore, we can frequently encounter current followers with two outputs (double-output current followers (DO-CFs)) [17-20] and three and more outputs (multiple-output current followers (MO-CFs)) [14], [16], [17], [21]. A operational transconductance amplifier has voltage and current terminals thus, it operates in the mixed mode. Depending on the number of outputs of this active element it is possible to come across OTA [11], [48] (having one output), balanced operational transconductance amplifier (BOTA) [10], [19], [51], (having two outputs of mutually opposite polarities) and multiple-output transconductance amplifier (MOTA) [19], [25], [49-52] with three or more outputs. The structure of these filters is characterized by higher circuit complexity and higher number of used active elements, but provide a greater variability of the proposal. The other approach is opposite to the first one when we use more

complex active elements so the number of used active elements can be lower and the proposed filtering structures appear to be simpler. These active elements are usually a particular composition of the simpler elements mentioned above. The disadvantage of this approach is more complex and more expensive proposal and implementation of given active elements on a chip. The literature presents filters which use different types of active elements based on Transconductance Amplifiers such as filters with Current Controlled Transconductance Amplifiers (CCTAs) [53-57], Current Differencing Transconductance Amplifiers (CDTAs) [58-64], Current Follower Transconductance Amplifiers (CFTAs) [5], [65-70] and Current Inverter Transconductance Amplifier (CITA) [71], [72]. Among other filtering structures which are employing this type of active elements there are filters using Current Differencing Buffered Amplifiers (CDBAs) [9], [73-77], Modified Current Differencing Unit (MCDU) [78], [79] and Operational Transresistance Amplifier (OTRA) [3], for instance.

A wide range of scientific papers, for example [12], [23], [44], [62], [80-85], focus on the proposal of universal filters allowing to obtain all standard transfer functions (low pass (LP), band pass (BP), high pass (HP), band stop (BS) and all pass (AP)) from the same circuit structure by suitable selection of used input and output terminals, or by reconfiguration of the filtering structure. Some of the works [7], [24], [29], [45], [47], [56], [70], [73], [78], [86] focus on the design of filters which provide only some types of transfer functions. These filtering structures are referred to as multifunctional filters. We can also come across filters which can provide only one type of transfer function [9], [17], [38], [65], [72], [75], [87-90].

Some filtering structures can provide all standard transfer functions without a necessity to change the circuit structure or position of the input voltage/current and at the same time take output responses directly from high-impedance output terminals of used active elements. These structures are often referred to as SIMO (Single-Input Multiple-Output) [22], [29], [47], [49], [50], [71], [80], [91], or SITO (Single-Input Triple-Output) [15], [21], [34], [41], [54], [66], [67], [74] because we theoretically need only three transfer functions (high pass, band pass, low pass) to implement all five standard filtering functions. Band-stop and all-pass transfer functions can be easily obtained by summing particular outputs of the circuit (in case of the current-mode signal processing). Other frequent structures are referred to as MISO (Multiple-Input Single-Output) [27], [30], [53], [55], [82], [85], [86], or TISO (Triple-Input Single-Output) [31], [33], [35], [37], [43], [44], [68]. These types of structures typically require either copies of the input voltage/current signal, or the structure must be reconfigured in order to provide a different function. These structures can provide one transfer function at the same time. Structures with more inputs and outputs are designated as MIMO (Multiple-Input Multiple-Output) [16], [24], [32], [40], [69], [81]. The last possible type is SISO (Single-Input Single-Output) [73], [75], [88], [90]. The structure of these filters must be physically adjusted to obtain different functions, or there are also so-called reconfigurable

filters [78], [79] when the transfer function can be switched electronically using controllable elements suitably placed in the structure.

The controllability of some characteristic filter parameters such as the pole frequency, quality factor, bandwidth, or gain in the pass-band area provides higher variability of use in the industry, or possibility to fineadjust or autoadjust the particular parameter in the final application. Thus, the frequency filters with the ability to control some of these parameters are highly advantageous. The controllability can be divided depending on how the control is achieved. The controllability of the filter can be achieved electronically by adjusting one or more parameters of active element(s) for example [19], [36], [38], [55], [57], [64], [84], [85], partly electronically by adjusting one parameter of used active element(s) and value of some passive part(s) [37], [63] for instance, or solely passively by changing values of passive elements, e.g. [40], [43], [46], [77]. Typical adjustable parameters of active elements used to control some of the characteristic filter parameters are transconductance g_m [19], [37], [55], [57], [63], [64], [84], and current gain B (A) [37], [38], [84], [85]. These parameters are usually controlled by DC voltage/current. Other possible parameter used for adjustability is intrinsic resistance R_X of used active element controlled by DC current [36]. If we are talking about a passive control, an adjustment of values of resistors (capacitors) [40], [43], [46], [63], [77] is also being used.

Some of the papers [17], [22], [25], [47], [69] are aimed at a comparison of single ended (S-E) and fully-differential (F-D) structures, single-ended and fully-differential filters respectively. The F-D structures in comparison to the S-E structures benefit from the advantages such as greater dynamic range of the processed signals, better power supply rejection ratio, lower harmonic distortions and greater attenuation of common-mode signals. The F-D structures have also a few drawbacks such as the larger area taken on the chip which results in higher power consumption. Also, the design of the F-D circuits is more complex than in case of S-E structures [91]. We can also mention so-called pseudo-differential filters [93-96]. The pseudo-differential structures consist of both differential input and output, but the inner structure of the filter is single-ended. These structures still can provide high attenuation of common-mode signals when their inner structure is less complex in comparison to the F-D structures [93]. However, other benefits of F-D structures are not applicable in case of the pseudo-differential filters.

There are multiple methods how to design single-ended frequency filters. One of the basic ways how to propose frequency filters is using autonomous circuit design method [7], [10], [97-100]. Autonomous circuits can be described as circuits of passive and active elements having no excitation source and no input or output terminals. These circuits are solely described by a determinant of their admittance matrix which represents the left part of the characteristic equation of the analyzed circuit. Such a circuit can be then used as a base element to design various types of frequency filters. The proposal can be intuitive when an experienced designer proposes these circuits directly, or the proposal can be generalized

when using a full admittance network connected to a desired number of generalized active elements. There is also a method based on extension of autonomous circuits [99] which is related to autonomous circuit design. This method is usually used to design filters of higher orders. Other method frequently used for the proposal of frequency filters is synthetic immittance system method [8], [88], [89], [99], [101] based on the fact it is possible to design synthetic elements of higher orders. These elements consist of serial or parallel combinations of D or E type two-port network which can be suitably connected to the circuitry of frequency-dependent voltage or current dividers in order to create filters of the demanded order. We can also mention signal-flow graphs (SFGs) method [65], [81], [90], [99], [102] which is based on so-called Mason-Coates (M-C) graphs. Using this method represents an easy approach to solve the transfer functions of relatively complex circuits. We can directly propose circuits of frequency filters using this method when following the rules of M-C graphs. This method was used to design filters presented in this thesis. SFGs method is described in chapter 4 in more detail.

There are two general ways how to propose fully-differential frequency filters. The first one is to directly propose the filter in its F-D form. Such a procedure requires an experienced designer who designs the F-D structures intuitively. To do this, signal-flow graphs method can be suitably used. However, a mathematical calculation of the F-D structures is far more complex than the proposal of the S-E structures due to the higher number of loops of the analyzed circuit. The other easier way how to propose the F-D filters is by transformation of the S-E filters into their F-D form by mirroring passive components around the active elements based on particular transformation method. The number of passive components will increase approximately two times in comparison to the number of passive components used in the S-E structure. Active elements are either replaced by their F-D equivalents with differential inputs and outputs, or they are also being mirrored which will again increase their number by twice. The values of the passive components after they were mirrored have to be determined all over when this is dependent on what type of transformation is used. This method is divided into the transformation of vertical structures and transformation of horizontal structures [103]. If we use the transformation of horizontal structures, the passive components of the horizontal branches of the circuit are being mirrored. In this case, the values of the horizontal components are dependent on the type of given passive element. The values of capacitors are doubled, while the values of resistors are halved. Inductors are replaced by transformers with mutually opposite winding when the number of windings is even. The values and positions of vertical components stay unchanged. In case of the vertical transformation, those passive components which are located in the horizontal branches are being mirrored. The values of capacitors located in the vertical branches have the half values of those capacitors used in the S-E structures, values of resistor are doubled. The mirroring of inductors follows the same rules as in the previous transformation. An example of the transformation of vertical and horizontal structures can be seen in Figure 1.1.

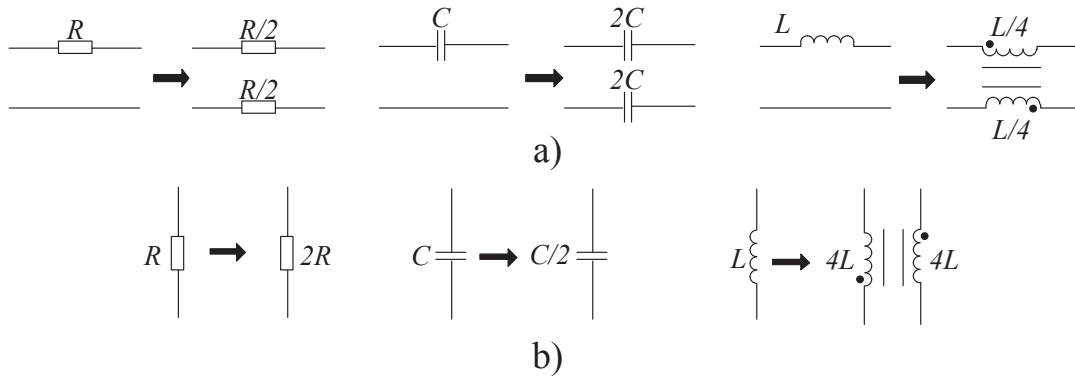


Figure 1.1 Examples of the transformation of S-E to F-D structures: a) horizontal structures, b) vertical structures

As already mentioned some active elements can be also transformed into their F-D equivalents. By a fully-differential active element we understand an element which has at least one differential input and output and the processed signal is then given by the difference of two input signals, output signals respectively. An example of such transformation is the transformation of a Current Follower (CF) into its F-D form as shown in Figure 1.2. In order to obtain a fully-differential current follower, additional input and output terminal which will have the opposite polarity in comparison to the original terminals must be added. The resulting active element is called Fully-Differential Current Follower (FD-CF).

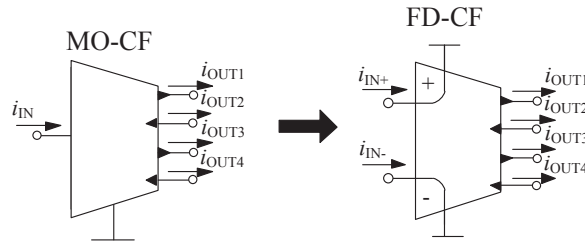


Figure 1.2 Principle of the transformation of an active device from S-E to F-D form: MO-CF transformed into FD-CF

In comparison to standard (integer-order) filters, the slope of attenuation of the fractional-order filters is given by the equation $20 \cdot (n + \alpha)$, where n is an unsigned non-zero integer number and α is a real number in the range $0 < \alpha < 1$ [104]. The design of fractional-order filters is rather more complicated than the proposal of standard (integer-order) filters. There are two basic ways how to propose a fractional-order filter.

The first way is based on creation of a special fractional-order element (FOE) [105-109]. Usually it is a capacitor. These fractional-order elements are then used in a conventional filter structure. The one of the most common method how to create a fractional-order capacitor is using an RC ladder network [106], [110] thanks to its easy implementation. The disadvantage

of this general way how to create fractional-order filters is that the order of created filter has a fixed value and cannot be electronically controlled.

The other possible way is an approximation of fractional-order Laplacian operator s^α using an integer-order transfer function of higher order. The second-order approximation is most commonly used [104], [106], [111], but it is also possible to use an approximation of higher orders than the second-order approximation [104]. To create a $(1+\alpha)$ -order filter, a conventional third-order filter is then used. Due to reasons of stability, it is necessary to design a filtering structure with the order lower than 2 [104]. In case we want to create a fractional-order filter of higher orders, a cascade combination of an integer-order and fractal $1 + \alpha$ filter is implemented. The advantage of this design method in comparison to using FOEs is that filters which are consisting of tunable active elements can be capable of electronic control of their order, or some other parameter such as the pole frequency, or quality factor [112], [113]. The disadvantage of this approach is complexity and higher number of active elements in the filtering structure.

Most commonly proposed type of fractional-order filter is a low-pass transfer function filter with Butterworth characteristics [104], [107], [108] [111-116]. It is also possible to come across papers proposing high-pass fractional-order filters [111], [117], or band-pass filters [104], [118]. A fractional-order filter with Chebyshev characteristics can be found for example in [109], [112].

2 Thesis Goals

The main aim of the work is the proposal and analysis of fully-differential frequency filters operating in the current-mode. Great emphasis will be paid to a comparison of the F-D structures and their corresponding S-E forms. The thesis is possible to divide into three parts.

The first part is to propose new second-order current-mode filtering structures especially fully-differential ones using non-standard active elements such as current conveyors, operational transconductance amplifiers, current amplifiers, current followers and their fully-differential equivalents. The proposed filters are going to be firstly designed in their S-E form using signal-flow graphs method and then transformed into the F-D structures using the transformation of horizontal structures so a mutual comparison of the S-E and F-D structures is possible. One of the main goals of this thesis is the emphasis laid upon the versatility of the proposed filters and the ability to control some of the typical filter parameters such as the pole frequency, or the quality factor of the filter by suitable use of controllable active elements. The design correctness and functionality of the proposed filters are going to be supported by simulations and in some cases also by experimental measurements. The simulations will be carried out using accurate second and third level simulation models of used active elements which are based on the measurement of characteristics of the real elements. The experimental measurements will be performed by measurements of implemented filters in a form of printed circuit boards (PCBs) using simple V/I, I/V converters [119] and chips of available active elements, in particular the universal current conveyor which can be used to implement a variety of active elements such as the current follower and operational transconductance amplifier, for instance. Subsequently, a comparison of the properties of S-E and F-D filters will be made. Each S-E filter and corresponding F-D filter will be presented together in the same chapter because of their easier comparison. Furthermore, the sensitivity [120] and parasitic [19] analysis of chosen proposal is going to be carried out.

The second part is the proposal and analysis of fractional-order frequency filters when also the possibility of creation of these filters in their fully-differential forms and following comparison of the S-E and F-D structures will be analyzed. One of the chosen conditions is again the ability to control some of the characteristic filter parameter, in this case, its order and pole frequency. The design procedure is the same as for the previous part. The filters are firstly designed in their S-E forms and then transformed into the F-D structures.

The last part consist of the analysis of existing design methods used for the proposal of frequency filters especially differential filters and subsequent modification of a chosen existing design method with respect to the specific needs and characteristics of differential structures. A practical applicability and versatility of this method is going to be also analyzed.

3 Definition of Single-Ended and Fully-Differential Current Transfers

This chapter describes relations of single-ended and fully-differential current transfers. A comparison of the ability of S-E and F-D structures to suppress the influence of common-mode signals is also included.

3.1 Definition of Single-Ended Current Transfers

The single-ended current transfer is defined as the proportion of the output and input current. There are two basic convention how to represent the direction of the currents. According to the convention in [121], the currents flow inside a block both at input and output. In this case, the output current is presented flowing inside a block however, the current transfer contains a minus sign, which means that the output current is actually flowing out which is in consistency with the representation of the current transfer used by signal-flow graphs where the transfer from the input to the output is always considered going in one direction. The other definition [122] represents the output currents flowing outside a block when the current transfer is positive. This definition of the current transfer is also consistent with signal-flow graphs. This particular representation of the current transfer is used in this thesis.

Figure 3.1 shows the second of above mentioned definitions of the simple current transfer.

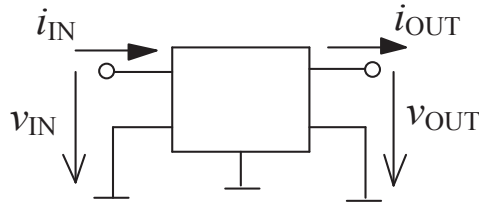


Figure 3.1 Structure used to illustrate the single-ended general current transfer

The current transfer from Figure 3.1 is given by:

$$K_i = \frac{i_{OUT}}{i_{IN}}. \quad (3.1)$$

One of the disadvantages of the single-ended transfer in comparison to the fully-differential transfer is that any common-mode signal (i_{CM}) which is added to the input current is being reflected to the output as well as shown in Figure 3.2.

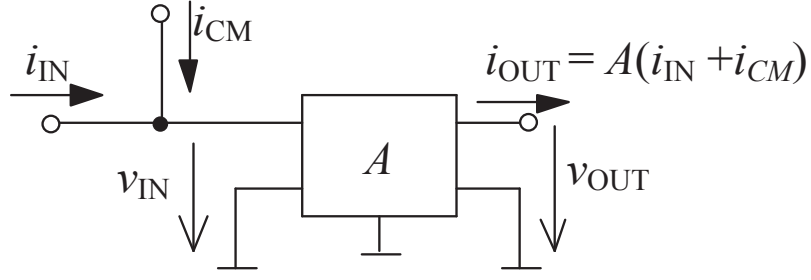


Figure 3.2 Influence of a common-mode signal added to the input current on the output current of the S-E structure with gain A .

3.2 Definition of Fully-Differential Current Transfers

The fully-differential current transfer is defined as the proportion of the differential output and differential input current. The direction of the currents can be represented according to the same conventions mentioned in the previous section. Figure 3.3 shows the definition from [122] when the output currents flow outside the block which respects the current transfer of the signal-flow graphs method where the transfer from the input to the output is, as already mentioned, always considered going in one direction.

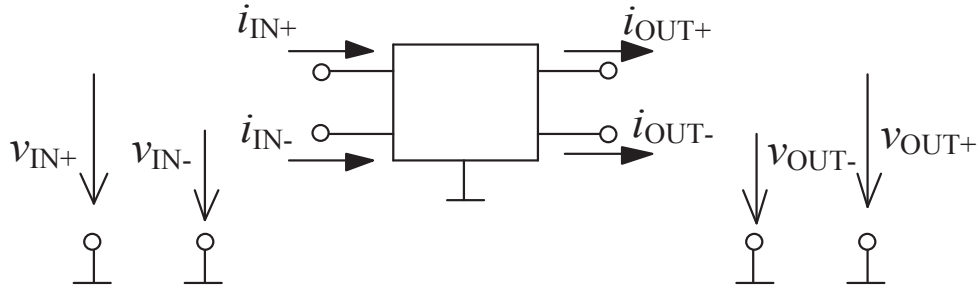


Figure 3.3 Structure used to illustrate the fully-differential general current transfer

If the differential input and output current are described by:

$$i_{IN\ DIF} = i_{IN+} - i_{IN-}, \quad (3.2)$$

$$i_{OUT\ DIF} = i_{OUT+} - i_{OUT-}, \quad (3.3)$$

then the differential current transfer is given as:

$$K_i = \frac{i_{OUT\ DIF}}{i_{IN\ DIF}}. \quad (3.4)$$

As already mentioned in chapter 1, the F-D structures provide, besides others, theoretically infinite attenuation of common-mode signals. Figure 3.4 demonstrates the ability of the F-D structures to suppress common-mode signals.

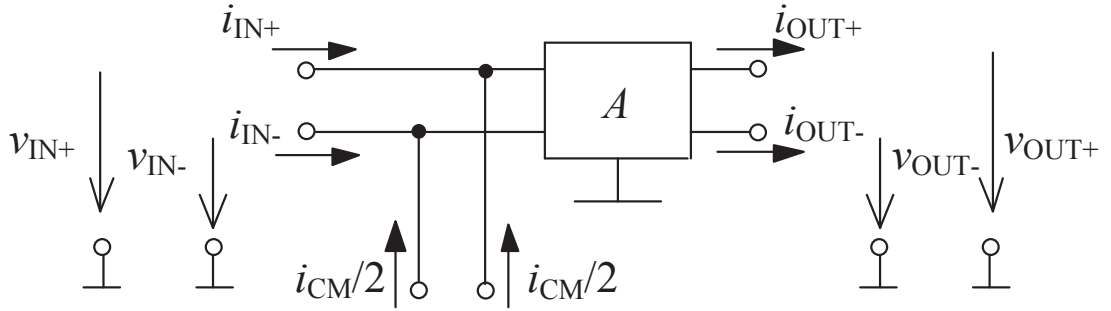


Figure 3.4 Influence of a common-mode signal added to the input differential current on the output differential current of the F-D structure.

In case of that both inputs have the same properties, the common-mode signal can be completely canceled as demonstrated by the following equations:

$$i_{OUT+} = B((i_{IN+} + i_{CM}/2) - (i_{IN-} + i_{CM}/2)) = B(i_{IN+} - i_{IN-}), \quad (3.5)$$

$$i_{OUT-} = -B((i_{IN+} + i_{CM}/2) - (i_{IN-} + i_{CM}/2)) = -B(i_{IN+} - i_{IN-}). \quad (3.6)$$

4 Signal-Flow Graphs Design Method

This well recognized method was used in the proposal of filters presented in chapter 6. Therefore, it would be appropriate to describe this method in more detail.

Signal-flow graphs were originally proposed by S. J. Mason in 1953 in order to describe and solve linear algebraic equations [123]. Later on, generalized Coates graphs [124] have appeared. Mixed Mason-Coates' (M-C) graphs [125] can be used for the analysis and synthesis of linear electrical networks. These graphs can be understood as diagrams of nodes which represent variables and directed branches defining mutual relationships between nodes of the analyzed structure. There is a parallel between signal-flow graphs and block diagrams. Nevertheless, the transformation of a block diagram into a transfer function requires successive application of fundamental relationships. In case of the signal-flow graphs, only Mason formula is required to obtain the transfer function. Thus, using this method represents an easy approach to solve the transfer functions of relatively complex circuits.

Manson's gain formula is given by the following relation:

$$K = \frac{1}{\Delta} \sum_i P_i \Delta_i, \quad (4.1)$$

where P_i is gain of i -th forward path and Δ stands for the determinant of the graph. The determinant is given by the following equation:

$$\Delta = P - \sum_i P_i \Delta_i + \sum_j P_j \Delta_j - \sum_k P_k \Delta_k + \dots, \quad (4.2)$$

where P represents self-loop products, P_i stands for individual loop gains, Δ_i are then loop gain terms which do not touch the i -th forward path, P_j are products of two non-touching loops, Δ_j symbolizes loop gain terms which do not touch the j -th forward path, P_k interprets products of three non-touching loops, Δ_k represents loop gain terms which do not touch the k -th forward path etc.

The proposed filters were designed using simplified M-C graphs. These simplified graphs are used for easier and more transparent presentation especially of the F-D structures which would be rather complex and difficult to follow in case of using modified M-C graphs. To show the design process when proposing a filter using signal-flow graphs let us have an example. The aim of the proposal is to design a second-order universal current-mode frequency filter which employs current followers as basic building blocks. The next condition of the proposal is that the proposed filter possesses ability to electronically control its pole frequency by changing values of unspecified adjustable active elements. The denominator (in its general form) of all transfer functions of the proposed filter takes form of:

$$D(s) = s^2 C_1 C_2 + s C_1 G_2 n_1 + G_1 G_2 n_1 n_2, \quad (4.3)$$

where C_1, C_2 define values of used capacitances of the filter and G_1, G_2 define values of used conductances which determine the pole frequency of the filter and n_1 and n_2 are controllable parameters of used adjustable active elements. Based on the rules of SFGs, the pole frequency of the filter having the denominator stated in (4.3) can be changed without disturbing the quality factor of the filter when $n_1 = n_2$. In this particular case, digitally adjustable current amplifiers were selected as controllable active elements. The pole frequency can be then controlled without the disturbance of the quality factor by adjusting current gains A of the DACA elements when $A_1 = A_2$. The denominator of the filter turns into:

$$D(s) = s^2 C_1 C_2 + s C_1 G_2 A_1 + G_1 G_2 A_1 A_2. \quad (4.4)$$

Equation (4.4) shows the final desired form of the denominator of the filter we want to propose. From this point, we can start designing the filter according to the rules of signal-flow graphs. The proposed filter is the second-order frequency filter thus, we are supposed to start with two self-loops as is shown in Figure 4.1.



Figure 4.1 Starting point of the design of the 2nd-order filter – Two non-touching self-loops (simplified M-C graph)

The denominator of the graph from Figure 4.1 is equal to:

$$D(s) = s^2 C_1 C_2 + s C_1 G_2 + s C_2 G_1 + G_1 G_2. \quad (4.5)$$

As can be seen the denominator contains some undesired terms. These terms can be eliminated by adding non-touching loops as demonstrated in Figure 4.2.

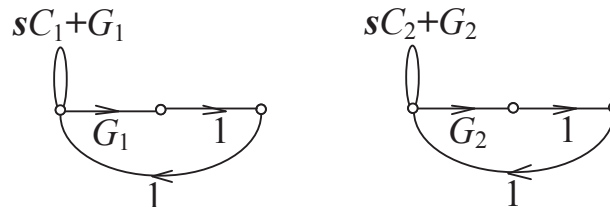


Figure 4.2 Second step of the design - Two loops (simplified M-C graph)

The denominator of the signal-flow graph from Figure 4.2 is:

$$D(s) = s^2 C_1 C_2. \quad (4.6)$$

The next step involves adding the main loop in order to obtain the next term of the chosen denominator. This graph modification can be seen in Figure 4.3.

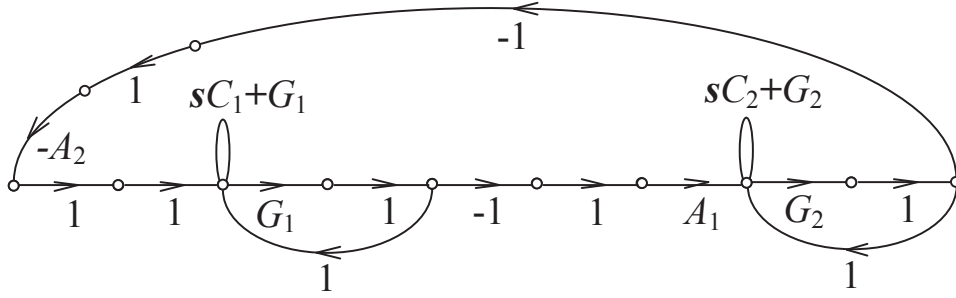


Figure 4.3 Third step of the design – Addition of main loop (simplified M-C graph)

The denominator of the filter turns into:

$$D(s) = s^2 C_1 C_2 + G_1 G_2 A_1 A_2. \quad (4.7)$$

The final step is adding the last loop in order to acquire the remaining term of the denominator. The resulting graph is depicted in Figure 4.4.

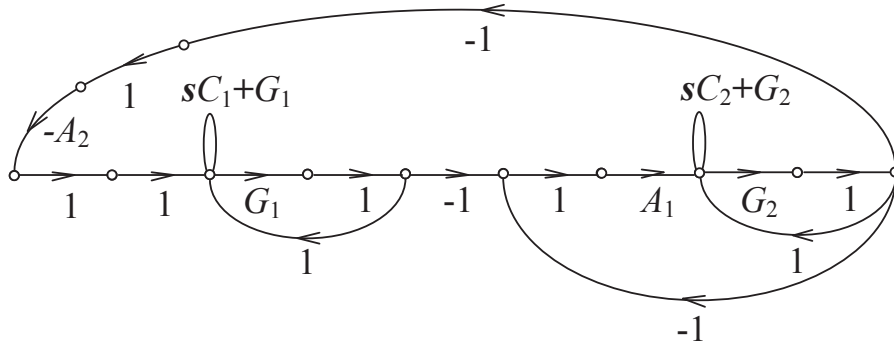


Figure 4.4 Resulting simplified M-C graph of the proposed filter

The denominator of the graph from Figure 4.4 is equal to:

$$D(s) = s^2 C_1 C_2 + s C_1 G_2 A_1 + G_1 G_2 A_1 A_2. \quad (4.8)$$

As can be seen the denominator from equation (4.8) is identical with the desired form of the denominator stated at the beginning of the proposal. The resulting M-C graph can be complemented with input and output terminals suitably placed in the graph as shown in Figure 4.5. The M-C graph of the proposed filter can be easily transformed into a corresponding circuit structure. This particular proposal is consistent with the proposed filter from chapter 6.4.

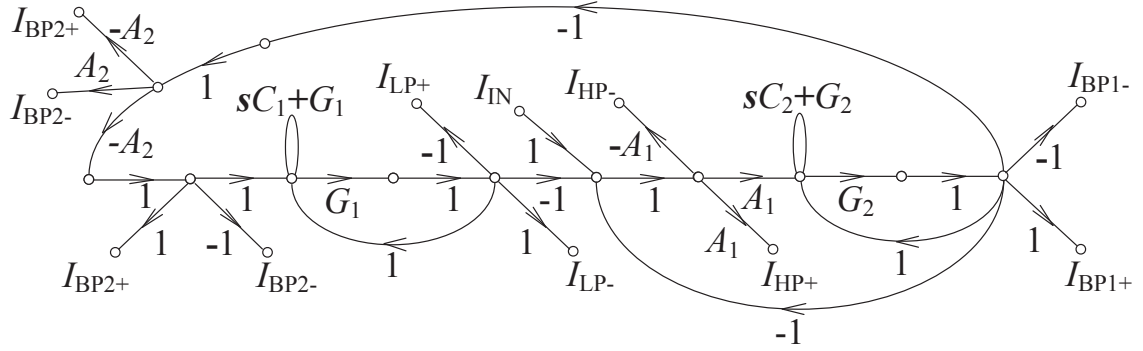


Figure 4.5 Resulting simplified M-C graph of the proposed filter with designated input and output terminals

5 Description of Used Active Elements

Active elements used to design filters that are included in this work are CFs [126], OTAs [127], ACAs [128] and OTRAs [129]. The voltage of each terminal of every presented active element is in relation to the ground as demonstrated in Figure 5.1, for instance.

The proposed filters in chapter 6 are simulated using behavioral simulation models which are described in this chapter. For simulations of current followers, operational transconductance amplifiers and operational transresistance amplifiers, the second-level and third-level behavioral simulation model of a universal current conveyor (UCC) with suitably connected terminals so it is able to emulate these active elements was used. The DACA has its own second-level and third-level behavioral simulation models.

Proposed fractional-order filters in chapter 7 were simulated using transistor-level simulation models. These models of active elements are described in this chapter as well. Simulation models of all these used active elements are implemented with 0.18 μm CMOS technology. The supply voltage for these models is ± 1 V. The number of outputs of all these active elements can be easily changed depending on current requirements of individual circuit structures of proposed filters.

5.1 Universal Current Conveyor

A universal current conveyor (UCC) [130] was developed in cooperation of Brno University of Technology and ON Semiconductor design center in CMOS 0.35 μm technology with designation UCC-N1B_0520. One UCC-N1B_0520 chip contains one UCC and one second-generation current conveyor with balanced output (CCII+/-). A schematic symbol of the UCC element is shown in Figure 5.1 a). Figure 5.1 b) illustrates a schematic symbol of the CCII+/-.

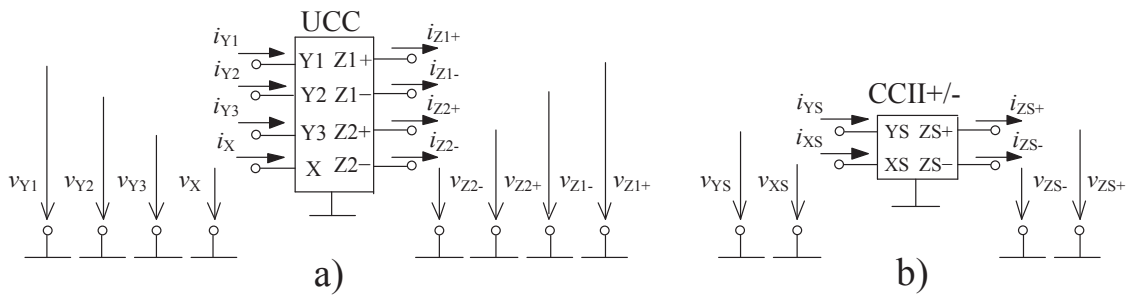


Figure 5.1 Schematic symbol of: a) UCC, b) CCII+/-

The UCC allows to realize all known types of current conveyors by appropriate connection of the terminals of this active element. The UCC can be also used to implement some other active elements such as OTA, or CF. The current followers, operational transconductance

amplifiers and operational transresistance amplifiers used in this work were implemented by the UCC.

Terminals Y1, Y2 and Y3 are high-impedance voltage inputs, X is a low-impedance current input and Z terminals are high-impedance current outputs which copy the current from terminal X with positive or negative polarity. The UCC can be described by hybrid matrix:

$$\begin{bmatrix} i_{Y1} \\ i_{Y2} \\ i_{Y3} \\ u_X \\ i_{Z1+} \\ i_{Z1-} \\ i_{Z2+} \\ i_{Z2-} \end{bmatrix} = \begin{bmatrix} 0 & 0 & 0 & 0 & 0 & 0 & 0 & 0 \\ 0 & 0 & 0 & 0 & 0 & 0 & 0 & 0 \\ 0 & 0 & 0 & 0 & 0 & 0 & 0 & 0 \\ 1 & -1 & 1 & 0 & 0 & 0 & 0 & 0 \\ 0 & 0 & 0 & 1 & 0 & 0 & 0 & 0 \\ 0 & 0 & 0 & -1 & 0 & 0 & 0 & 0 \\ 0 & 0 & 0 & 1 & 0 & 0 & 0 & 0 \\ 0 & 0 & 0 & -1 & 0 & 0 & 0 & 0 \end{bmatrix} \begin{bmatrix} u_{Y1} \\ u_{Y2} \\ u_{Y3} \\ i_X \\ u_{Z1+} \\ u_{Z1-} \\ u_{Z2+} \\ u_{Z2-} \end{bmatrix}. \quad (5.1)$$

As it was already stated above, the UCC-N1B_0520 chip also contains CCII+/- element which can be described by:

$$\begin{bmatrix} i_{YS} \\ u_{XS} \\ i_{ZS+} \\ i_{ZS-} \end{bmatrix} = \begin{bmatrix} 0 & 0 & 0 & 0 \\ 1 & 0 & 0 & 0 \\ 0 & 1 & 0 & 0 \\ 0 & -1 & 0 & 0 \end{bmatrix} \begin{bmatrix} u_{YS} \\ i_{XS} \\ u_{ZS+} \\ u_{ZS-} \end{bmatrix}. \quad (5.2)$$

A second-level simulation macromodel of the UCC is depicted in Figure 5.2. This macromodel has been used in simulations of the filters from chapters 6.2 - 6.5. As obvious, this simulation model imitates non-ideal input and output impedances of individual terminals of the UCC element. The parameters of the components within the simulation model are designed that way so the impedances of individual terminals correspond with the real element [131].

For simulations of filter in chapter 6.6 and on, a third-level model of universal current conveyor (taken directly from its simulation model in PSpice) illustrated in Figure 5.3 was used. Besides the imitation of input and output impedances, this model includes current limitations of the inputs and outputs and also elements limiting bandwidths of inter-terminal transfers. Detailed description of this model can be found in [131].

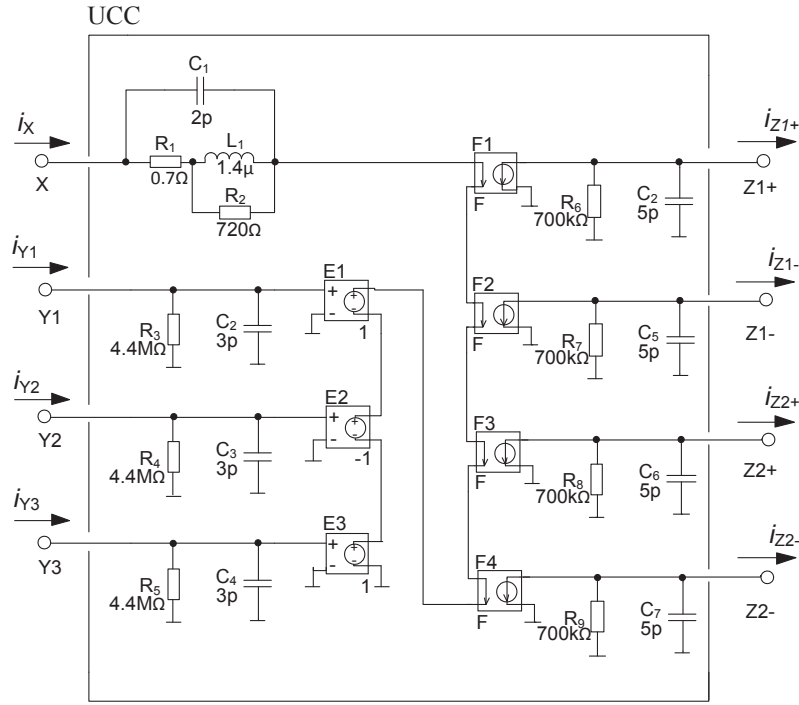


Figure 5.2 Second-level simulation macromodel of the UCC

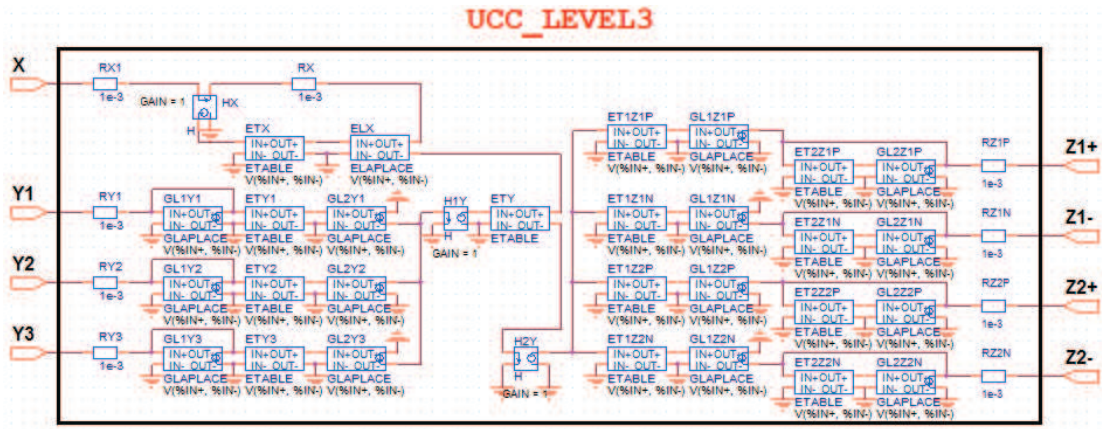


Figure 5.3 Third-level simulation macromodel of the UCC

5.2 Current Followers

In this work, the proposed filters which are using current followers in their structure are employing double-output current followers (DO-CFs) and multiple-output current followers (MO-CFs). The DO-CF consists of two outputs when the MO-CF consists of three or more outputs. Current followers are used to create either lossless or lossy integrators which are basic building blocks used in design of frequency filters. Additional outputs of this active element can be used to create feedbacks, which allow us to cancel out undesired terms

of the denominator of the filter, or to obtain particular transfer function right from the high-impedance outputs of this element. The MO-CF was originally presented in [126]. A schematic symbol, M-C graph, simplified M-C graph and possible implementation of the MO-CF element with four outputs can be seen in Figure 5.4 a), b), c), d) respectively. Figure 5.4 e) shows a schematic symbol of a FD-CF. In case of the implementation of the MO-CF by the UCC, all Y terminals are grounded, X serves as an input and Z terminals as outputs.

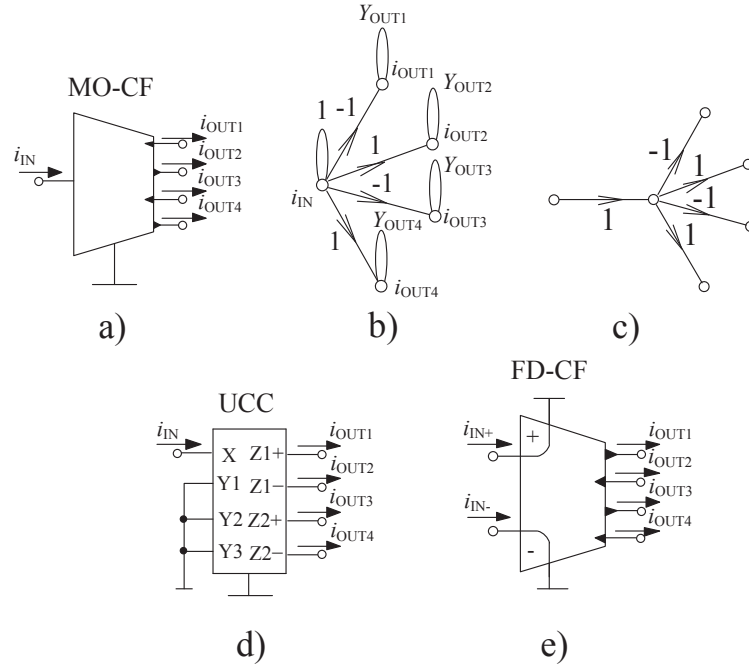


Figure 5.4 a) schematic symbol of the MO-CF, b) modified M-C graph of the MO-CF, c) simplified M-C graph of the MO-CF, d) possible implementation of the MO-CF using the UCC, e) schematic symbol of the FD-CF

The MO-CF element has one input and four output terminals. The relations between the input and output terminals of this active element are described by the following equations:

$$i_{OUT1} = i_{OUT3} = i_{IN}, \quad (5.3)$$

$$i_{OUT2} = i_{OUT4} = -i_{IN}. \quad (5.4)$$

The FD-CF from Figure 5.4 e) has a differential input and its behavior can be described by:

$$i_{OUT1} = i_{OUT3} = (i_{IN+} - i_{IN-}), \quad (5.5)$$

$$i_{OUT2} = i_{OUT4} = -(i_{IN+} - i_{IN-}). \quad (5.6)$$

The MO-CF element in chapter 6 was either modeled by the second-level model of the UCC from Figure 5.2, or the third-level model from Figure 5.3 depending on that if the filter was only simulated, or also implemented.

Figure 5.5 shows the transistor-level model of MO-CF element used in chapter 7 including the transistor dimensions. This simulation model was taken from [132].

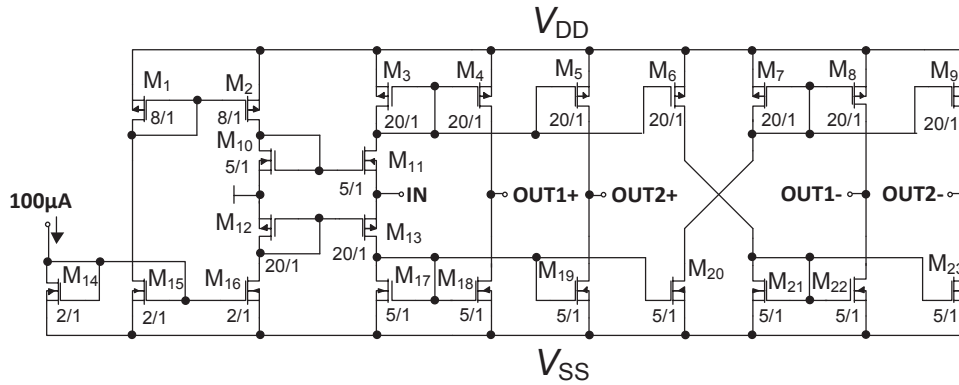


Figure 5.5 Used transistor-level model of the MO-CF element [132]

This particular implementation of the MO-CF consists of one input and four output terminals. Theoretical relations between input and output terminals are described by relations (5.3) and (5.4). The MO-CF can be easily transformed into a FD-CF when the branch between transistors M_{10} and M_{12} is used as the second input instead of being grounded.

5.3 Operational Transconductance Amplifiers

This active element is not working purely in the current mode, but it is frequently used in current-mode circuits as a basic building element. An ideal OTA element is a voltage-controlled current source (VCCS) with transconductance g_m . The operational transconductance amplifiers have a voltage differential input and either one current output (OTA) two current outputs with mutually opposite polarities (balanced operational transconductance amplifier (BOTA)), or three or more current outputs (MOTA). A schematic symbol, modified M-C graph and simplified M-C graph of the BOTA element are shown in Figure 5.6 a), b) and c). A schematic symbol and possible implementation of the MOTA element using the UCC are depicted in Figure 5.6 d), e). In case of the implementation of the MOTA using the UCC, Y_1 and Y_2 terminals serve as inputs, Y_3 is grounded, X is connected to a grounded resistor. Transconductance of this type of implementation is then inversely dependent on the value of the resistor R which is connected to X terminal.

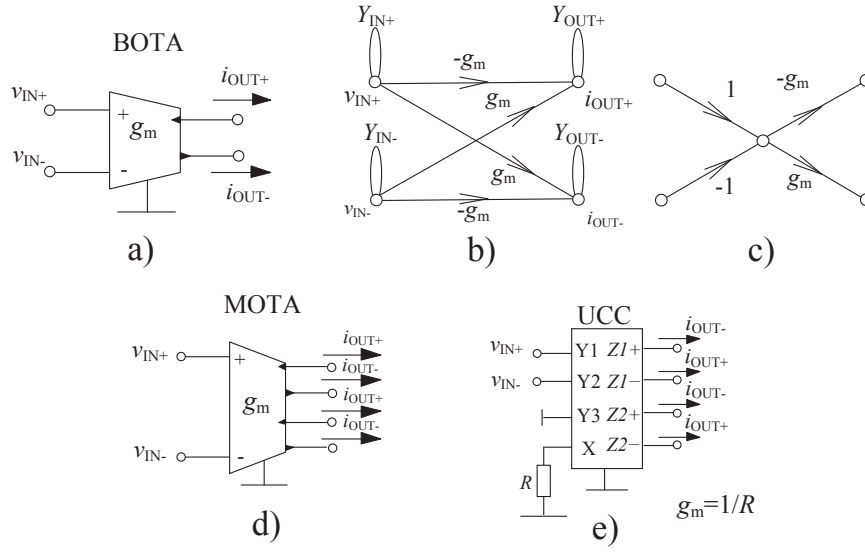


Figure 5.6 a) schematic symbol of the BOTA, b) modified M-C graph of the BOTA, c) simplified M-C graph of the BOTA, d) schematic symbol of the MOTA, e) possible implementation of the MOTA using the UCC

The BOTA and MOTA consist of a voltage differential input and two or more current outputs. Relations between input and output terminals are described as:

$$i_{OUT+} = -i_{OUT-} = g_m (v_{IN+} - v_{IN-}). \quad (5.7)$$

The MOTA element in chapter 6 was either modeled by the second-level model of the UCC from Figure 5.2, or the third-level model from Figure 5.3.

A transistor-level model of the MOTA element used for PSpice simulations in chapter 7 including the transistor dimensions is illustrated in Figure 5.7. The transconductance of this particular implementation of the MOTA element is controlled by bias DC current I_{set} . The dependence of transconductance of the used transistor-level simulation model of the MOTA element on bias current I_{set} is presented in Figure 5.8.

This particular implementation of the MOTA element consists of two input and four output terminals. Relations between input and output terminals are described by equation (5.7). This transistor-level model was taken from [133]. The dimensions of some transistors stated in [133] were slightly adjusted in order to decrease the difference between positive and negative outputs.

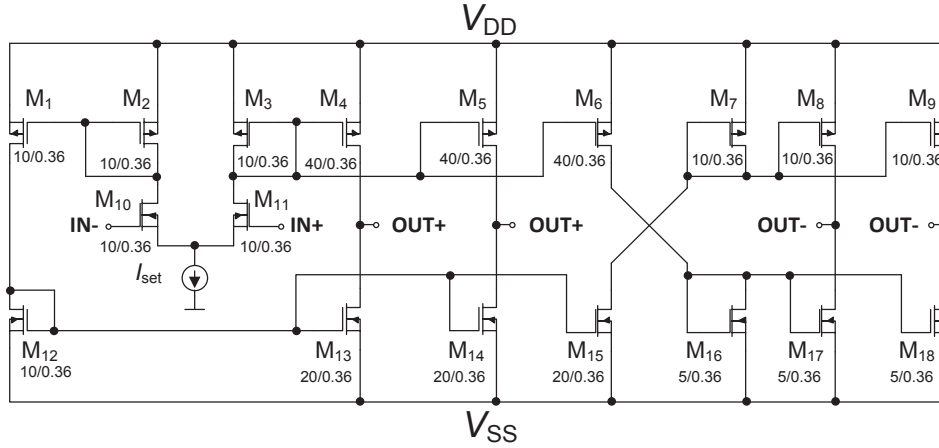


Figure 5.7 Used transistor-level model of the MOTA element [133]

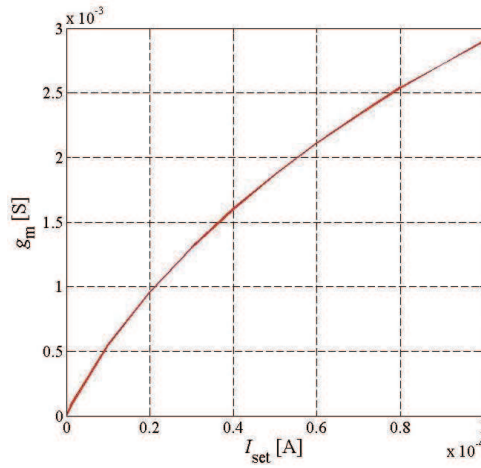


Figure 5.8 Dependence of g_m on I_{set} of the MOTA transistor-level simulation model

5.4 Adjustable Current Amplifiers

Adjustable current amplifiers are current-mode active elements with a low-impedance current input(s) and current high-impedance current output(s) with ability to control their gain. The gain of these elements is being controlled by some external parameter usually DC voltage and current. A schematic symbol of the ACA element is depicted in Figure 5.9 a). Figure 5.9 b) c) and d) shows a schematic symbol of the digitally adjustable current amplifier, modified M-C graph of this element, simplified M-C graph respectively.

The DACA element was developed in cooperation of Brno University of Technology and ON Semiconductor design center in CMOS 0.35 μm technology. The DACA consists of a differential input and differential output and its gain is controlled via 3-bit word in range from 1 to 8 with step of 1. An alternative circuit solution of the DACA element is presented in Figure 5.9 e). It consists of two inputs and four outputs and it is formed by one universal

voltage conveyor (UVC) [55], one EL2082 [134] and one UCC. The gain of this circuit can be controlled continuously in range of 0 to 5 by DC voltage.

The DACA element can be described by the following relations:

$$i_{ID} = i_{IN+} - i_{IN-}, \quad (5.8)$$

$$i_{OD} = i_{OUT+} - i_{OUT-}, \quad (5.9)$$

$$i_{OD} = 2Ai_{ID}, \quad (5.10)$$

$$i_{OUT+} = A(i_{IN+} - i_{IN-}), \quad (5.11)$$

$$i_{OUT-} = -A(i_{IN+} - i_{IN-}), \quad (5.12)$$

where i_{ID} is a differential input current, i_{OD} is the differential output current and A stands for the current gain of this element.

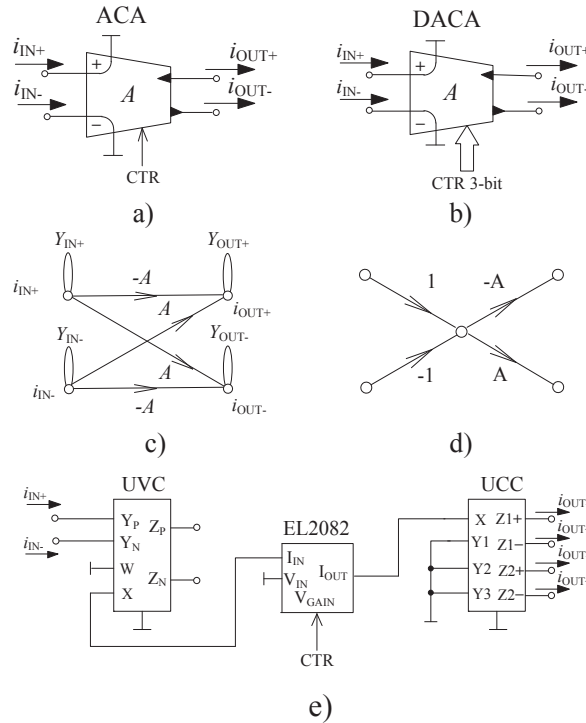


Figure 5.9 a) schematic symbol of the ACA, b) schematic symbol of the DACA, c) modified M-C graph of the DACA, d) simplified M-C graph of the DACA, e) alternative implementation of the DACA using one UCC, UVC and EL2082

A second-level simulation macromodel which has been used in simulations of the proposed filters from chapters 6.2 - 6.5 and 6.8 is presented in Figure 5.10. This model is used for filters which were proposed with the alternative circuit solution of the DACA element so the control of its current gain is continuous instead of discrete steps of the real DACA element. This simulation model imitates non-ideal input and output impedances of individual terminals of the DACA element.

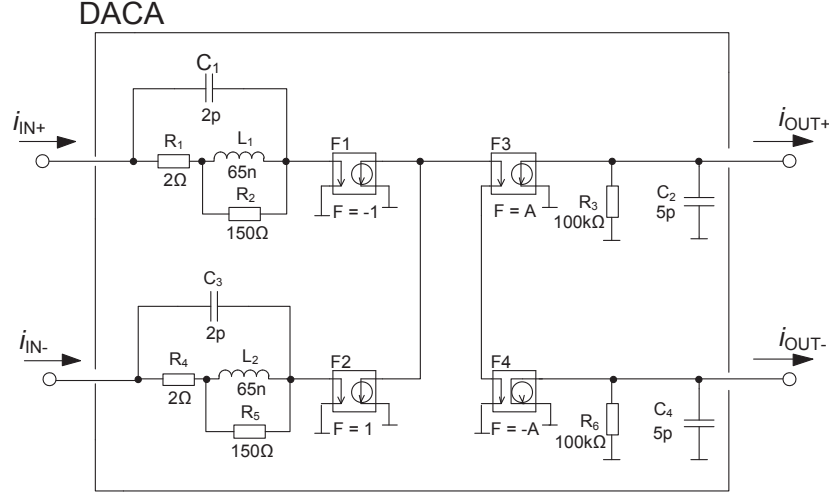


Figure 5.10 Second-level simulation macromodel of the DACA

A simulation macromodel used for simulations of the filter from chapter 6.6 is illustrated in Figure 5.11. This simulation model is used for the filter which is implemented with the real DACA element. It is the third-level simulation macromodel which imitates input and output impedances of individual terminals of the DACA and also imitates current limitations of these terminals. In this model, the values of output impedances and current limitations are depended on the actual chosen value of gain. Detailed information about this simulation model of the DACA element can be found in [135].

Table I summarizes values of the current gains of the DACA element depending on chosen 3-bit word. A_{THEOR} represents the theoretical value of actual gain when A_{REAL} is the actual obtained gain for particular word. These values are based on the worst case values obtained from measurement of ten DACA chips.

Table I Theoretical and actual values of current gains of the DACA element

3-bit word	000	001	010	011	100	101	110	111
A_{THEOR} [-]	1	2	3	4	5	6	7	8
A_{REAL} [-]	0.80	1.60	2.49	3.30	4.13	4.94	5.81	6.61

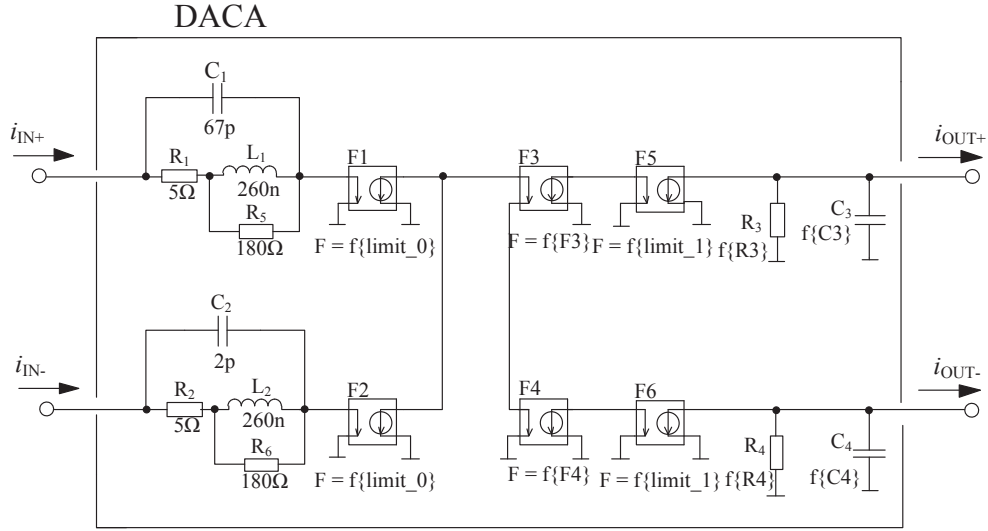


Figure 5.11 Third-level simulation macromodel of the DACA

Figure 5.12 depicts a transistor-level model of the ACA element including the transistor dimensions. The current gain (B label used in this case) of this particular implementation of a transistor-level model of the ACA element is controlled by current I_{setB} . The dependence of current gain B of the used transistor-level simulation model of the ACA element on control current I_{setB} is shown in Figure 5.13. This simulation model was taken from [14].

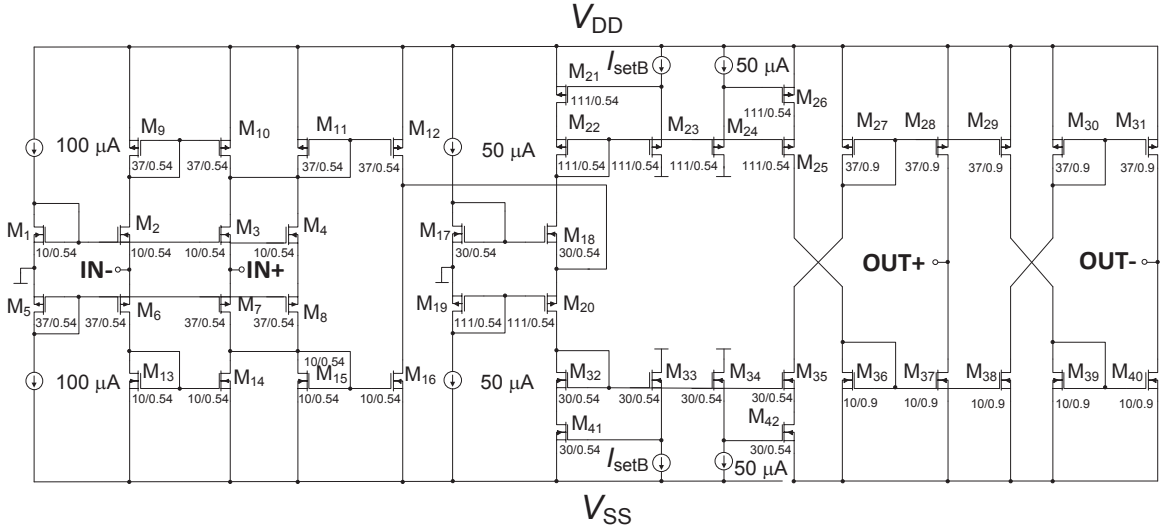


Figure 5.12 Used transistor-level model of the ACA element [14]

This particular transistor-level model implementation of the ACA consists of two input and two output terminals. This active element can be described by the following relation:

$$I_{\text{OUT}+} = -I_{\text{OUT}-} = B \cdot (I_{\text{IN}+} - I_{\text{IN}-}).$$

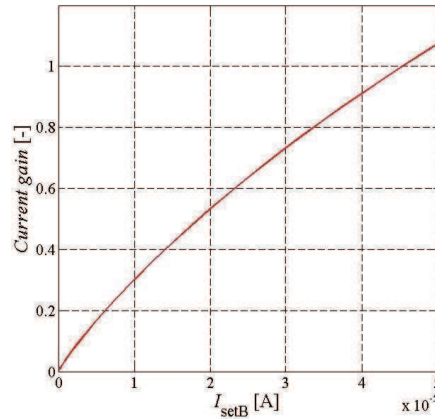


Figure 5.13 Dependence of B on I_{setB} of the ACA transistor-level simulation model

5.5 Operational Transresistance Amplifiers

An OTRA originally presented in [129] is an active element with a current input and voltage output(s). A schematic symbol, modified M-C graph, simplified M-C graph of the OTRA element and its possible implementation using two UCC-N1B_0520 chips can be seen in Figure 5.14. This particular implementation of the OTRA element consists of two current inputs and two voltage outputs and its transresistance can be set by resistor R_T connected between CCII and UCCs the way shown in Figure 5.14 d).

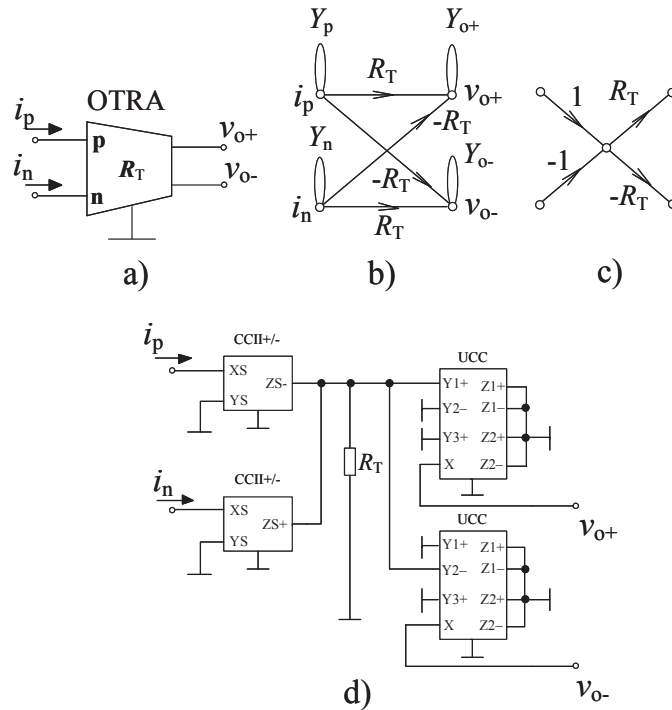


Figure 5.14 Operational transresistance amplifier: a) schematic symbol, b) modified M-C graph, c) simplified M-C graph, d) possible implementation of the OTRA using two UCC-N1B_0520 chips

Relations between input and output terminals of the OTRA element can be described as:

$$v_{o+} = R_T(i_p - i_n), \quad (5.13)$$

$$v_{o-} = -R_T(i_p - i_n), \quad (5.14)$$

where i_p and i_n are currents of p and n input terminals of this element.

5.6 Concluding Summary of the Chapter

Current followers are very simple active components which are suitable for the current-mode circuits. The disadvantage of their usage is that the filters employing CFs require resistors which increases the complexity of the circuit. The other disadvantage is that additional (controllable) active elements must be placed in the circuit structure in order to achieve electronic control of some of the typical filter parameters such as the pole frequency, quality factor etc.

The transconductance amplifiers are also suitable for the current-mode circuits although the circuits employing this type of active elements are not working purely in the current mode. The advantage of this active element is the ability to control its transconductance so it is possible to electronically control some of the filter parameters and it does not require additional resistors in comparison to CFs. The OTAs are also suitable for use in F-D structures because it has a voltage differential input.

The DACA amplifier can be suitably added in the circuit structure in order to enable control of some of the filter parameters. Since they have current inputs and current outputs they are idea to combine with current followers which do not posses electronic controllability. The alternative circuit of the DACA element also provides a continuous control and possesses four outputs in default which is advantageous for usage in F-D structures.

The OTRA amplifier can be also added in circuit structure in order to enable control of some of the filter parameters. Its inclusion in the circuit structure is slightly more difficult than in case of the DACA because of its voltage outputs which cannot be directly connected to the current input of the filter. Thus, the OTRA element is appropriate to combine with the OTA, or some other active element with voltage inputs.

6 Newly Proposed Filtering Structures

This chapter contains new proposals of the fully-differential (F-D) frequency filters working in the current mode. These filters are either firstly proposed in their single-ended (S-E) form and then transformed into the F-D forms, or proposed in the F-D forms based on existing structures. All presented responses are non-inverting transfer functions unless stated otherwise. The models of particular active elements used in case of simulations are described in chapter 5. All S-E filters are firstly design using signal-flow graph design method. The F-D filters are then created from the corresponding S-E filters by the transformation of horizontal structures. All the proposed filters are the second-order current-mode filters. Band-pass and all-pass transfer functions can be easily obtained by summing particular outputs of the circuit because the proposed structures are the SIMO type filters. Another important feature of the proposed structures is a low input and high output impedance which allows simple cascading of these structures in order to create higher-order filters. Since floating capacitors are not suitable for practical implementation, all implemented filter are designed with grounded capacitors as shown later. The proposals are then verified using SNAP program and PSpice simulations using available simulation models of used active elements. The actual functionality of the proposed filters is, in some cases, also supported by experimental measurements. If the experimental measurement has been carried out, chips of available active elements have been used the way stated in chapter 5. The measurement has been performed using network analyzer Agilent 4395A together with simple V/I and I/V converters. In case of F-D measurement, single-ended voltage to differential voltage, two V/I and differential current to single-ended voltage converters [119] were used. Figure 6.1 shows a block diagram of the measurement of the S-E filters working in the current mode. A block diagram of the measurement of the F-D current-mode filters is illustrated in Figure 6.2. All experimental measurements are affected by limitations and parasitic parameters of used V/I and I/V (V/I_{DIF} , I_{DIF}/V) converters. The magnitude response of the S-E V/I - I/V converters is depicted in Figure 6.3 and the magnitude response of the V/I_{DIF} - I_{DIF}/V converters is shown in Figure 6.4.

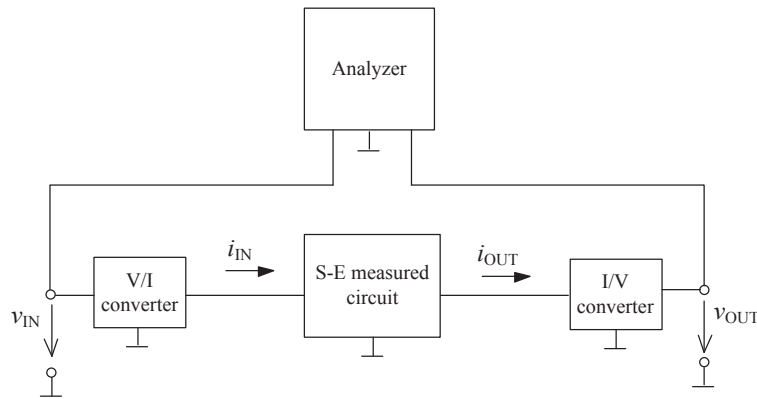


Figure 6.1 Block diagram of the measurement of the S-E filters

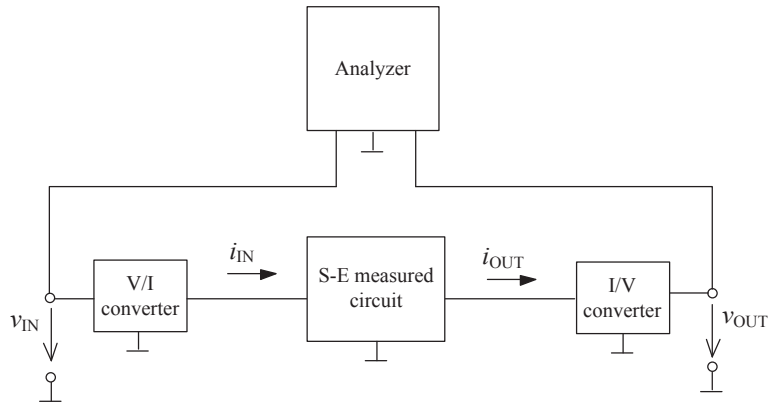


Figure 6.2 Block diagram of the measurement of the F-D filters

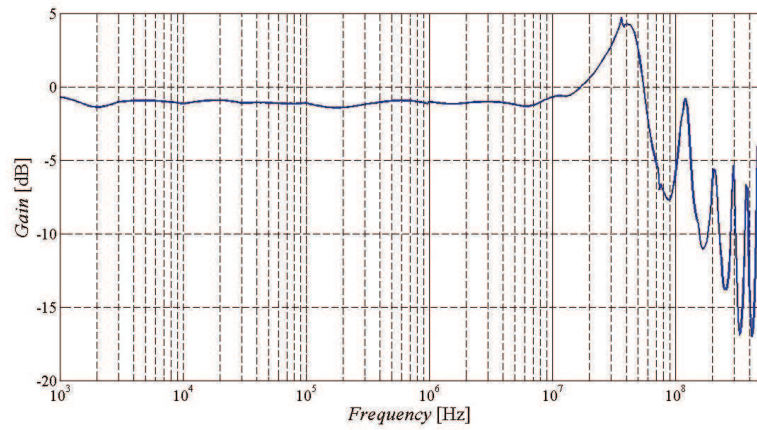


Figure 6.3 Magnitude response of the S-E V/I - I/V converters

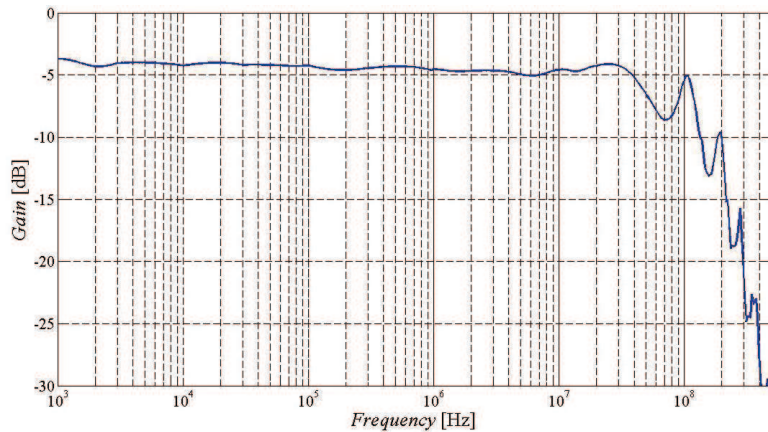


Figure 6.4 Magnitude response of the V/I_{DIF} - I_{DIF}/V converters

From the Figure 6.3 can be seen that the S-E V/I, I/V converters are suitable to use up to 30 MHz. The suitability of the V/I_{DIF} - I_{DIF}/V converters is up to 50 MHz. The gain of the converters above these frequencies is highly inconsistent. This inconsistency is

affecting measured results. All experimental measurements are also affected by parasitic capacitances of PCBs of implemented filters and parasitic capacitances of cables used to connect the measured filter with converters and analyzer. All these features are significantly affecting experimental results at higher frequencies.

6.1 General Conception of a Filter with Three CFs

Figure 6.5 shows a general structure of a second-order universal filter based on the FLF topology employing three CFs from [80]. This conception is based on the fact that it is possible to design frequency filters by suitable setting of integrators as basic building blocks. The structure consists of three MO-CFs creating lossy and lossless integrators. The advantage of this is a low input and high output impedance of given structure which in case of the current mode allows simple chaining of these blocks in cascade. In case of the design of the current-mode frequency filters, it is advantageous that when the output responses are taken directly from current outputs of used active elements. For this reason, it is advantageous to use multiple-output active elements such as MO-CFs in order to have more responses from high-impedance outputs of active element if possible in both polarities.

The denominator of the filter is:

$$D(s) = s^2 C_1 C_2 + s C_2 G_1 + G_1 G_2. \quad (6.1)$$

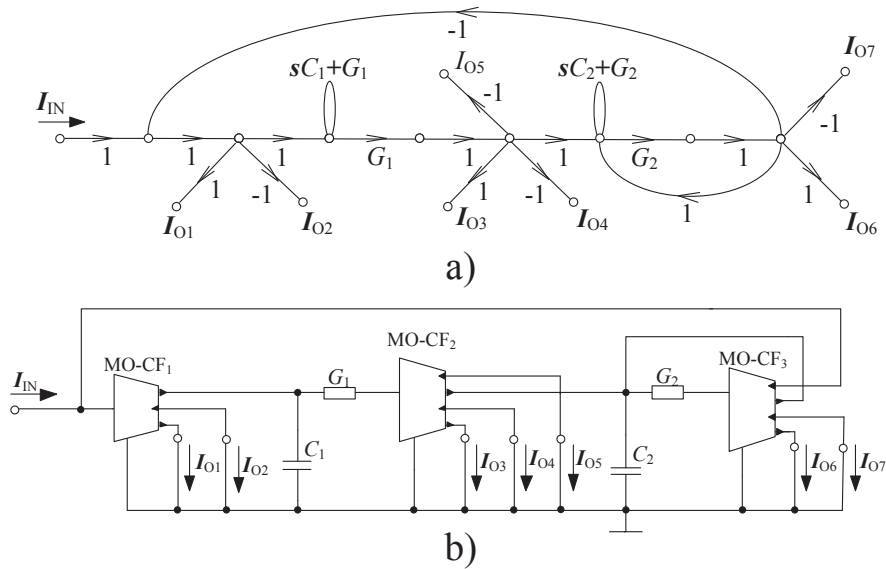


Figure 6.5 General conception of a filter with three MO-CFs: a) simplified M-C graph, b) circuit structure

Relations of the pole frequency and quality factor of the filter are given by the following equations:

$$f_0 = \frac{1}{2\pi} \sqrt{\frac{G_1 G_2}{C_1 C_2}}, \quad Q = \sqrt{\frac{G_2 C_1}{G_1 C_2}}, \quad (6.2), (6.3)$$

where f_0 is the pole frequency and Q stands for the quality factor of the filter.

The filter can provide the following functions:

$$K_{LP}(s) = \frac{I_{O6}}{I_{IN}} = -\frac{I_{O7}}{I_{IN}} = \frac{G_1 G_2}{D}, \quad (6.4)$$

$$K_{BP}(s) = \frac{I_{O3}}{I_{IN}} = -\frac{I_{O4}}{I_{IN}} = -\frac{I_{O5}}{I_{IN}} = \frac{s C_2 G_1}{D}, \quad (6.5)$$

$$K_{HP}(s) = \frac{I_{O1} + I_{O4}}{I_{IN}} = \frac{I_{O1} + I_{O5}}{I_{IN}} = -\frac{I_{O2} + I_{O3}}{I_{IN}} = \frac{s^2 C_1 C_2}{D}, \quad (6.6)$$

$$K_{BS}(s) = \frac{I_{O1} + I_{O4} + I_{O6}}{I_{IN}} = \frac{I_{O1} + I_{O5} + I_{O6}}{I_{IN}} = -\frac{I_{O2} + I_{O3} + I_{O7}}{I_{IN}} = \frac{s^2 C_1 C_2 + G_1 G_2}{D}, \quad (6.7)$$

$$K_{AP}(s) = \frac{I_{O1} + I_{O4} + I_{O5} + I_{O6}}{I_{IN}} = \frac{s^2 C_1 C_2 - s C_2 G_1 + G_1 G_2}{D}. \quad (6.8)$$

From obtainable transfer functions is obvious that the filter is universal because it provides all standard transfer functions (LP, BP, HP, BS, AP). All transfer functions except all-pass function can be obtained in both polarities. Note that the high-pass transfer function is obtained by summing two outputs. This conception is used to propose filters in chapters 6.2, 6.3, 6.4 and 6.5.

6.2 Universal Filter with Three CFs and Two DACs

6.2.1 Filter proposal

This proposal is based on a previously presented filter from chapter 6.1. The circuit structure has been complemented with two digitally adjustable current amplifiers which were suitably added in the circuit structure so it is possible to electronically control the pole frequency. Figure 6.6 shows the proposed S-E filter. The other advantage of this new proposal is that high-pass transfer function can be obtained directly from the outputs of the follower

MO-CF₁ in comparison to the previously proposed filter when it was necessary to sum the outputs of the two active components, in order to obtain this function. I presented the proposal described in this chapter in [136].

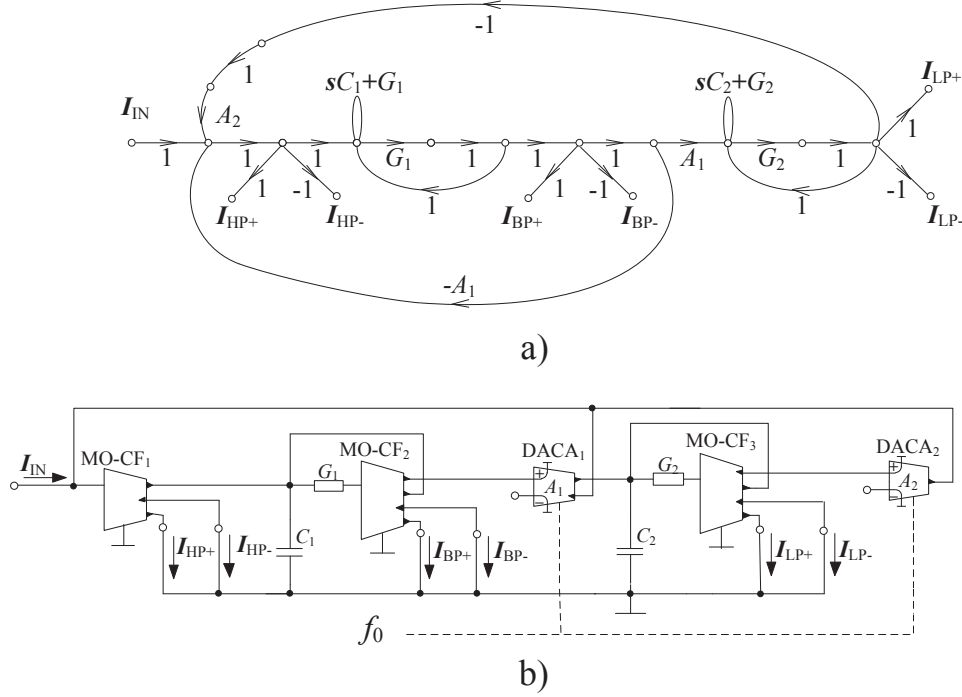


Figure 6.6 Single-ended form of the proposed filter with three MO-CFs and two DACAs: a) simplified M-C graph, b) circuit structure

The F-D version of the proposed filter was created from the S-E structure by mirroring passive parts and also active elements. The F-D filter is also proposed with non-differential current followers instead of fully differential current followers in order of easier possible future implementation in a form of PCB. The differential structure of the proposed filter is presented in Figure 6.7. It consists of two DO-CFs, four MO-CFs and two DACAs.

The denominator for all available transfer functions of these filters is given by:

$$D(s) = s^2 C_1 C_2 + s C_2 G_1 A_1 + G_1 G_2 A_1 A_2. \quad (6.9)$$

From equation (6.9) is obvious that it is possible to control the pole frequency of the filter without disturbing the quality factor of the filter by adjusting current gains of the DACA elements when $A_1 = A_2 = A$.

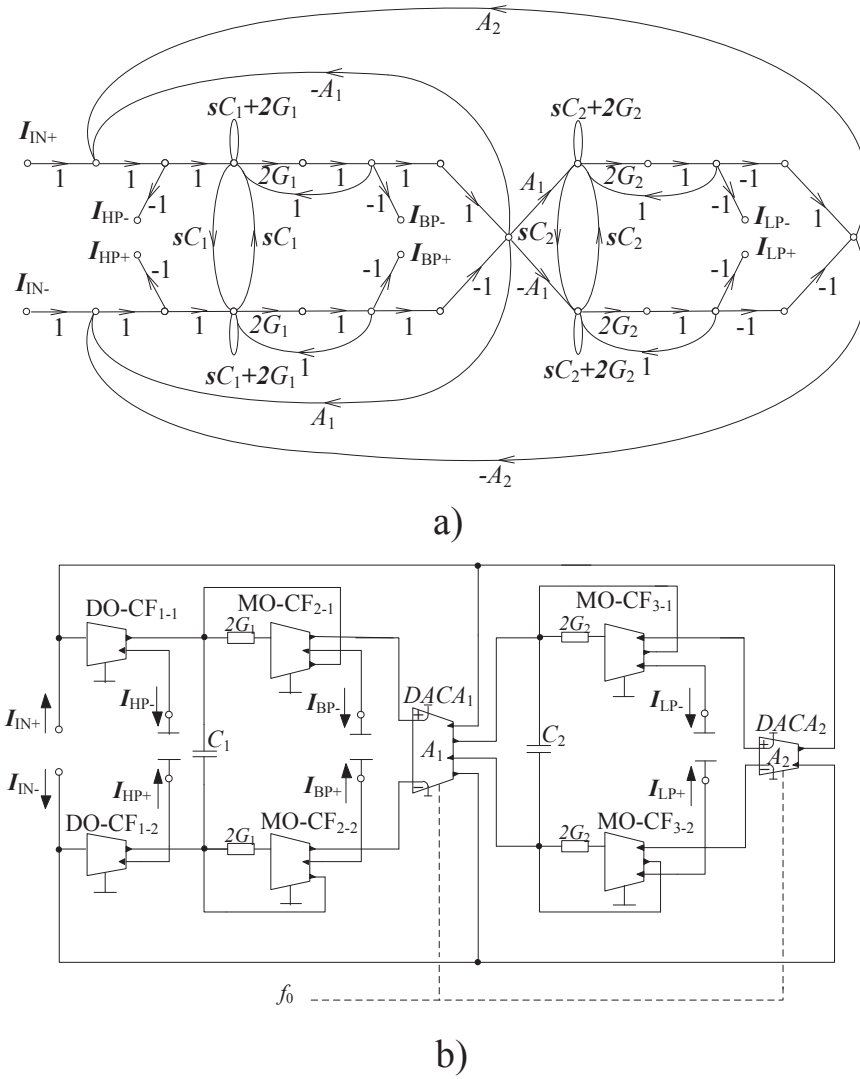


Figure 6.7 Fully-differential form of the proposed filter with three MO-CFs and two DACs: a) simplified M-C graph, b) circuit structure

The pole frequency and quality factor are defined accordingly:

$$f_0 = \frac{A}{2\pi} \sqrt{\frac{G_1 G_2}{C_1 C_2}}, \quad Q = \sqrt{\frac{G_2 C_1}{G_1 C_2}}. \quad (6.10), (6.11)$$

In order to obtain the same particular transfer functions for the F-D form of filter, parameter A is replaced by $2A$. The values of parameters G_1 , G_2 are also twice higher in comparison to the values used for the S-E filter which results from the method described in chapter 1.

Obtainable transfer functions of these filters are given as follows:

$$\frac{I_{LP+}}{I_{IN}} = -\frac{I_{LP-}}{I_{IN}} = \frac{G_1 G_2 A_1}{D}, \quad (6.12)$$

$$\frac{I_{BP+}}{I_{IN}} = -\frac{I_{BP-}}{I_{IN}} = \frac{sC_2 G_1}{D}, \quad (6.13)$$

$$\frac{I_{HP+}}{I_{IN}} = -\frac{I_{HP-}}{I_{IN}} = \frac{s^2 C_1 C_2}{D}, \quad (6.14)$$

$$I_{BS} = \frac{I_{HP+} + I_{LP+}}{I_{IN}} = -\frac{I_{HP-} + I_{LP-}}{I_{IN}} = \frac{s^2 C_1 C_2 + G_1 G_2 A_1}{D}, \quad (6.15)$$

$$I_{AP} = \frac{I_{HP+} + I_{BP-} + I_{LP+}}{I_{IN}} = -\frac{I_{HP-} + I_{BP+} + I_{LP-}}{I_{IN}} = \frac{s^2 C_1 C_2 - sC_2 G_1 + G_1 G_2 A_1}{D}. \quad (6.16)$$

From the equations (6.12) - (6.16) is obvious that it is possible to obtain all standard transfer functions. From the equations it is evident that high-pass transfer function corresponds with the particular term of the denominator and it will have unity gain in pass-band area regardless the values of parameter A . For these filters, the analysis of five possible inputs in order to determinate what filter functions can obtained from individual outputs was made. For the sake of clarity, only analysis with input I_{IN1} is included here. All analyzed variants can be found in [136].

6.2.2 Simulation Results

For the PSpice simulations, the values of passive elements and specific filter parameters have been chosen as follows: the starting pole frequency $f_0 = 1$ MHz, starting quality factor $Q = 0.707$ (Butterworth approximation), default current gains $A_1 = A_2 = 1$ (half values in case of the F-D form of the filter) and values of capacitors were set $C_1 = C_2 = 100$ pF. Values of resistors were calculated accordingly: $R_1 = Q/(2\pi f_0 C_1) = 1125 \Omega$ and $R_2 = 1/(4\pi^2 f_0^2 C_1 C_2 R_1) = 2252 \Omega$. These values were left unchanged instead of being rounded to correspond with realistically obtainable values so the parasitic characteristics of the models of used active elements are more apparent.

As already mentioned conductances G_1 , G_2 for the F-D filter must be of double values thus, the resistors of the F-D filter have half the values of resistors of the S-E filter. All output responses depicted in this chapter are inverting filtering functions. Instead of the DACA element, an alternative circuit of the DACA presented in section 5.4 was used. Therefore, the values chosen to verify ability to tune the pole frequency of filters are solely demonstrational and do not necessary correspond with values which can be obtained using a real element of the DACA.

Figure 6.8 illustrates obtained LP, BP, HP and BS transfer functions for both S-E and F-D form of the filter. The slope of attenuation of obtained HP transfer functions (blue lines) is 39 dB per decade, 18 dB per decade for BP functions (red lines) and in case of LP transfer functions it is 38 dB per decade. The biggest attenuation of the BS function is -40 dB. The slope of attenuation of individual transfer functions of the F-D filter is slightly higher. This is mainly caused by lower values of resistors used for the F-D filter in comparison to the values of resistors of the S-E filter.

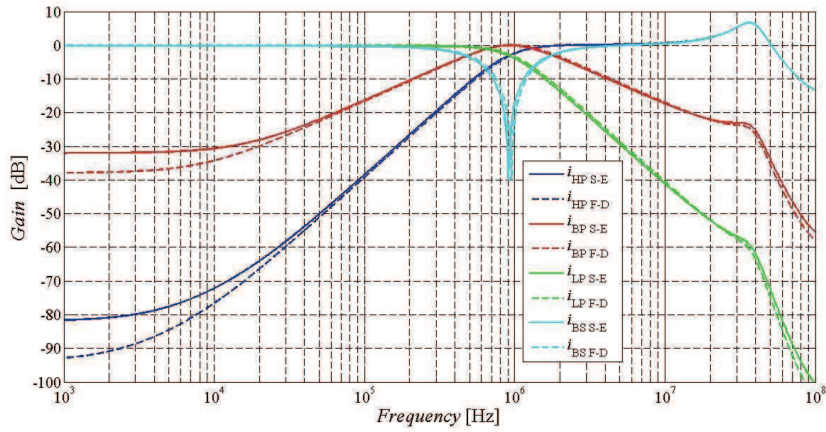


Figure 6.8 Output responses of the S-E filter from Fig. 6.6 (solid lines) and of the F-D filter from Fig. 6.7 (dashed lines): high-pass, band-pass, low-pass, band-stop transfer functions (simulation results)

Demonstration of the possibility to tune the pole frequency of the S-E and F-D filter by changing the values of transfer gains of the DACA elements can be seen in Figure 6.9. The HP transfer function was used as an example. Values of current gains A_1 and A_2 were set accordingly 0.5, 1, 2 (0.25, 0.5, 1 in case of the F-D structure). Values of the pole frequency obtained from simulations can be compared in Table II. From the table can be seen that the values of the pole frequency obtained from the F-D filter are closer to the theoretical values.

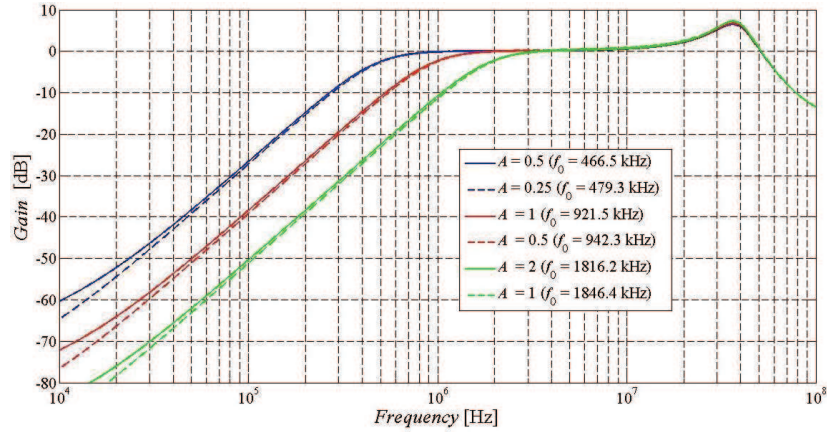


Figure 6.9 Demonstration of ability to control the pole frequency (simulation results) in case of the S-E filter from Fig. 6.6 (solid lines) and of the F-D filter from Fig. 6.7 (dashed lines) when $A_1 = A_2$ were set 0.5, 1, 2

Table II Comparison of obtained values of the pole frequency

	$A_{1,2}$ S-E/ $A_{1,2}$ F-D [-]		
Frequency [kHz]	0.5/0.25	1/0.5	2/1
Calculated	500.0	999.9	1999.8
Simulated S-E	466.5	921.5	1816.2
Simulated F-D	479.3	942.3	1846.4

Gain, group delay and phase characteristics of all pass transfer functions are depicted in Figure 6.10. The blue lines represent all-pass transfer function of the S-E form of the proposed filter and the red lines then show obtained all-pass transfer function of the F-D form of the filter. From the graph can be see that the filter is suitable only approximately up to frequency of 10 MHz because of bandwidth limitations and parasitic characteristics of used active elements, bandwidth limitations of used converters and parasitic capacitances of cables and PCB.

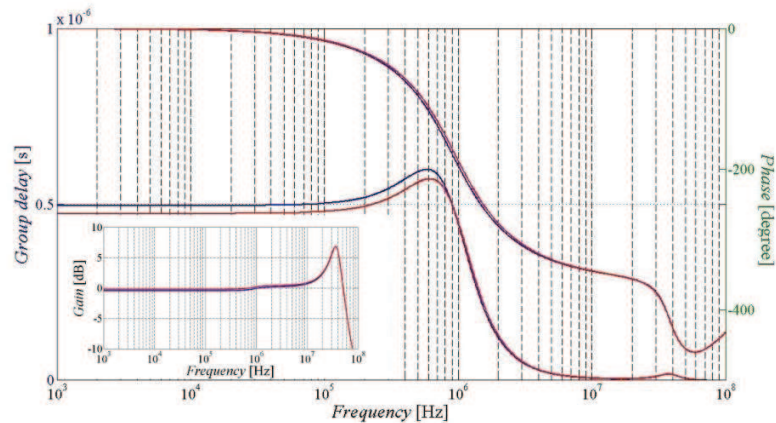


Figure 6.10 Output responses (simulation results) of all-pass filter characteristics (gain, group delay and phase) of the S-E filter from Fig. 6.6 (blue lines) and of the F-D filter from Fig. 6.7 (red lines)

6.2.3 Sensitivity Analysis

The analysis of the proposed S-E and F-D filter also includes a relative sensitivity analysis [120]. The S-E filter from Figure 6.6 contains 17 parameters ($C_1, C_2, G_1, G_2, A_1, A_2, n_{11}, n_{12}, n_{13}, n_{21}, n_{22}, n_{23}, n_{24}, n_{31}, n_{32}, n_{33}, n_{34}$). Coefficients n_{11} to n_{34} represent individual outputs of each current follower in the circuit structure. The change of any of these parameters can significantly influence the characteristics of the filter. When taking all these parameters into consideration, the denominator of the S-E filter turns into:

$$D_{real}(s) = s^2 b_2 + s b_1 + b_0, \quad (6.17)$$

where

$$b_2 = -C_1 C_2, \quad (6.18)$$

$$b_1 = -G_1 C_2 - G_1 n_{22} C_2 - G_1 n_{21} A_1 C_2 n_{11} - C_1 G_2 - C_1 G_2 n_{32}, \quad (6.19)$$

$$b_0 = -G_1 n_{21} A_1 G_2 n_{32} n_{11} - G_1 n_{22} G_2 - G_1 n_{22} G_2 n_{32} - G_1 G_2 - G_1 G_2 n_{32} - G_1 n_{21} A_1 G_2 n_{11} - G_1 n_{21} A_1 G_2 n_{31} A_2 n_{11}. \quad (6.20)$$

The real transfer functions are given by the following equations:

$$K_{LP\ real}(s) = \frac{I_{LP\ real}}{D_{real}}, \quad (6.21)$$

$$K_{BP\ real}(s) = \frac{I_{BP\ real}}{D_{real}}, \quad (6.22)$$

$$K_{HP\ real}(s) = \frac{I_{HP\ real}}{D_{real}}, \quad (6.23)$$

$$K_{BS\ real}(s) = \frac{I_{BS\ real}}{D_{real}}, \quad (6.24)$$

where

$$\mathbf{I}_{LP\ real} = G_1 n_{21} A_1 G_2 n_{34} n_{11}, \quad (6.25)$$

$$\mathbf{I}_{BP\ real} = s(G_1 n_{24} C_2 n_{11}) + G_1 n_{24} G_2 n_{11} + G_1 n_{24} G_2 n_{32} n_{11}, \quad (6.26)$$

$$\begin{aligned} \mathbf{I}_{HP\ real} = & s^2(C_1 C_2 n_{13}) + s(C_1 G_2 n_{32} n_{13} + C_1 G_2 n_{13} + G_1 n_{22} C_2 n_{13} + G_1 C_2 n_{13}) + \\ & + G_1 G_2 n_{13} + G_1 G_2 n_{32} n_{13} + G_1 n_{22} G_2 n_{32} n_{13} + G_1 n_{22} G_2 n_{13}, \end{aligned} \quad (6.27)$$

$$\begin{aligned} \mathbf{I}_{BS\ real} = & s^2(C_1 C_2 n_{13}) + s(C_1 G_2 n_{32} n_{13} + C_1 G_2 n_{13} + G_1 C_2 n_{13} n_{22} + G_1 C_2 n_{13}) + G_1 G_2 n_{13} + \\ & + G_1 G_2 n_{13} n_{22} + G_1 G_2 n_{32} n_{13} + G_1 G_2 n_{32} n_{13} n_{22} + G_1 A_1 G_2 n_{34} n_{11} n_{21}. \end{aligned} \quad (6.28)$$

A relation for a relative sensitivity analysis of a transfer function is given by [120]:

$$S_{R-q_i}^K = \frac{q_i}{K} \frac{\partial K}{\partial q_i}, \quad (6.29)$$

where q_i represents particular circuit parameter such as C_1 , A_1 etc.

The relative sensitivity of the module of transfer is then given as [120]:

$$S_{R-q_i}^{|K(j\omega)|} = \text{Re}\{S_{R-q_i}^{K(j\omega)}\}. \quad (6.30)$$

Figure 6.11 to Figure 6.14 gradually show the relative sensitivity of the module of transfer to above mentioned parameters for LP, BP, HP and BS transfer functions when $f_0 = 1$ MHz. AP transfer function was not included in this analysis because of its excessive complexity (especially in case of the F-D filter). Mathematical expression of individual sensitivities was performed using the program Maple. Individual calculations are not included due to their large volume and because it brings practically no additional information. From the graphs is obvious that all sensitivities to individual parameters are low (they are up to one). The biggest sensitivity is around the pole frequency of the filter (1 MHz) which is well known fact.

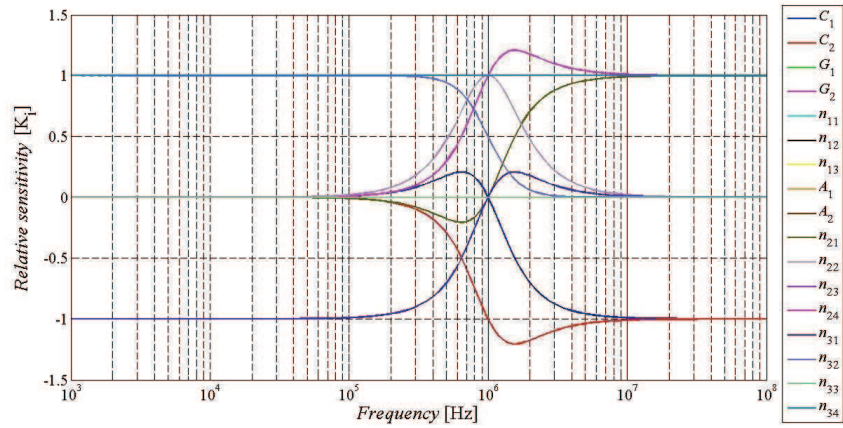


Figure 6.11 Relative sensitivity of the module of transfer of LP of the S-E filter for individual parameters depending on the frequency ($f_0 = 1$ MHz)

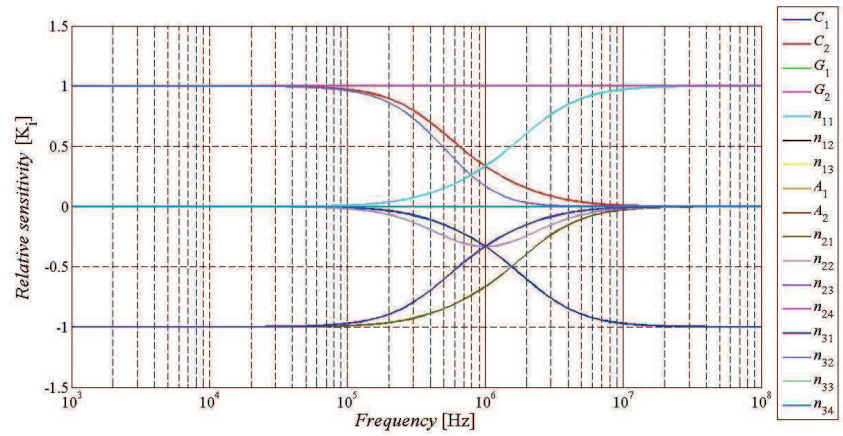


Figure 6.12 Relative sensitivity of the module of transfer of BP of the S-E for individual parameters depending on the frequency ($f_0 = 1$ MHz)

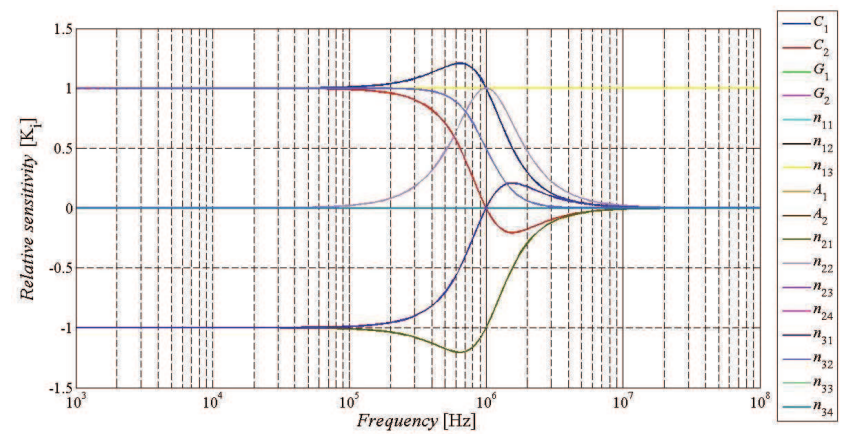


Figure 6.13 Relative sensitivity of the module of transfer of HP of the S-E for individual parameters depending on the frequency ($f_0 = 1$ MHz)

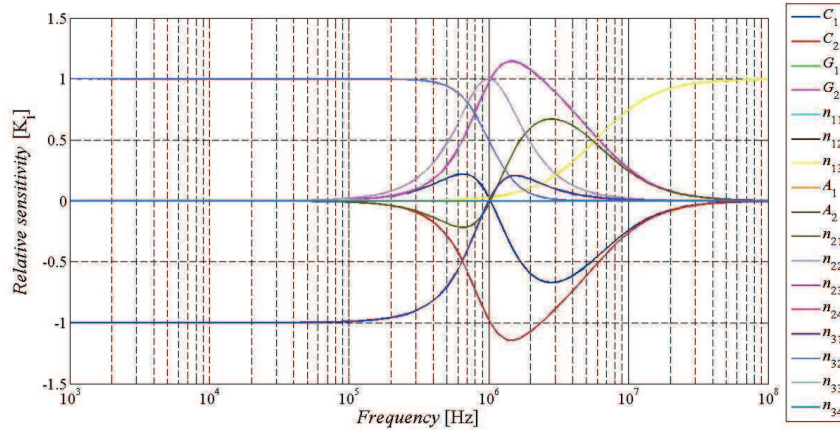


Figure 6.14 Relative sensitivity of the module of transfer of BS of the S-E for individual parameters depending on the frequency ($f_0 = 1$ MHz)

The F-D filter from Figure 6.7 contains 22 parameters ($C_1, C_2, G_1, G_2, A_1, A_2, n_{11}, n_{12}, n_{13}, n_{14}, n_{21}, n_{22}, n_{23}, n_{24}, n_{25}, n_{26}, n_{31}, n_{32}, n_{33}, n_{34}, n_{35}, n_{36}$) Coefficients n_{11} to n_{34} again stand for individual outputs of each current follower in the circuit structure.

The denominator of the F-D filter has the form:

$$D_{real}(s) = s^2 b_2 + s b_1 + b_0, \quad (6.31)$$

The equations of the sensitivity analysis of the F-D filter were moved to Appendices due to their large volume. Individual terms of the denominator of the F-D filter are given by equations (A.1) to (A.3). The real transfer functions of the F-D filter in their general form are given by equations (6.21) to (6.24). Numerators of the transfer functions of the F-D filter are given by equations (A.4) to (A.7).

The relative sensitivity of the module of transfer to given parameters for LP and BP, transfer functions of the F-D filter when $f_0 = 1$ MHz is calculated the same way as for the S-E filter (using equations (6.29) and (6.30)). The relative sensitivity of the module of transfer of HP and BS transfer function was not possible to calculate in real time because of the excessive complexity of numerator of these functions. The relative sensitivity of the module of transfer of LP and BP transfer functions of the F-D filter are illustrated in Figure 6.15 and Figure 6.16. As can be seen from graphs, individual sensitivities of the F-D filter are low. Both LP and BP are the most sensitive to parameter n_{23} whose sensitivity reaches two at frequencies below the pole frequency and parameter n_{32} when the sensitivity reaches two around the pole frequency.

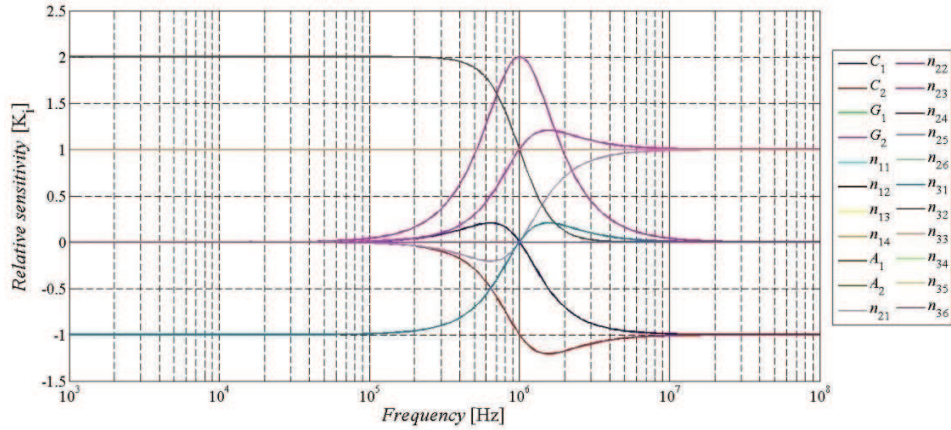


Figure 6.15 Relative sensitivity of the module of transfer of LP of the F-D filter for individual parameters depending on the frequency ($f_0 = 1$ MHz)

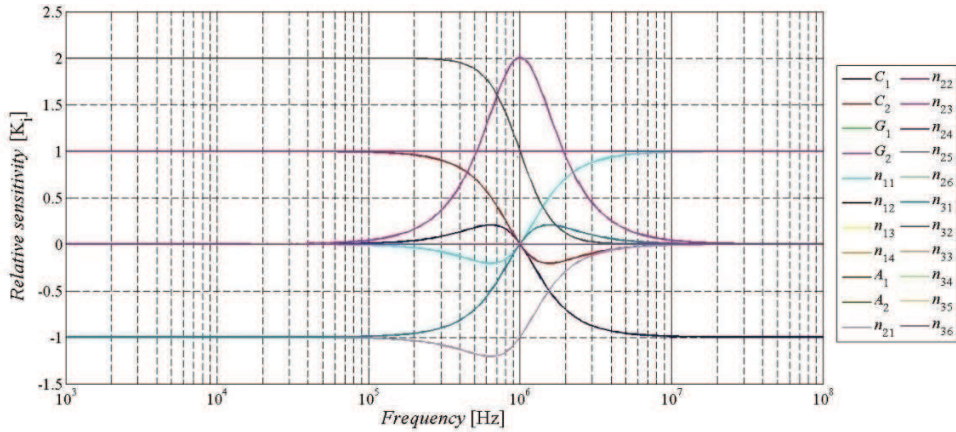


Figure 6.16 Relative sensitivity of the module of transfer of BP of the F-D for individual parameters depending on the frequency ($f_0 = 1$ MHz)

6.3 Universal Filter with Three CFs and Three DACAs

6.3.1 Filter proposal

This filtering structure is also based on the filter from chapter 6.1. There are three DACA elements suitably added in the circuit structure so it is possible to electronically control not only the pole frequency, but also the quality factor of the filter without disturbing each other. The proposed filter is illustrated in Figure 6.17. The filter as well benefits from the advantage that high-pass transfer function can be obtained directly from the outputs of the follower MO-CF₁. I have also presented this proposal in [136].

The F-D form of the filter was again created by mirroring passive and active elements so the F-D filter, as well, proposed with non-differential current followers in order of easier possible implementation in a form of PCB. Figure 6.18 shows the F-D version of the proposed filter. It consists of two DO-CFs, four MO-CFs and three DACAs.

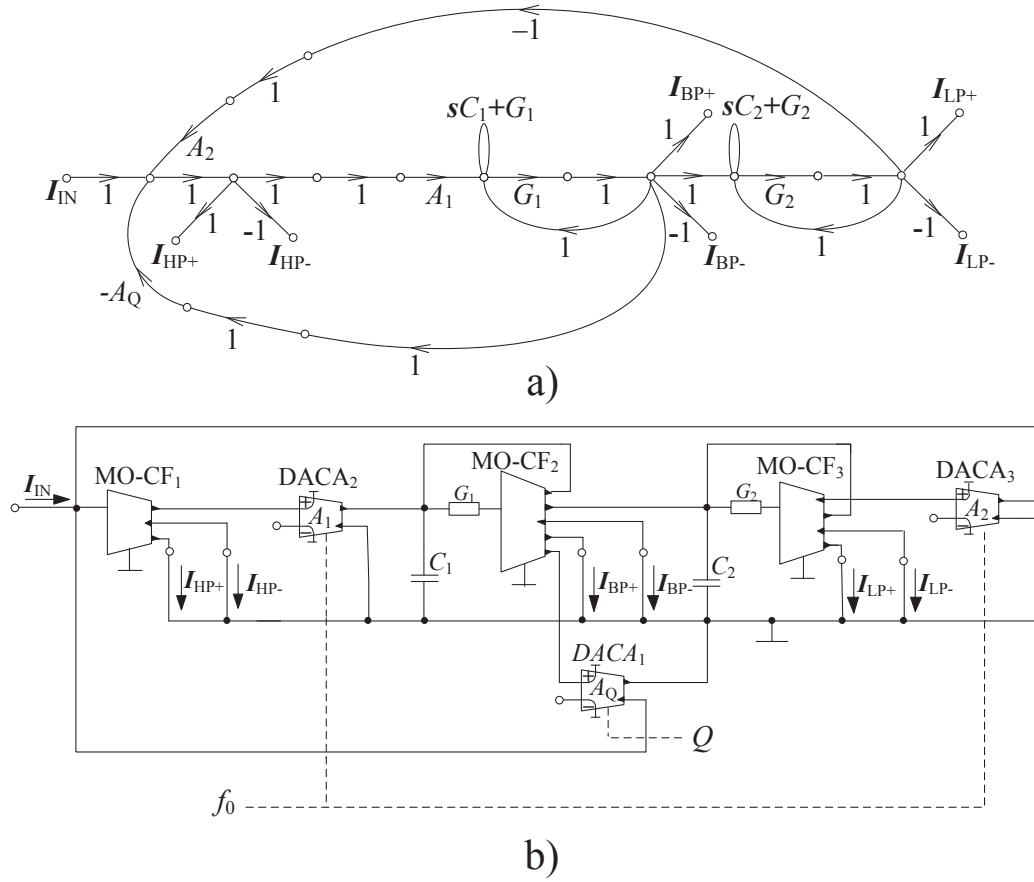


Figure 6.17 Single-ended form of the proposed filter with three MO-CFs and three DACs: a) simplified M-C graph, b) circuit structure

The denominator which is common for all transfer functions of the filter is given as:

$$D(s) = s^2 C_1 C_2 + s C_2 G_1 A_1 A_Q + G_1 G_2 A_1 A_2. \quad (6.32)$$

From the denominator of the transfer functions of the filter can be seen that it is possible to control the pole frequency without disturbing the quality factor by changing the values of the current gains A_1 and A_2 when $A_1 = A_2 = A$. The quality factor of the filter can be controlled without disturbing the pole frequency by changing current gain A_Q .

The relations for the pole frequency and quality factor of the filter are described by the following equations:

$$f_0 = \frac{A}{2\pi} \sqrt{\frac{G_1 G_2}{C_1 C_2}}, \quad Q = \frac{1}{A_Q} \sqrt{\frac{G_2 C_1}{G_1 C_2}}. \quad (6.33), (6.34)$$

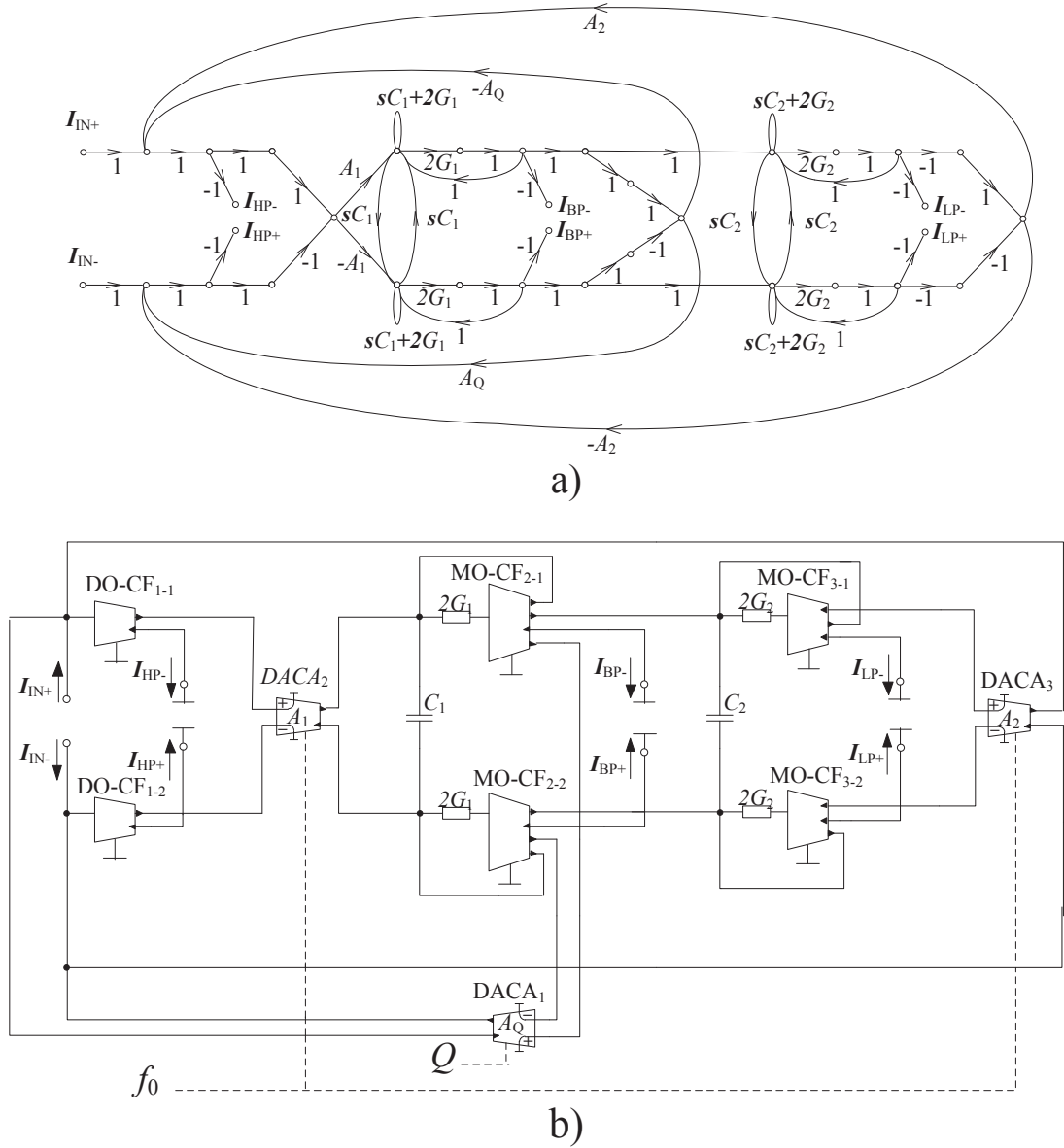


Figure 6.18 Fully-differential form of the proposed filter with three MO-CFs and three DACAs: a) simplified M-C graph, b) circuit structure

Again applies that in order to obtain the same particular pole frequency for the F-D filter, parameters A_1 and A_2 are replaced by $2A$ in comparison to the S-E form of the filter. Similarly, the value of parameter A_Q is halved to achieve the same quality factor. The values of parameters G_1 , G_2 are also twice higher in comparison to the values used for the S-E filter.

The transfer functions of both S-E and F-D filters are described by:

$$\frac{I_{LP+}}{I_{IN}} = -\frac{I_{LP-}}{I_{IN}} = \frac{G_1 G_2 A_1}{D}, \quad (6.35)$$

$$\frac{I_{BP+}}{I_{IN}} = -\frac{I_{BP-}}{I_{IN}} = \frac{sC_2 G_1}{D}, \quad (6.36)$$

$$\frac{I_{HP+}}{I_{IN}} = -\frac{I_{HP-}}{I_{IN}} = \frac{s^2 C_1 C_2}{D}, \quad (6.37)$$

$$I_{BS} = \frac{I_{HP+} + I_{LP+}}{I_{IN}} = -\frac{I_{HP-} + I_{LP-}}{I_{IN}} = \frac{s^2 C_1 C_2 + G_1 G_2 A_1}{D}, \quad (6.38)$$

$$I_{AP} = \frac{I_{HP+} + I_{BP-} + I_{LP+}}{I_{IN}} = -\frac{I_{HP-} + I_{BP+} + I_{LP-}}{I_{IN}} = \frac{s^2 C_1 C_2 - sC_2 G_1 + G_1 G_2 A_1}{D}. \quad (6.39)$$

These equations show that the filter provides all standard transfer functions. High-pass transfer function corresponds with the particular term of the denominator thus, it has unity gain in pass band area regardless values of parameter A . As in the previous case, the analysis of five possible inputs was made. Only the analysis with input I_{IN1} has been included. All analyzed variants can be again found in [136].

6.3.2 Simulation Results

The values of passive elements and specific filter parameters were set the same way as for the filter in subsection 6.2. That means the starting pole frequency $f_0 = 1$ MHz, starting quality factor $Q = 0.707$ (Butterworth approximation), capacitors were set $C_1 = C_2 = 100$ pF. Resistors had again values $R_1 = 1125 \Omega$, $R_2 = 2252 \Omega$. Current gains $A_1 = A_2 = 1$ (half values in case of the F-D form of the filter) and A_Q equals 1 as well (0.5 for the F-D transfer functions).

All output responses illustrated in this chapter are inverting filtering functions. The alternative circuit solution of the DACA element has been used. Therefore, the values chosen for the control of the pole frequency and quality factor of proposed filters are solely demonstrational and do not necessary correspond with values which can be obtained using a real element of the DACA.

Output responses of low-pass, band-pass, high-pass and band-stop transfer functions of the S-E and F-D form of the proposed filter are shown in Figure 6.19. The slope of attenuation of obtained HP transfer functions (blue lines) is 39 dB per decade, 19 dB per decade for BP functions (red lines) and in case of LP transfer functions it is 37 dB per decade. The biggest attenuation of the BS function is -40 dB. The slope of attenuation of individual transfer functions of the F-D filter is slightly steeper which is mainly given by lower values of resistors used for the F-D filter.

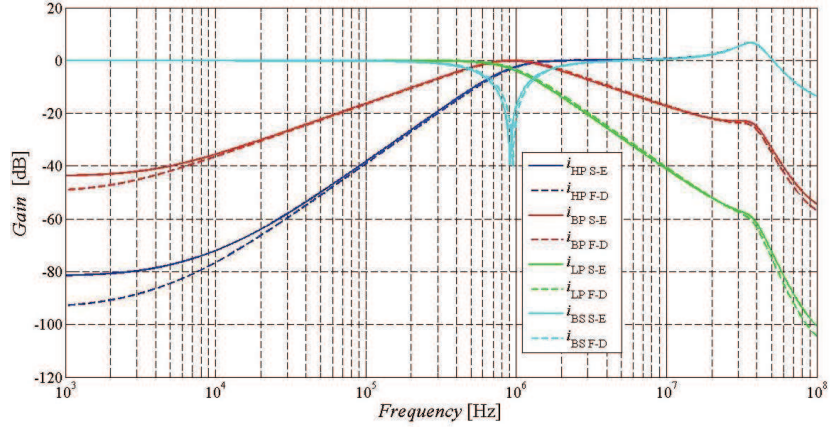


Figure 6.19 Output responses of the S-E filter from Fig. 6.17 (solid lines) and of the F-D filter from Fig. 6.18 (dashed lines): high-pass, band-pass, low-pass, band-stop transfer functions (simulation results)

The ability to adjust the pole frequency of the S-E and F-D filter by changing the values of transfer gains A_1 and A_2 is depicted in Figure 6.20. The HP transfer function was used for this example. Values of current gains A_1 and A_2 were set the same way as for the filter in subsection 6.2 (i. e. 0.5, 1, 2 in case of the S-E filter and 0.25, 0.5, 1 for the F-D filter). The value of parameter A_Q was not changing. Table III compares the values of the pole frequency obtained from simulations of the S-E and F-D filter. It can be seen that the values of the pole frequency obtained from the F-D filter are closer to the theoretical values.

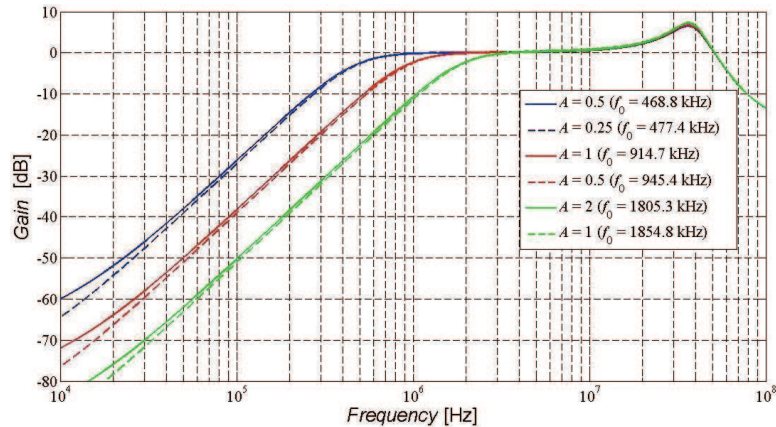


Figure 6.20 Demonstration of ability to control the pole frequency (simulation results) in case of the S-E filter from Fig. 6.17 (solid lines) and of the F-D filter from Fig. 6.18 (dashed lines) when $A_1 = A_2$ were set 0.5, 1, 2

Table III Comparison of obtained values of the pole frequency

	$A_{1,2}$ S-E/ $A_{1,2}$ F-D [-]		
Frequency [kHz]	0.5/0.25	1/0.5	2/1
Calculated	500.0	999.9	1999.8
Simulated S-E	468.8	914.7	1805.3
Simulated F-D	477.4	945.4	1854.8

Figure 6.21 illustrates controllability of the quality factor of the filter. The ability to change the quality factor is achieved by changing the current gain A_Q . For the presentation, BP transfer function has been selected as an example. Values of parameter A_Q are selected accordingly: 0.1, 0.5 and 1, which corresponds with values of 0.05, 0.25 and 0.5 for the F-D filter. Values of current gains A_1 and A_2 remain unchanged. The theoretical and simulated values of the quality factor for given values of A_Q are summarized in Table IV. By comparison is obvious that the values of the quality factor obtained from the F-D filter are slightly higher than the values of the S-E filter.

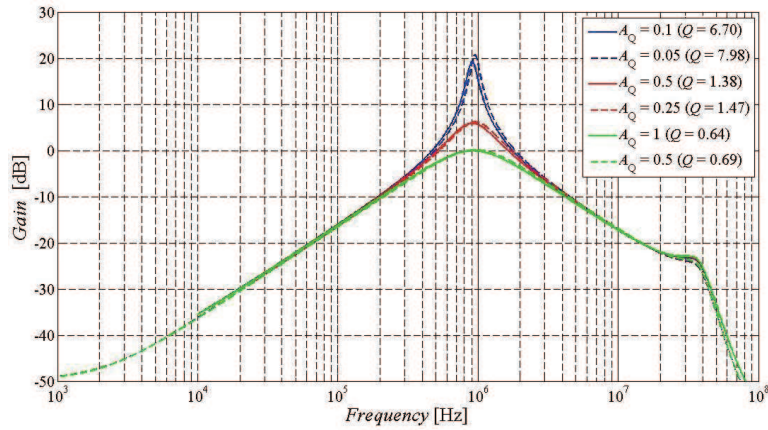


Figure 6.21 Demonstration of ability to control the quality factor (simulation results) in case of the S-E filter from Fig. 6.17 (solid lines) and of the F-D filter from Fig. 6.18 (dashed lines) when A_Q was 0.1, 0.5, 1

Table IV Comparison of obtained values of the quality factor

	A_Q S-E/ A_Q F-D [-]		
Q [-]	0.1/0.05	0.5/0.25	1/0.5
Calculated	7.07	1.41	0.71
Simulated S-E	6.70	1.38	0.64
Simulated F-D	7.98	1.47	0.69

Figure 6.22 shows gain, group delay and phase characteristics of all pass transfer function of the S-E and F-D filter. The blue lines represent all-pass transfer function of the S-E form of the filter and the red lines show obtained all-pass transfer function of the F-D form of the filter. Even this all-pass filter, as in the previous case, is usable approximately up to 10 MHz because of the bandwidth limitations and parasitic characteristics of the models used

active elements, bandwidth limitations of used converters and parasitic capacitances of cables and PCB.

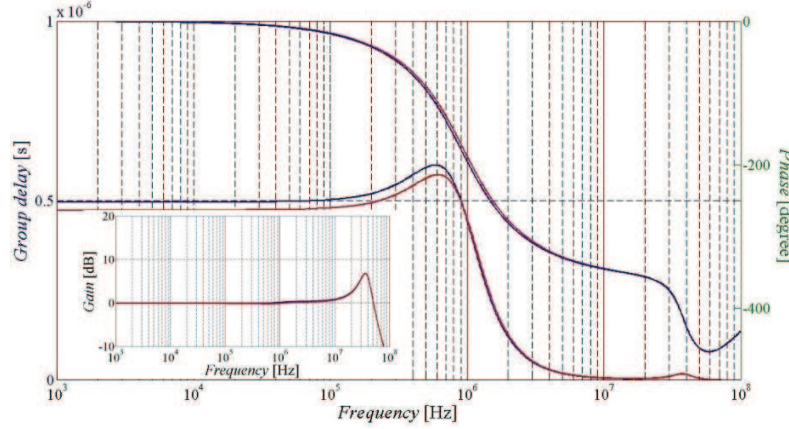


Figure 6.22 Output responses (simulation results) of all-pass filter characteristics (gain, group delay and phase) of the S-E filter from Fig. 6.17 (blue lines) and of the F-D filter from Fig. 6.18 (red lines)

6.4 Universal Filter with Three CFs and Two DACAs

6.4.1 Filter proposal

Another possible circuits solution of a second-order universal filter based on the conception from chapter 6.1 which uses three MO-CF and two DACA elements is presented in Figure 6.23. The difference between this filter and the filter from chapter 6.1 is that the structure from chapter 6.1 is based on Follow-the-Leader Feedback (FLF) topology [104] in comparison to Inverse Follow-the-Leader Feedback (IFLF) topology [115] used in this case. The DACA elements are suitably placed in the circuit structure that it is possible to electronically control the pole frequency. The analysis of obtainable transfer functions depending on chosen input has been made. Input placed before DACA₁ when the filter provides all standard filtering functions has been chosen for further analysis. My research described in this chapter is published in [137].

The F-D form of the filter is shown in Figure 6.24. It was created by mirroring passive and active elements. The F-D structure of the proposed filter is designed with non-differential current followers in order to simplify possible future implementation of the filter. In case of practical implementation, it would be possible to use the DACA elements to substitute fully-differential followers. The filter employs two DO-CFs, four MO-CFs and two DACAs.

The denominator of the filter is described by the following equation:

$$D(s) = s^2 C_1 C_2 + s C_1 G_2 A_1 + G_1 G_2 A_1 A_2. \quad (6.40)$$

The pole frequency of the filter can be electronically controlled without disturbing the quality factor by current gains of the DACA elements when $A_1 = A_2 = A$ which is evident from the equation (6.40).

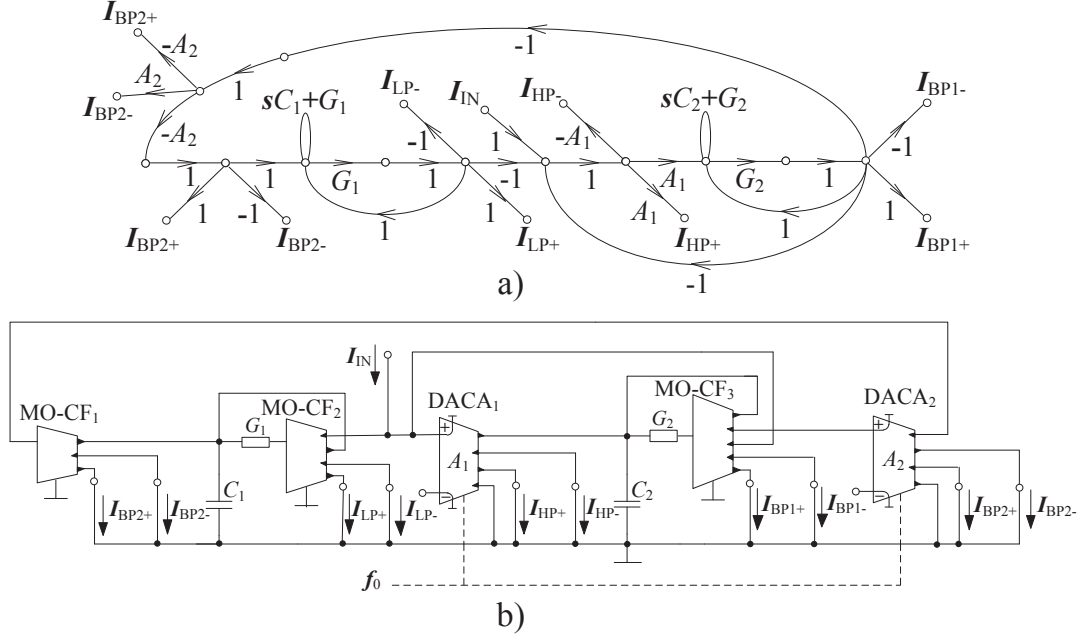


Figure 6.23 Single-ended form of the proposed filter with three MO-CFs and two DACAs:
a) simplified M-C graph, b) circuit structure

The pole frequency and quality factor of the filter are described by the following relations:

$$f_0 = \frac{A}{2\pi} \sqrt{\frac{G_1 G_2}{C_1 C_2}}, \quad Q = \sqrt{\frac{G_2 C_1}{G_1 C_2}}. \quad (6.41), (6.42)$$

To obtain the same particular transfer functions of the F-D form of filter, parameter A is replaced by $2A$. The values of parameters G_1 , G_2 must be also twice higher in comparison to the values used for the S-E filter.

The proposed S-E and F-D filter can provide the following transfer functions:

$$\frac{I_{LP+}}{I_{IN}} = -\frac{I_{LP-}}{I_{IN}} = \frac{G_1 G_2 A_1 A_2}{D}, \quad (6.43)$$

$$\frac{I_{BP1+}}{I_{IN}} = -\frac{I_{BP1-}}{I_{IN}} = \frac{sC_1 G_2 A_1}{D}, \quad (6.44)$$

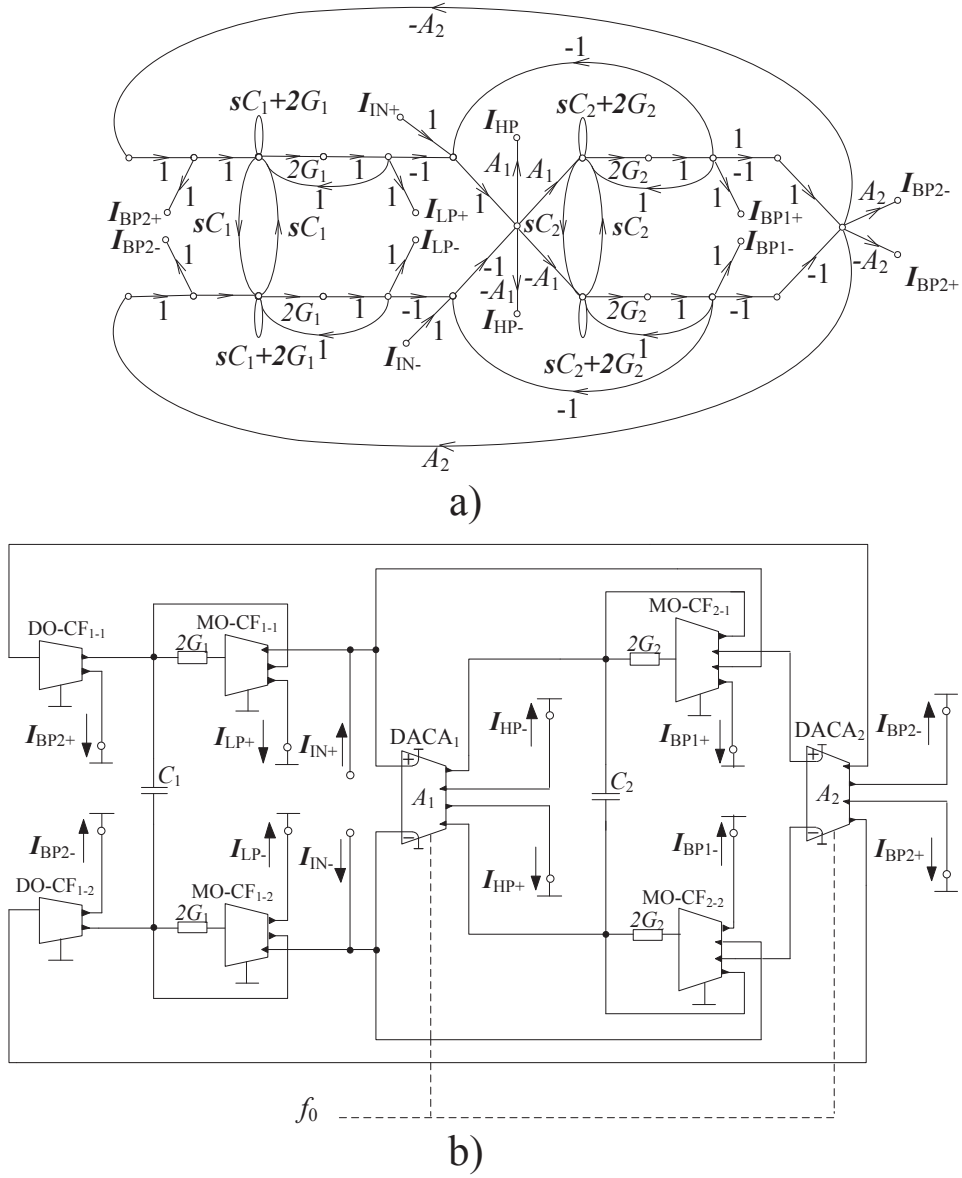


Figure 6.24 Fully-differential form of the proposed filter with three MO-CFs and two DACs: a) simplified M-C graph, b) circuit structure

$$\frac{I_{BP2+}}{I_{IN}} = -\frac{I_{BP2-}}{I_{IN}} = \frac{sC_1 G_2 A_1 A_2}{D}, \quad (6.45)$$

$$\frac{I_{HP+}}{I_{IN}} = -\frac{I_{HP-}}{I_{IN}} = \frac{s^2 C_1 C_2 A_1}{D}, \quad (6.46)$$

$$I_{BS} = \frac{I_{HP+} + I_{LP+}}{I_{IN}} = -\frac{I_{HP-} + I_{LP-}}{I_{IN}} = \frac{s^2 C_1 C_2 A_1 + G_1 G_2 A_1 A_2}{D}, \quad (6.47)$$

$$\begin{aligned} I_{AP1} &= \frac{I_{HP+} + I_{BP1-} + I_{LP+}}{I_{IN}} = -\frac{I_{HP-} + I_{BP1+} + I_{LP-}}{I_{IN}} = \\ &= \frac{s^2 C_1 C_2 A_1 - s C_1 G_2 A_1 + G_1 G_2 A_1 A_2}{D}, \end{aligned} \quad (6.48)$$

$$\begin{aligned} I_{AP2} &= \frac{I_{HP+} + I_{BP2-} + I_{LP+}}{I_{IN}} = -\frac{I_{HP-} + I_{BP2+} + I_{LP-}}{I_{IN}} = \\ &= \frac{s^2 C_1 C_2 A_1 - s C_1 G_2 A_1 A_2 + G_1 G_2 A_1 A_2}{D}. \end{aligned} \quad (6.49)$$

We can obtain all standard transfer functions and thus, the filter is universal. The proposed filter also provides two different band-pass and all-pass functions. BP1 function is more advantageous since this function corresponds with the particular term of the denominator and it will have unity gain pass band area regardless values of parameter A . AP1 transfer function is more advantageous for the same reason. Also, low-pass transfer function corresponds with the particular term of the denominator therefore, it has unity gain in pass band area regardless values of parameter A .

6.4.2 Simulation Results

Simulation results were carried out using these starting values of passive elements and specific filter parameters: default f_0 has been set to 1 MHz, quality factor Q equals 0.707 (Butterworth approximation), capacitors $C_1 = C_2 = 100$ pF, current gains of DACA elements are $A_1 = A_2 = 1$ (0.5 in case of the F-D transfer functions). Values of resistors R_1 and R_2 were calculated accordingly: $R_1 = 1/(2\pi f_0 C_1 Q) = 2252 \Omega$ and $R_2 = 1/(4\pi^2 f_0^2 C_1 C_2 R_1) = 1126 \Omega$. The values of resistors were not rounded for reasons mentioned in chapter 6.2.

The alternative circuit solution of the DACA element has been used. Therefore, the values chosen for the control of the pole frequency and quality factor of proposed filters are solely demonstrational and do not necessary correspond with values which can be obtained using a real element of the DACA amplifier.

Figure 6.25 shows obtained low-pass, band-pass, high-pass and band-stop transfer functions of the S-E and F-D filter. BP transfer function presented in the graph is BP1. The slope of attenuation of obtained HP transfer functions (blue lines) is 38 dB per decade, 19 dB per decade for BP functions (red lines) and in case of LP transfer functions it is 39 dB per decade.

The biggest attenuation of the BS function is -40 dB. The slope of attenuation of individual transfer functions of the F-D filter is slightly greater which is mainly given by the fact that the values of resistors used for the S-E filter are twice as big as in case of the F-D filter.

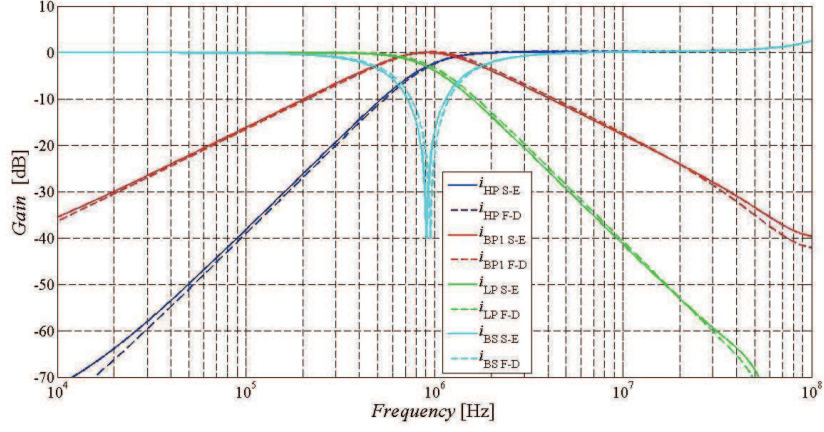


Figure 6.25 Output responses of the S-E filter from Fig. 6.23 (solid lines) and of the F-D filter from Fig. 6.24 (dashed lines): high-pass, band-pass, low-pass, band-stop transfer functions (simulation results)

Figure 6.26 demonstrates the ability to control the pole frequency of the S-E and F-D filter when changing values of current gains A_1 and A_2 . LP transfer function was selected for the illustration. Selected values of parameters A are 0.5, 1 and 2 which corresponds with values 0.25, 0.5 and 1 in case of the F-D filter. Simulated values of the pole frequency of the S-E and F-D filter can be compared in Table V. When comparing the values of the pole frequency from the table it can be seen that the pole frequencies obtained from the F-D filter are closer to the theoretical values.

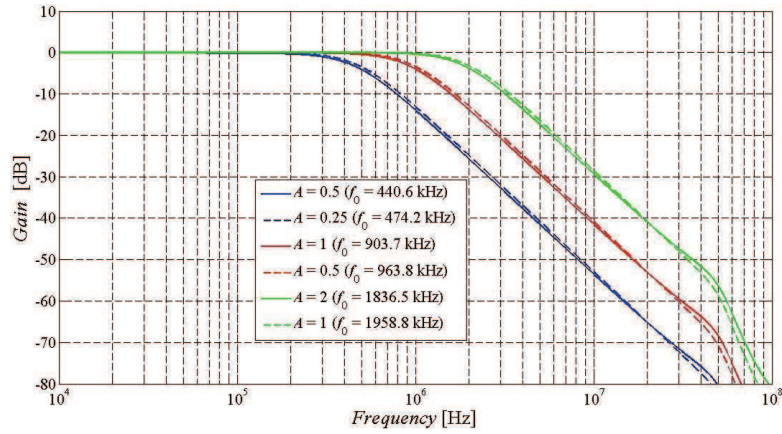


Figure 6.26 Demonstration of ability to control the pole frequency (simulation results) in case of the S-E filter from Fig. 6.23 (solid lines) and of the F-D filter from Fig. 6.24 (dashed lines) when $A_1 = A_2$ were set 0.5, 1, 2

Table V Comparison of obtained values of the pole frequency

	$A_{1,2}$ S-E/ $A_{1,2}$ F-D [-]		
Frequency [kHz]	0.5/0.25	1/0.5	2/1
Calculated	499.7	999.5	1998.9
Simulated S-E	440.6	903.7	1836.5
Simulated F-D	474.2	963.8	1958.8

Characteristics of gain, group delay and phase of the all pass (AP1) transfer function of the S-E and F-D filter are illustrated in Figure 6.27. All-pass transfer function of the S-E filter is represented by blue lines when all-pass transfer function of the F-D filter is represented by red lines. These all-pass filters are suitable to use approximately up to 30 MHz because the transfer function at higher frequencies is already affected by bandwidth limitations and parasitic characteristics of the models used active elements, bandwidth limitations of used converters etc.

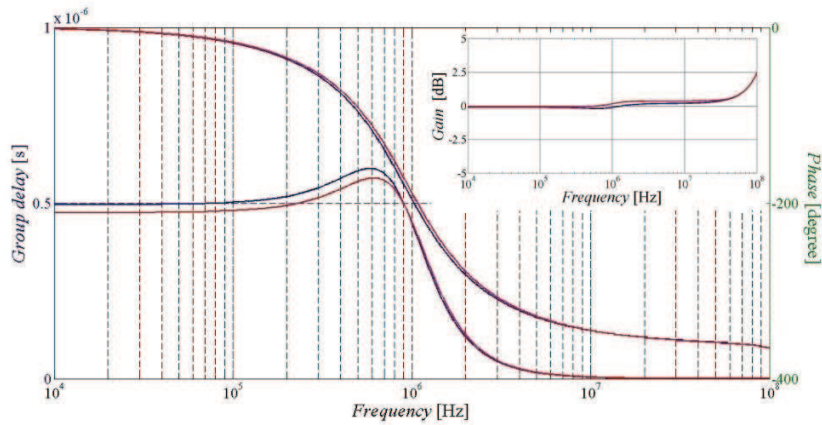


Figure 6.27 Output responses (simulation results) of all-pass filter characteristics (gain, group delay and phase) of the S-E filter from Fig. 6.23 (blue lines) and of the F-D filter from Fig. 6.24 (red lines)

6.4.3 Parasitic Analysis

The parasitic analysis [19] of the S-E and F-D filter was carried out in this case. The parasitic analysis deals mainly with input and output characteristics of used active elements. Significant parasitic admittances (Y_{S1} - Y_{S5} and Y_{P1} - Y_{P5}) of the S-E filter caused by the non-ideal input and output characteristics of used active elements are depicted in Figure 6.28. Typical input and output parameters of a CF are $R_{IN\ CF} \sim 2\Omega$, $C_{IN\ CF} \sim 3\text{ pF}$, $R_{OUT\ CF} \sim 200\text{ k}\Omega$ and $C_{OUT\ CF} \sim 0.6\text{ pF}$ [19]. Characteristic input and output parameters in case of the DACA element ($R_{IN\ DACA} \sim 2\Omega$, $C_{IN\ DACA} \sim 2\text{ pF}$, $R_{OUT\ DACA} \sim 100\text{ k}\Omega$ and $C_{OUT\ DACA} \sim 5\text{ pF}$) are based on its simulation model from chapter 5.4. Capacitances of individual pins of the active elements (approximately 1 pF each) are not included because all circuit is meant to be in its final implementation in the integrated form. Individual inputs and outputs of each used active element are expected to have very similar characteristics,

therefore, the positive and negative inputs/outputs are considered having the same parasitic characteristics.

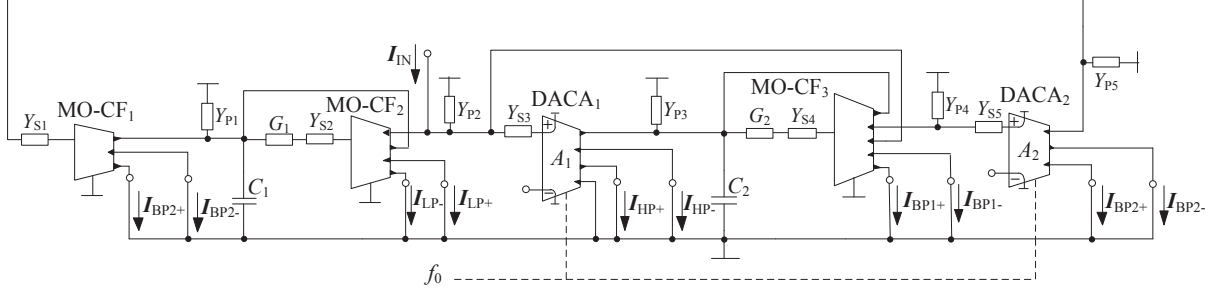


Figure 6.28 S-E filter from Figure 6.23 with depicted main parasitic admittances being considered

The parasitic admittances from Figure 6.28 can be described as:

$$Y_{S1} = G_{S1} + sC_{S1} = \frac{1}{R_{IN\ CF_1}} + sC_{IN\ CF_1}, \quad (6.50)$$

$$Y_{S2} = G_{S2} + sC_{S2} = \frac{1}{R_{IN\ CF_2}} + sC_{IN\ CF_2}, \quad (6.51)$$

$$Y_{S3} = G_{S3} + sC_{S3} = \frac{1}{R_{IN\ DACA_1}} + sC_{IN\ DACA_1}, \quad (6.52)$$

$$Y_{S4} = G_{S4} + sC_{S4} = \frac{1}{R_{IN\ CF_3}} + sC_{IN\ CF_3}, \quad (6.53)$$

$$Y_{S5} = G_{S5} + sC_{S5} = \frac{1}{R_{IN\ DACA_2}} + sC_{IN\ DACA_2}, \quad (6.54)$$

$$Y_{P1} = G_{P1} + sC_{P1} = \frac{1}{R_{OUT\ CF_1}} + \frac{1}{R_{OUT\ CF_2}} + s(C_{OUT\ CF_1} + C_{OUT\ CF_2}), \quad (6.55)$$

$$Y_{P2} = G_{P2} + sC_{P2} = \frac{1}{R_{OUT\ CF_2}} + \frac{1}{R_{OUT\ CF_3}} + s(C_{OUT\ CF_2} + C_{OUT\ CF_3}), \quad (6.56)$$

$$Y_{P3} = G_{P3} + sC_{P3} = \frac{1}{R_{OUT CF_3}} + \frac{1}{R_{OUT DAC_A1}} + s(C_{OUT CF_3} + C_{OUT DAC_A1}), \quad (6.57)$$

$$Y_{P4} = G_{P4} + sC_{P4} = \frac{1}{R_{OUT CF_3}} + sC_{OUT CF_3}, \quad (6.58)$$

$$Y_{P5} = G_{P5} + sC_{P5} = \frac{1}{R_{OUT DAC_A2}} + sC_{OUT DAC_A2}. \quad (6.59)$$

Figure 6.29 shows the F-D filter with significant parasitic admittances caused by the non-ideal input and output characteristics of used active elements. Since the F-D structure was created by mirroring the S-E form of the filter, all parasitic admittances have the same form as in case of the S-E filter (equations (6.50) to (6.59)). Also as mentioned before we consider that individual inputs and outputs of each used active element have very similar characteristics therefore, admittances of both positive and negative branch are calculated the same way.

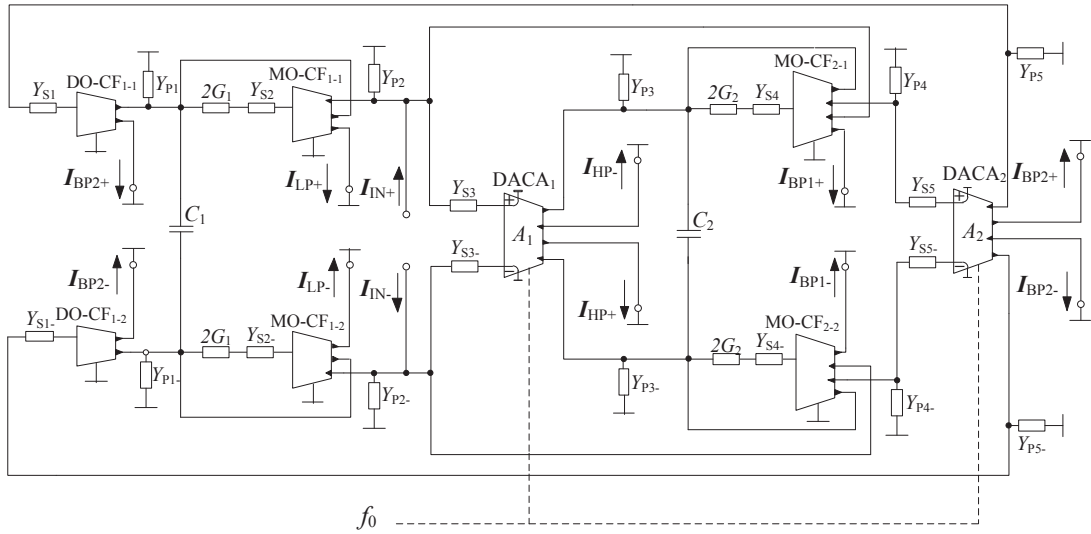


Figure 6.29 F-D filter from Figure 6.24 with depicted main parasitic admittances

Admittances Y_{P1} and Y_{P3} have the most significant impact on the S-E and F-D circuit. Admittance Y_{P1} influences all transfer functions when Y_{P3} influences mainly high-pass transfer function. The biggest influence of serial parasitic conductances is caused by conductances G_{S2} and G_{S4} which cause a frequency shift because they are added to conductance G_1 , G_2 respectively. The biggest influence of parallel parasitic capacitances is caused by C_{P1} and C_{P2}

which again cause a frequency shift because they are added to capacitances C_1 and C_2 . Serial parasitic capacitances have minimal influence. All this applies for both S-E and F-D filter.

Figure 6.30 illustrates BP1 transfer function of the S-E filter for chosen values of R_{P1} (10 k Ω , 50 k Ω , 100 k Ω , 200 k Ω , 500 k Ω) when the C_{P1} is equal to 1.2 pF. It can be seen that smaller values of R_{P1} decrease the attenuation of the BP1 response in its stop band at lower frequencies. The same can be said about S-E HP transfer function in Figure 6.32. The only difference is that this time it is caused by influence of R_{P3} . Figure 6.31 shows the influence of parameter C_{P2} (for values 0.1 pF, 1 pF, 10 pF, 50 pF and 100 pF) when R_{P2} was 100 k Ω on BP2 transfer function of the S-E filter. It is evident that higher values of C_{P2} cause a frequency shift to lower values. The influence of R_{P1} the C_{P1} is 1.2 pF on BS transfer function is shown in Figure 6.33. Lower values of R_{P1} decrease the attenuation of the stop band area of the BS function.

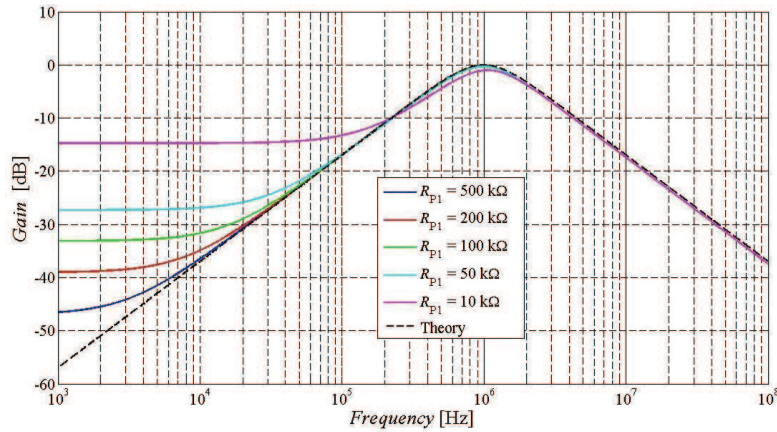


Figure 6.30 Influence of R_{P1} parasitic characteristic on BP1 response of the S-E filter when C_{P1} was 1.2 pF

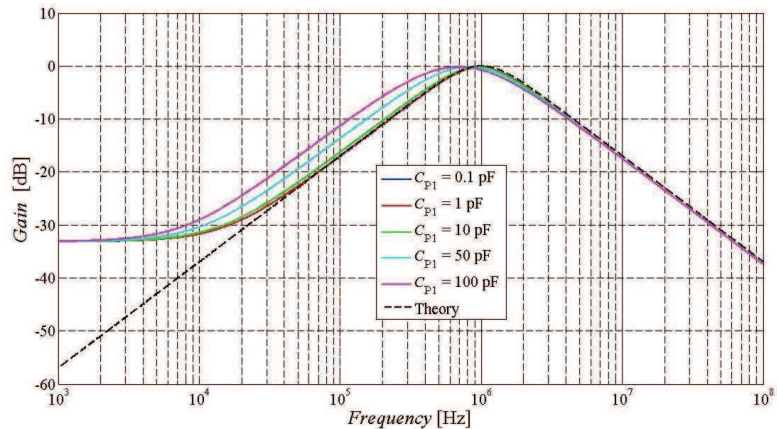


Figure 6.31 Influence of C_{P1} parasitic characteristic on BP2 response of the S-E filter when R_{P1} was 100 k Ω

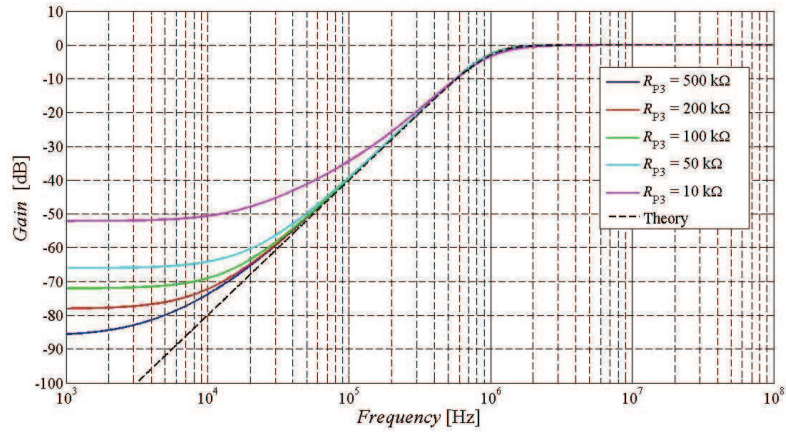


Figure 6.32 Influence of R_{P3} parasitic characteristic on HP response of the S-E filter when C_{P3} was 2.6 pF

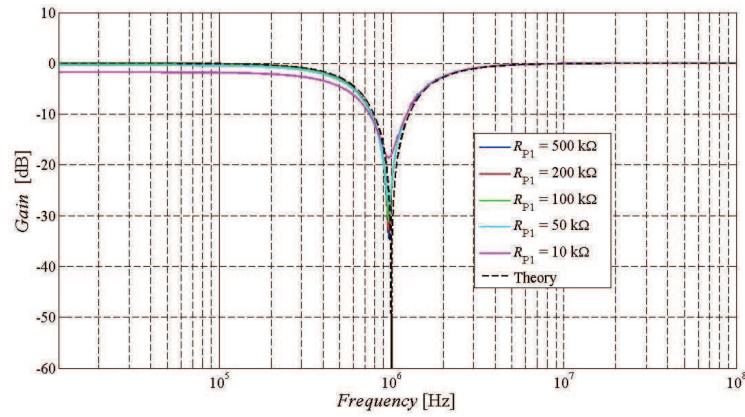


Figure 6.33 Influence of R_{P1} parasitic characteristic on BS response of the S-E filter when C_{P1} was 1.2 pF

Figures Figure 6.34 to Figure 6.37 depict the influence of the same parameters (and same chosen values) on same transfer function of the F-D filter. From graphs can be seen that the influence of parasitic parameters is in case of the F-D transfer function slightly less distinctive.

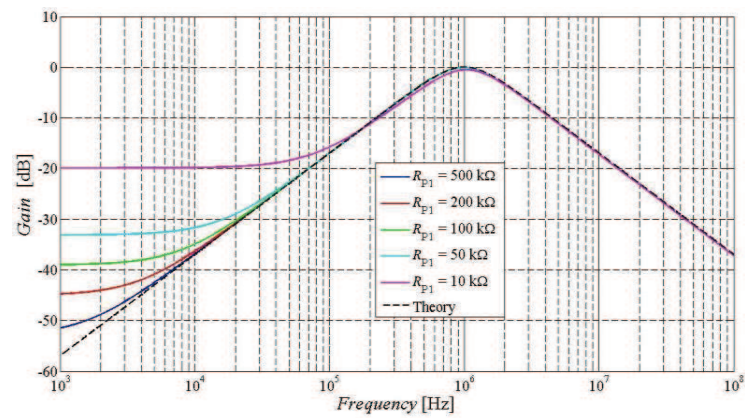


Figure 6.34 Influence of R_{P1} parasitic characteristic on BP1 response of the F-D filter when C_{P1} was 1.2 pF

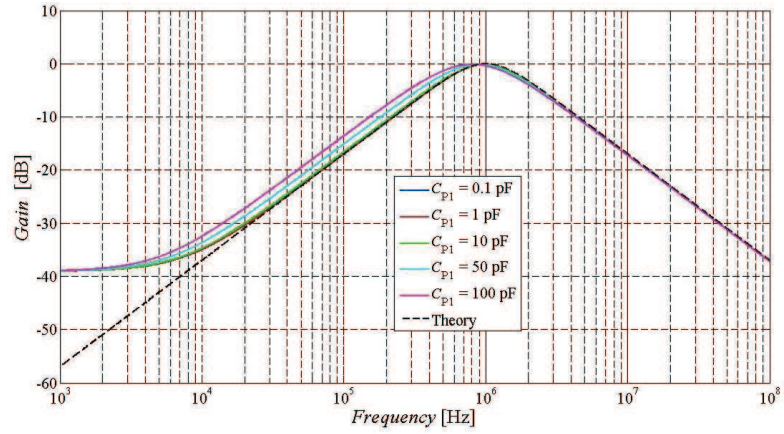


Figure 6.35 Influence of C_{P1} parasitic characteristic on BP2 response of the F-D filter when R_{P1} was 100 k Ω

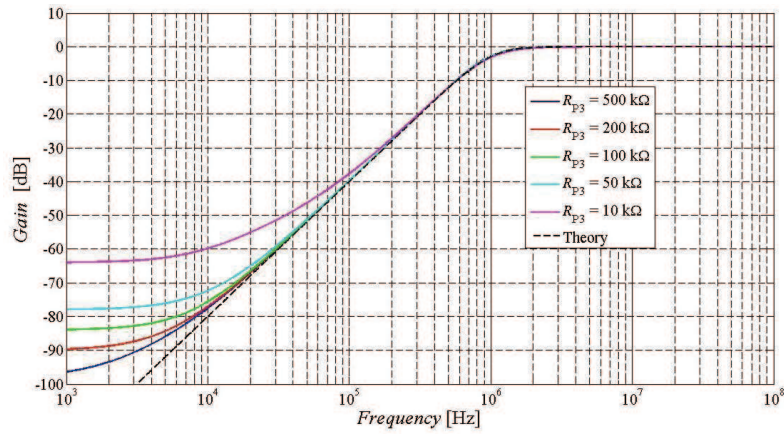


Figure 6.36 Influence of R_{P3} parasitic characteristic on HP response of the F-D filter when C_{P3} was 2.6 pF

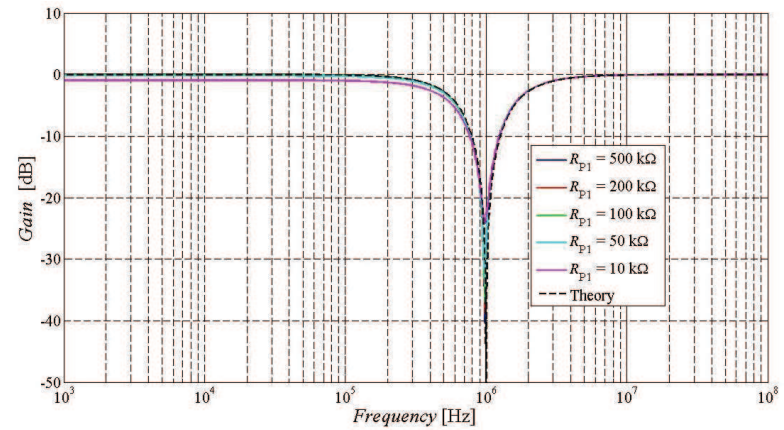


Figure 6.37 Influence of R_{P1} parasitic characteristic on BS response of the F-D filter when C_{P1} was 1.2 pF

6.5 Universal Filter with Two CFs and Two DACAs

6.5.1 Filter proposal

By further analysis of the filter from chapter 6.4 has been discovered that the structure of this filter can be simplified by removing MO-CF₁ (DO-CF₁₋₁ and DO-CF₁₋₂ in case of the F-D form) because it is possible to obtain all standard transfer functions and the filter is thus versatile without responses taken from the outputs of this omitted active element. Figure 6.38 shows the modified filter. It consists of two MO-CF and two DACA elements. For this filter, four possible inputs were analyzed. To obtain all standard types of transfer functions, the input of the circuit must be placed before DACA₁ has to be used therefore this input is selected for subsequent presentation of the functionality of the S-E and F-D filter. I have published the proposal presented in this chapter in [137].

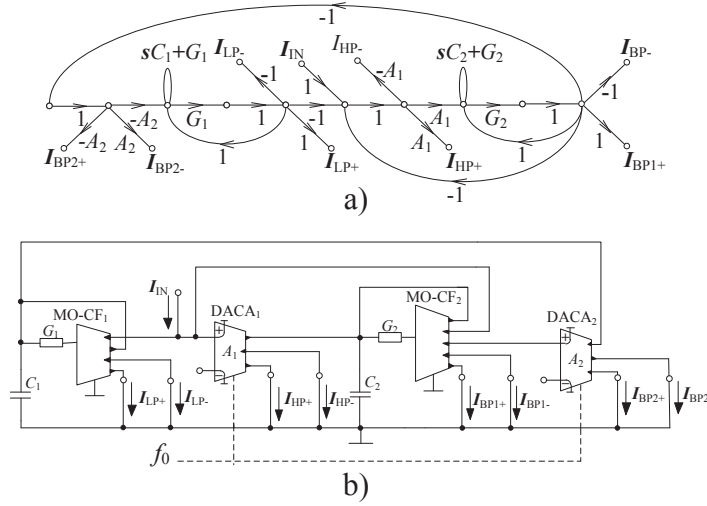


Figure 6.38 Single-ended form of the proposed filter with two MO-CFs and two DACAs:
a) simplified M-C graph, b) circuit structure

The F-D form of the proposed filter was again created from the S-E structure by mirroring passive parts and active elements. The F-D filter is proposed with non-differential current for the sake of easier possible implementation in a form of PCB. Figure 6.39 presents the F-D structure of the proposed filter. The filter is formed by four MO-CFs and two DACAs.

The denominator of all transfer functions of the filter is given as:

$$D(s) = s^2 C_1 C_2 + s C_1 G_2 A_1 + G_1 G_2 A_1 A_2. \quad (6.60)$$

As it can be seen it is the same denominator as for the filter in chapter 6.4. Therefore, the pole frequency of the filter can be electronically controlled without disturbing the quality factor by changing values of current gains when maintaining a simple condition $A_1 = A_2 = A$.

Relations for the pole frequency and quality factor of the filter are described as:

$$f_0 = \frac{A}{2\pi} \sqrt{\frac{G_1 G_2}{C_1 C_2}}, \quad Q = \sqrt{\frac{G_2 C_1}{G_1 C_2}}. \quad (6.61), (6.62)$$

Again applies that in order to obtain the same particular transfer functions for both the S-E and F-D form of the filter, parameter A is replaced by $2A$. The values of parameters G_1 , G_2 must be also twice higher that it was in case of the values used for the S-E filter.

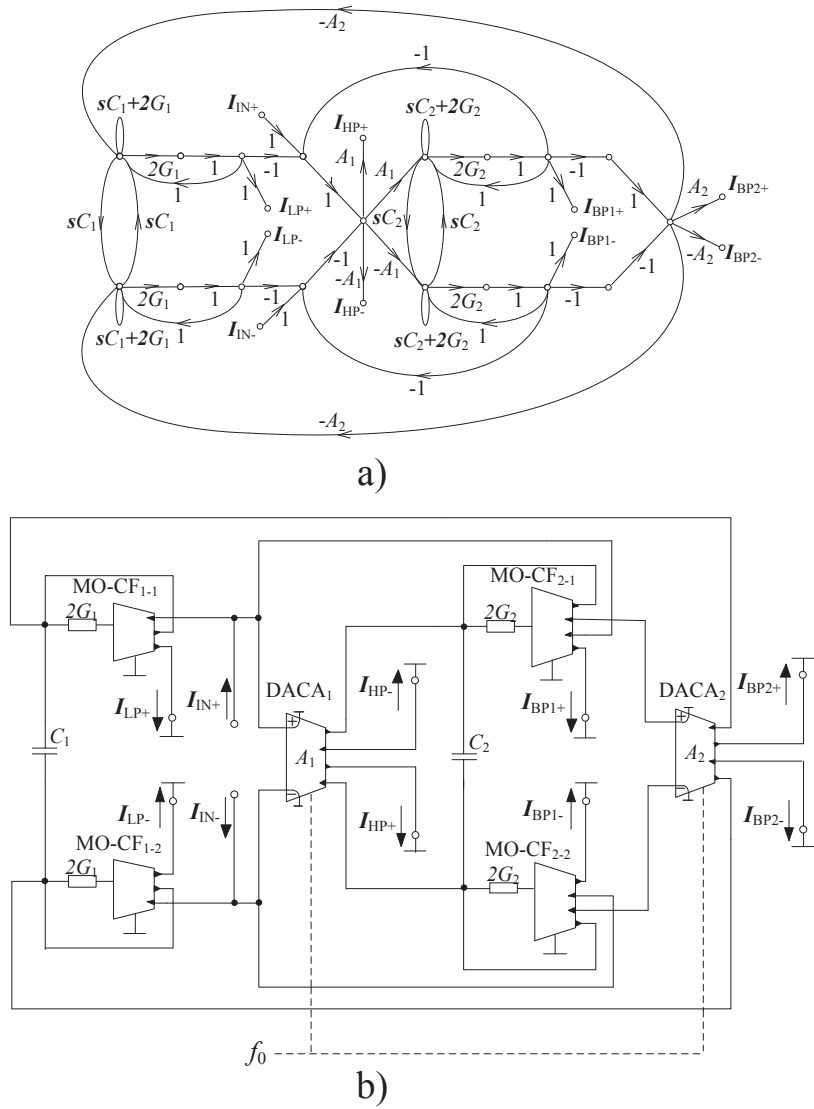


Figure 6.39 Fully-differential form of the proposed filter with two MO-CFs and two DACAs:
a) simplified M-C graph, b) circuit structure

The transfer functions are given by the following equations:

$$\frac{I_{LP+}}{I_{IN}} = -\frac{I_{LP-}}{I_{IN}} = \frac{G_1 G_2 A_1 A_2}{D}, \quad (6.63)$$

$$\frac{I_{BP1+}}{I_{IN}} = -\frac{I_{BP1-}}{I_{IN}} = \frac{s C_1 G_2 A_1}{D}, \quad (6.64)$$

$$\frac{I_{BP2+}}{I_{IN}} = -\frac{I_{BP2-}}{I_{IN}} = \frac{s C_1 G_2 A_1 A_2}{D}, \quad (6.65)$$

$$\frac{I_{HP+}}{I_{IN}} = -\frac{I_{HP-}}{I_{IN}} = \frac{s^2 C_1 C_2 A_1}{D}, \quad (6.66)$$

$$I_{BS} = \frac{I_{HP+} + I_{LP+}}{I_{IN}} = -\frac{I_{HP-} + I_{LP-}}{I_{IN}} = \frac{s^2 C_1 C_2 A_1 + G_1 G_2 A_1 A_2}{D}, \quad (6.67)$$

$$\begin{aligned} I_{AP1} &= \frac{I_{HP+} + I_{BP1-} + I_{LP+}}{I_{IN}} = -\frac{I_{HP-} + I_{BP1+} + I_{LP-}}{I_{IN}} = \\ &= \frac{s^2 C_1 C_2 A_1 - s C_1 G_2 A_1 + G_1 G_2 A_1 A_2}{D}, \end{aligned} \quad (6.68)$$

$$\begin{aligned} I_{AP2} &= \frac{I_{HP+} + I_{BP2-} + I_{LP+}}{I_{IN}} = -\frac{I_{HP-} + I_{BP2+} + I_{LP-}}{I_{IN}} = \\ &= \frac{s^2 C_1 C_2 A_1 - s C_1 G_2 A_1 A_2 + G_1 G_2 A_1 A_2}{D}. \end{aligned} \quad (6.69)$$

As in case of the filter from chapter 6.4 we can obtain all standard transfer functions. The filter provides two different band-pass and all-pass functions. As for the previous filter, it applies that BP1 and AP1 are more advantageous transfer functions. For each transfer function again applies that the transfer function which corresponds with the specific term of the denominator of the filter will always have unity gain in the pass band area regardless the values of the parameters A_1 and A_2 . For other transfer functions applies that their gain will change depending on parameters A .

6.5.2 Simulation Results

The values of passive elements and specific filter parameters were the same as for the filter from chapter 6.4. E. g. the starting pole frequency equals 1 MHz, starting quality factor $Q = 0.707$ (Butterworth approximation), the values of capacitors were $C_1 = C_2 = 100$ pF. Values of resistors were $R_1 = 2252 \Omega$ and $R_2 = 1126 \Omega$ (without being rounded because of previously mentioned reasons). Current gains were chosen $A_1 = A_2 = 1$ (half values in case of the F-D form of the filter).

The alternative circuit solution of the DACA element has been again used. Therefore, the values used to control the pole frequency of proposed filter are solely demonstrational and do not necessary correspond with values which can be obtained using a real element of the DACA amplifier.

Simulated responses of low-pass, band-pass, high-pass and band-stop transfer functions of the S-E and F-D filter are shown in Figure 6.40. BP1 transfer function was used for the presentation. The slope of attenuation of obtained HP transfer functions (blue lines) is 38 dB per decade, 19 dB per decade for BP functions (red lines) and in case of LP transfer functions it is 39 dB per decade. The biggest attenuation of the BS function is -40 dB. Transfer functions obtained from the F-D filter have steeper slope of attenuation than the functions of the S-E filter. This fact is mainly given by values of resistors which are twice as big in case of the S-E filter.

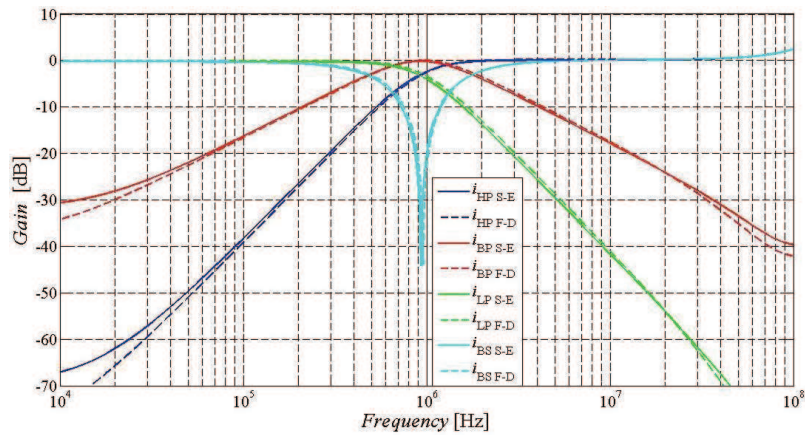


Figure 6.40 Output responses of the S-E filter from Fig. 6.38 (solid lines) and of the F-D filter from Fig. 6.39 (dashed lines): high-pass, band-pass, low-pass, band-stop transfer functions (simulation results)

Demonstration of controllability of the pole frequency of the proposed S-E and F-D filter by changing the values of current gains A_1 and A_2 is illustrated in Figure 6.41. In this case, BP transfer function was selected for the presentation. The values of current gains A_1 and A_2 were set 0.5, 1 and 2 (0.25, 0.5 and 1 for the F-D filter). The pole frequencies obtained from simulations are compared in Table VI. From the table can be seen that the values of the pole frequency obtained from the F-D filter are closer to the theoretical values.

Table VI Comparison of obtained values of the pole frequency

	$A_{1,2}$ S-E/ $A_{1,2}$ F-D [-]		
Frequency [kHz]	0.5/0.25	1/0.5	2/1
Calculated	499.7	999.5	1998.9
Simulated S-E	465.6	920.5	1853.5
Simulated F-D	483.1	981.8	1940.8

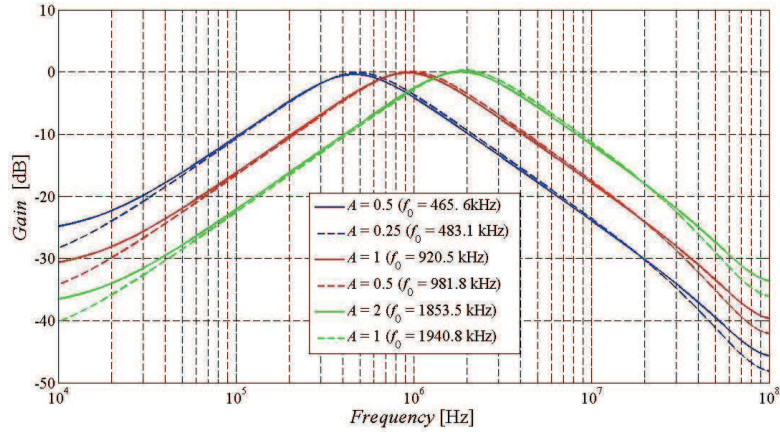


Figure 6.41 Demonstration of ability to control the pole frequency (simulation results) in case of the S-E filter from Fig. 6.38 (solid lines) and of the F-D filter from Fig. 6.39 (dashed lines) when $A_1 = A_2$ were set 0.5, 1, 2

Figure 6.42 depicts gain, group delay and phase of the all pass (AP1) transfer function of the S-E and F-D filter. The blue lines are characteristics of the S-E filter and the red lines are characteristics of the F-D filter. From the graph it can be seen that all-pass filters are suitable to use approximately up to 30 MHz because of bandwidth limitations and parasitic characteristics of the models of used active elements.

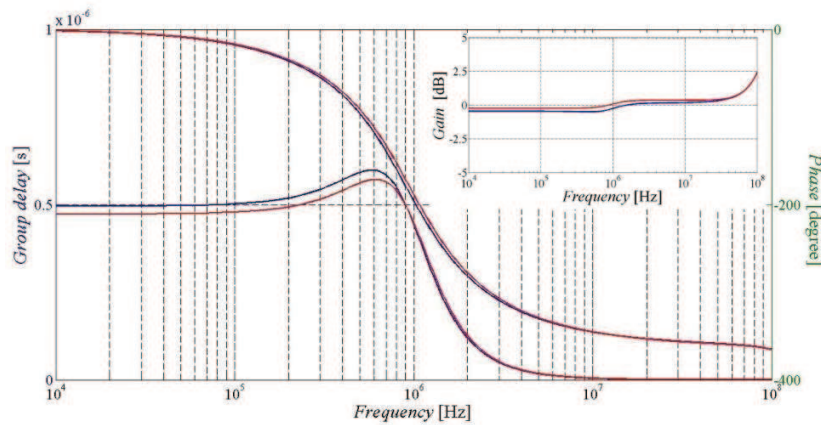


Figure 6.42 Output responses (simulation results) of all-pass filter characteristics (gain, group delay and phase) of the S-E filter from Fig. 6.38 (blue lines) and of the F-D filter from Fig. 6.39 (red lines)

6.5.3 Sensitivity Analysis

The S-E and F-D filter was subjected to the sensitivity analysis. The S-E filter from Figure 6.38 contains 15 parameters ($C_1, C_2, G_1, G_2, A_1, A_2, n_{11}, n_{12}, n_{13}, n_{14}, n_{21}, n_{22}, n_{23}, n_{24}, n_{25}$) where parameters n are individual outputs of each current follower in the circuit structure. The sensitivity analysis was carried out the same way as in the chapter 6.2 using relations (6.29) and (6.30).

The denominator of the S-E filter when considering all these parameters is:

$$D_{real}(s) = s^2 b_2 + s b_1 + b_0, \quad (6.70)$$

where

$$b_2 = C_1 C_2, \quad (6.71)$$

$$b_1 = C_2 G_1 + n_{21} C_1 G_2 + C_1 G_2 + n_{22} A_1 C_1 G_2 + C_2 G_1 n_{12}, \quad (6.72)$$

$$b_0 = n_{23} A_1 A_2 G_1 G_2 n_{11} + G_1 G_2 + n_{21} G_1 G_2 + n_{21} G_1 G_2 n_{12} + G_1 G_2 n_{12} + n_{22} A_1 G_1 G_2 n_{12} + n_{22} A_1 G_1 G_2. \quad (6.73)$$

The real transfer functions of the S-E filter are given as follows:

$$K_{LP\ real}(s) = \frac{I_{LP\ real}}{D_{real}}, \quad (6.74)$$

$$K_{BP1\ real}(s) = \frac{I_{BP1\ real}}{D_{real}}, \quad (6.75)$$

$$K_{BP2\ real}(s) = \frac{I_{BP2\ real}}{D_{real}}, \quad (6.76)$$

$$K_{HP \text{ real}}(s) = \frac{I_{HP \text{ real}}}{D_{\text{real}}}, \quad (6.77)$$

$$K_{BS \text{ real}}(s) = \frac{I_{BS \text{ real}}}{D_{\text{real}}}, \quad (6.78)$$

where

$$I_{LP \text{ real}} = n_{23}A_1A_2G_1G_2n_{14}, \quad (6.79)$$

$$I_{BP1 \text{ real}} = s(n_{25}A_1C_1G_2) + n_{25}A_1G_1G_2 + n_{25}A_1G_1G_2n_{12}, \quad (6.80)$$

$$I_{BP2 \text{ real}} = s(n_{23}A_1A_2C_1G_2) + n_{23}A_1A_2G_1G_2 + n_{23}A_1A_2G_1G_2n_{12}, \quad (6.81)$$

$$\begin{aligned} I_{HP \text{ real}} = & s^2(A_1C_2C_1) + s(A_1C_2G_1n_{12} + A_1C_2G_1 + n_{21}A_1C_1G_2 + A_1C_1G_2) + A_1G_1G_2 + \\ & + A_1G_1G_2n_{12} + n_{21}A_1G_1G_2n_{12} + n_{21}A_1G_1G_2, \end{aligned} \quad (6.82)$$

$$\begin{aligned} I_{BS \text{ real}} = & s^2(A_1C_2C_1) + s(A_1C_2G_1n_{12} + A_1C_2G_1 + n_{21}A_1C_1G_2 + A_1C_1G_2) + A_1G_1G_2n_{12} - \\ & - n_{23}A_1A_2G_1G_2n_{14} + A_1G_1G_2 + n_{21}A_1G_1G_2 + n_{21}A_1G_1G_2n_{12}. \end{aligned} \quad (6.83)$$

Figure 6.43 to Figure 6.47 depict the relative sensitivity of the module of transfer to given parameters for LP, BP1, BP2, HP and BS transfer functions when $f_0 = 1$ MHz. From the graphs can be seen that all sensitivities to individual parameters are low (they are up to one) except BS transfer function (up to eight in case of parameters C_1 , C_2 , G_1 , G_2 , A_2 , n_{14} and n_{23}). The biggest sensitivity is again around the pole frequency. Higher sensitivity in case of BS transfer function is mainly given because of higher complexity of the numerator of this function.

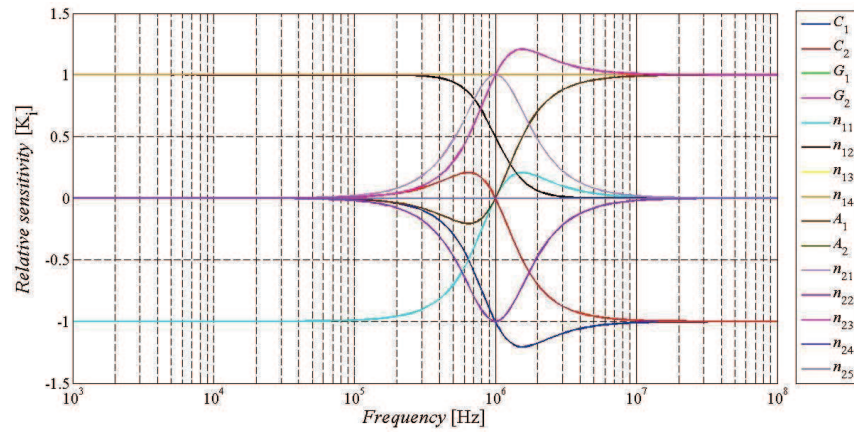


Figure 6.43 Relative sensitivity of the module of transfer of LP of the S-E filter for individual parameters depending on the frequency ($f_0 = 1$ MHz)

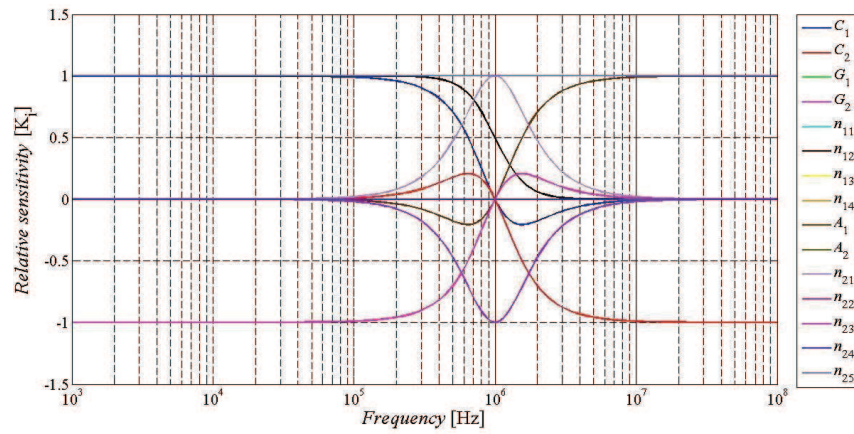


Figure 6.44 Relative sensitivity of the module of transfer of BP1 of the S-E for individual parameters depending on the frequency ($f_0 = 1$ MHz)

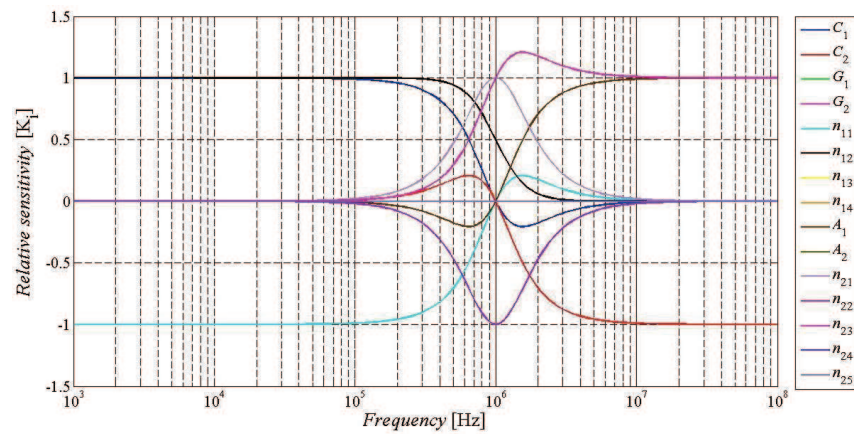


Figure 6.45 Relative sensitivity of the module of transfer of BP2 of the S-E for individual parameters depending on the frequency ($f_0 = 1$ MHz)

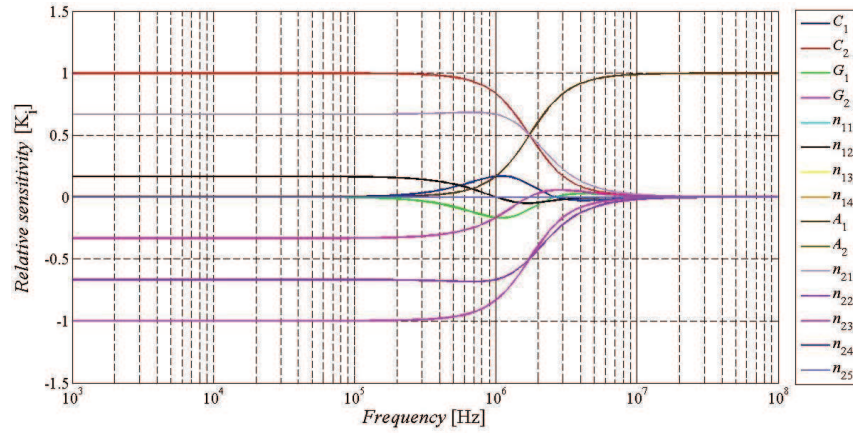


Figure 6.46 Relative sensitivity of the module of transfer of HP of the S-E for individual parameters depending on the frequency ($f_0 = 1$ MHz)

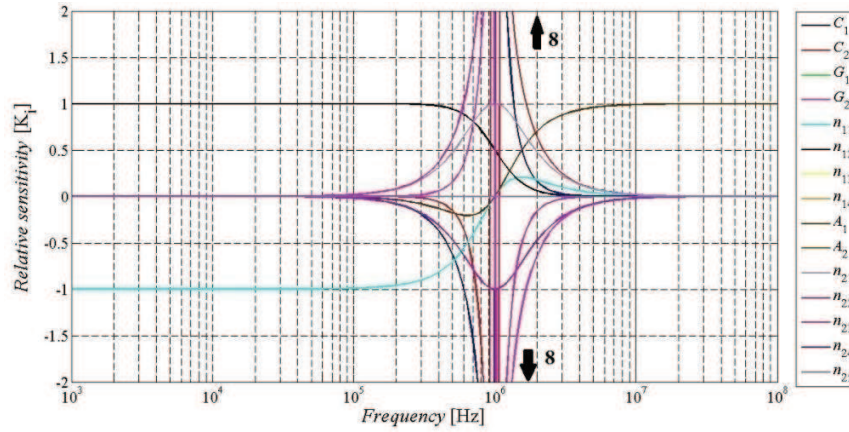


Figure 6.47 Relative sensitivity of the module of transfer of BS of the S-E for individual parameters depending on the frequency ($f_0 = 1$ MHz)

The F-D filter from Figure 6.39 contains 20 parameters ($C_1, C_2, G_1, G_2, A_1, A_2, n_{11}, n_{12}, n_{13}, n_{14}, n_{15}, n_{16}, n_{21}, n_{22}, n_{23}, n_{24}, n_{25}, n_{26}, n_{27}, n_{28}$) where parameters n_{11} to n_{34} again stand for individual outputs of each current follower in the circuit structure.

The denominator of the F-D filter is given as:

$$D_{real}(s) = s^2 b_2 + s b_1 + b_0, \quad (6.84)$$

The equations of the sensitivity analysis of the F-D filter were again moved to Appendices due to their large volume. Individual terms of the denominator of the F-D filter are given by equations (B.1) to (B.3). The real transfer functions of the F-D filter in their general form are given by equations (6.74) to (6.78). Numerators of the transfer functions of the F-D filter are given by equations (B.4) to (B.8).

Figure 6.48 to Figure 6.52 illustrate the relative sensitivity of the module of transfer to given parameters for LP, BP1, BP2, HP and BS transfer functions of the F-D filter when $f_0 = 1$ MHz. Individual sensitivities of the F-D filter are low except BS transfer function where the sensitivity reaches up to eight similarly to the S-E BS function. LP, BP1, BP2 and HP are the most sensitive to parameters n_{12} and n_{21} whose sensitivity reaches two. The sensitivity of BS transfer function reaches up to eight for parameters C_1 , C_2 , G_1 , G_2 , A_2 , n_{13} and n_{22} .

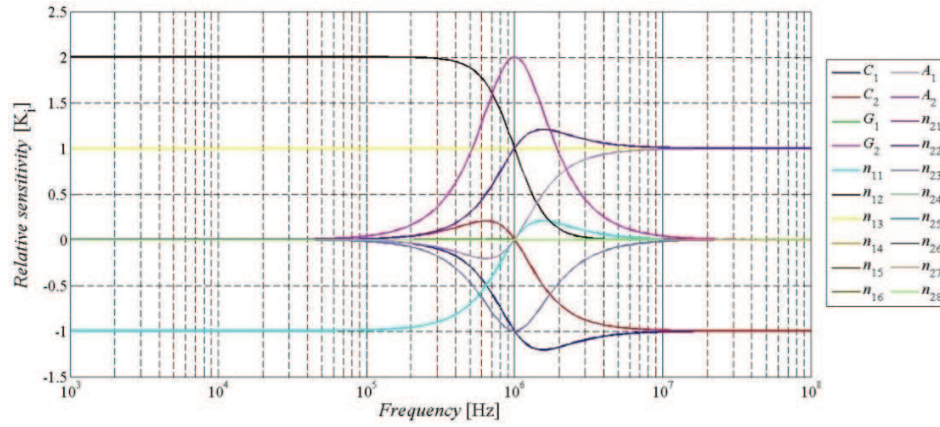


Figure 6.48 Relative sensitivity of the module of transfer of LP of the F-D filter for individual parameters depending on the frequency ($f_0 = 1$ MHz)

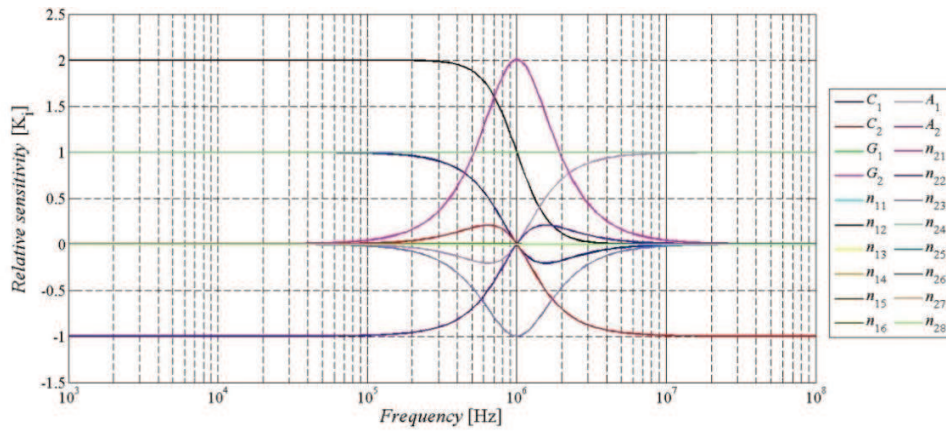


Figure 6.49 Relative sensitivity of the module of transfer of BP1 of the F-D for individual parameters depending on the frequency ($f_0 = 1$ MHz)

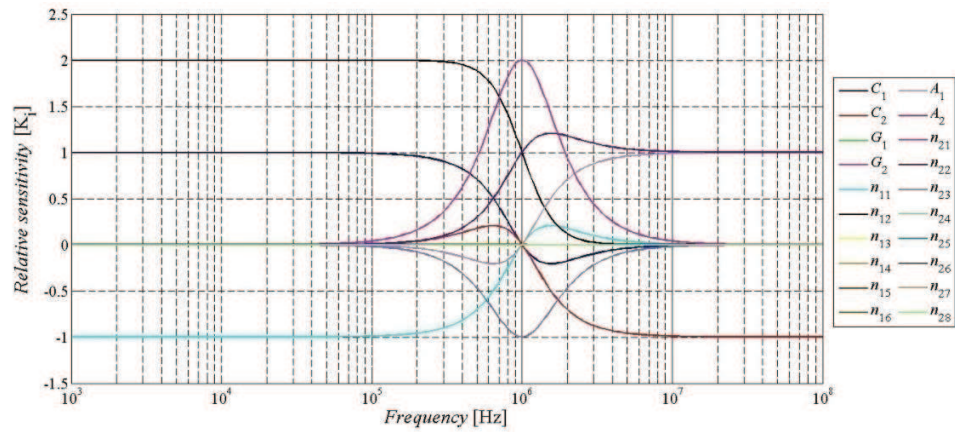


Figure 6.50 Relative sensitivity of the module of transfer of BP2 of the F-D for individual parameters depending on the frequency ($f_0 = 1$ MHz)

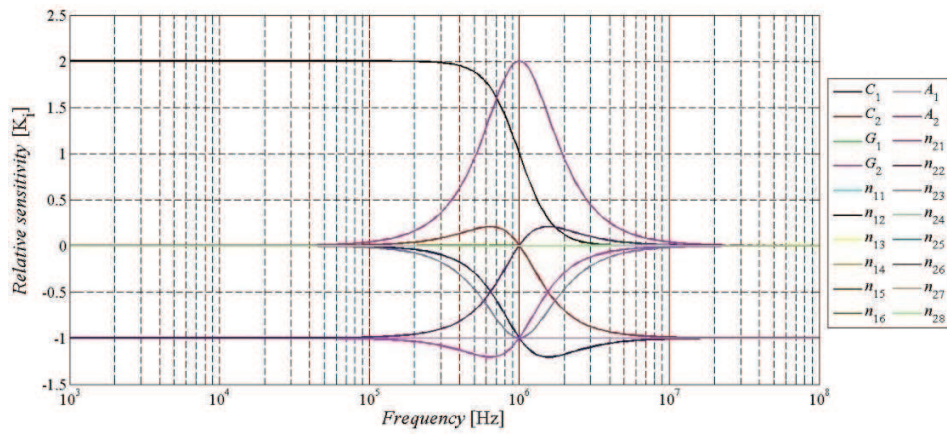


Figure 6.51 Relative sensitivity of the module of transfer of HP of the F-D for individual parameters depending on the frequency ($f_0 = 1$ MHz)

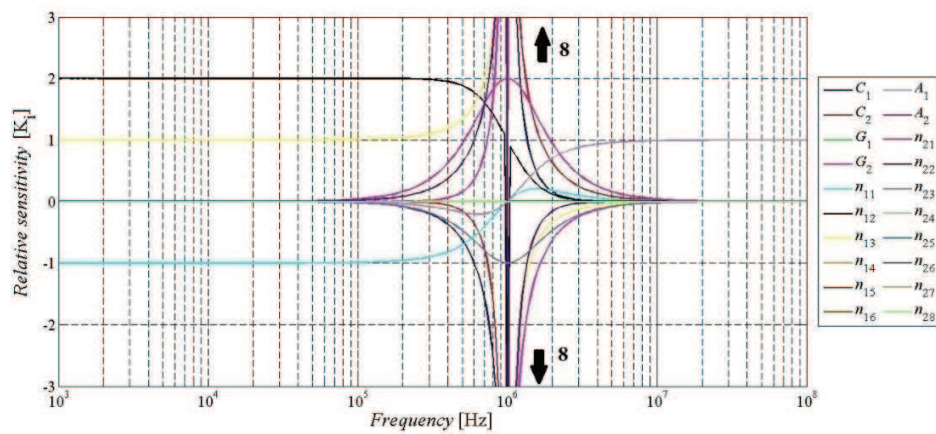


Figure 6.52 Relative sensitivity of the module of transfer of BS of the F-D for individual parameters depending on the frequency ($f_0 = 1$ MHz)

6.6 Universal Filter with Three CFs and Two DACAs

6.6.1 Filter proposal

Figure 6.53 presents a modified version of the filtering structure from chapter 6.2. The modification consists in that the positions of elements MO-CF₂ and DACA₁ and then MO-CF₃ and DACA₂ have been swapped. The modified version benefits from the fact that used DACA elements in the F-D structure now require only up to two outputs in comparison to the F-D filter from chapter 6.2 where DACA₁ required four outputs. Therefore, it is possible to use the chips of the DACA element (which posses of two outputs) without any requirement of additional active elements which would be necessary to multiply the number of the outputs of the DACA elements. The other advantage is that all obtainable transfer functions correspond with particular term of the denominator of the filter thus, all transfer functions have the unity gain in pass-band area regardless the values of current gains A_1 and A_2 . This S-E and F-D filter was also implemented in form of PCBs and experimental measurement has been made. I have published the S-E and F-D filter from this chapter in [138].

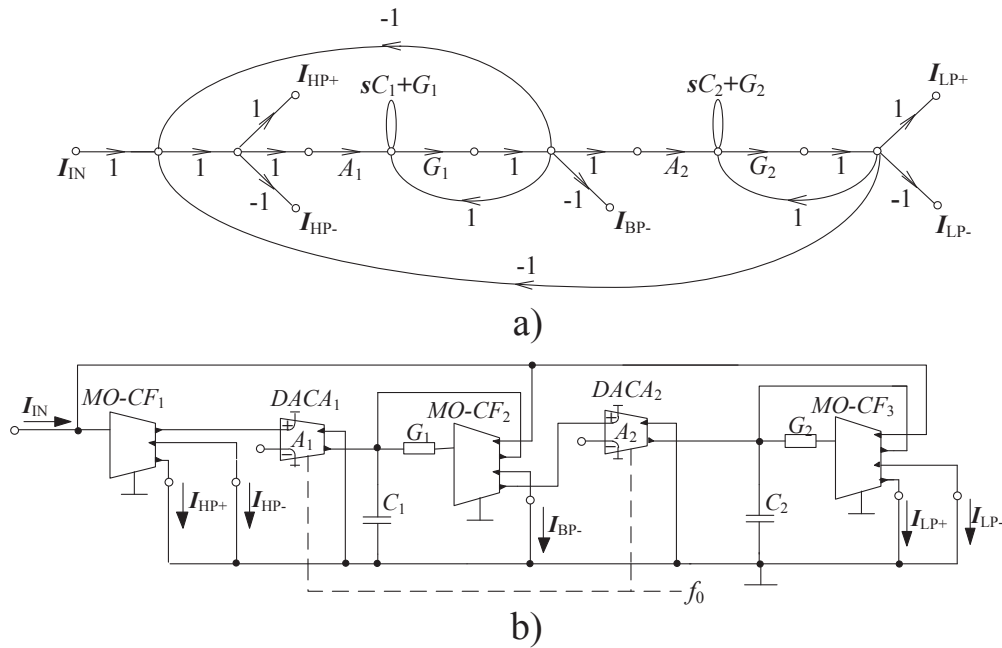


Figure 6.53 Single-ended form of the filter with three MO-CFs and two DACAs:
a) simplified M-C graph, b) circuit structure

The F-D form of the filter from Figure 6.53 is illustrated in Figure 6.54. It is proposed with non-differential current followers in order of easier implementation in a form of PCB. The circuit structure of the F-D filter is created by two DO-CF, four MO-CF and two DACAs. In case of the implementation, floating capacitors have been replaced by grounded capacitors in

each branch as shown in Figure 6.54 c). The value of these capacitors is twice as high as selected values of capacitors from the S-E filter in order to compensate the pole frequency of the F-D transfer function in comparison to the S-E function.

The denominator of all transfer functions of this S-E and F-D filter is given by:

$$D(s) = s^2 C_1 C_2 + s C_2 G_1 A_1 + G_1 G_2 A_1 A_2. \quad (6.85)$$

The denominator of the filter shows that it is possible to control the pole frequency of the filter without disturbing the quality factor by changing the values of the current gains A_1 and A_2 when $A_1 = A_2 = A$.

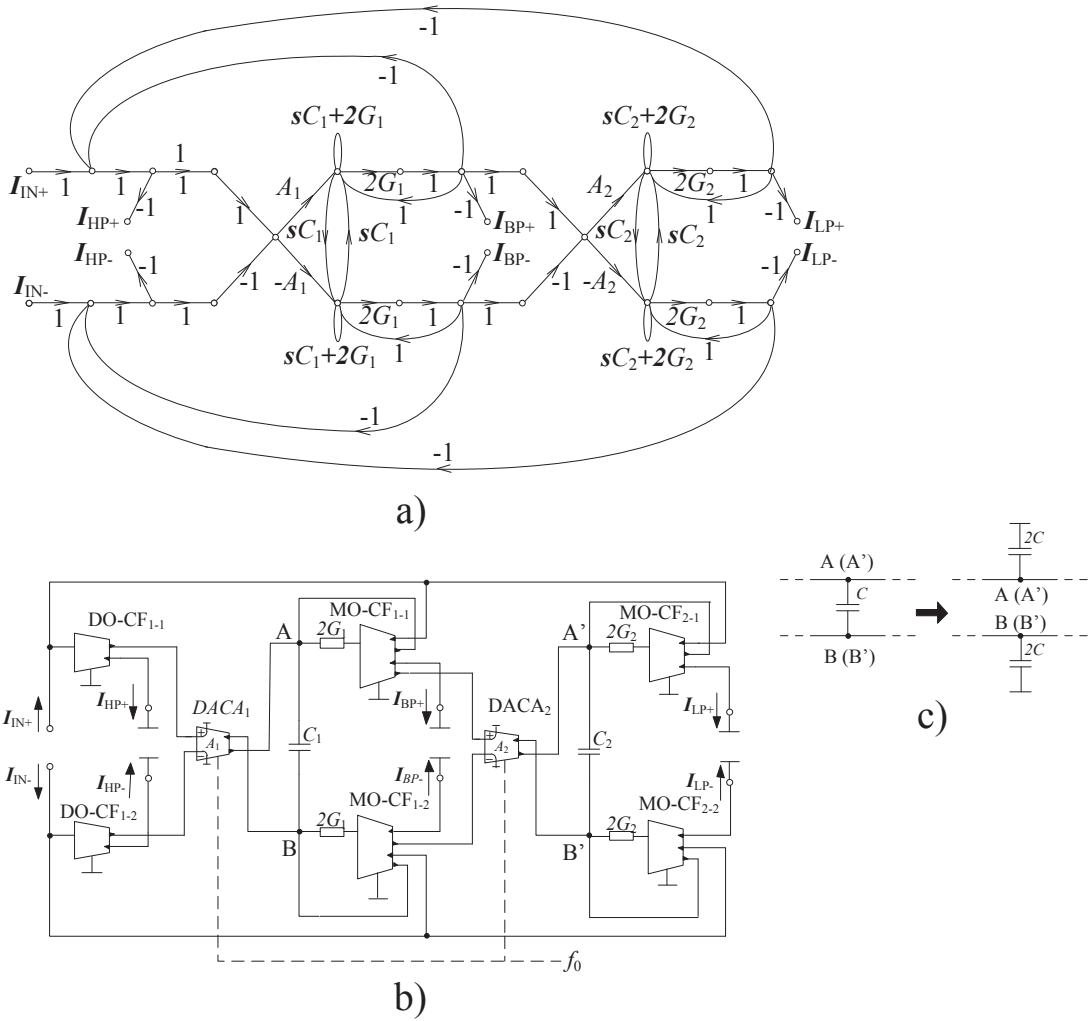


Figure 6.54 Fully-differential form of the filter with three MO-CFs and two DACAs: a) simplified M-C graph, b) circuit structure, c) implementation of non-floating capacitors

The relations of the pole frequency and quality factor of the filter are represented by the following equations:

$$f_0 = \frac{A}{2\pi} \sqrt{\frac{G_1 G_2}{C_1 C_2}}, \quad Q = \sqrt{\frac{G_2 C_1}{G_1 C_2}}. \quad (6.86), (6.87)$$

Again applies that values parameters G_1 , G_2 of the F-D filter are twice higher in comparison to the values used for the S-E filter.

Obtainable transfer functions of both S-E and F-D filter are given as:

$$\frac{I_{LP+}}{I_{IN}} = -\frac{I_{LP-}}{I_{IN}} = \frac{G_1 G_2 A_1 A_2}{D}, \quad (6.88)$$

$$\frac{I_{BP+}}{I_{IN}} = -\frac{I_{BP-}}{I_{IN}} = \frac{s C_2 G_1 A_1}{D}, \quad (6.89)$$

$$\frac{I_{HP+}}{I_{IN}} = -\frac{I_{HP-}}{I_{IN}} = \frac{s^2 C_1 C_2}{D}, \quad (6.90)$$

$$I_{BS} = \frac{I_{HP+} + I_{LP+}}{I_{IN}} = -\frac{I_{HP-} + I_{LP-}}{I_{IN}} = \frac{s^2 C_1 C_2 + G_1 G_2 A_1 A_2}{D}, \quad (6.91)$$

$$I_{AP} = \frac{I_{HP+} + I_{BP+} + I_{LP+}}{I_{IN}} = -\frac{I_{HP-} + I_{BP-} + I_{LP-}}{I_{IN}} = \frac{s^2 C_1 C_2 - s C_2 G_1 A_1 + G_1 G_2 A_1 A_2}{D}. \quad (6.92)$$

From the equations (6.88) - (6.92) can be seen that the proposed S-E and F-D filter provides all standard transfer functions. All transfer functions correspond with particular term of the denominator and thus, they have the unity gain in pass band area regardless values of current gains of the DACA elements. In case of the S-E filter, LP, HP and BS transfer functions can be obtained either positive or negative. As it is for the F-D filter, all available transfer functions can be obtained in both polarities.

6.6.2 Simulation and Experimental Results

Values of passive elements and specific filter parameters selected for PSpice simulations and experimental measurement are following: values of capacitors were set $C_1 = C_2 = 330$ pF, the quality factor of the filter $Q = 0.707$ (Butterworth approximation), starting values of current gains $A_1 = A_2 = 1$, G_1 equals 0.909 mS which corresponds with a resistor value of 1100 Ω . The starting pole frequency was set to 300 kHz. Remaining G_2 was calculated according to the relation: $G_2 = 2\pi f_0 C_2 Q = 0.4398$ mS which is approximately 2274 Ω .

A resistor of value $2200\ \Omega$ was used which results in $f_0 = 310.0\ \text{kHz}$ ($241.5\ \text{kHz}$ when taking real values of gain of the DACA element into consideration).

A comparison of the simulation and experimental results of LP, BP, HP and BS transfer functions of the S-E filter are shown in Figure 6.55. HP transfer functions (blue lines) have the slope of attenuation of 39 dB per decade, BP functions (red lines) have 17 dB per decade and LP functions have 36 dB per decade. The slope of attenuation of simulated and measured functions is almost the same. The biggest attenuation of the BS function is 32 dB in case of the simulations and 37 dB for the measured filter. The biggest difference between simulation and experimental results is at lower and higher frequencies. The difference at lower frequencies is given mainly by that the output-impedances of actual used active elements are not high enough. The difference at higher frequencies is given mainly because of bandwidth limitations and parasitic characteristics of used V/I, I/V converters and active elements and also parasitic capacitances of cables and PCB. That also applies for the F-D filter.

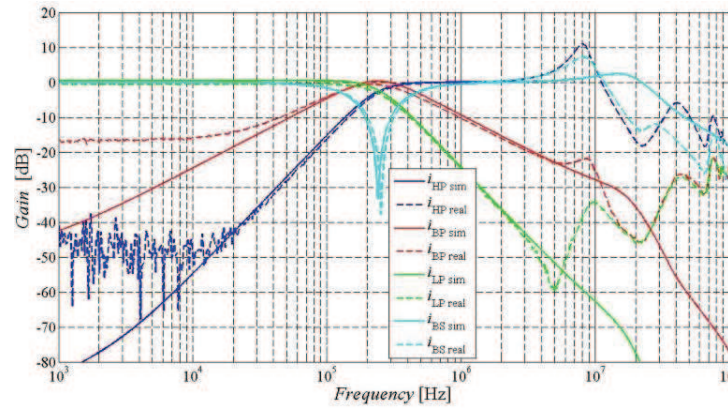


Figure 6.55 Comparison of transfer functions high-pass, band-pass, low-pass and band-stop of the S-E proposed filter from Fig. 6.53: simulation (solid lines) and experimental results (dashed lines)

Figure 6.56 shows the ability to control the pole frequency of the S-E filter without disturbing its quality factor by changing the values of current gains A_1 and A_2 . LP transfer function was used for the illustration. The values of current gains were set 1, 2, 3, 4. The pole frequencies obtained from simulations and measurement are summarized in Table VII. The simulation results are closer to the theory nevertheless, the measured results also prove design correctness.

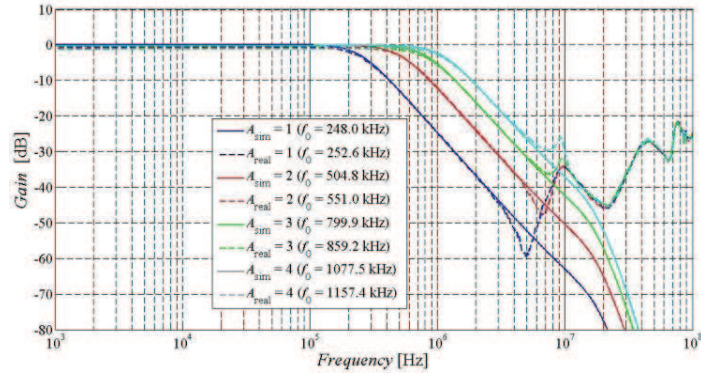


Figure 6.56 Demonstration of ability to control the pole frequency in case of the S-E filter from Fig. 6.53: simulation (solid lines) and experimental (dashed lines) results when parameter A was set to 1, 2, 3, 4

Table VII Comparison of obtained values of the pole frequency

	$A_{1,2}$ [-]			
Frequency [kHz]	1	2	3	4
Calculated	241.5	494.2	771.7	1022.8
Simulated	248.0	504.8	799.9	1077.5
Measured	252.6	551.0	859.2	1157.4

A comparison of the simulation and experimental results of LP, BP, HP and BS transfer functions of the F-D filter is depicted in Figure 6.57. The slope of attenuation of obtained HP transfer functions (blue lines) is 35 dB per decade, 17 dB per decade for BP functions (red lines) and in case of LP transfer functions it is 39 dB per decade. The biggest attenuation of the BS function is 43 dB in case of the simulated results and 11 dB for the measured results. The slope of attenuation of independent transfer functions is almost the same for both simulation and experimental results. From this graph, we can see bigger differences between simulated and measured results which are given mainly because individual chips of the DACA elements have a rather wide range of their parameters such as the current gain and output impedance.

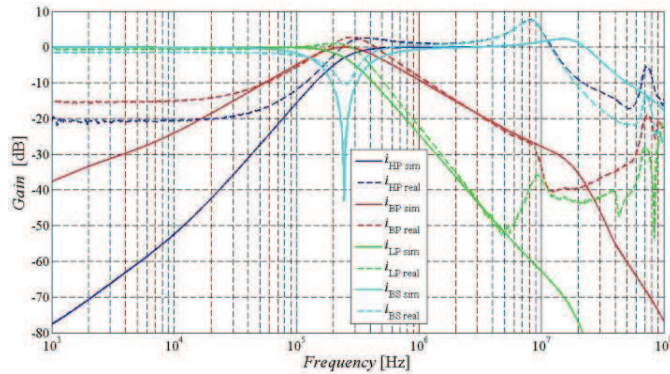


Figure 6.57 Comparison of transfer functions high-pass, band-pass, low-pass and band-stop of the F-D proposed filter from Fig. 6.54: simulation (solid lines) and experimental results (dashed lines)

The ability to control the pole frequency of the F-D filter without disturbing its quality factor by changing the values of current gains A_1 and A_2 is illustrated in Figure 6.58. LP transfer function was chosen as an example. The values of current gains were set 1, 2, 3, 4. The values of pole frequencies obtained from simulations and measurement can be compared in Table VIII. By comparison can be seen that the values obtained from simulations are closer to the calculated values. The values of the pole frequency of the F-D filter are slightly higher.

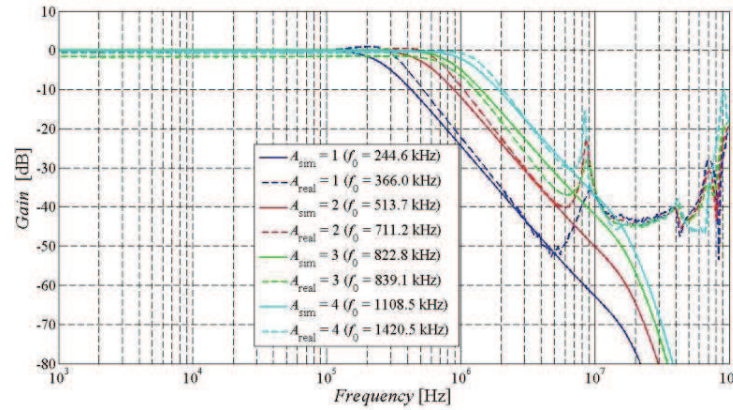


Figure 6.58 Demonstration of ability to control the pole frequency in case of the F-D filter from Fig. 6.54: simulation (solid lines) and experimental (dashed lines) results when parameter A was set to 1, 2, 3, 4

Table VIII Comparison of obtained values of the pole frequency

	$A_{1,2} [-]$			
Frequency [kHz]	1	2	3	4
Calculated	241.5	494.2	771.7	1022.8
Simulated	244.6	513.7	822.8	1108.5
Measured	366.0	711.2	839.1	1420.5

Figure 6.59 and Figure 6.60 compare experimental results of the S-E and F-D filter. Bigger differences between the S-E and F-D filter can be seen. This is given mainly because of a rather wide range of parameters such as the current gain and output impedance of individual chips of the DACA element. A comparison of measured pole frequencies of the S-E and F-D filter can be made from Table IX. The pole frequencies of the S-E filter are closer to the calculated values. The values of the pole frequency of the F-D filter are higher than the theoretical values which is again given by a wide range of parameters of individual DACA chips.

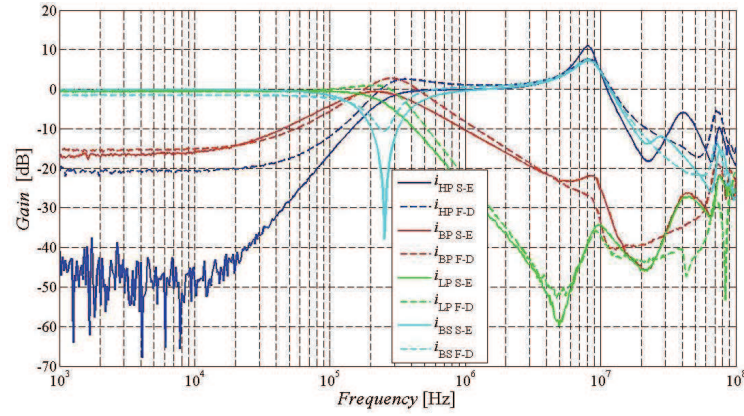


Figure 6.59 Comparison of transfer functions high-pass, band-pass, low-pass and band-stop of experimental results: the S-E filter from Fig. 6.53 (solid lines) and the F-D filter from Fig. 6.54 (dashed lines)

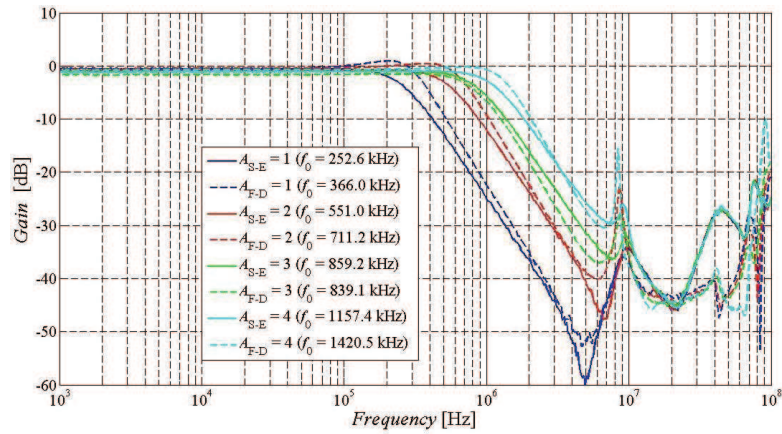


Figure 6.60 Demonstration of ability to control the pole frequency in case of experimental results: the S-E filter from Fig. 6.53 (solid lines) and the F-D filter from Fig. 6.54 (dashed lines)

Table IX Comparison of obtained values of the pole frequency

	$A_{1,2}$ [-]			
Frequency [kHz]	1	2	3	4
Calculated	241.5	494.2	771.7	1022.8
Measured S-E	252.6	551.0	859.2	1157.4
Measured F_D	366.0	711.2	839.1	1420.5

6.7 General Conception of a Filter with Two OTAs and One CF

Figure 6.61 shows a second-order universal filter with minimal number of used active elements taken from [51]. The filter consists of two OTA elements (BOTA and MOTA) and one CF (DO-CF). Even though the filter has a current input and output, it contains mixed-mode active elements so, it is not working purely in the current-mode. Nevertheless, the filter has a low input and high output impedance allowing simple chaining in cascade. The filter

possesses ability to control the pole frequency by changing values of transconductances of OTAs. All output responses are taken directly from current outputs of used active elements.

The denominator which is common for all obtainable transfer functions is given as:

$$D(s) = s^2 C_1 C_2 + s C_2 g_{m1} + g_{m1} g_{m2}. \quad (6.93)$$

The pole frequency and quality factor of the filter are described by the following relations:

$$f_0 = \frac{1}{2\pi} \sqrt{\frac{g_{m1} g_{m2}}{C_1 C_2}}, \quad Q = \sqrt{\frac{g_{m2} C_1}{g_{m1} C_2}}. \quad (6.94), (6.95)$$

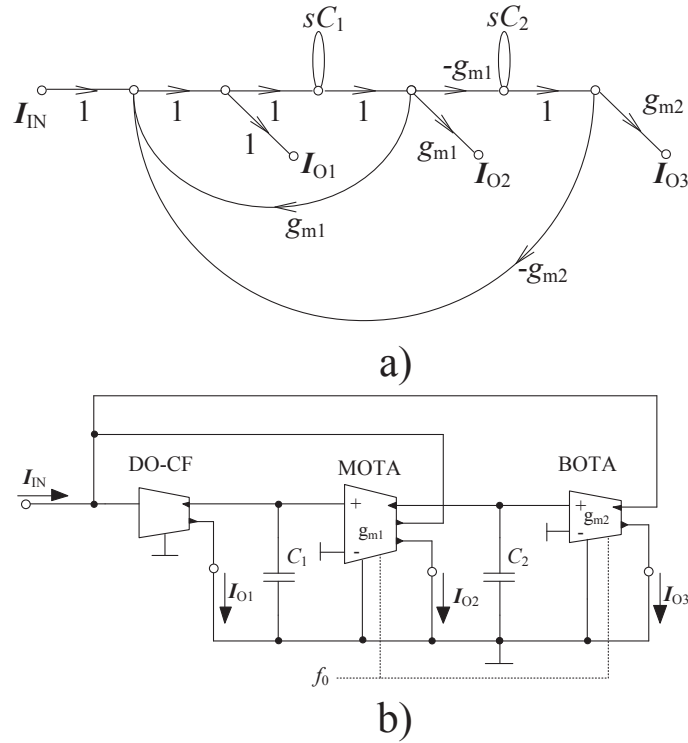


Figure 6.61 General conception of a filter with two OTAs and one CF: a) simplified M-C graph, b) circuit structure

From equation (6.94) is obvious that the pole frequency can be controlled without disturbing the quality factor of the filter by changing values of transconductances g_{m1} and g_{m2} when $g_{m1} = g_{m2}$.

The transfer functions of the filter are given by:

$$K_{LP}(s) = \frac{I_{O3}}{I_{IN}} = \frac{g_{m1} g_{m2}}{D}, \quad (6.96)$$

$$K_{BP-}(s) = \frac{I_{O2}}{I_{IN}} = \frac{sC_2g_{m1}}{D}, \quad (6.97)$$

$$K_{HP}(s) = \frac{I_{O1}}{I_{IN}} = \frac{s^2C_1C_2}{D}, \quad (6.98)$$

$$K_{BS}(s) = \frac{I_{O1} + I_{O3}}{I_{IN}} = \frac{s^2C_1C_2 + g_{m1}g_{m2}}{D}, \quad (6.99)$$

$$K_{AP}(s) = \frac{I_{O1} + I_{O2} + I_{O3}}{I_{IN}} = \frac{s^2C_1C_2 - sC_2g_{m1} + g_{m1}g_{m2}}{D}. \quad (6.100)$$

From equations (6.96) to (6.100) is obvious that the filter is universal it provides all standard transfer functions (LP, BP, HP, BS, AP). All transfer functions excluding BP are positive. This conception was used to propose filters in chapters 6.8, 6.9 and 6.10.

6.8 Universal Filter with Two OTAs, One CF and One DACA

6.8.1 Filter proposal

The aim of the proposal was to design a second-order universal current-mode frequency filter using transconductance amplifiers (one BOTA and one MOTA elements) as basic building blocks. The DACA element was added in the circuit structure to control the quality factor of the filter. The proposed filter enables to control the pole frequency without disturbing the quality factor of the filter by simultaneous change of transconductances g_{m1} , g_{m2} . The quality factor of the filter can be electronically controlled by adjusting the current gain of the DACA element. I have presented the research from this chapter in [139]. The S-E form of the filter is shown in Figure 6.62.

The F-D form of the filter can be seen in Figure 6.63. The filter consists of two MOTAs, one DACA and one FD-CF. The FD-CF is implemented by the DACA element. Floating capacitors are replaced by grounded capacitors the way shown in Figure 6.63 c). These capacitors are, similarly to previous cases, twice as high as capacitors used in the S-E filter.

The denominator of transfer functions of the S-E and F-D filter is described by:

$$D(s) = s^2 C_1 C_2 + s C_2 g_{m1} A + g_{m1} g_{m2}. \quad (6.101)$$

As it can be seen the pole frequency can be controlled electronically without disturbing the quality factor by adjusting values of transconductances g_{m1} and g_{m2} when $g_{m1} = g_{m2}$. The quality factor of the filter can be electronically controlled without disturbing its pole frequency by changing the current gain A .

The pole frequency and the quality factor can be described by the following relations:

$$f_0 = \frac{1}{2\pi} \sqrt{\frac{g_{m1} g_{m2}}{C_1 C_2}}, \quad Q = \frac{1}{A} \sqrt{\frac{g_{m2} C_1}{g_{m1} C_2}}. \quad (6.102), (6.103)$$

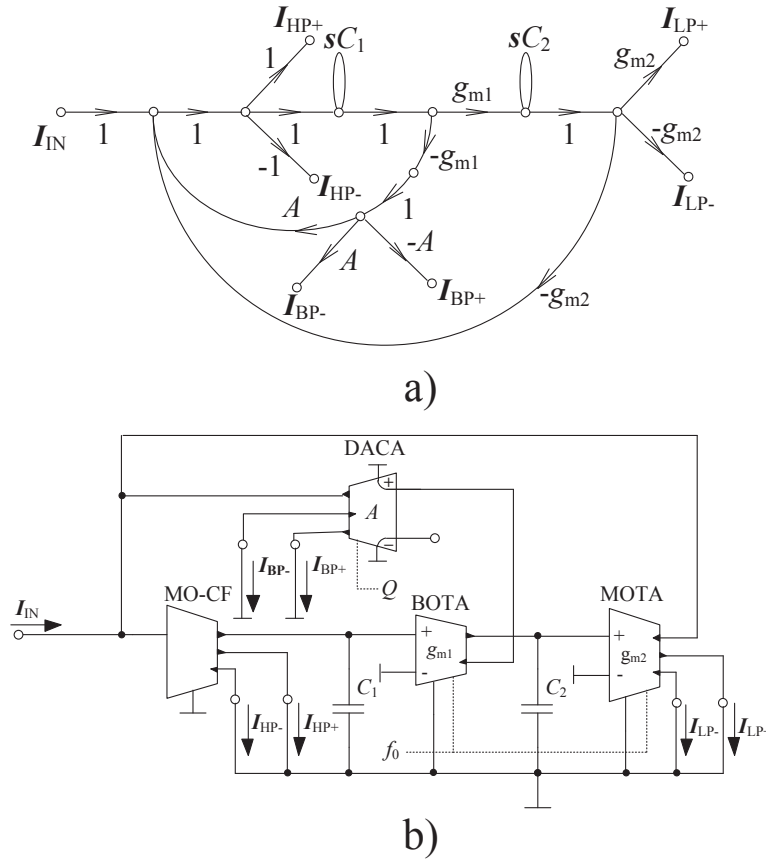


Figure 6.62 Single-ended form of the filter with two OTAs, one DACA and one MO-CF:
a) simplified M-C graph, b) circuit structure

In order to obtain the same transfer functions for both the S-E and F-D filter, factor A used for the F-D structure is replaced by $2A$. The values of g_{m1} , g_{m2} of the F-D filter must be twice higher than in case of S-E transconductances.

The proposed S-E and F-D filter provides the following transfer functions:

$$\frac{I_{LP+}}{I_{IN}} = -\frac{I_{LP-}}{I_{IN}} = \frac{g_{m1}g_{m2}}{D}, \quad (6.104)$$

$$\frac{I_{BP+}}{I_{IN}} = -\frac{I_{BP-}}{I_{IN}} = \frac{sC_2g_{m1}A}{D}, \quad (6.105)$$

$$\frac{I_{HP+}}{I_{IN}} = -\frac{I_{HP-}}{I_{IN}} = \frac{s^2C_1C_2}{D}, \quad (6.106)$$

$$I_{BS} = \frac{I_{HP+} + I_{LP+}}{I_{IN}} = -\frac{I_{HP-} + I_{LP-}}{I_{IN}} = \frac{s^2C_1C_2 + g_{m1}g_{m2}}{D}, \quad (6.107)$$

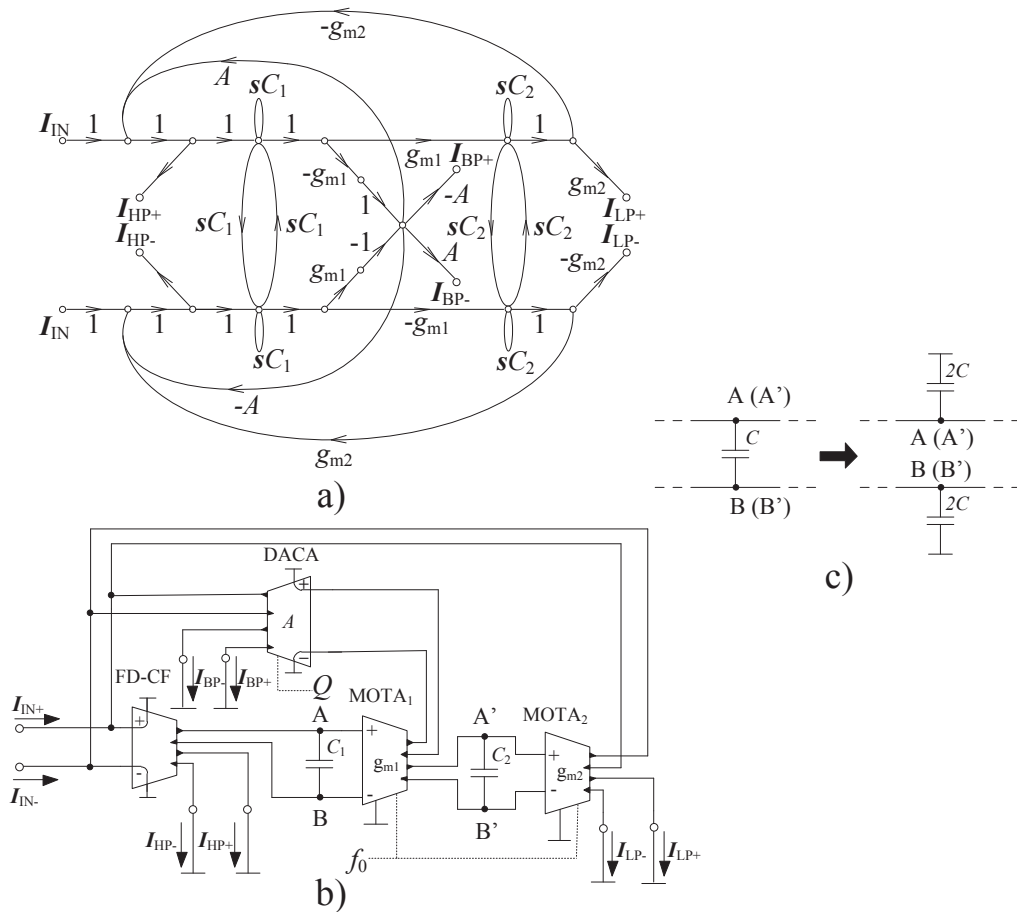


Figure 6.63 Fully-differential form of the filter with two OTAs, one DACA and one CF: a) simplified M-C graph, b) circuit structure, c) implementation of non-floating capacitors

$$I_{AP} = \frac{I_{HP+} + I_{BP-} + I_{LP+}}{I_{IN}} = -\frac{I_{HP-} + I_{BP+} + I_{LP-}}{I_{IN}} = \frac{s^2 C_1 C_2 - s C_2 g_{m1} A + g_{m1} g_{m2}}{D}. \quad (6.108)$$

As can be seen the proposed S-E and F-D filter provides all standard transfer functions. All transfer functions correspond with particular term of the denominator and they have the unity gain in pass band area regardless values of transconductances g_{m1} and g_{m2} and current gain A of the DACA element. All obtainable transfer functions of the S-E and F-D filter can be obtained in both polarities.

6.8.2 Simulation and Experimental Results

The values of passive elements and specific filter parameters were set as follows: the starting pole frequency equals 500 kHz, the starting quality factor $Q = 0.707$ (Butterworth approximation), values of conductances g_{m1} , g_{m2} were set to 1 mS, the starting current gain of DACA element has been chosen $A = 1$. Only values of capacitors C_1 and C_2 remain to be determined. These values were calculated as follows: $C_1 = (g_{m1} Q A) / (2\pi f_0) = 225$ pF, $C_2 = g_{m2} / (2\pi f_0 A Q) = 450$ pF. Hence, for the simulations and experimental measurement $C_1 = 220$ pF and $C_2 = 440$ pF have been used.

The alternative circuit solution of the DACA element has been used. Therefore, the values used to control the quality factor of the S-E and F-D filter are solely demonstrational and do not necessary correspond with values which can be obtained using a real element of the DACA amplifier. The reason why the alternative solution of the DACA element is used instead of the DACA chip is that in case of the F-D we need 4 outputs otherwise it would not be possible to obtain the band-pass transfer function. It would be possible to use a current follower in order to copy and multiply the output signal of the DACA element, but that would increase the number of active elements on the PCB. Another advantage is that the quality factor of the filters can be controlled continuously instead of being limited by discrete steps.

Simulation and experimental results of low-pass, band-pass, high-pass and band-stop transfer functions of the S-E form of the proposed filter are depicted in Figure 6.64. High-pass transfer function (blue lines) has the slope of attenuation 38 dB per decade. The slope of attenuation of band-pass function (red lines) is 19 dB per decade. Low-pass transfer function (green lines) was 39 dB per decade. The highest attenuation of band-pass function is at -35 dB in case of simulations and -25 dB of measured function. The transfer functions obtained from experimental measurement have slightly lower attenuation than simulated transfer functions. Differences between simulated and measured results at higher frequencies are mainly given by bandwidth limitations of used real active elements and also by limitations of used converters etc. The measured results are also affected by input/output impedances (they are not low/high enough) of the active elements in the structure. The input impedance

of the DACA element is the most dominant parasitic element at higher frequencies. That applies for all measured results.

Possibility to control the pole frequency of the S-E filter without disturbing its quality factor by changing values of transconductances when $g_{m1} = g_{m2} = g_m$ is presented in Figure 6.65. LP transfer function has been selected as an example. The values of transconductances were set 0.5 mS (resistor 2000 Ω has been used), 1 mS (1000 Ω) and 1.96 mS (510 Ω).

Table X compares obtained values of the pole frequency. It can be seen that the pole frequencies obtained from simulations are closer to the theoretical values. Nonetheless, measured results are also satisfactory and confirm design correctness and correct operation of both filters.

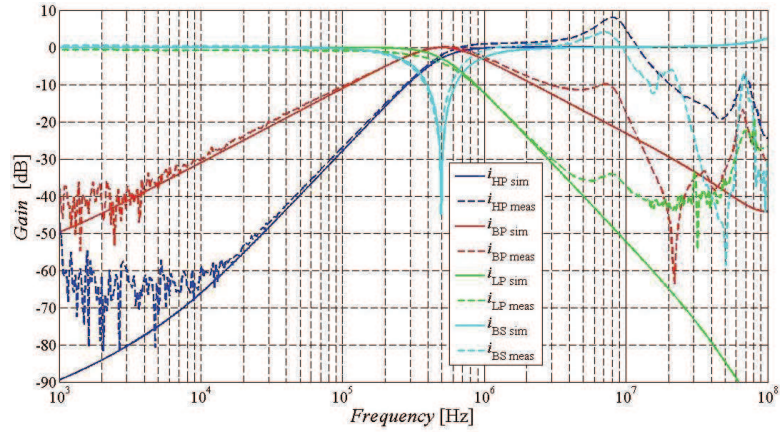


Figure 6.64 Comparison of transfer functions high-pass, band-pass, low-pass and band-stop of the S-E proposed filter from Fig. 6.62: simulation (solid lines) and experimental results (dashed lines)

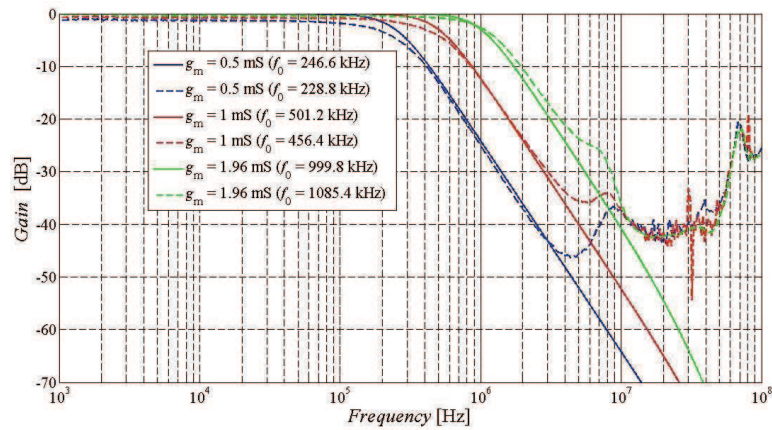


Figure 6.65 Demonstration of ability to control the pole frequency in case of the S-E filter from Fig. 6.62: simulation (solid lines) and experimental (dashed lines) results when g_{m1} and g_{m2} were set to 0.5 mS, 1 mS, 1.96 mS

Table X Comparison of obtained values of the pole frequency

	$g_{m1,2}$ [mS]		
Frequency [kHz]	0.5	1	1.96
Calculated	255.8	511.5	1003.0
Simulated	246.6	501.2	999.8
Measured	228.8	456.4	1085.4

Figure 6.66 illustrates possibility to control the quality factor of the filter without disturbing the pole frequency by adjusting current gain A . For the presentation, BP transfer function was chosen to be the example. Values of parameter A were selected accordingly: 0.25, 0.5 and 1. Table XI compares obtained values of the quality factor. Both simulated and measured values of the quality factor are in good agreement with the theory. There are slightly bigger differences for higher values of the quality factor.

Table XI Comparison of obtained values of the quality factor

	A [-]		
Q [-]	0.25	0.5	1
Calculated	2.83	1.41	0.71
Simulated	3.08	1.49	0.73
Measured	3.26	1.39	0.67

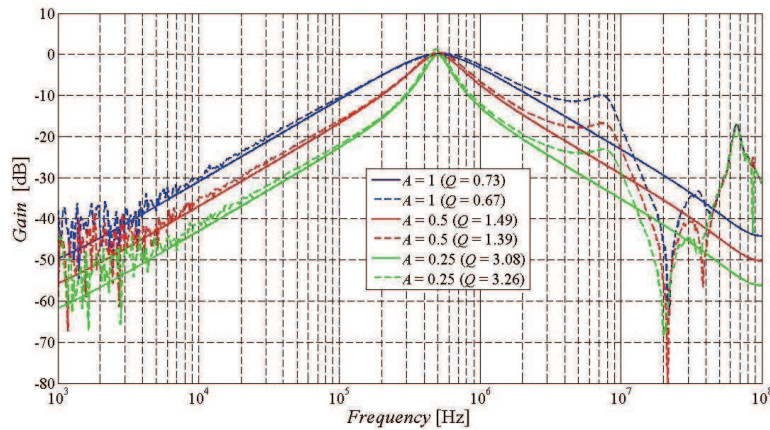


Figure 6.66 Demonstration of ability to control the quality factor in case of the S-E filter from Fig. 6.62: simulation (solid lines) and experimental (dashed lines) results when A was set to 0.5 mS, 1 mS, 1.96 mS

Low-pass, band-pass, high-pass and band-stop transfer functions of the F-D form obtained from simulations and experimental measurement are shown in Figure 6.67. The slope of attenuation of high-pass transfer functions (blue lines) is 39 dB per decade, in case of band-pass functions (red lines), it is 20 dB per decade and 40 dB per decade for low-pass functions (green lines). The highest attenuation of band-stop transfer functions (turquoise lines) is at -47

dB in case of simulations and -35 dB in case of measured function. The measured function of high-pass function has slightly lower attenuation than the simulated function, approximately the same slope in case of band-pass and slightly higher slope for low-pass function.

Figure 6.68 illustrates ability to control the pole frequency of the F-D filter without disturbing the quality factor by changing values of transconductances g_{m1} , g_{m2} . LP transfer function was again selected as an example. The values of transconductances of the F-D filter were set 1 mS (1000 Ω), 1.96 mS (510 Ω) and 3.92 mS (parallel combination of two 510 Ω resistors).

Table XII summarizes values of the pole frequency obtained from simulations and experimental measurement. The values obtained from the experimental measurement are slightly higher than the calculated values. The difference is becoming more obvious at higher frequencies.

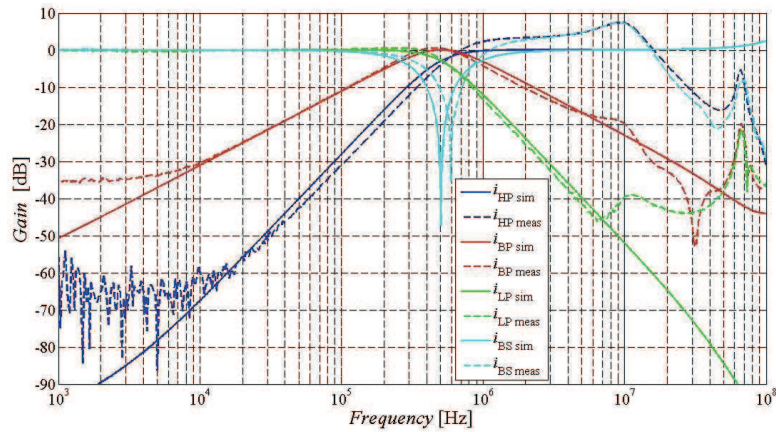


Figure 6.67 Comparison of transfer functions high-pass, band-pass, low-pass and band-stop of the F-D proposed filter from Fig. 6.63: simulation (solid lines) and experimental results (dashed lines)

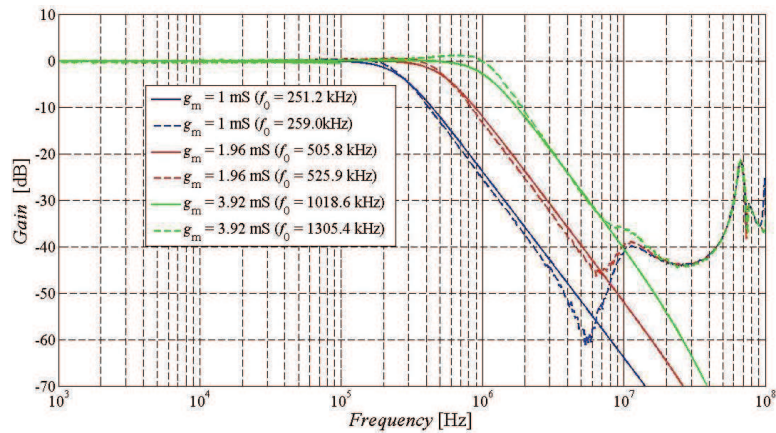


Figure 6.68 Demonstration of ability to control the pole frequency in case of the F-D filter from Fig. 6.63:

simulation (solid lines) and experimental (dashed lines) results when g_{m1} and g_{m2} were set to 1 mS, 1.96 mS and 3.92 mS

Table XII Comparison of obtained values of the pole frequency

	$g_{m1,2}$ [mS]		
Frequency [kHz]	1	1.96	3.92
Calculated	255.8	511.5	1003.0
Simulated	251.2	505.8	1018.6
Measured	259.0	525.9	1305.4

Possibility to control the quality factor of the filter without disturbing the pole frequency by changing the value of the current gain of the DACA element can be seen in Figure 6.69. BP transfer function has been chosen for the presentation. Values of parameter A are halved in comparison to the values used for the S-E filter (e. g. 0.125, 0.25, 0.5). A comparison of simulated and measured values of the quality factor is given in Table XIII. The values of the quality factor obtained from experimental measurement are significantly higher than the theoretical values. Also the pole frequency is slightly shifting when the quality factor changes. Nevertheless, the experimental measurement of the F-D filter proves the correctness and functionality of the proposed filter.

Table XIII Comparison of obtained values of the quality factor

	A [-]		
Q [-]	0.125	0.25	0.5
Calculated	2.83	1.41	0.71
Simulated	2.87	1.41	0.71
Measured	3.42	2.02	0.91

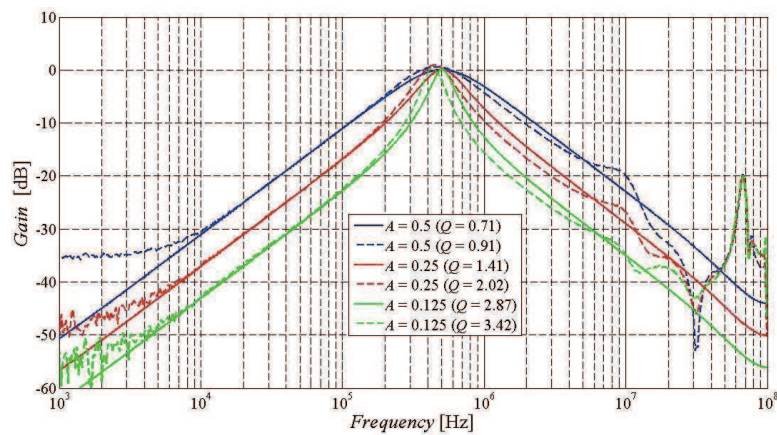


Figure 6.69 Demonstration of ability to control the quality factor in case of the F-D filter from Fig. 6.63:

simulation (solid lines) and experimental (dashed lines) results when A was set to 0.5 mS, 1 mS, 1.96 mS

A comparison of the experimental measurement of low-pass, band-pass, high-pass and band-stop transfer functions of the S-E and F-D filter are shown in Figure 6.70. From the graph can be seen that the F-D transfer functions have slightly higher attenuation than in case of the S-E functions, which is mainly given by that the values of conductances used in F-D structures must be twice the values used in case of S-E structures in order to obtain the same pole frequency for both filters. It can be seen that the filters can be suitably used approximately up to frequency of 6 MHz because of bandwidth limitations and parasitic characteristics of used active elements. Results are also affected by limitations of used converters and parasitic capacitances of cables and PCB. Obtained slopes of attenuation of individual transfer functions are compared in text above.

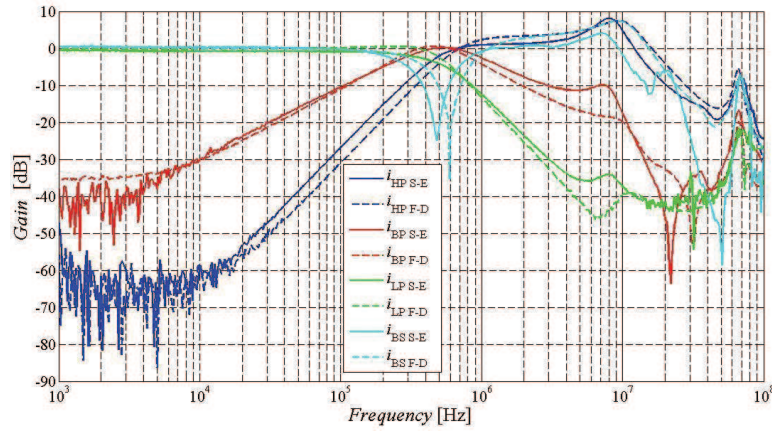


Figure 6.70 Comparison of transfer functions high-pass, band-pass, low-pass and band-stop of experimental results: the S-E filter from Fig. 6.62 (solid lines) and the F-D filter from Fig. 6.63 (dashed lines)

Figure 6.71 compares the experimental results of the ability to control the pole frequency of the S-E and F-D filter without disturbing the quality factor by changing values of transconductances g_{m1} , g_{m2} . Obtained values of measured pole frequencies can be compared in Table XIV. The values of transconductances used in the S-E filter (before the slash) and the F-D filter (after the slash) are given in the table. The pole frequencies of the F-D filter are at lower frequencies closer to calculated values than values obtained from the S-E filter. The slopes of attenuation are greater in case of the F-D filter.

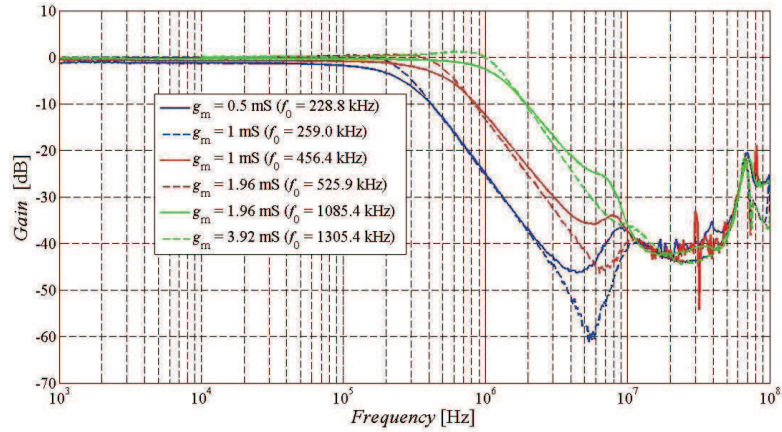


Figure 6.71 Comparison of possibility to control the pole frequency when comparing experimental results: S-E filter from Fig. 6.62 (solid lines), F-D filter from Fig. 6.63 (dashed lines)

Table XIV Comparison of obtained values of the pole frequency

	$g_{m1,2}$ S-E/ $g_{m1,2}$ F-D [mS]		
Frequency [kHz]	0.5/1	1/1.96	1.96/3.92
Calculated	255.8	511.5	1003.0
Mesured S-E	228.8	456.4	1085.4
Mesured F-D	259.0	525.9	1305.4

The experimental results showing the ability to control the quality factor of the S-E and F-D filter without disturbing the pole frequency by changing the value of the current gain A are illustrated in Figure 6.72. Table XV provides a comparison of measured quality factors obtained from the S-E and F-D filter. The values of the quality factor obtained from the S-E are closer to the theoretical values. The values obtained from the F-D filter are significantly higher than the calculated values. Also the pole frequency of the F-D is slightly shifting for higher values of the quality factor.

Table XV Comparison of obtained values of the quality factor

	A S-E/ A F-D [-]		
Q [-]	0.25/0.125	0.5/0.25	1/0.5
Calculated	2.83	1.41	0.71
Mesured S-E	3.26	1.39	0.67
Mesured F-D	3.42	2.02	0.91

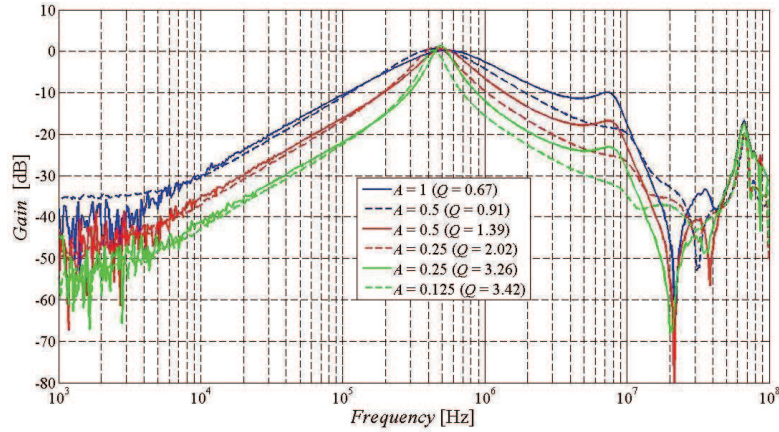


Figure 6.72 Comparison of possibility to adjust the quality factor when comparing experimental results: S-E filter from Fig. 6.62 (solid lines), F-D filter from Fig. 6.63 (dashed lines)

The analysis of this proposal also includes a comparison of the dynamic range of the proposed S-E and F-D filter. For this matter, measurement of the DC transfer function of the all-pass S-E and F-D filter was carried out. This comparison is shown in Figure 6.73. The input DC current was set in range from -3 mA to 3 mA with 5 uA step using current source Agilent B2902A and multimeters Agilent 34410A. From the graph it can be seen that the dynamic range of the F-D filter (from -1.1 mA to 1.3 mA) is significantly greater than the dynamic range of the S-E filter (from -0.8 mA to 0.55 mA).

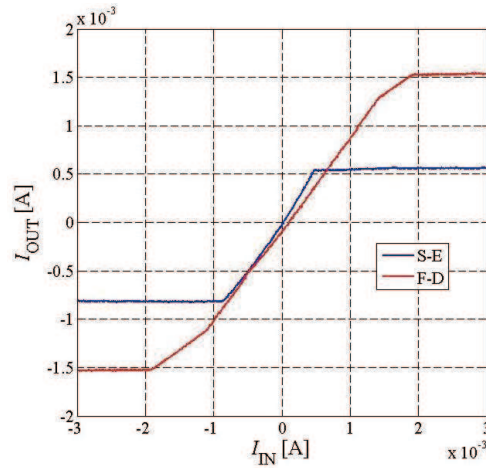


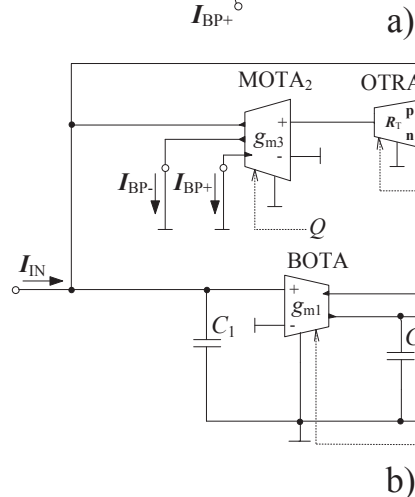
Figure 6.73 Comparison of the dynamic range of proposed S-E and F-D filter (experimental results): S-E filter from Fig. 6.62 (blue line), F-D filter from Fig. 6.63 (red line)

6.9 Multifunctional Filter with Three OTAs and One OTRA

6.9.1 Filter proposal

The proposed filter is a second-order multifunctional current-mode frequency filter employing three OTAs and one OTRA. The proposed filter possesses ability to control

My proposal from this chapter is presented in [140].



a) simplified M-C graph, b) circuit structure

three MOTAs and one OTRA. Floating capacitors were replaced by grounded capacitors the

way shown in Figure 6.75 c). These capacitors have double the value of capacitors used in the S-E filter.

The denominator which is common for all obtainable transfer functions of these filters is given by:

$$D(s) = s^2 C_1 C_2 + s C_2 g_{m1} R_T g_{m3} + g_{m1} g_{m2}. \quad (6.109)$$

From equation (6.109) can be seen that it is possible to control the pole frequency of the filter without disturbing the quality factor by changing values of transconductances g_{m1} and g_{m2} simultaneously. The quality factor can be controlled without disturbing the pole frequency by changing values of transconductance g_{m3} or/and transresistance R_T .

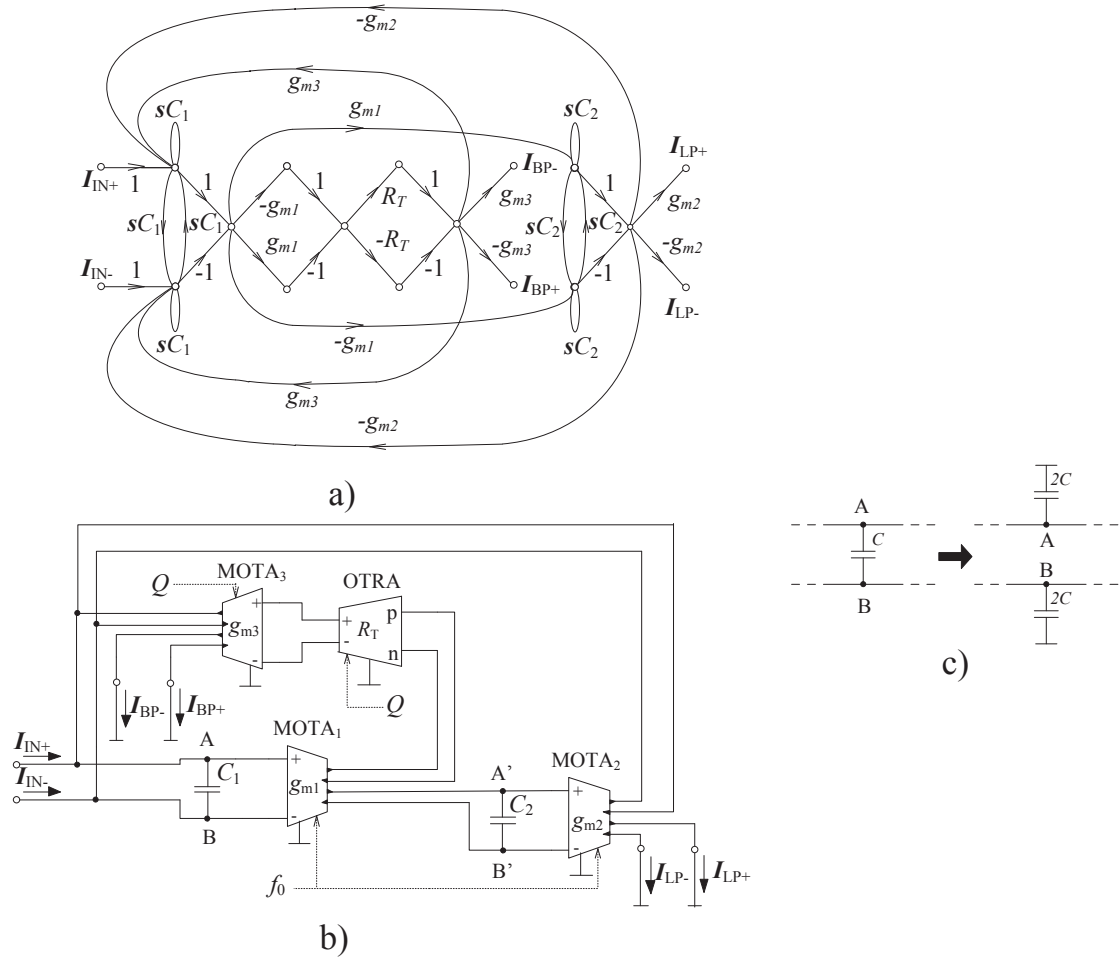


Figure 6.75 Fully-differential form of the proposed filter with three OTAs and one OTRA:
a) simplified M-C graph, b) circuit structure, c) implementation of non-floating capacitors

The relations describing the pole frequency and quality factor of the filter are given as:

$$f_0 = \frac{1}{2\pi} \sqrt{\frac{g_{m1}g_{m2}}{C_1C_2}}, \quad Q = \frac{1}{g_{m3}R_T} \sqrt{\frac{g_{m2}C_1}{g_{m1}C_2}}. \quad (6.110), (6.111)$$

To obtain the same transfer functions for the S-E and F-D filter, the values of transconductances g_{m1} , g_{m2} of the F-D filter must be twice higher than in case of S-E transconductances in order to obtain the same pole frequencies. The values of transconductance g_{m3} of the F-D filter must be twice higher than the values used for the S-E filter and the values of transresistance R_T in case of the F-D filter must be 1/4 of the values of the S-E filter. However, the values of transresistance R_T used for the F-D structure would be already rather small. To avoid reaching the parameter limitations, the values of g_{m3} were left unchanged resulting in that the values of R_T will decrease only with the ratio 1:2 instead of 1:4.

The proposed S-E and F-D filter provides the following transfer functions:

$$\frac{I_{LP+}}{I_{IN}} = -\frac{I_{LP-}}{I_{IN}} = \frac{g_{m1}g_{m2}}{D}, \quad (6.112)$$

$$\frac{I_{BP+}}{I_{IN}} = -\frac{I_{BP-}}{I_{IN}} = \frac{sC_2g_{m1}R_Tg_{m3}}{D}. \quad (6.113)$$

From the equation (6.112) and (6.113) can be seen that the proposed filter provides low-pass and band-pass transfer functions. Both transfer functions of the S-E and F-D filter can be obtained in both polarities. The nominator of each of transfer function corresponds with particular term of the denominator, thus, these functions have the unity gain in pass-band area regardless the values of transconductances g_{m1} , g_{m2} , g_{m3} and transresistance R_T .

6.9.2 Simulation and Experimental Results

The starting values of passive elements and specific filter parameters for the simulations and experimental measurement were selected accordingly: values of transconductances g_{m1} , g_{m2} were set to 0.5 mS (resistors of value 2 k Ω (1 k Ω in case of the F-D structure)), capacitors $C_1 = C_2 = 470$ pF. Depending on these values of transconductances and capacitors, the starting pole frequency equals 169.3 kHz. The starting value of the quality factor of the filter was $Q = 0.707$ (Butterworth approximation). The starting value of transconductance g_{m3} is equal to 1.96 mS (resistor of value 510 Ω was used). Transresistance R_T was calculated as follows: $R_T = 1/(g_{m3}Q)\sqrt{(C_1g_{m2})/(C_2g_{m1})}$

721.36 Ω . Therefore, a resistor of value 680 Ω (340 Ω in case of the F-D structure) has been used which results in $Q = 0.75$.

A comparison of the simulation and experimental results of LP transfer function of the S-E filter when changing the pole frequency is presented in Figure 6.76. The slope of attenuation of obtained LP transfer functions is 40 dB per decade and it is slightly steeper in case of the experimental results. The biggest difference between the simulation and experimental results can be seen at higher frequencies. This difference is given mainly because of the bandwidth limitations and parasitic characteristics of used active elements and bandwidth limitations of converters etc. That also applies for results of the F-D filter. Values of transconductances g_{m1} , g_{m2} were selected 0.5 mS (2000 Ω), 1 mS (1000 Ω) and 1.96 mS (510 Ω). Values of the pole frequencies obtained from the simulations and experimental measurement are compared in Table XVI. The simulated values of the quality factor are closer to theoretical values nevertheless, the measured results also prove design correctness of the proposed S-E filter.

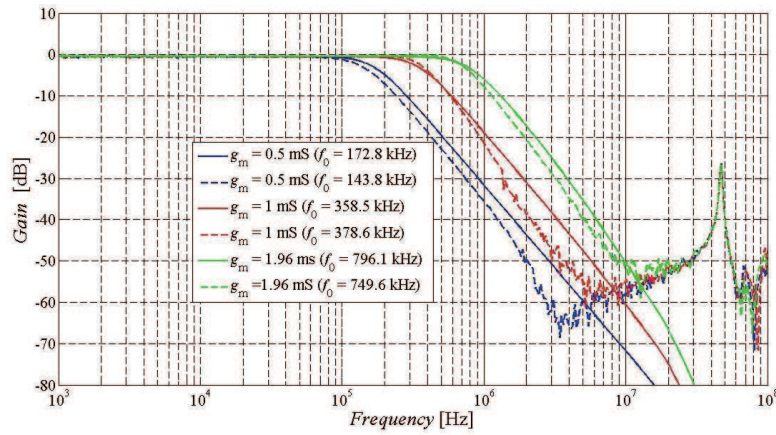


Figure 6.76 Demonstration of ability to control the pole frequency in case of the S-E filter from Fig. 6.74: simulation (solid lines) and experimental (dashed lines) results when g_{m1} and g_{m2} were set to 0.5 mS, 1 mS, 1.96 mS.

Table XVI Comparison of obtained values of the pole frequency

	$g_{m1,2}$ [mS]		
Frequency [kHz]	0.5	1	1.96
Calculated	169.3	338.6	677.3
Simulated	172.8	358.5	796.1
Measured	143.8	378.6	749.6

The simulation and experimental results of band-pass transfer function of the S-E filter when changing the quality factor are shown in Figure 6.77. In this case, the control of the quality factor is done through changing values of transconductance g_{m3} when R_T is fixed to value 680 Ω . The difference between simulation and experimental results at lower frequencies is mainly given by that the output-impedances of actual used active elements are not high enough. That

also applies for the remaining results. The values of g_{m3} were set to 0.5 mS (2000 Ω), 1 mS (1000 Ω) and 1.96 mS (510 Ω). Table XVII summarizes obtained values of the quality factor of the S-E filter. The obtained values of the quality factor are relatively close to the theoretical values.

Table XVII Comparison of obtained values of the quality factor

	g_{m3} [mS]		
Q [-]	1.96	1	0.5
Calculated	0.75	1.47	2.94
Simulated	0.76	1.47	3.12
Measured	0.82	1.65	2.92

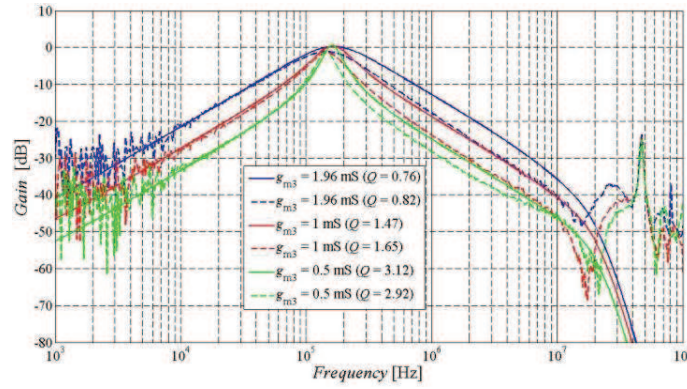


Figure 6.77 Demonstration of ability to control the quality factor in case of the S-E filter from Fig. 6.74: simulation (solid lines) and experimental (dashed lines) results when g_{m3} was set to 0.5 mS, 1 mS, 1.96 mS

Figure 6.78 illustrates simulation and experimental results of band-pass transfer function of the S-E filter when adjusting the quality factor by changing the values of transresistance R_T (g_{m3} is fixed to 1.96 mS). The values of R_T were set to 680 Ω , 510 Ω and 330 Ω . The values of the quality factor obtained from the simulation and experimental results are compared in Table XVIII. The obtained results are in good agreement with the theory.

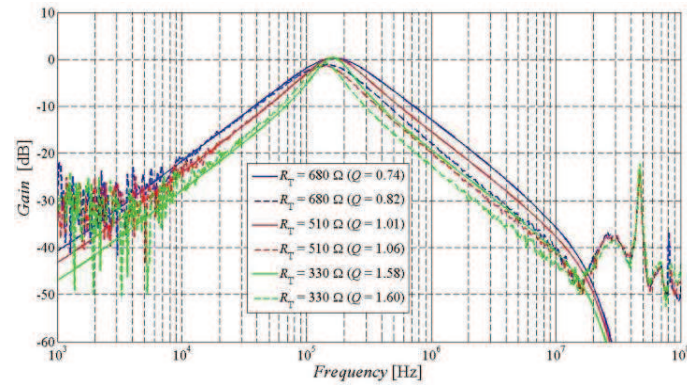


Figure 6.78 Demonstration of ability to control the quality factor in case of the S-E filter from Fig. 6.74: simulation (solid lines) and experimental (dashed lines) results when R_T was set to 680 Ω , 510 Ω , 330 Ω

Table XVIII Comparison of obtained values of the quality factor

	R_T [Ω]		
Q [-]	680	510	330
Calculated	0.75	1.00	1.55
Simulated	0.74	1.01	1.58
Measured	0.82	1.06	1.60

Figure 6.79 shows simulation and experimental results of LP transfer function of the F-D filter when changing the pole frequency by changing values of transconductances g_{m1} , g_{m2} . The slope of attenuation of obtained LP transfer functions is 40 dB per decade and it is slightly steeper in case of the experimental results. Transconductances g_{m1} , g_{m2} were set to 1 mS (1000 Ω), 1.96 mS (510 Ω) and 3.92 mS (parallel combination of two 510 Ω resistors). The obtained values of the pole frequency can be compared in Table XIX. The values obtained from simulations are slightly higher than the measured results.

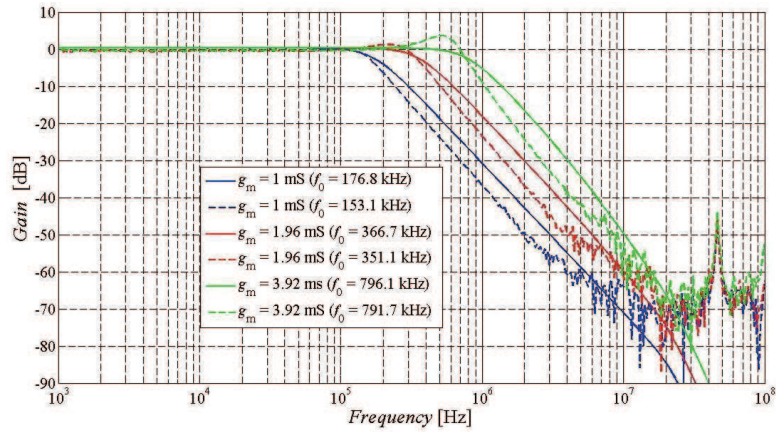


Figure 6.79 Demonstration of ability to control the pole frequency in case of the F-D filter from Fig. 6.75: simulation (solid lines) and experimental (dashed lines) results when g_{m1} and g_{m2} were set to 1 mS, 1.96 mS, 3.92 mS.

Table XIX Comparison of obtained values of the pole frequency

	$g_{m1,2}$ [mS]		
Frequency [kHz]	1	1.96	3.92
Calculated	169.3	338.6	677.3
Simulated	176.8	366.7	796.1
Measured	153.1	351.1	792.0

Output responses of band-pass transfer function of the F-D filter obtained from the simulations and experimental measurement are depicted in Figure 6.80. The control of the quality factor is achieved by changing values of transconductance g_{m3} when R_T is fixed to value 340 Ω . Used values of transconductance g_{m3} are 0.5 mS (2000 Ω), 1 mS (1000 Ω) and 1.96 mS (510 Ω). A comparison of obtained values of the quality factor can be made from

Table XX. It can be seen that the measured values of the quality factor are rather higher than the expected values.

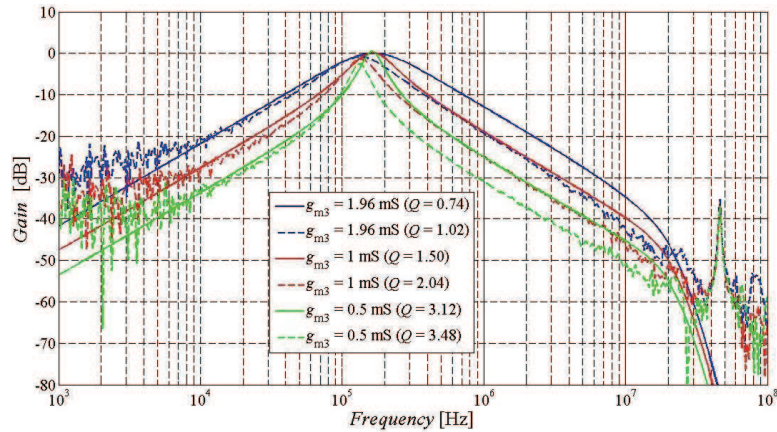


Figure 6.80 Demonstration of ability to control the quality factor in case of the F-D filter from Fig. 6.75: simulation (solid lines) and experimental (dashed lines) results when g_{m3} was set to 0.5 mS, 1 mS, 1.96 mS

Table XX Comparison of obtained values of the quality factor

	g_{m3} [mS]		
Q [-]	1.96	1	0.5
Calculated	0.75	1.47	2.94
Simulated	0.74	1.50	3.12
Measured	1.02	2.04	3.48

Figure 6.81 compares simulation and experimental results of band-pass transfer function of the F-D filter when changing the quality factor of the filter by changing values of transresistance R_T (g_{m3} is fixed to 1.96 mS). The values of R_T were set to 340 Ω (parallel combination of two 680 Ω resistors), 255 Ω (parallel combination of two 510 Ω resistors) and 165 Ω (parallel combination of two 330 Ω resistors). The values of obtained quality factors are summarized in Table XXI. The measured values are again higher than the calculated values. The simulated values are almost the same as the theoretical values.

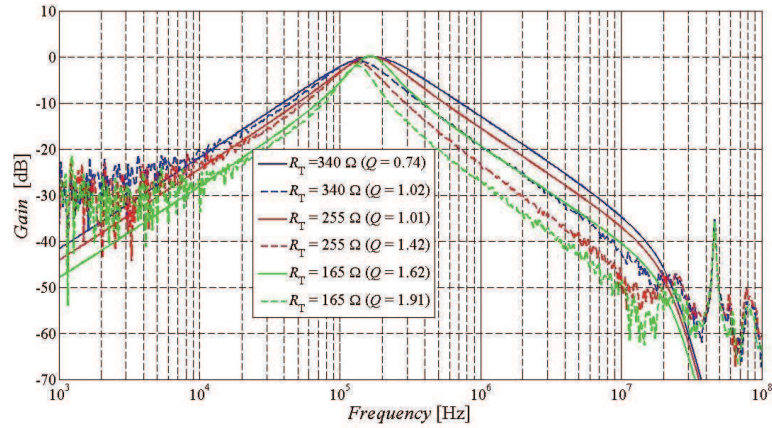


Figure 6.81 Demonstration of ability to control the quality factor in case of the F-D filter from Fig. 6.75: simulation (solid lines) and experimental (dashed lines) results when R_T was set to 340 Ω , 255 Ω , 165 Ω

Table XXI Comparison of obtained values of the quality factor

	R_T [Ω]		
Q [-]	340	255	165
Calculated	0.75	1.00	1.55
Simulated	0.74	1.01	1.62
Measured	1.02	1.42	1.91

A comparison experimental results of LP transfer function of the S-E and F-D filter when changing the pole frequency by changing values of transconductances g_{m1} , g_{m2} is given in Figure 6.82. Transconductances g_{m1} , g_{m2} were set to 0.5 mS, 1 mS and 1.96 mS (1 mS, 1.96 mS and 3.92 mS in case of the F-D structure). The obtained values of the pole frequency can be compared in Table XXII. From the table can be seen that the measured values of the quality factor of the F-D filter are for lower quality factors closer to the calculated values.

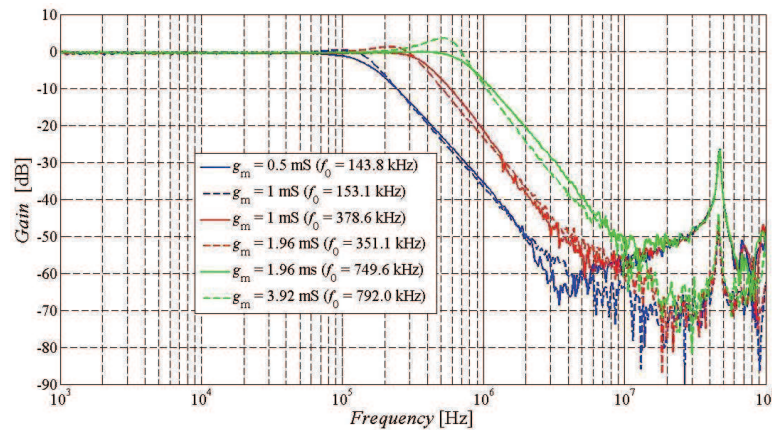


Figure 6.82 Comparison of possibility to control the pole frequency when comparing experimental results: S-E filter from Fig. 6.74 (solid lines), F-D filter from Fig. 6.75 (dashed lines)

Table XXII Comparison of obtained values of the pole frequency

	$g_{m1,2}$ S-E/ $g_{m1,2}$ F-D [mS]		
Frequency [kHz]	0.5/1	1/1.96	1.96/3.92
Calculated	169.3	338.6	677.3
Measured S-	143.8	378.6	749.6
Measured F-D	153.1	351.1	792.0

Figure 6.83 illustrates a comparison of the experimental results of band-pass transfer function of the S-E and F-D filter. Transconductances g_{m1} , g_{m2} were set to 0.5 mS, 1 mS and 1.96 mS in both cases when R_T was 680 Ω in case of the S-E filter and 340 Ω for the F-D filter. Table XXIII compares values of measured quality factors of the S-E and F-D filter. By comparison it can be seen that the values of the F-D filter are rather higher than the expected values.

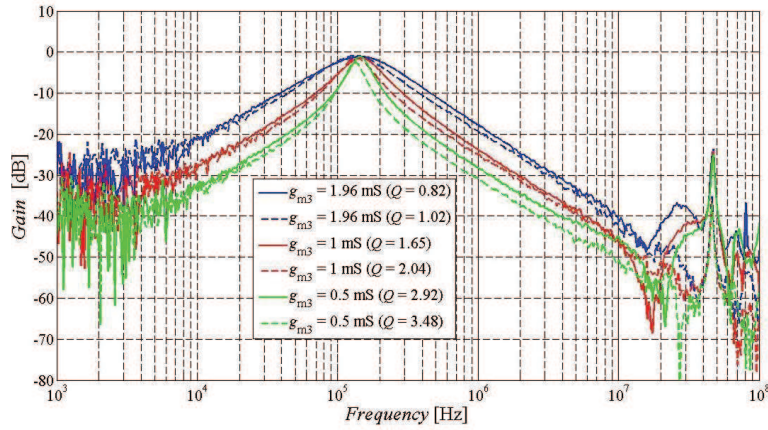


Figure 6.83 Comparison of possibility to control the quality factor when comparing experimental results: S-E filter from Fig. 6.74 (solid lines), F-D filter from Fig. 6.75 (dashed lines) when g_{m3} was set to 0.5 mS, 1 mS, 1.96 mS

Table XXIII Comparison of obtained values of the quality factor

	g_{m3} S-E/ g_{m3} F-D [mS]		
Q [-]	1.96	1	0.5
Calculated	0.75	1.47	2.94
Measured S-E	0.82	1.65	2.92
Measured F-D	1.02	2.04	3.48

The experimental results of band-pass transfer function of the S-E and F-D filter are compared in Figure 6.84. The values of R_T when changing the quality factor of the S-E filter were set to 680 Ω , 510 Ω and 330 Ω and the values of resistors used for the F-D filter were 340 Ω (parallel combination of two 680 Ω resistors), 255 Ω (parallel combination of two 510 Ω resistors) and 165 Ω (parallel combination of two 330 Ω resistors). Obtained values of the quality factor are summarized in Table XXIV. Even in this case, the values of the S-E filter are closer to calculated values when the values of the F-D filter are higher.

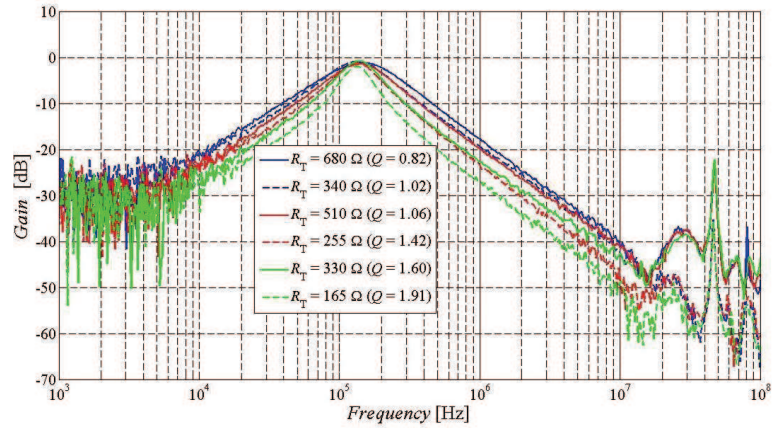


Figure 6.84 Comparison of possibility to control the quality factor when comparing experimental results: S-E filter from Fig. 6.74 (solid lines), F-D filter from Fig. 6.75 (dashed lines)

Table XXIV Comparison of obtained values of the quality factor

	R_T S-E/ R_T F-D [Ω]		
Q [-]	680/340	510/255	330/165
Calculated	0.75	1.00	1.55
Measured S-E	0.82	1.06	1.60
Measured F-D	1.02	1.42	1.91

6.9.3 Parasitic Analysis

The analysis of the proposed S-E and F-D filter also includes their parasitic analysis with input and output characteristics of used active elements. Figure 6.85 and Figure 6.86 show the proposed S-E and F-D filter with significant parasitic admittances (Y_{P1} - Y_{P4} and Y_{S1} - Y_{S2}). As stated before all parasitic admittances of the F-D filter are the same as in case of the S-E filter. Since we consider that individual inputs and outputs of each used active element have very similar characteristics, admittances of both positive and negative branch of the F-D filter are calculated the same way. Characteristic input and output parameters of the OTA element are $R_{IN\ OTA} \sim 1\text{ G}\Omega$, $C_{IN\ OTA} \sim 1\text{ pF}$, $R_{OUT\ OTA} \sim 200\text{ k}\Omega$ and $C_{OUT\ OTA} \sim 0.6\text{ pF}$ [19]. Characteristic input and output parameters of the OTRA element are $R_{IN\ OTRA} \sim 1\ \Omega$, $C_{IN\ OTRA} \sim 2\text{ pF}$, $R_{OUT\ OTRA} \sim 2\ \Omega$ and $C_{OUT\ OTRA} \sim 2\text{ pF}$. As mentioned before capacitances of individual pins of the active elements (approximately 1 pF each) are not included because all circuit is meant to be in its final implementation in the integrated form. Individual inputs and outputs of each used active element are expected to have very similar characteristics.

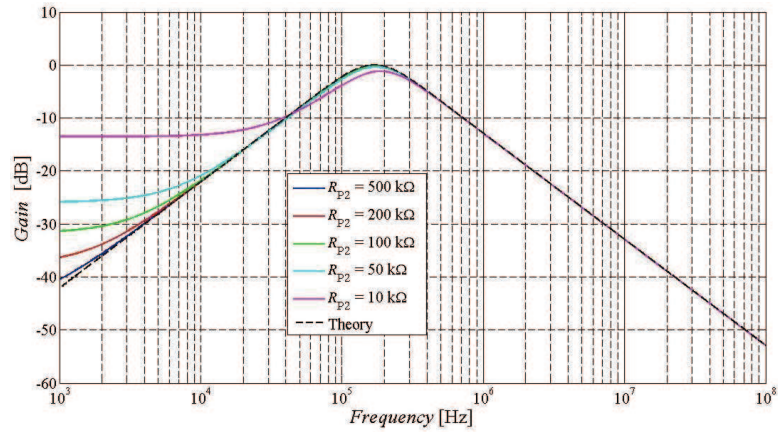


Figure 6.87 Influence of R_{P2} parasitic characteristic on BP response of the S-E filter when C_{P2} was 1.6 pF

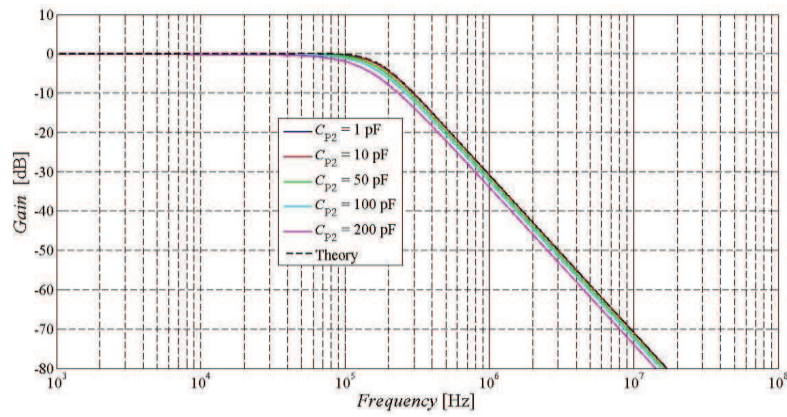


Figure 6.88 Influence of C_{P2} parasitic characteristic on LP response of the S-E filter when R_{P2} was 200 kΩ

Figure 6.89 illustrates the influence of R_{P2} on BP transfer function of the F-D filter when Figure 6.90 shows the influence of C_{P2} on LP transfer function of the F-D filter. It can be seen that the influence of parasitic parameters is slightly less significant than in case of the S-E filter. In case of the influence of C_{P2} it is because the capacitors C_1 , C_2 have twice the value of the capacitors of the S-E filter.

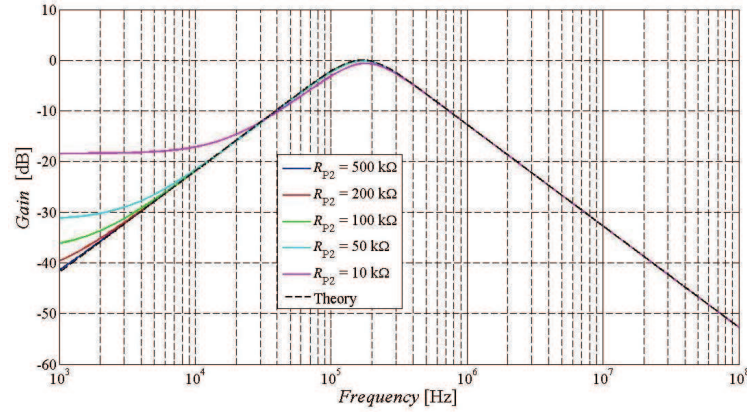


Figure 6.89 Influence of R_{P2} parasitic characteristic on BP response of the F-D filter when C_{P2} was 1.6 pF

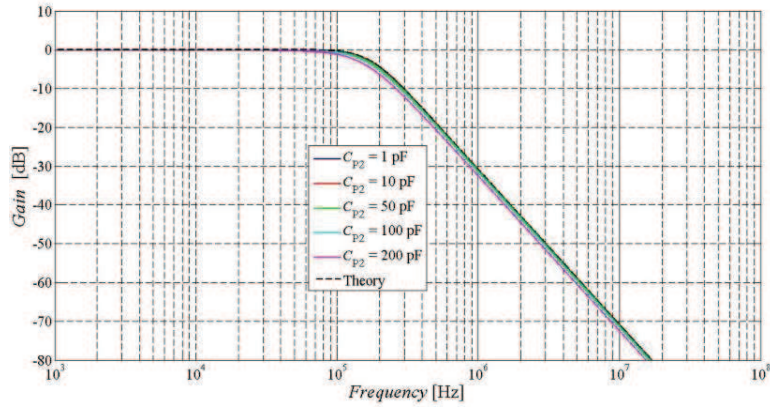


Figure 6.90 Influence of C_{P2} parasitic characteristic on LP response of the F-D filter when R_{P2} was 200 kΩ

6.10 Universal Filter with Three OTAs, One CF and One OTRA

6.10.1 Filter proposal

The last proposed filter of this chapter is based on the proposal from chapter 6.9. The circuit structure from chapter 6.9 has been complemented by one additional CF element, so the filter can provide all standard transfer functions and behaves as universal. It is still possible to electronically control the pole frequency and quality factor of the filter without disturbing each other. The proposed filter is shown in Figure 6.91. It employs one BOTAs, two MOTAs one MO-CF and one OTRA. I have published the proposal in this chapter in [141].

The F-D form of the proposed filter can be seen in Figure 6.92. It was created by mirroring passive parts around active elements. It consists of three MOTAs, one fully-differential OTRA and one FD-CF. In case of implementation, the floating capacitors are replaced by grounded capacitors as it is shown in Figure 6.92 c). The values of these capacitors must be again twice as much as the value of capacitors used in the S-E filter.

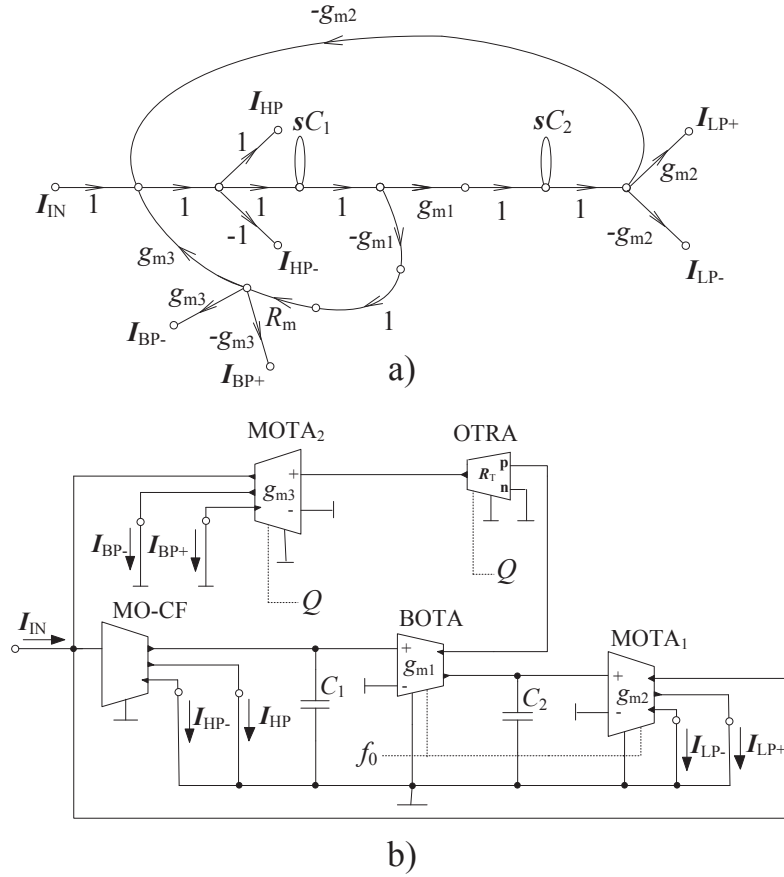


Figure 6.91 Single-ended form of the proposed filter with three OTAs, one CF and one OTRA:
a) simplified M-C graph, b) circuit structure

The denominator for all transfer functions is given by:

$$D(s) = s^2 C_1 C_2 + s C_2 g_{m1} g_{m3} R_T + g_{m1} g_{m2}. \quad (6.120)$$

From equation (6.120) is obvious that it is possible to control the pole frequency of the filter without disturbing the quality factor by changing values of transconductances g_{m1} , g_{m2} when $g_{m1} = g_{m2}$. It is also possible to control the quality factor of the filter without disturbing the pole frequency by changing values of transconductance g_{m3} or/and transresistance R_T .

The pole frequency and quality factor are defined according to the following relations:

$$f_0 = \frac{1}{2\pi} \sqrt{\frac{g_{m1} g_{m2}}{C_1 C_2}}, \quad Q = \frac{1}{g_{m3} R_T} \sqrt{\frac{g_{m2} C_1}{g_{m1} C_2}}. \quad (6.121), (6.122)$$

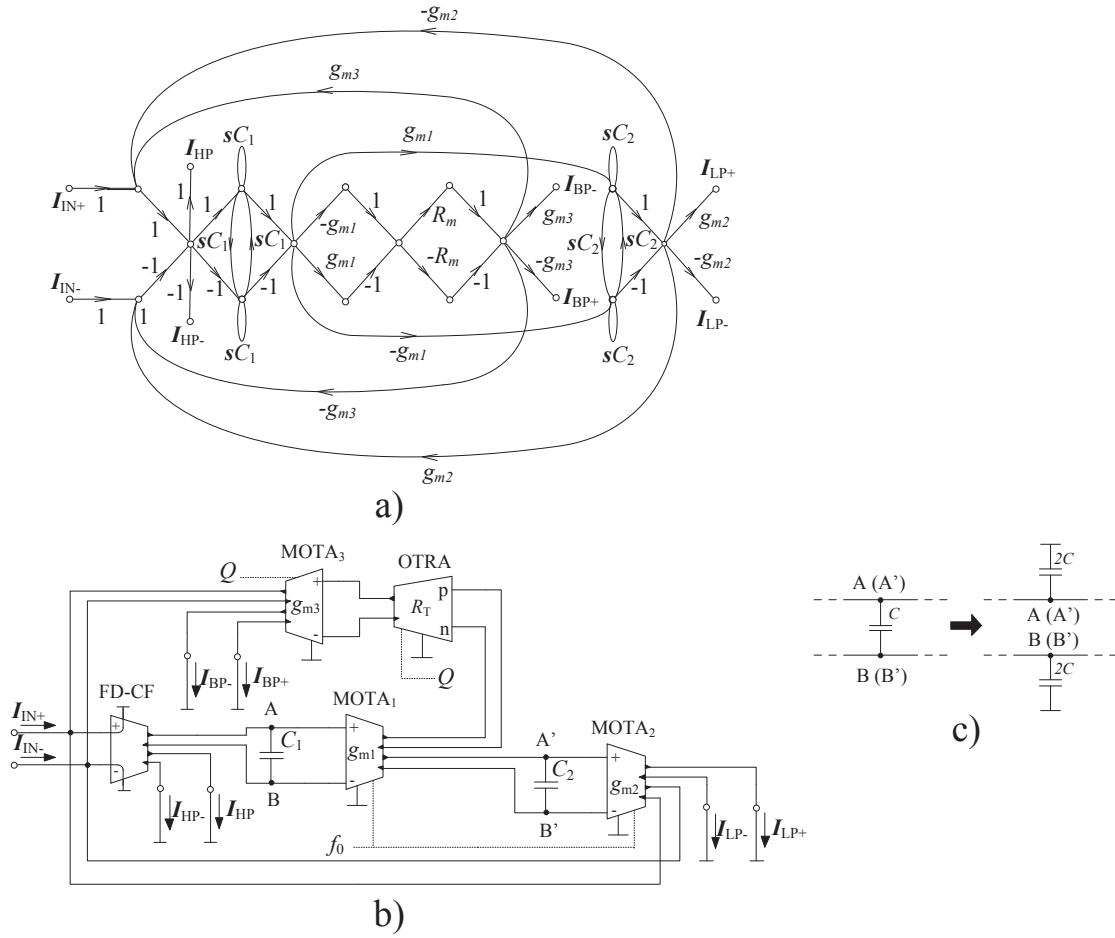


Figure 6.92 Fully-differential form of the proposed filter with three OTAs, one CF and one OTRA:
a) simplified M-C graph, b) circuit structure, c) implementation of non-floating capacitors

In order to obtain the same pole frequency of particular transfer functions for the F-D form of filter, transconductances g_{m1} g_{m2} must be twice higher than transconductances used for the S-E filter. To obtain the same quality factor of the filter for both S-E and F-D filter, values of transconductance g_{m3} used in case of the F-D filter must be twice the values of the S-E filter. The values of transresistance R_T of the F-D filter must be four times lower.

All obtainable transfer functions of these filters are given as follows:

$$\frac{I_{LP+}}{I_{IN}} = -\frac{I_{LP-}}{I_{IN}} = \frac{g_{m1}g_{m2}}{D}, \quad (6.123)$$

$$\frac{I_{BP+}}{I_{IN}} = -\frac{I_{BP-}}{I_{IN}} = \frac{sC_2g_{m1}g_{m3}R_T}{D}, \quad (6.124)$$

$$\frac{I_{HP+}}{I_{IN}} = -\frac{I_{HP-}}{I_{IN}} = \frac{s^2 C_1 C_2}{D}, \quad (6.125)$$

$$I_{BS} = \frac{I_{HP+} + I_{LP+}}{I_{IN}} = -\frac{I_{HP-} + I_{LP-}}{I_{IN}} = \frac{s^2 C_1 C_2 + g_{m1} g_{m2}}{D}, \quad (6.126)$$

$$\begin{aligned} I_{AP} &= \frac{I_{HP+} + I_{BP-} + I_{LP+}}{I_{IN}} = -\frac{I_{HP-} + I_{BP+} + I_{LP-}}{I_{IN}} = \\ &= \frac{s^2 C_1 C_2 - s C_2 g_{m1} g_{m3} R_T + g_{m1} g_{m2}}{D}. \end{aligned} \quad (6.127)$$

The equation (6.123) up to (6.127) prove that the proposed filter is universal because it provides all standard transfer functions. All transfer functions correspond with particular term of the denominator and they have the unity gain in pass band area regardless values of transconductances g_{m1} and g_{m2} g_{m3} and transresistance R_T . Also, all transfer functions can be obtained for both polarities.

6.10.2 Simulation and Experimental Results

In this particular case, the F-D form of the filter was not implemented. Therefore, the simulation and experimental results were carried out to verify appropriate function of the S-E proposed filter only.

Values of the specific filter parameters and passive parts for the PSpice simulations and experimental measurements have been stated accordingly: the starting pole frequency $f_0 = 500$ kHz, the starting value of the quality factor $Q = 0.707$ (Butterworth approximation), values of capacitors were chosen to be $C_1 = 470$ pF and $C_2 = 47$ pF. The values of the capacitances were set like this in order to acquire the same value of transconductance g_{m1} , g_{m2} , so it is easier to control the pole frequency of the filter. The values of transconductances g_{m1} and g_{m2} were calculated accordingly: $g_{m1,2} = 2\pi f_0 \sqrt{C_1 C_2} = 0.467$ mS. Thus, resistors of value of 2 k Ω which corresponds with transconductances of value 0.5 mS were selected. The starting pole frequency is then equal to 535.4 kHz. The starting value of transresistance R_T is equal to 510 Ω . Only transconductance g_{m3} remains to be determined. This parameter is calculated as follows: $g_{m3} = 1/(QR_T) \sqrt{(g_{m2} C_1)/(g_{m1} C_2)} = 8.77$ mS which is approximately 114 Ω . Therefore, a resistor of value 110 Ω has been used. Recalculated quality factor for these values is 0.682 .

Figure 6.93 shows the simulation and experimental results of low-pass, band-pass, high-pass and band-stop transfer functions of the S-E filter. High-pass transfer functions (blue lines) have the slope of attenuation of 38 dB per decade, band-pass functions (red lines) have 19 dB per decade and in case of low-pass transfer functions it is 40 dB per decade. The biggest attenuation of the band-stop function is -27 dB in case of the simulated results and -35 dB for the measured results. The slope of attenuation of independent transfer functions is almost the same for both simulation and measurement of the S-E filter. The measured results are affected mostly by input/output impedances (they are not low/high enough) of the active elements in the structure. The output impedance of the BOTA is the most dominant parasitic element mainly at lower frequencies because it is connected to node with C_2 . Internal node of the OTRA with R_T connected also significantly affects measured results at higher frequencies because output impedance of the first stage (CCII) is not high enough with respect to R_T values. The results are also affected by bandwidth limitations of used converters and parasitic capacitances of cables and PCB. That applies for all presented results.

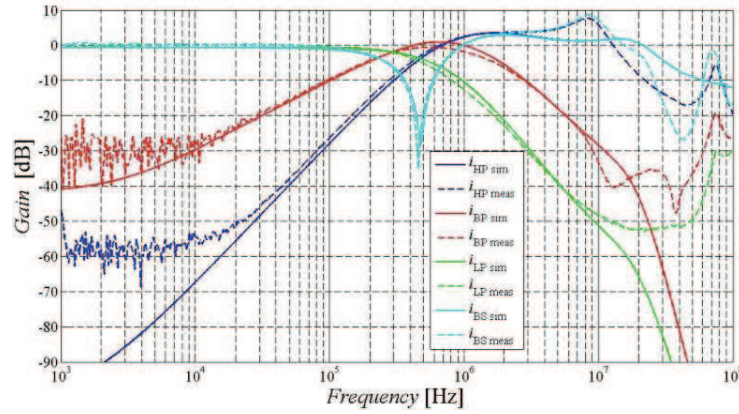


Figure 6.93 Comparison of transfer functions high-pass, band-pass, low-pass and band-stop of the S-E proposed filter from Fig. 6.91: simulation (solid lines) and experimental results (dashed lines)

The ability to control the pole frequency of the S-E filter is illustrated in Figure 6.94. LP transfer function was chosen as the example. The values of transconductances g_{m1} and g_{m2} were chosen 0.256 mS (3900 Ω), 0.5 mS (2000 Ω), 1 mS (1000 Ω). Table XXV summarizes values of simulated and measured pole frequencies. The values of pole frequencies obtained from simulations are closer to the theoretical values.

Table XXV Comparison of obtained values of the pole frequency

	$g_{m1,2}$ [mS]		
Frequency [kHz]	0.256	0.5	1
Calculated	274.6	535.4	1070.8
Simulated	232.2	464.2	1140.2
Measured	197.1	369.5	1335.2

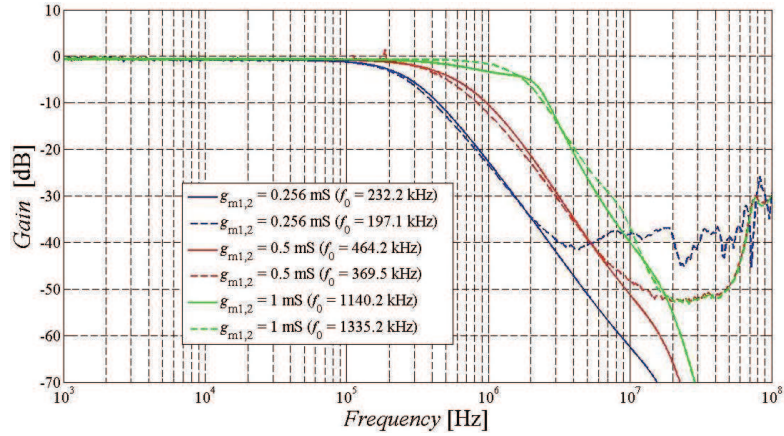


Figure 6.94 Demonstration of ability to control the pole frequency in case of the S-E filter from Fig. 6.91: simulation (solid lines) and experimental (dashed lines) results when g_{m1} and g_{m2} were set to 0.256 mS, 0.5 mS, 1 mS.

The simulation and experimental results of the ability to control the quality factor of the filter by changing the values of transconductance g_{m3} are shown in Figure 6.95. BP transfer function was chosen for the illustration. The values of transconductance g_{m3} were 9.09 mS (110 Ω), 4.55 mS (220 Ω) and 2.33 mS (430 Ω). The values of transresistance R_T is fixed to 510 Ω . Obtained values of the quality factor are included in Table XXVI. The measured results show slightly lower values of the quality factor than values obtained from simulations.

Table XXVI Comparison of obtained values of the quality factor

	g_{m3} [mS]		
Q [-]	9.09	4.55	2.33
Calculated	0.68	1.36	2.67
Simulated	0.50	1.37	3.22
Measured	0.47	1.10	2.83

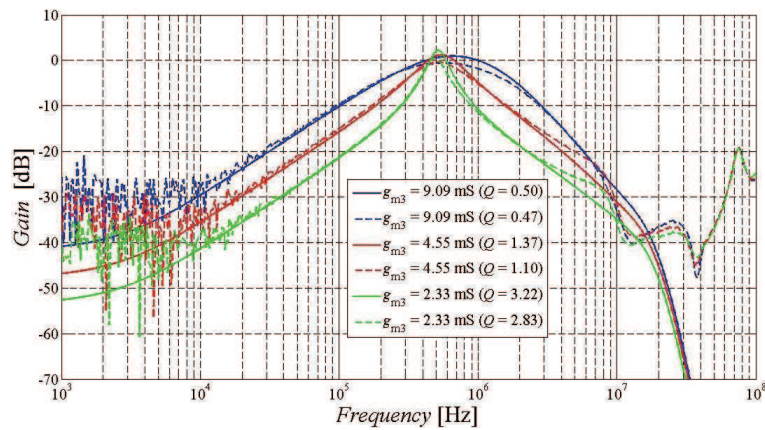


Figure 6.95 Demonstration of ability to control the quality factor in case of the S-E filter from Fig. 6.91: simulation (solid lines) and experimental (dashed lines) results when g_{m3} was set to 2.33 mS, 4.55 mS, 9.09 mS

Figure 6.96 illustrates the simulation and experimental results of band-pass transfer function of the S-E filter when adjusting the quality factor by changing values of transresistance R_T (g_{m3} is fixed to 9.09 mS). The values of R_T were 510 Ω , 255 Ω (parallel combination of two 510 Ω resistors) and 120 Ω . Table XXVII compares obtained values of the quality factor of the filter. It can be seen that the simulation results are closer to the theory for lower values of the quality factor.

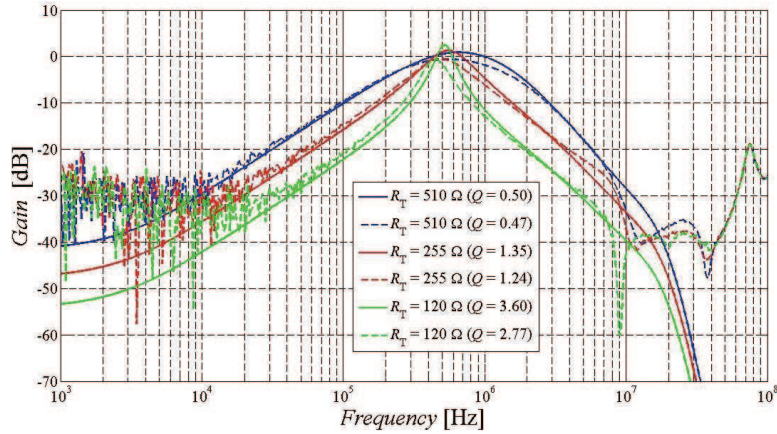


Figure 6.96 Demonstration of ability to control the quality factor in case of the S-E filter from Fig. 6.91: simulation (solid lines) and experimental (dashed lines) results when R_T was set to 510 Ω , 255 Ω , 120 Ω

Table XXVII Comparison of obtained values of the quality factor

	R_T [Ω]		
Q [-]	510	255	120
Calculated	0.68	1.36	2.90
Simulated	0.50	1.35	3.60
Measured	0.47	1.24	2.77

6.11 Concluding Summary of the Chapter

In this chapter, eight proposed second-order current-mode filtering structures in their S-E and also F-D form using CFs and OTAs as basic building blocks have been presented. Four proposals are supported by simulations and the rest four proposals are supported by simulations and also by experimental measurement of implemented filters. The first proposed S-E and F-D filter is supported by simulations and complemented with the sensitivity analysis of both S-E and F-D filter. The second S-E and F-D filter is supported by simulations. Simulations and parasitic analysis were carried out in case of the S-E and F-D filter from chapter 6.4. The next proposal contains simulations and sensitivity analysis of the S-E and F-D filter. The design correctness and functionality of the S-E and F-D filter from chapter 6.6 and 6.8 are proved by simulations and also experimental measurement. Chapter 6.9 contains simulations, experimental results and parasitic analysis of the S-E and F-D

proposed filter. The last presented filter is supported by simulations and experimental measurement of the S-E filter.

When comparing the S-E and F-D structures, the transfer functions of the F-D filters have a slightly steeper slope of attenuation than the S-E filters. This is given mainly because of halved values of resistors of the F-D structures in comparison to the S-E structures. From the schemes it is obvious that the F-D filters have a more complex circuit structure. From tables it can be seen that obtained pole frequencies of the F-D filters are usually closer to the theoretical values and the quality factors of F-D structures are closer to the theoretical values when the quality factors of F-D transfer functions are usually higher.

7 Proposal of Fractional-Order Filters

The proposed filters in this chapter were simulated using the transistor-level simulation models presented in chapter 5. Simulation models of all used active elements are implemented with 0.18 μm CMOS technology and the supply voltage for all these models is ± 1 V.

7.1 $(1+\alpha)$ -Order Low-Pass Filter with Three MO-CFs and Five ACAs

7.1.1 Filter proposal

The proposed filter is a fractional $(1+\alpha)$ -order low-pass filter with Butterworth characteristics using multi-output current followers and adjustable current amplifiers. The second-order approximation of Laplacian operator was used to propose the filter. The filter possesses ability to electronically control its order and also the pole frequency. It is based on Follow-the-Leader Feedback topology. It would be also possible to obtain high-pass transfer function by adding one MO-CF at the beginning of the circuit structure. Note that all parameters would have to be recalculated to obtain high-pass function. The section presents only the F-D fractional-order filter which is based on the previously presented S-E fractional-order filter from [142]. The description of the S-E filter and all made design steps are included only because of a comparison with the F-D structure and due to the fact that the reader can understand how the proposal of this filter in its S-E form was made.

The transfer function of a $(1+\alpha)$ -order low-pass Butterworth filter is given as [117]:

$$K_{1+\alpha}^{LP}(s) = \frac{k_1}{s^\alpha (s + k_2) + k_3}, \quad (7.1)$$

where

$$k_1 = 1, \quad (7.2)$$

$$k_2 = 1.0683\alpha^2 + 0.161\alpha + 0.3324, \quad (7.3)$$

$$k_3 = 0.2937\alpha + 0.71216. \quad (7.4)$$

Coefficients k_1 , k_2 and k_3 are used in order to shape the pass band region while keeping the desired fractional-order slope of attenuation of the stop band region [117].

Using the second-order approximation of fractional Laplacian operator, a $(1+\alpha)$ -order low-pass transfer function turns into [117]:

$$K_{1+\alpha}^{LP}(s) \cong \frac{k_1}{a_0} \frac{a_2 s^2 + a_1 s + a_0}{s^3 + b_2 s^2 + b_1 s + b_0}, \quad (7.5)$$

where

$$\begin{aligned} a_0 &= \alpha^2 + 3\alpha + 2 \\ a_1 &= 8 - 2\alpha^2, \\ a_2 &= \alpha^2 - 3\alpha + 2 \end{aligned} \quad (7.6)$$

and

$$\begin{aligned} b_0 &= \frac{a_0 k_3 + a_2 k_2}{a_0} \\ b_1 &= \frac{a_1(k_2 + k_3) + a_2}{a_0} \\ b_2 &= \frac{a_1 + a_0 k_2 + a_2 k_3}{a_0} \end{aligned} \quad (7.7)$$

Using the transfer function given in (7.5), it is possible to create a block diagram of a fractional-order low-pass filter. Figure 7.1 illustrates a resulting block diagram of given filter when Follow-the-Leader Feedback topology has been used.

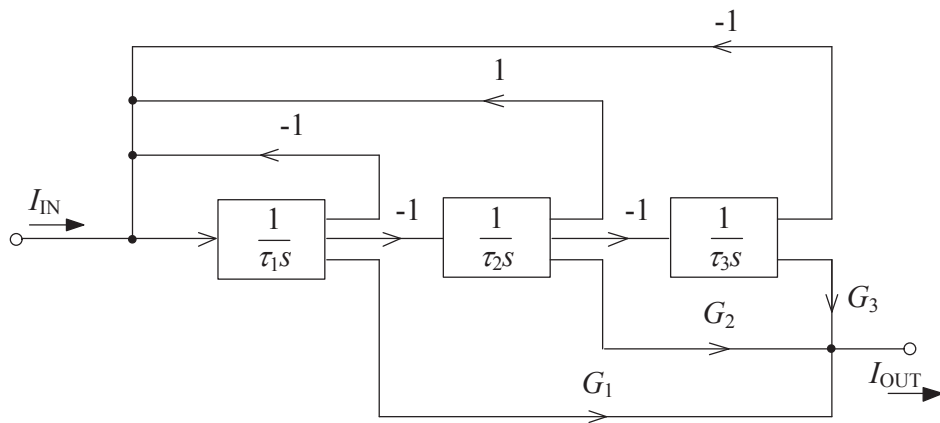


Figure 7.1 Block diagram of the third-order FLF topology filter leading to $(1 + \alpha)$ -order low-pass filter

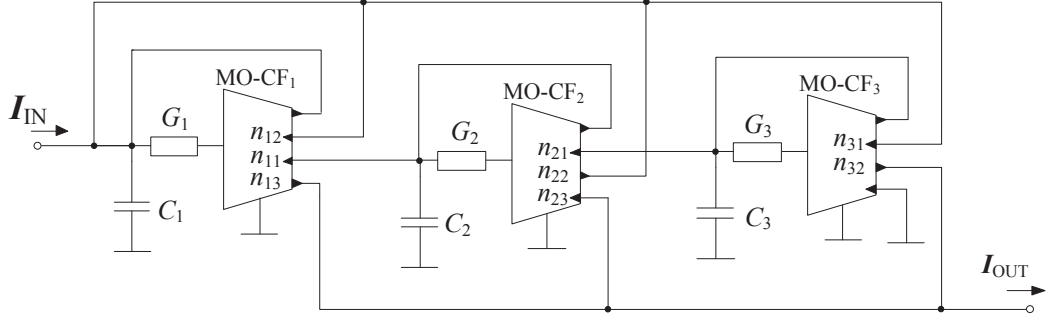


Figure 7.2 Initial circuit structure of the proposed S-E $(1 + \alpha)$ -order low-pass filter

The transfer function of this block diagram is:

$$K(s) = \frac{I_{OUT}}{I_{IN}} = \frac{\frac{G_1}{\tau_1} s^2 + \frac{G_2}{\tau_1 \tau_2} s + \frac{G_3}{\tau_1 \tau_2 \tau_3}}{s^3 + \frac{1}{\tau_1} s^2 + \frac{1}{\tau_1 \tau_2} s + \frac{1}{\tau_1 \tau_2 \tau_3}}. \quad (7.8)$$

The values of G and τ parameters can be determined when comparing particular terms of equations (7.5) and (7.8). These values then define transfers of individual branches of the proposed filter.

The circuit structure of the fractional $(1+\alpha)$ -order low-pass filter can be then designed based on the block diagram in Figure 7.1. The designed S-E filter constructed by three MO-CF elements with designated transfers of individual branches (from n_{11} to n_{32}) is shown in Figure 7.2.

Transfers (n_{11} to n_{32}) can be calculated the same way as parameters G and τ . These transfers then determine the resulting order of the transfer function.

The transfer function of the filter is described by the following relation:

$$K(s) = \frac{I_{OUT}}{I_{IN}} = \frac{N(s)}{D(s)}, \quad (7.9)$$

where

$$N(s) = G_1 C_2 C_3 n_{13} s^2 + G_1 G_2 C_3 n_{11} n_{23} s + G_1 G_2 G_3 n_{11} n_{21} n_{32}, \quad (7.10)$$

$$D(s) = C_1 C_2 C_3 s^3 + G_1 C_2 C_3 n_{12} s^2 + G_1 G_2 C_3 n_{11} n_{22} s + G_1 G_2 G_3 n_{11} n_{21} n_{31}. \quad (7.11)$$

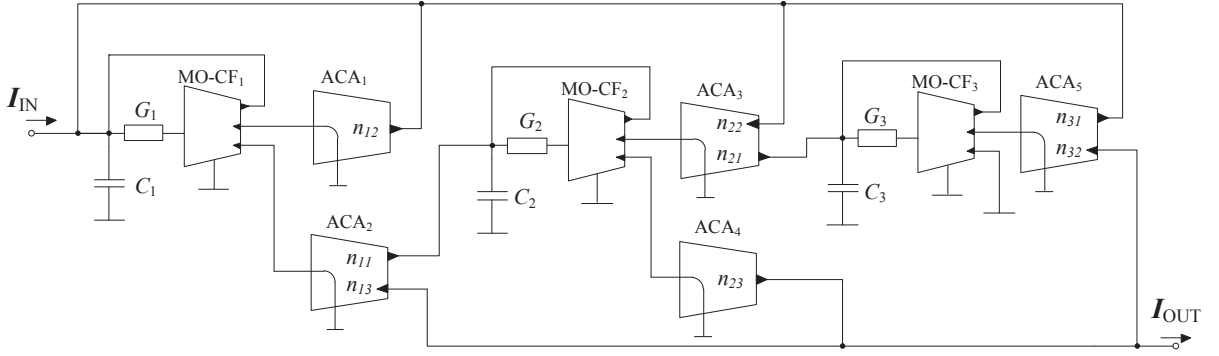


Figure 7.3 Modified circuit structure of the S-E proposed $(1 + \alpha)$ -order low-pass filter

There are multiple ways how to set transfers of individual branches of the proposed filter, for example, by combination of resistors of specific values using current dividers (when the value of each transfer is smaller than 1), or different types of current amplifiers (if we do not want to be restricted by values smaller than 1 and consequently, being restricted in values of orders and pole frequencies which can be obtained). As it is obvious from equations (7.10) and (7.11) it would be necessary to use eight current amplifiers for this particular design. Therefore, the calculation of the transfers has been made that way so some transfers (n_{11} with n_{13} , n_{21} with n_{22} and n_{31} with n_{32} , respectively) have the same value and can be combined in order to decrease number of active elements in the final circuit structure. This modified circuit structure of the proposed filter is presented in Figure 7.3. It consists of three MO-CFs, three resistors, three grounded capacitors and five ACAs.

The F-D form of the proposed $(1 + \alpha)$ -order low-pass filter is shown in Figure 7.4. It consists of three FD-CFs and five ACAs. It was created from the S-E structure by mirroring passive parts. The values of current gains B of the F-D filter must be a half of the values used for the S-E filter. The F-D filter was proposed with grounder capacitors which must have twice the value of capacitors used in the S-E filter. The values of parameters G_1 , G_2 and G_3 are also twice higher in comparison to the values used for the S-E filter.

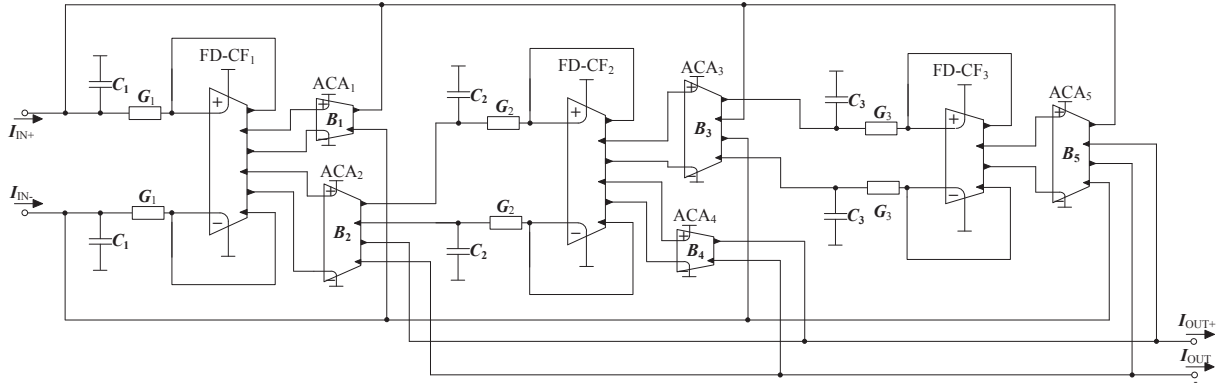


Figure 7.4 Circuit structure of the F-D proposed $(1 + \alpha)$ -order low-pass filter

7.1.2 Simulation results

To verify functionality of the proposed S-E and F-D filter, Pspice simulations using transistor-level models described in chapter 5 were carried out. Selected starting values of passive parts and parameters of the filter were set as follows: the starting pole frequency equals 100 kHz, default order 1.5 ($\alpha = 0.5$), values of resistors $R_1 = R_2 = R_3 = 2 \text{ k}\Omega$ and capacitors $C_1 = 75 \text{ pF}$, $C_2 = 43 \text{ pF}$ and $C_3 = 390 \text{ pF}$.

The proposed filter possesses ability to electronically control its order by changing values of transfers n_{11} to n_{32} . This ability was tested for three different values of parameter α (0.2, 0.5, 0.8). Table XXVIII summarizes values of used passive parts and calculated values of transfers n_{11} to n_{32} for selected values of parameter α .

Table XXVIII Used values of passive parts and transfers n_{11} - n_{32} for selected values of parameter α

α [-]	0.2	0.5	0.8
C_1 [pF]	75		
C_3 [pF]	43		
C_3 [pF]	390		
$R_1 = R_2 = R_3$ [k Ω]	2		
$n_{11} = n_{13}$ [-]	0.0483	0.0177	0.0042
n_{12} [-]	0.3387	0.2500	0.2234
$n_{21} = n_{22}$ [-]	0.3799	0.8300	3.0248
n_{23} [-]	0.2794	0.5080	1.4217
$n_{31} = n_{32}$ [-]	0.1121	0.1398	0.1628

Figure 7.5 shows a comparison of the simulation results of the S-E filter and the theory for these chosen values. The values of passive parts and transfers n_{11} - n_{32} were taken from Table XXVIII. Theoretical values of the slope of attenuation (dashed lines) for chosen values of α and values of the slope of attenuation obtained from simulations (solid lines) corresponding with these chosen values of parameter α are compared in Table XXIX. From

the table it is obvious that the values of the slope of attenuation obtained from simulations are in good agreement with the theory except the value for order 1.8 where the slope of attenuation was steeper than the theoretical expectations. That is mainly given by already too small value of transfer n_{11} , n_{13} respectively. Nonetheless, the simulation results confirm the proper design of the S-E $(1 + \alpha)$ -order low-pass filter.

Table XXIX Theoretical and simulated values of the slope of attenuation of the proposed S-E filter

α [-]	0.2	0.5	0.8
Theoretical slope of attenuation [dB/dec]	24.0	30.0	36.0
Simulated slope of attenuation [dB/dec]	23.8	29.4	37.9

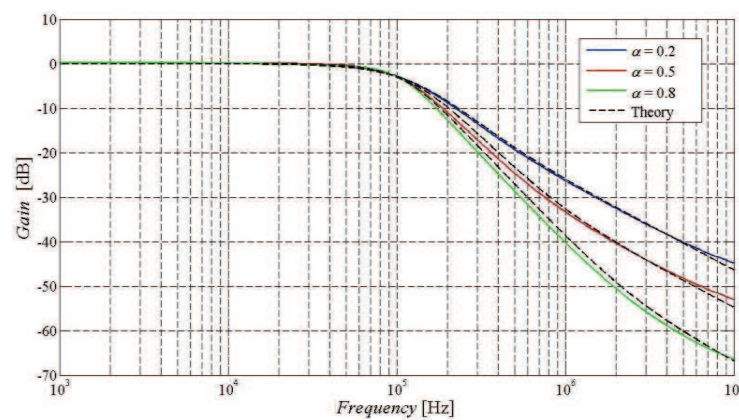


Figure 7.5 Comparison of theoretical and simulated S-E transfer functions when α was set to 0.2, 0.5 and 0.8

A comparison of simulation results of the S-E and F-D filter when changing its order is depicted in Figure 7.6. The values of parameter α were set as stated above. The obtained slopes of attenuation of the transfer function of the S-E and F-D filter for these chosen values are summarized in Table XXX. The values of the slope of attenuation of the F-D are almost the same as values obtained from the S-E filter.

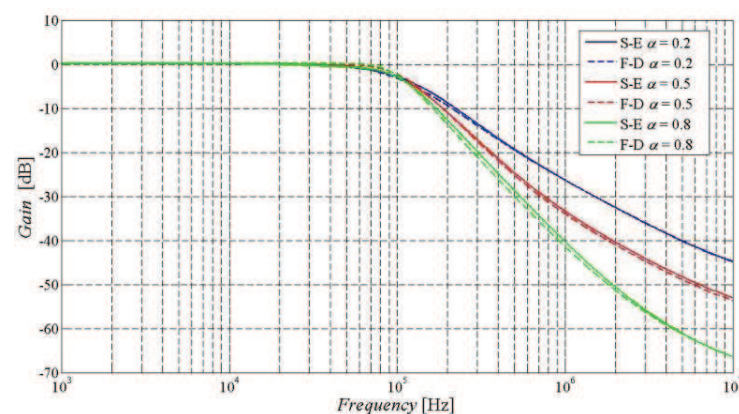


Figure 7.6 Comparison of simulated transfer functions of the S-E filter from Fig. 7.3 (solid lines) and the F-D filter from Fig. 7.4 (dashed lines) when α was set to 0.2, 0.5, and 0.8

Table XXX Comparison of obtained slopes of attenuation

α [-]	0.2	0.5	0.8
Simulated slope of attenuation S-E [dB/dec]	23.8	29.4	37.9
Simulated slope of attenuation F-D [dB/dec]	23.1	29.9	37.6

Figure 7.7 compares simulation results of the S-E and F-D filter when changing the pole frequency. The pole frequency of the S-E and F-D filter can be either controlled electronically by changing values of transfers n_{11} - n_{32} , or it can be controlled by changing values of passive parts. Ability to control the pole frequency electronically was chosen for the illustration since the electronic control is more advantageous. The selected values of the pole frequency are 50 kHz, 100 kHz and 200 kHz when the order of the filter is fixed to 1.5 ($\alpha = 0.5$). The used values of passive parts and transfers n_{11} to n_{32} are stated in Table XXXI. Obtained values of the pole frequency are compared in Table XXXII. From the table can be seen that the obtained values of the pole frequency are close to the theoretical values.

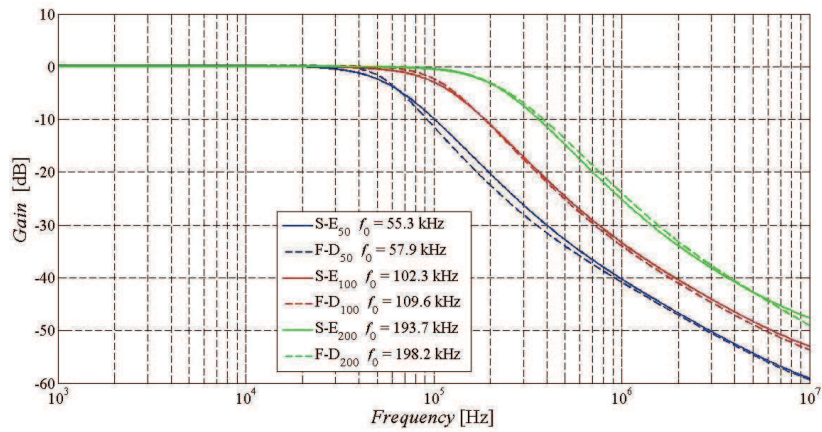


Figure 7.7 Comparison of ability to control the pole frequency of the S-E filter from Fig. 7.3 (solid lines) and the F-D filter from Fig. 7.4 (dashed lines)

Table XXXI Used values of passive parts and transfers n_{11} - n_{32} for selected values of f_0

f_0 [kHz]	50	100	200
C_1 [pF]	75		
C_2 [pF]	43		
C_3 [pF]	390		
$R_1 = R_2 = R_3$ [k Ω]	2		
$n_{11} = n_{13}$ [-]	0.0089	0.0177	0.0354
n_{12} [-]	0.1250	0.2500	0.5000
$n_{21} = n_{22}$ [-]	0.4150	0.8300	1.6600
n_{23} [-]	0.2540	0.5080	1.0160
$n_{31} = n_{32}$ [-]	0.0699	0.1398	0.2796

Table XXXII Comparison of obtained pole frequencies

f_0 [kHz]	50	100	200
Simulated pole frequency S-E [kHz]	55.3	102.3	193.7
Simulated pole frequency F-D [kHz]	57.9	109.6	198.2

7.2 $(1+\alpha)$ -Order Low-Pass Filter with Three OTAs Two ACAs and One CF

7.2.1 Filter proposal

The proposal is focused on the design of a S-E and F-D $(1+\alpha)$ -order low-pass filter with Butterworth characteristics which employs three OTAs two ACAs and one CF. I present this research in [143]. The proposed filter is based on Inverse Follow-the-Leader Feedback topology. The initial design procedure of this filter is the same as for the filter in chapter 7.1 (all the way from equation (7.1) to equation (7.7)). A possible block diagram of a $(1+\alpha)$ -order low-pass filter based on IFLF topology is illustrated in Figure 7.8.

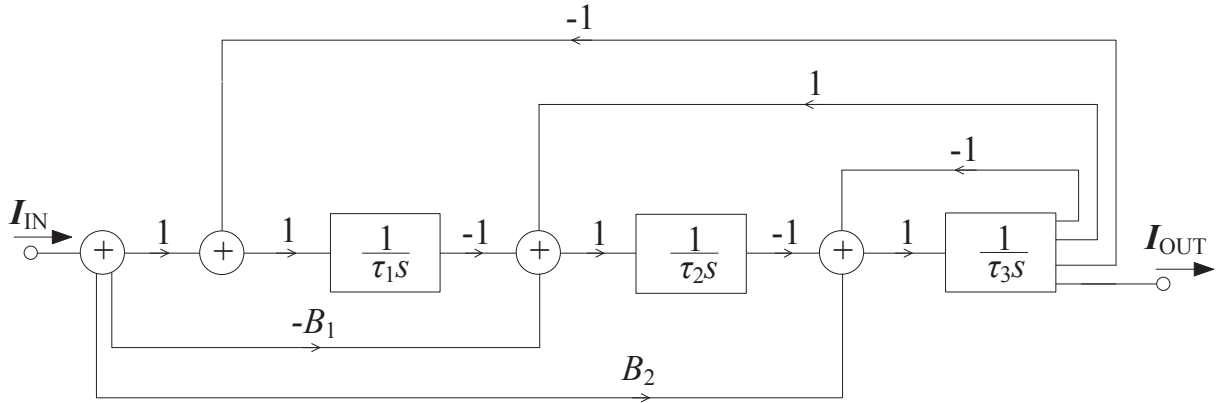


Figure 7.8 Block diagram of the third-order IFLF topology filter leading to $(1 + \alpha)$ -order low-pass filter

The transfer function of this block diagram is given as:

$$K(s) = \frac{I_{OUT}}{I_{IN}} = \frac{\frac{B_2}{\tau_3} s^2 + \frac{B_1}{\tau_2 \tau_3} s + \frac{1}{\tau_1 \tau_2 \tau_3}}{s^3 + \frac{1}{\tau_3} s^2 + \frac{1}{\tau_2 \tau_3} s + \frac{1}{\tau_1 \tau_2 \tau_3}}. \quad (7.12)$$

The values of B and τ parameters can be determined when comparing particular terms of equations (7.5) and (7.12).

Figure 7.9 shows the circuit structure of the fractional $(1+\alpha)$ -order low-pass filter which is based on the block diagram from Figure 7.8. It consists of two OTAs, two ACAs, one MOTA and one MO-CF. Thus, the proposed filter contains of six active elements. It would be possible to reduce the number of active elements by two in case the parameters B_1 and B_2 were set solely passively (by current dividers), however that would narrow the range of the adjustability of these parameters and also it would not be possible to control order of the filter electronically as shown later.

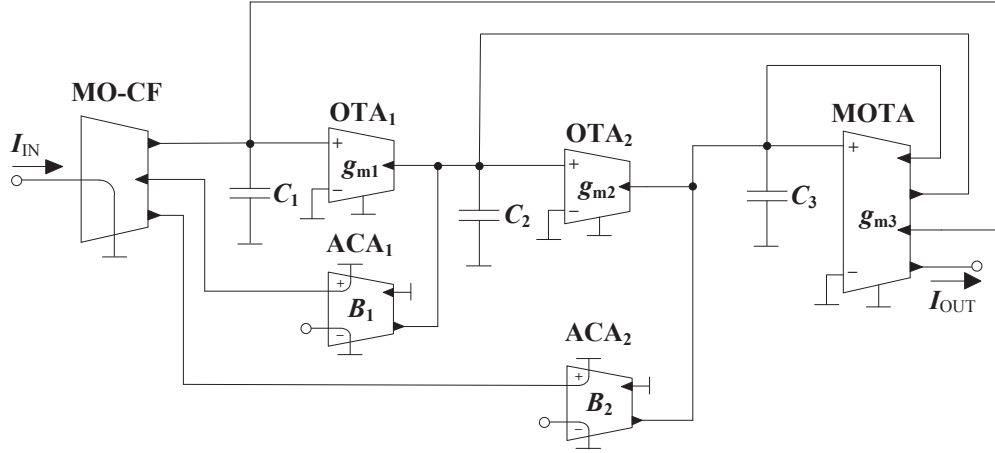


Figure 7.9 Single-ended form of the proposed S-E $(1 + \alpha)$ -order low-pass filter

The transfer function of the proposed S-E and F-D filter is given by the following relation:

$$K(s) = \frac{I_{OUT}}{I_{IN}} = \frac{N(s)}{D(s)}, \quad (7.13)$$

where

$$N(s) = C_1 C_2 g_{m3} B_2 s^2 + C_1 g_{m2} g_{m3} B_1 s + g_{m1} g_{m2} g_{m3}, \quad (7.14)$$

$$D(s) = C_1 C_2 C_3 s^3 + C_1 C_2 g_{m3} s^2 + C_1 g_{m2} g_{m3} s + g_{m1} g_{m2} g_{m3} n_{31}. \quad (7.15)$$

The F-D form of the proposed $(1 + \alpha)$ -order low-pass filter is presented in Figure 7.10. The F-D filter was created from the S-E filter by mirroring of passive parts. It consists of two BOTAs, one MOTA, two ACAs and one FD-CF. The values of current gains B of the F-D filter must be half of the values used for the S-E filter. The F-D filter is proposed with grounded capacitors instead of floating ones. These capacitors must have twice the value of capacitors of the S-E filter.

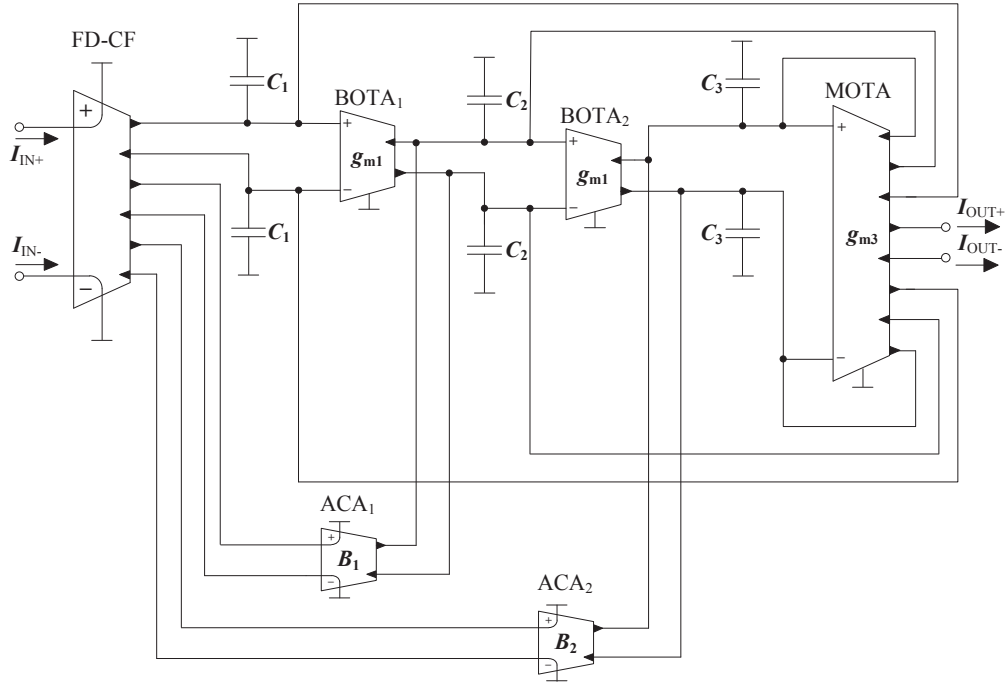


Figure 7.10 Fully-differential form of the proposed $(1 + \alpha)$ -order low-pass filter

7.2.2 Simulation results

Pspice simulations of the S-E and F-D filter were performed using transistor-level models described in chapter 5. The values of passive and active elements were selected accordingly: capacitors $C_1 = 820$ pF, $C_2 = C_3 = 560$ pF, the starting pole frequency is equal to 100 kHz, starting value of the filter order is 1.5 ($\alpha = 0.5$), transconductances $g_{m1} = 146$ μ S, $g_{m2} = 376$ μ S, $g_{m3} = 934$ μ S and current gains $B_1 = 0.6$ and $B_2 = 0.068$.

The proposed S-E and F-D filter possesses ability to electronically control the order of the filter by changing values of transconductances g_{m1} , g_{m2} , g_{m3} and transfers B_1 and B_2 . This ability was simulated for five values of parameter α (0.1, 0.3, 0.5, 0.7, 0.9). Calculated values of passive and active elements for chosen values of parameter α are given in Table XXXIV.

Table XXXIII Used values of passive and active elements for selected values of parameter α

α [-]	0.1	0.3	0.5	0.7	0.9
C_1 [pF]	820				
$C_2 = C_3$ [pF]	560				
g_{m1} [μ S]	112	133	147	174	210
g_{m2} [μ S]	340	370	370	417	417
g_{m3} [μ S]	1499	1181	909	909	954
B_1 [-]	0.76	0.7	0.61	0.515	0.428
B_2 [-]	0.17	0.117	0.07	0.033	0.008

Figure 7.11 shows a comparison of the simulation results of the S-E and F-D filter when changing its order. The values of passive and active elements used for the simulations are summarized in Table XXXIII. The obtained slopes of attenuation of the transfer function of the S-E and F-D filter for selected values of parameter α can be compared in Table XXXIV. The values of the slope of attenuation of the F-D filter are closer to the theoretical values.

Table XXXIV Comparison of obtained slopes of attenuation

α [-]	0.1	0.3	0.5	0.7	0.9
Theoretical slope of attenuation [dB/dec]	22.0	26.0	30.0	34.0	38.0
Simulated slope of attenuation S-E [dB/dec]	20.8	25.5	30.2	34.5	36.6
Simulated slope of attenuation F-D [dB/dec]	21.2	26.0	30.6	34.4	37.0

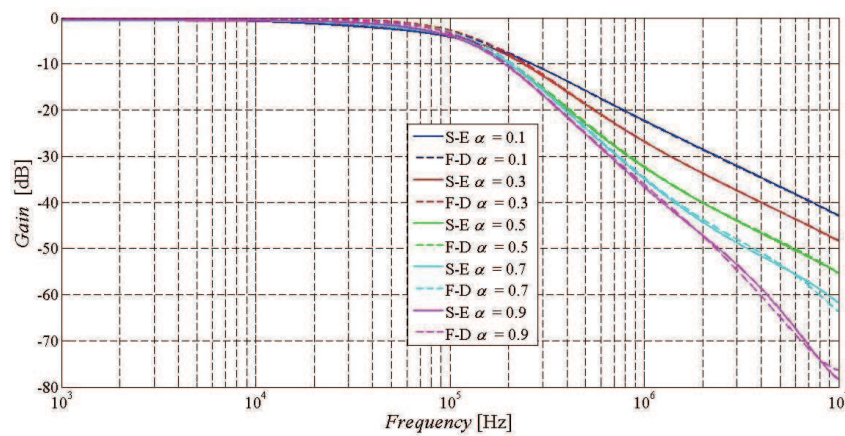


Figure 7.11 Comparison of simulated transfer functions of the S-E filter from Fig. 7.9 (solid lines) and the F-D filter from Fig. 7.10 (dashed lines) when α was set to 0.1, 0.3, 0.5, 0.7 and 0.9

A comparison of phase responses of the transfer functions from Figure 7.11 are illustrated in Figure 7.12. It can be seen that the phase responses correspond with the particular order. For example, the phase response of 1.1 order ends slightly above 90 degrees, or the phase response of 1.3 order is getting close to 117 degrees etc.

A comparison of the simulation results of the S-E and F-D filter when changing the pole frequency can be seen in Figure 7.13. The values of the pole frequency selected for the illustration are 50 kHz, 75 kHz, 100 kHz, 150 kHz and 200 kHz when the order of the filter is fixed to 1.5 ($\alpha = 0.5$). The used values of passive and active elements are stated in Table XXXV. Obtained values of the pole frequency are compared in Table XXXVI. The obtained pole frequencies of the F-D filter are closer to the theoretical values. The values of the pole frequency of the F-D filter are slightly above the theoretical values when the values of the S-E filter are lower. This fact is being more evident with increasing frequency.

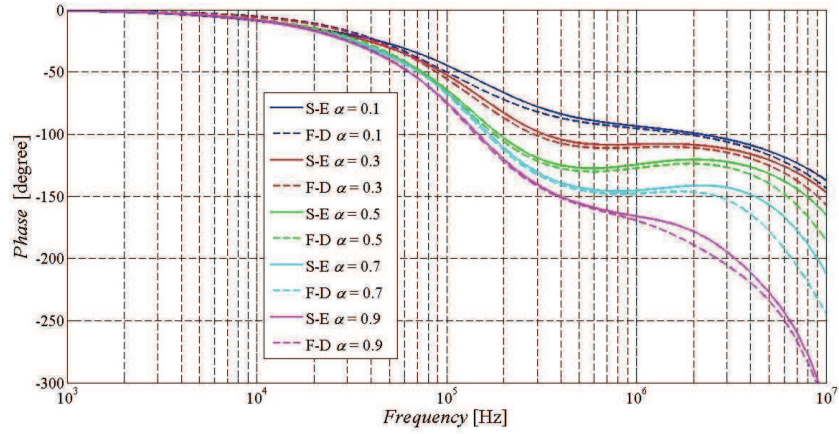


Figure 7.12 Comparison of phase responses of the S-E filter from Fig. 7.9 (solid lines) and the F-D filter from Fig. 7.10 (dashed lines) when controlling the order

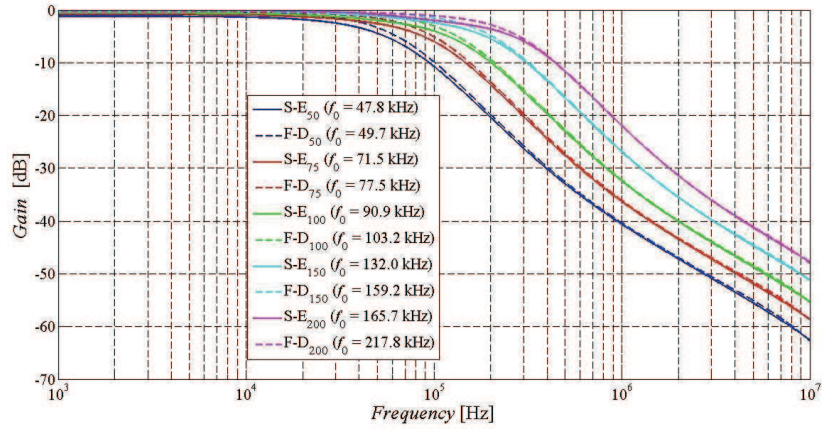


Figure 7.13 Comparison of ability to control the pole frequency of the S-E filter from Fig. 7.9 (solid lines) and the F-D filter from Fig. 7.10 (dashed lines)

Table XXXV Used values of passive parts and transfers n_{11} - n_{32} for selected values of f_0

f_0 [kHz]	50	75	100	150	200
C_1 [pF]	820				
$C_2 = C_3$ [pF]	560				
g_{m1} [μ S]	74	110	147	220	294
g_{m2} [μ S]	182	278	370	556	769
g_{m3} [μ S]	465	667	909	1333	1818
B_1 [-]	0.61				
B_2 [-]	0.07				

Table XXXVI Comparison of obtained pole frequencies

f_0 [kHz]	50	75	100	150	200
Simulated slope of attenuation S-E [dB/dec]	47.8	71.5	90.9	132.0	165.7
Simulated slope of attenuation F-D [dB/dec]	49.7	77.5	103.2	159.2	217.8

Figure 7.14 shows phase responses corresponding with the transfer functions from Figure 7.13. Bigger differences between the responses of the S-E and F-D filter can be seen at higher frequencies.

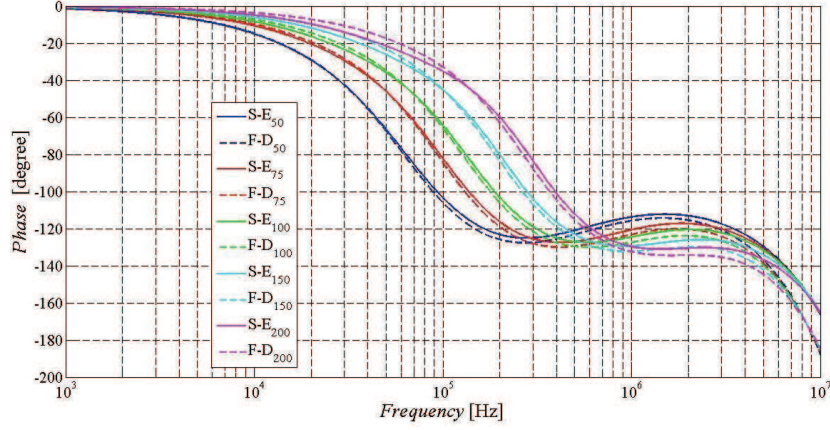


Figure 7.14 Comparison of phase responses of the S-E filter from Fig. 7.9 (solid lines) and the F-D filter from Fig. 7.10 (dashed lines) when controlling the pole frequency

7.3 Concluding Summary of the Chapter

This chapter includes two structures of a fractional-order LP frequency filters. The first filter is proposed in its F-D form based on the previously proposed fractional-order filter. The second filter is proposed in the S-E and F-D variant. The filters are proposed with CFs, OTAs and ACAs as active elements. Both filters possess ability to electronically control their order and pole frequency. The simulation results were obtained using transistor-level simulation models of used active elements.

The obtained results confirm the possibility to propose this type of filters in their F-D form. Furthermore, the obtained results of F-D structures show that both pole frequencies and orders of the F-D filters are closer to the theoretical values than in case of the S-E filters.

8 Modified Design Method

This chapter presents a modified version of the horizontal structures transformation method described in chapter 1. This modified design method is intended for frequency filters using current followers as basic building blocks. An adjustment of the method so it is suitable for filters employing OTAs can be easily made. To transform for example a partial structure from Figure 8.1 a) into a corresponding F-D structure using the transformation of horizontal structures, the passive components placed in the horizontal branches of the circuit are being mirrored. In this case it means the resistor (conductance G) is mirrored around the CF. As mentioned before if the horizontal components are resistors, the values of these resistors of a resulting F-D circuit have half the value (that is $2G$ if the resistors are denoted as conductances) of the resistors of the S-E circuit when the values and positions of vertical components (capacitor C) stay unchanged as shown in Figure 8.1 b). The disadvantage of this method is that originally grounded capacitor C turns into a floating capacitor which is not suitable for implementation and integrability of such a circuit. Therefore, the next logical step of the transformation into the F-D structure is to replace the floating capacitor by grounded capacitors (one for each branch of the F-D structure) as used in case of implementation of proposed filters in chapters 6.6, 6.8, 6.9 and 6.10 and as demonstrated in Figure 8.1 c). This is one additional step of the design which must be taken into consideration. The values of these capacitors are twice as high as used values of capacitors of the S-E structure. Note that we have ended up with doubled values of conductances and capacitances to compensate the F-D transfer function in comparison to the initial values of passive components of the S-E structure. Thus the slope of attenuation of individual transfer functions of the F-D structure is going to be slightly steeper because of lower values of resistors used for the S-E and F-D structures. In case of a comparison of S-E and F-D structures when this approach is used we are actually trying to compare a slightly different transfer functions and consequently receive less information when comparing the S-E and F-D structures.

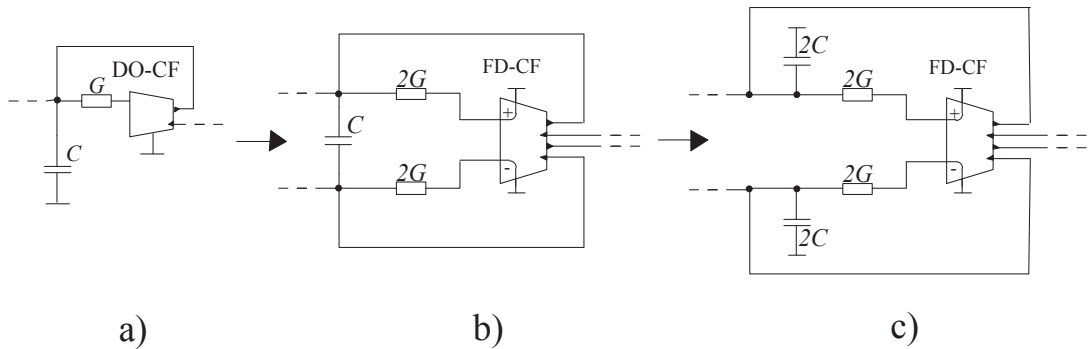


Figure 8.1 Design steps: a) initial S-E structure, b) the F-D structure created by the transformation of horizontal structures, c) the F-D structure with grounded capacitors

When using the transformation of horizontal structures, the values of the mirrored resistors of the F-D structure must have halved values to compensate the pole frequency of the F-D. Then again when splitting the floating capacitor into two grounded ones, the values of these capacitors need to be adjusted due to halved values of resistors of the F-D structure in comparison to the S-E structure so the pole frequency of the resulting F-D transfer function stays the same as the pole frequency of the S-E function. The modified transformation method takes these facts into consideration. The modified method is considering the grounded capacitors of the F-D structure right from the beginning and thus, the values of resistors and capacitors of the F-D structure can stay the same as values of passive elements of the S-E structure. Figure 8.2 illustrates the transformation of the same S-E structure from Figure 8.1 using the modified method. The transformation consists of one step when the resulting F-D structure in Figure 8.2 b) already contains the grounded capacitors and all passive components have the same values as the passive components of the S-E structure. This way, it is possible that the slope of attenuation of the F-D transfer functions is more like the slope of attenuation of the S-E transfer functions than it is in case of the original transformation of horizontal structures as shown later. The modified method was tested in case of ten simulated filters and six implemented filters and in each case proved to be more suitable for the design of F-D filters than the original transformation of horizontal structures. Chosen results are included for the illustration.

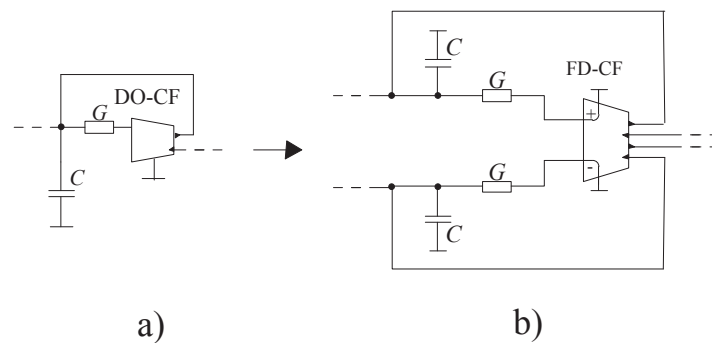


Figure 8.2 Design steps: a) initial S-E structure, b) the F-D structure created by the modified design method

That the transfer function of the F-D structure from Figure 8.1 c) created based on the horizontal structures transformation method and the F-D structure from Figure 8.2 b) based on the modified method is the same is supported mathematically using M-C graphs. Figure 8.3 depicts simplified M-C graphs of the F-D structure from Figure 8.1 c) and the F-D structure from Figure 8.2 b).

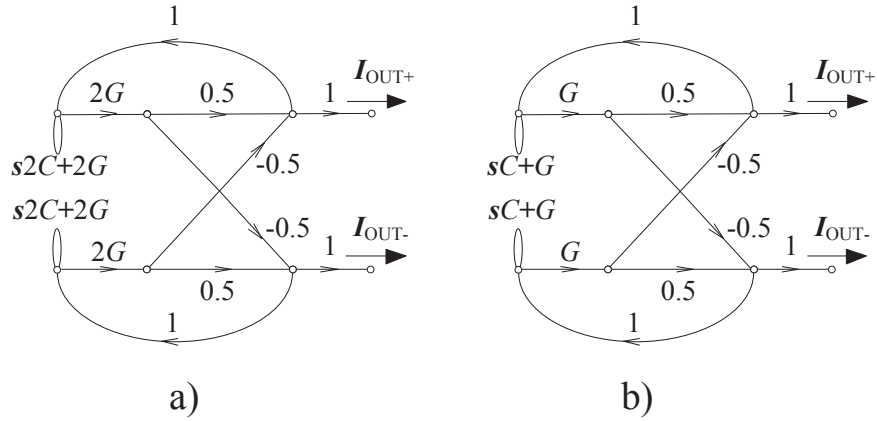


Figure 8.3 Simplified M-C graph: a) of the F-D structure from Figure 8.1 c), b) of the F-D structure from Figure 8.2 b)

The denominator of the simplified M-C graph from Figure 8.3 a) is calculated as:

$$\begin{aligned}
 D(s) &= (s2C + 2G) \cdot (s2C + 2G) - (0.5 \cdot 2G \cdot (s2C + 2G)) - (0.5 \cdot 2G \cdot (s2C + 2G)) - \\
 &- (-0.5 \cdot -0.5 \cdot 2G \cdot 2G) + 0.5 \cdot 0.5 \cdot 2G \cdot 2G = 4s^2C^2 + 4sCG + 4sCG + 4G^2 - 2sCG - \quad (8.1) \\
 &- 2G^2 - 2sCG - 2G^2 - G^2 + G^2 = 4s^2C^2 + 4sCG.
 \end{aligned}$$

The numerator of the corresponding F-D structure (when taking the response from the outputs of the FD-CF) is:

$$N(s) = 4sCG + 4G^2. \quad (8.2)$$

As can be seen all terms of the denominator and numerator contain "4" which will cancel each other and the resulting transfer of the F-D structure from Figure 8.1 c) is given as:

$$K(s) = \frac{sCG + G^2}{s^2C^2 + sCG}. \quad (8.3)$$

The denominator of the simplified M-C graph of the F-D structure from Figure 8.2 b) shown in Figure 8.3 b) is calculated as:

$$\begin{aligned}
 D(s) &= (sC + G) \cdot (sC + G) - (0.5 \cdot G \cdot (sC + G)) - (0.5 \cdot G \cdot (sC + G)) - \\
 &- (-0.5 \cdot -0.5 \cdot G \cdot G) + 0.5 \cdot 0.5 \cdot G \cdot G = s^2C^2 + sCG + sCG + G^2 - 0.5sCG \quad (8.4) \\
 &- 0.5G^2 - 0.5sCG - 0.5G^2 - 0.25G^2 + 0.25G^2 = s^2C^2 + sCG.
 \end{aligned}$$

The numerator of the corresponding F-D structure (when taking the response from the outputs of the FD-CF) is:

$$N(s) = sCG + G^2. \quad (8.5)$$

The resulting transfer of this F-D structure is given as:

$$K(s) = \frac{sCG + G^2}{s^2C^2 + sCG}. \quad (8.6)$$

It can be seen that the transfers of the F-D structure from Figure 8.1 c) created using the horizontal structures transformation method and the F-D structure from Figure 8.2 b) based on the modified method presented in the equations (8.3) and (8.6) are identical and the modified design method can be used instead of the transformation of horizontal structures without any change in the transfer of the resulting F-D structure.

Figure 8.4 shows a comparison of the simulations of BP transfer function of the filter from chapter 6.2. The values of passive elements and filter parameters were the same as stated in chapter 6.2. The S-E transfer function is presented by blue line, the transfer function of the F-D structure created by the transformation of horizontal structures (conductances of the S-E filter were replaced by $2G$) when the F-D structures contains floating capacitors as show in Figure 8.1 b) is represented by green line, the function of the same structure with grounded capacitors (having the twice the value of the floating capacitors) is presented by cyan line, the red line represents the transfer function obtained when using the modified design method. From the graph can be seen that the function obtained when using the modified design method better follows the S-E transfer function. Also the attenuation of the this transfer function at lower frequencies is better than in case of the transfer function of the F-D created by the transformation of horizontal structures.

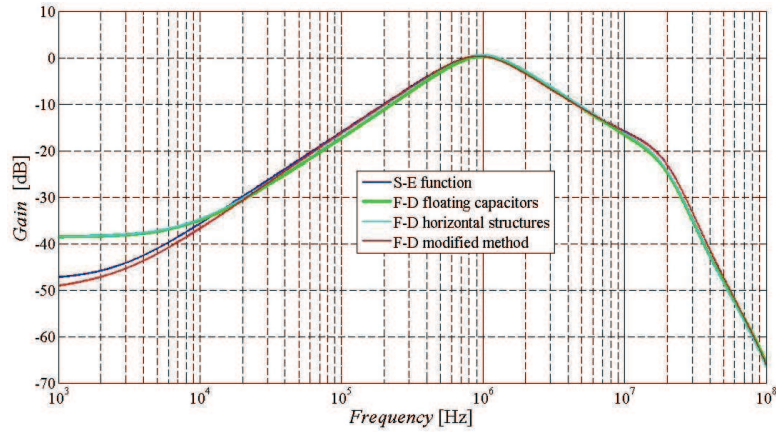


Figure 8.4 Comparison of simulated BP function of the proposed filter from chapter 6.2: S-E transfer function (blue line), F-D function obtained after the transformation of horizontal structures with floating capacitors (green line), F-D function obtained after the transformation of horizontal structures with grounded capacitors (cyan line), F-D function obtained using the modified method (red line)

Figure 8.5 compares the DC function of obtained BP transfer functions from Figure 8.4. The DC function of the BP transfer function of the F-D filter created using the modified method better follows the DC function of the S-E BP function. Also the linearity of this DC function is greater than in case of other two F-D structures.

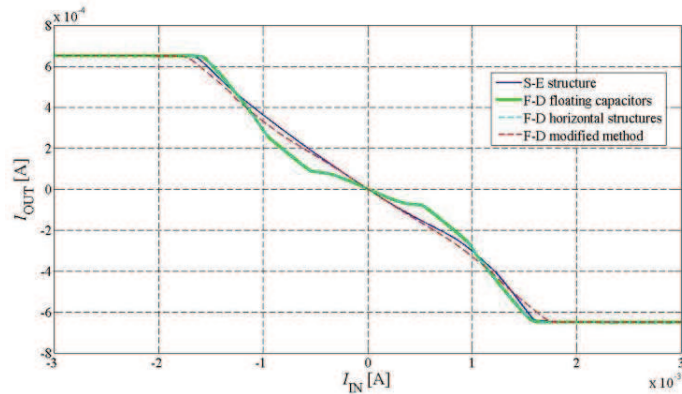


Figure 8.5 Comparison of simulated DC function of BP function of the proposed filter from chapter 6.2: S-E transfer function (blue line), F-D function obtained after the transformation of horizontal structures with floating capacitors (green line), F-D function obtained after the transformation of horizontal structures with grounded capacitors (cyan line), F-D function obtained using the modified method (red line)

A comparison of the simulation results of HP transfer function of the proposed filter from chapter 6.4 is depicted in Figure 8.6. The values of passive elements and specific filter parameters correspond with those used in chapter 6.4. The representation of individual transfer functions is the same as for Figure 8.4. It can be seen that the F-D transfer function obtained when using the modified method can better follow the S-E transfer function and it has greater attenuation at lower frequencies.

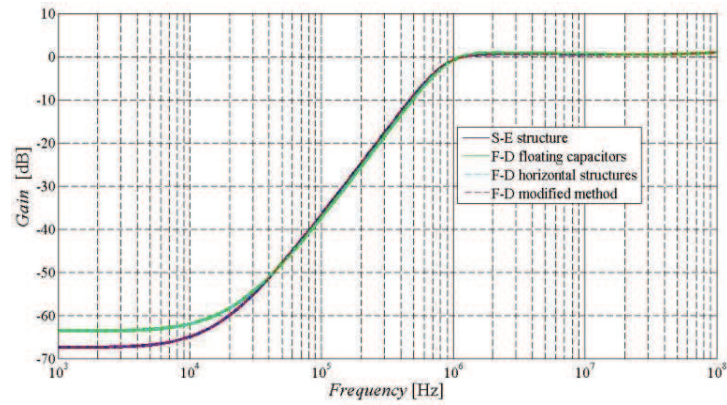


Figure 8.6 Comparison of simulated HP function of the proposed filter from chapter 6.4: S-E transfer function (blue line), F-D function obtained after the transformation of horizontal structures with floating capacitors (green line), F-D function obtained after the transformation of horizontal structures with grounded capacitors (cyan line), F-D function obtained using the modified method (red line)

Figure 8.7 compares the simulation results of LP transfer function of the proposed filter from chapter 6.6. The values of passive elements and specific filter parameters have the same values as stated in chapter 6.6. The transfer functions are represented the same way as in case of Figure 8.4 and Figure 8.6. By comparison, the transfer function obtained from the F-D structure created by the modified method has slightly lower attenuation at higher frequencies than the transfer function from the F-D structure when using the transformation of the horizontal structures, but it is more consistent with the slope of attenuation of the S-E transfer function. Figure 8.8 shows phases of the illustrated LP transfer functions from Figure 8.7. It can be seen that the phase of LP function which is obtained from the F-D structure created by the modified method can better follow the phase of the S-E structure.

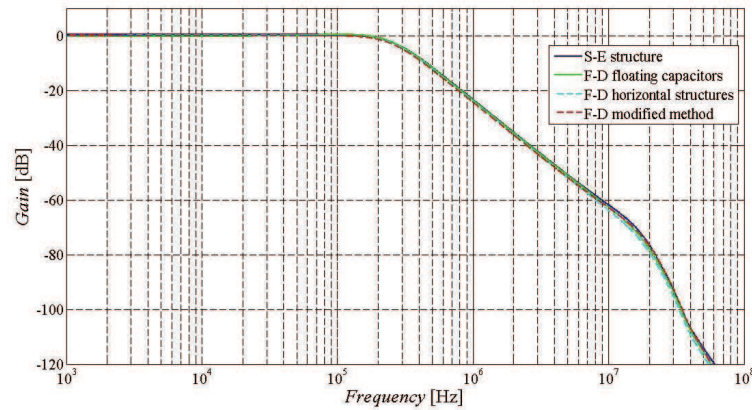


Figure 8.7 Comparison of simulated LP function of the proposed filter from chapter 6.6: S-E transfer function (blue line), F-D function obtained after the transformation of horizontal structures with floating capacitors (green line), F-D function obtained after the transformation of horizontal structures with grounded capacitors (cyan line), F-D function obtained using the modified method (red line)

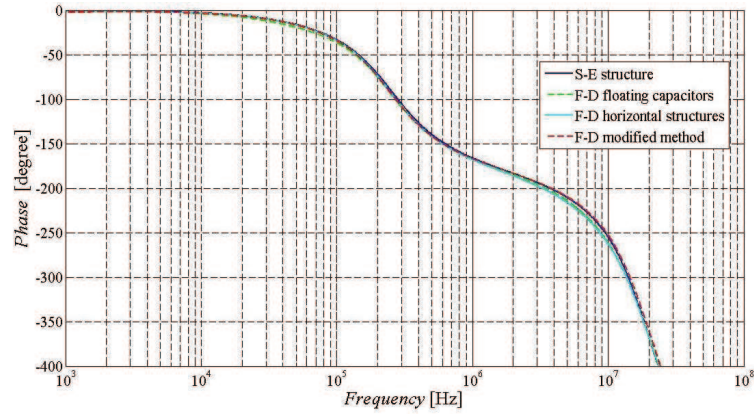


Figure 8.8 Comparison of phases of simulated LP function of the proposed filter from chapter 6.6: S-E transfer function (blue line), F-D function obtained after the transformation of horizontal structures with floating capacitors (green line), F-D function obtained after the transformation of horizontal structures with grounded capacitors (cyan line), F-D function obtained using the modified method (red line)

The simulation results of LP transfer functions of the filter from chapter 6.5 are compared in Figure 8.9. The values of passive elements and specific filter parameters have the same values as described in chapter 6.5 except the values of current gains of the DACA elements which were in case of the S-E filter set to $A_1 = A_2 = 2$ (half values for the F-D structure). From the graph can be seen that the transfer function obtained when using the modified design method better follows the S-E transfer function.

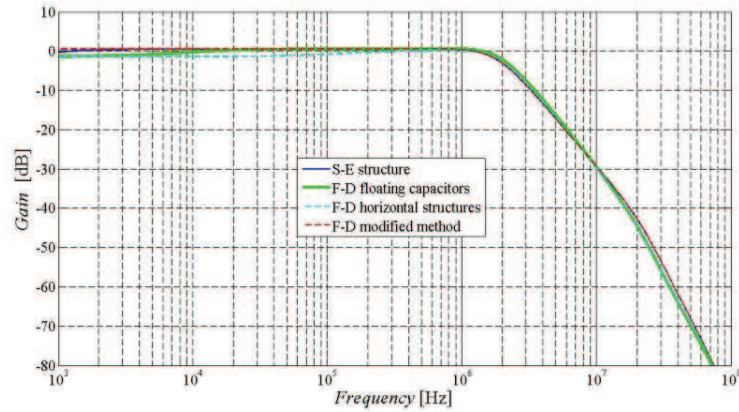


Figure 8.9 Comparison of simulated LP functions of the proposed filter from chapter 6.5: S-E transfer function (blue line), F-D function obtained after the transformation of horizontal structures with floating capacitors (green line), F-D function obtained after the transformation of horizontal structures with grounded capacitors (cyan line), F-D function obtained using the modified method (red line)

Figure 8.10 shows a comparison of measured LP transfer functions of the filter from chapter 6.5. The values of passive elements and specific filter parameters are the same as stated for transfer functions in Figure 8.9. The transfer function of the S-E filter is represented by blue line, the transfer function of the F-D structure created by the transformation of horizontal structures with grounded capacitors by green line and the transfer function obtained from the F-D structure created by the modified method is represented by red line. It can be seen

that the transfer function obtained from the F-D structure created by the transformation of horizontal structures has a slightly higher slope of attenuation than the S-E transfer function. The slopes of attenuation of the S-E transfer function and the transfer function obtained when using the modified method are nearly identical.

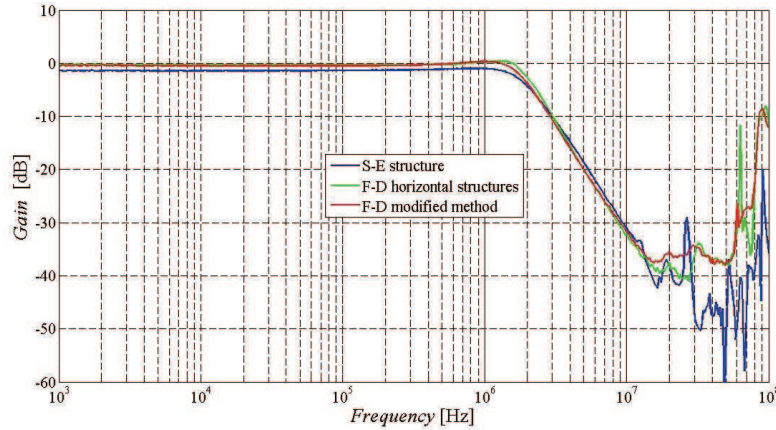


Figure 8.10 Comparison of measured LP functions of the proposed filter from chapter 6.5: S-E transfer function (blue line), F-D function obtained after the transformation of horizontal structures with grounded capacitors (green line), F-D function obtained using the modified method (red line)

9 Conclusion

The thesis was mainly aimed at the proposal of fully-differential frequency filters working in the current mode and employing non-standard active elements. Great emphasis was paid to a comparison of the F-D structures and their corresponding S-E forms. The work was divided into three main parts namely the proposal of new second-order current-mode filtering structures especially fully-differential ones, the proposal of fractional-order frequency filters in both single-ended and fully-differential forms and finally a modification of the transformation of horizontal structures design method with respect to the specific needs and characteristics of differential structures. The design correctness and functionality of the proposed filters are verified by SNAP program, PSpice simulations and in some cases also by experimental measurement. Chapter 1 gives an overview of the basics and development in the field of analogue filtering structures. The main goals of the thesis are stated in chapter 2. Chapter 3 provides definition of single-ended and fully-differential current transfers. Chapter 4 describes signal-flow graphs (SFGs) design method which was used to propose the presented filters. Used active elements are described in chapter 5. Chapters 6 and 7 present the proposed filtering structures. The last chapter presents the modified design method and gives a comparison of obtained results together with horizontal structures transformation method.

Chapter 6 contains eight proposed second-order current-mode filtering structures in their S-E and also F-D form. In principle, all proposed filters are SIMO type filters which can provide

all (or at least more than one) transfer functions without a necessity to change the circuit structure or position of the input current. The first five filters based on current followers. The remaining three filtering structures are based on operational transconductance amplifiers as basic building blocks allowing to control the pole frequency and quality factor of the filter. The determinants of proposed filters have been chosen that way it is possible to control the pole frequency, quality factor of the filter, or both by suitable placement of digitally adjustable current amplifiers or operational transresistance amplifiers in the circuit structure as graphically demonstrated in the thesis. Differential structures were transformed from single-ended structures using the transformation of horizontal structures by mirroring passive components around the active elements, or in some cases also by mirroring active elements. The output response are always obtained directly from high-impedance outputs of used active elements so it is not necessary to obtain any of the output responses that would flow through the passive components, which is not, in case of implementation, appropriate. Since the floating capacitors are not suitable for implementation, all F-D filters are proposed with grounded capacitors. From the graphs it is obvious that the transfer functions of the differential filters have slightly higher slope of attenuation than in case of single-ended filters. This is mainly due to the fact that the F-D filters are using resistors of half values than the S-E filters. This fact then leads to the modification of the horizontal structures transformation method presented in chapter 8. From the measurement results of the possibility to control the pole frequency and quality factor of the S-E and F-D filter is possible to observe that the obtained pole frequencies of the F-D filters are usually closer to the theoretical values than in case of the S-E filters. Furthermore, the quality factors of F-D transfer functions are higher than the quality factors of S-E transfer function which are closer to the theoretical values. From the perspective of the author, the filter from chapter 6.8 is the most advantageous in case of implementation of the proposed filter in an integrated form because it can provide all standard transfer functions in both polarities, requires only four active elements and allows to electronic control its pole frequency and quality factor. Furthermore, the terms of each transfer function correspond with particular terms of the denominator thus, the individual transfer functions have the unity gain regardless the values of adjustable parameters. Filters from chapter 6.9 and 6.10 are advantageous because they possess dual parameter control of their quality factors so it is possible to adjust the quality factor in a wider range without reaching the parameter limitations. The filters based on current followers require additional active elements in order to provide the controllability of some of the filter parameter(s) which increases the number of used active elements and resulting circuit complexity. Therefore these filters are less advantageous in case of implementation of the proposed filters in an integrated form. All filters can seem rather complex, but the circuit structure of each filter can be adjusted for particular application (unused terminals can be removed, the number of active elements can be lowered in case of requirement of only some transfer function etc.).

Chapter 7 presents the proposal of two fractional order filters. One in its F-D and the second one in its S-E and F-D form. The first proposed filter is based on current followers and the second one on operational transconductance amplifiers. The proposal of the F-D structures is made the same way as in chapter 6. The possibility to propose these filters in their F-D form has been proved and the proposed F-D structures provide better properties as shown in case of controllability of the order and pole frequency of the filters when both slope of attenuation for individual values of parameter α and pole frequency of the F-D filter are closer to the theoretical values.

Finally chapter 8 presents the modified horizontal structures transformation method which was adjusted with respect to the specific needs and characteristics of differential structures. The modified method is intended for filtering structures using current followers. Its practical applicability was tested on ten simulated filters and six implemented filters and then compared with results obtained from the corresponding F-D structures created using the original horizontal structures transformation method and the corresponding S-E forms of these filters.

The research described in this work was adequately presented to the scientific community, as an author or coauthor I have published:

- 4 papers in impact factor journals (Advances in Electrical and Computer Engineering, Indian Journal of Engineering and Materials Sciences, Circuits Systems and Signal Processing, Journal of Circuits, Systems, and Computers)
- 4 papers in proceedings of international conferences (WSEAS Circuits, Systems, Control, Signals, Telecommunications and Signal Processing, Applied Electronics)
- 1 paper in international non-impact journal (WSEAS Transactions on Circuits)
- 7 papers in national non-impact journals (Elektrorevue, International Journal of Advances in Telecommunications, Electrotechnics, Signals and Systems)
- 6 papers in proceedings of national conferences (student IEEE)
- furthermore, I'm an author of 2 pedagogical texts.

References

- [1] CHANG C. M., AL-HASHIMI B. M., WANG C. L., HUNG C. W., Single fully differential current conveyor biquad filters, *In Proc. IEE Circuits, Devices and Systems*, 2003, vol. 150, Issue 5, pp. 394-398.
- [2] SOLIMAN A. M., Generation and classification of Ker-win–Huelsman–Newcomb circuits using the DVCC, *Int. J. Circ. Theor. Appl.*, 2009, vol. 37, pp. 835-855.
- [3] GHOSH M., PAUL S. K., RANJAN R. K., RANJAN A., Third Order Universal Filter Using Single Operational Transresistance Amplifier, *Journal of Engineering*, 2013, vol. 2013, pp. 1-6.
- [4] BEG P., KHAN I. A., MAHESHWARI S., SIDDIQI M. A., Digitally Programmable Fully Differential Filter, *Radioengineering*, 2011, vol. 20, no. 4, pp. 917-925.
- [5] TANGSRITAT W., Novel current-mode and voltage-mode universal biquad filters using single CFTA, *Indian Journal of Engineering and Materials Sciences*, 2010, vol. 17, pp. 99-104.
- [6] KACAR F., YESIL A., FDCCII-based electronically tunable voltage-mode biquad filter, *Int. J. Circ. Theor. Appl.*, 2012, vol. 40, pp. 377-383.
- [7] HERENC SAR N., VRBA K., Obecný přístup k návrhu kmitočtových filtrů pomocí autonomních obvodů" (The Common Approach to Frequency Filters Design Based on Autonomous Circuits), *Elektrorevue*, 2006, no. 40, pp. 40-1 - 40-17.
- [8] KOTON J., VRBA K., Electronically Tunable Frequency Filters Based on Transformation Cells, In *Proc. The 3rd International Conference Systems*, 2008, Cancun, Mexico, pp. 260-264.
- [9] KACAR F., MENEKAY S., Realization of a CMOS Current Differencing Buffer Amplifier and Its Filter Application, In *Proc. The 7th International Conference Electrical and Electronics Engineering*, 2011, Bursa, Turkey, pp. 337-340.
- [10] HERENC SAR N., VRBA K., Current conveyors-based circuits using novel transformation method, *IEICE Electronics Express*, 2007, vol. 4, no. 21, pp. 650-656.
- [11] ABUELMA'ATTI M. T., BENTRACIA A., A novel mixed-mode OTA-C universal filter, *International Journal of Electronics*, 2005, vol. 92, issue 7, pp. 375-383.
- [12] HORNG J. W., Current-Mode and Transimpedance-Mode Universal Biquadratic Filter using Multiple-Output CCII, *Indian Journal of Engineering and Materials Sciences*, 2010, vol. 17, no. 3, pp. 169-174.
- [13] PANDEY N., PAUL S. K., BHATTACHARYYA A., JAIN S. B., A new mixed mode biquad using reduced number of active and passive elements, *IEICE Electronics Express*, 2006, vol. 3, no. 6, pp. 115-121.
- [14] JERABEK J., KOTON J., SOTNER R., VRBA K., Adjustable band-pass filter with current active elements: two fully-differential and single-ended solutions, *Analog integrated circuits and signal processing*, 2013, vol. 74, no. 1, pp. 129-139.
- [15] SENANI R., GUPTA S. S., Current-Mode Universal Biquad Using Current Followers: A Minimal Realization, *Radioengineering*, 2011, vol. 20, no. 4, pp. 898-904.
- [16] JERABEK J., VRBA K., Řiditelný univerzální filtr s vícevýstupovými proudovými sledovači (A Controllable Universal Filter Using Multi-Output Current Followers), *Elektrorevue*, 2008, no. 35, pp. 35-1 - 35-10.

- [17] KOTON J., HERENC SAR N., VRBA K., JERABEK J., Digitally Adjustable Current Amplifier and its Application in Fully Differential Current-Mode Band-Pass Filter Design, *Elektrorevue*, 2010, no. 90, pp. 47-52.
- [18] PRASERTSOM D., TANGSRIRAT W., CMOS Digitally Controlled Current Follower and Its Application, *In Proc. of the 12th International Symposium on Integrated Circuits, ISIC '09*, 2009, Singapore, Republic of Singapore, pp. 486-489.
- [19] JERABEK J., SOTNER R., VRBA K., Tunable universal filter with current follower and transconductance amplifiers and study of parasitic influences, *Journal of Electrical Engineering*, 2011, vol. 62, no. 6, pp. 317-326.
- [20] TANGSRIRAT W., PRASERTSOM D., Electronically tunable low-component-count current-mode biquadratic filter using dual-output current followers, *Electr. Eng.*, 2007, vol. 90, pp. 33-37.
- [21] JERABEK J., SOTNER R., VRBA K., Comparison of the SITO Current-Mode Universal Filters Using Multiple-Output Current Followers, *In Proc. of The 35th International Conference on Telecommunications and Signal Processing*, 2012, Prague, Czech Republic, pp. 406-410.
- [22] JERABEK J., SOTNER R., VRBA K., KOUDAR I., Plně diferenční univerzální a říditelný filtr s proudovými aktivními prvky", (A Fully-Differential Universal Tunable Filter with Current Active Elements) *Elektrorevue*, 2010, no. 7, pp. 7-1 - 7-6.
- [23] JERABEK J., SOTNER R., VRBA K., Fully-differential current amplifier and its application to universal and adjustable filter, *In Proc. International Conference Applied Electronics (AE)*, 2010, Pilsen, Czech Republic, pp. 1-4.
- [24] KUBANEK D., VRBA K., Second-Order Multifunction Filter with Fully Differential Current Follower, *In Proc. International Conference Electrical and Electronics Engineering. 2009 ELECO*, 2009, Bursa, Turkey, pp. II-252 - II-255.
- [25] JERABEK J., VRBA K., Design of Fully Differential Filters with Basic Active Elements Working in the Current Mode, *Elektrorevue*, 2010, vol. 2010, no. 87, pp. 1-5.
- [26] YUCE E., Current-mode electronically tunable biquadratic filters consisting of only CCCIs and grounded capacitors, *Microelectronics Journal*, 2009, vol. 40, issue, pp. 1719-1725.
- [27] KUMNGERN M., Multiple-input single-output current-mode universal filter using translinear current conveyors, *Journal of Electrical and Electronics Engineering Research*, 2011, vol. 3, no. 9, pp. 162-170.
- [28] CHEN H., Current-mode dual-output ICCI-based tunable universal biquadratic filter with low-input and high-output impedances, *International Journal of Circuit Theory and Applications*, 2014, vol. 42, issue 4, pp. 376-393.
- [29] SOLIMAN A. M., Current mode filters using two output inverting CCII, *Int. J. Circ. Theor. Appl.*, 2008, vol. 36, pp. 875-881.
- [30] CHUNHUA W., HAIGUANG L., YAN Z., Universal current-mode filter with multiple inputs and one output using MOCCII and MO-CCCA, *International Journal of Electronics and Communications (AEÜ)*, 2009, vol. 63, pp. 448-453.
- [31] YUCE E., KIRCA Y. A., TOKAT S., Universal resistorless current-mode filters employing CCCIs, *Int. J. Circ. Theor. Appl.*, 2008, vol. 36, pp. 739-755.
- [32] CHEN H. P., CHU P. L., Versatile Universal Electronically Tunable Current-Mode Filter Using CCCII, *IEICE Electronic Express*, 2009, vol. 6, no. 2, pp. 122-128.

- [33] HORNG J. W., WU C. M., HERENC SAR N., Three-Input-One-Output Current-Mode Universal Biquadratic Filter Using One Differential Difference Current Conveyor, *Indian Journal of Pure and Applied Physics*, 2014, vol. 52, pp. 556-562.
- [34] KOTON J., HERENC SAR N., VRBA K., Single-Input Three-Output Current-Mode Filter Using Dual-Output Current Conveyors, *In Proc. Int. Conference on Electrical and Electronics Engineering - ELECO 2009*, 2009, Bursa, Turkey, pp. II-263-II-266.
- [35] CHANG C., HUANG T., TU S., HOU C., HORNG J., Universal Active Current Filter Using Single Second-Generation Current Controlled Conveyor, *Circuits Systems and Signal Processing*, 2008, vol. 1 no. 2, pp. 129-133.
- [36] SAGBAS M., FIDABOYLU K., Electronically tunable current-mode second order universal filter using minimum elements, *Electronics Letters*, 2004, vol. 40, issue 1, pp. 2-4.
- [37] JERABEK J., SOTNER R., VRBA K., Tiso Adjustable Filter with Controllable Controlled-Gain Voltage Differencing Current Conveyor, *Journal of Electrical Engineering*, 2014, vol. 65, issue 3, pp. 137-143.
- [38] SOTNER R., JERABEK J., SEVCIK B., DOSTAL T., VRBA K., Novel Solution of Notch/All-pass Filter with Special Electronic Adjusting of Attenuation in the Stop Band, *Elektronika ir Elektrotechnika*, 2011, vol. 113, no.7, pp. 37-42, 2011.
- [39] MINAEI' S., IBRAHIP M. A., KUNTUAN H., A New Current-Mode KHN-Biquad Using Differential Voltage Current Conveyor Suitable for IF Stages, *In Proc. The 7th International Symposium Signal Processing and Its Applications*, 2003, Paris, France, Vol. 1, pp. 249-252.
- [40] CHEN H., Tunable versatile current-mode universal filter based on plus-type DVCCs, *International Journal of Electronics and Communications (AEÜ)*, 2012, vol. 66, issue 4, pp. 332-339.
- [41] TEMIZYUREK C., MYDERRIZI I., Current-Mode Universal Filter Implemented with DVCCs, *In Proc. of The International Conference on Electrical and Electronics Engineering*, 2003, Bursa, Turkey, pp. 3-7.
- [42] JERABEK J., VRBA K., JELINEK M., Universal Fully-Differential Adjustable Filter with Current Conveyors and Current Amplifier in Comparison with Single-Ended Solution, *In Proc. of The 2011 International Conference on Applied Electronics*, 2011, Pilsen, Czech Republic, pp. 189-192.
- [43] CHEN H., WANG S., LI P., CHOU N., CHANG C., Single FDCCII-based current-mode universal biquadratic filter, *In Proc. The 2nd International Conference Consumer Electronics, Communications and Networks (CECNet)*, 2012, Yichang, China, pp. 2076-2079.
- [44] GÜR F., ANDAY F., Simulation of a novel current-mode universal filter using FDCCIIs, *Analog Integrated Circuits and Signal Processing*, 2009, vol. 60, no. 3, pp. 231-236.
- [45] KACAR F., METIN B., KUNTAM H., CICEKOGLU O., Current-Mode Multifunction Filters Using a Single FDCCII, *In Proc. International Conference Electrical and Electronics Engineering (ELECO)*, 2009, Bursa, Turkey, pp. II-54 - II-57.
- [46] KACAR F., KUNTMAN H., OZCAN S., New High Performance CMOS Fully Differential Current Conveyor, *Electroscope Applied Electronics* 2008, vol. 2008, no. III, pp. 1-4.
- [47] KOTON J., HERENC SAR N., VRBA K., KOUDAR I., Fully differential current-mode filters using digitally adjustable current amplifier, *Elektrrevue*, 2009, no. 45, pp. 45-1-45-4.
- [48] LEE CH., Multiple-Mode OTA-C Universal Biquad Filters, *Circuits, Systems and Signal Processing*, 2010, vol. 29, issue 2, pp. 263-274.

- [49] CHUNHUA W., LING Z., TAO L., A new OTA-C current-mode biquad filter with single input and multiple outputs, *International Journal of Electronics and Communications (AEÜ)*, 2008, vol. 62, pp. 232-234.
- [50] QADIR A., ALTAF T., Current Mode Canonic OTA-C Universal Filter with Single Input and Multiple Outputs, *In Proc. The 2nd International Conference Electronic Computer Technology (ICECT)*, 2010, Kuala Lumpur, Malaysia, pp. 32-24.
- [51] JERABEK, J., VRBA, K., JELINEK, M., Univerzální a řiditelný filtr s proudovými sledovači, transkonduktančními zesilovači a minimálním počtem komponent (A Universal Controllable filter with CFs, OTAs and Minimal Number of Components), *Elektrorevue*, 2010, vol. 2010, no. 46, pp. 1-5.
- [52] BIOLEK D., BIOLKOVA V., KOLKA Z., Universal current-mode OTA-C KHN biquad, *International Journal of Electronics, Circuits & Systems*, 2007, vol.1, no. 4, pp. 214.
- [53] JAIKLA W., SIRIPONGDEE S., SUWANJAN P., MISO current-mode biquad filter with independent control of pole frequency and quality factor, *Radioengineering*, 2012, vol. 21, no. 3, pp. 886-891.
- [54] SINGH S. V., MAHESHWARI S., MOHAN J., CHAUHAN D. S., Electronically tunable current-mode universal biquad filter based on the CCCCTA, *In Proc. of IEEE Int. Conf. on Advances in Recent Technologies in Comm. and Computing (ARTCOM)*, 2009, Kottayam, Kerala, pp. 424-429.
- [55] TOMAR R., SINGH S., CHAUHAN D., Current Processing Current Tunable Universal Biquad Filter Employing Two CCTAs and Two Grounded Capacitors, *Circuits and Systems*, 2013, vol. 4, no. 6, pp 443-450.
- [56] KUMNGERN M., TORTEANCHAI U., SARSITTHITHUM K., Current-Tunable Current-Mode Multifunction Filter Employing a Modified CCCCTA, *In Proc. 7th IEEE Conference Industrial Electronics and Applications (ICIEA)*, 2012, Singapore, Republic of Singapore, pp. 1794 - 1797.
- [57] SINGH S., MAHESHWARI S., CHAUHAN D., Universal Current-Controlled Current-Mode Biquad Filter Employing MO-CCCCTAs and Grounded Capacitors, *Circuits and Systems*, 2010, vol. 1, no. 2, pp. 35-40.
- [58] PRASAD D., BHASKAR D. R., SINGH A. K., Universal current-mode biquad filter using dual output current differencing transconductance amplifier, *International Journal of Electronics and Communications (AEÜ)*, 2009, vol. 63, issue 6, pp. 497-501.
- [59] TANGSRIRAT W., PUKKALANUN T., Structural generation of two integrator loop filters using CDTAs and grounded capacitors, *International Journal of Circuit Theory and Applications*, 2011, vol. 39, Issue 1, pp. 31-45.
- [60] KESKIN A. U., BIOLEK D., HANCIOGLU E., BIOLKOVA V., Current-mode KHN filter employing current differencing transconductance amplifiers, *International Journal of Electronics and Communications (AEÜ)*, 2006, vol. 60, pp. 443-446.
- [61] SHAH N. A., QUADRI M., IQUBAL S. Z., Realization of CDTA based current-mode universal filter, *Indian J. pure & applied physics*, 2008, vol. 46, pp. 283-285.
- [62] BIOLEK D., BIOLKOVA V., CDTA-C current-mode universal 2nd-order filter, *In Proc. of the 5th WSEAS Int. Conf. on Applied Informatics and Communications*, 2005, Malta, pp. 411-414.
- [63] DEHRAN M., SINGH I. P., SINGH K., SINGH R. K., Switched Capacitor Biquad Filter Using CDTA, *Circuits and Systems*, 2013, vol. 4, no. 6, pp. 438-442.
- [64] KACAR F., KUNTMAN H., A new, improved CMOS realization of CDTA and its filter applications, *Turkish Journal of Electrical Engineering & Computer Sciences*, 2011, vol. 19, issue 4, pp. 631.

- [65] INTAWICHAH K., TANGSRIRAT W., Signal-Flow Graph Realization of nth-Order Current-Mode Allpass Filters Using CFTAs, *In Proc. The 10th International Conference Electrical Engineering/Electronics, Computer, Telecommunications and Information Technology (ECTI-CON)*, 2013, Krabi, Thailand, pp. 1-6.
- [66] HERENC SAR N., KOTON J., VRBA K., LAHIRI A., CICEKOGLU O., Current-Controlled CFTA-Based Current-Mode SITO Universal Filter and Quadrature Oscillator, *In Proc. International Conference Applied Electronics (AE)*, 2010, Pilsen, Czech Republic, pp. 1-4.
- [67] TANGSRIRAT W., Single-input three-output electronically tunable universal current-mode filter using current follower transconductance amplifiers, *International Journal of Electronics and Communications (AEÜ)*, 2011, vol. 65, pp. 783-787.
- [68] TOMAR R. S., SINGH S. V., CHAUHAN C., Fully Integrated Electronically Tunable Universal Biquad Filter Operating in Current-Mode, *In Proc. the international Conference Signal Processing and Integrated Networks (SPIN)*, 2014, Noida, India, pp. 549-554.
- [69] TOMAR R. S., SINGH S. V., CHAUHAN D. S., Cascadable Low Voltage Operated Current-Mode Universal Biquad Filter, *WSEAS Transactions on Signal Processing*, 2014, vol. 10, pp. 345-353.
- [70] LAWANWISUT S., SIRIPRUCHYANUN M., A Current-Mode Multifunction Biquadratic Filter Using CFTAs, *Journal of KMUTNB*, 2012, vol. 22, no. 3, pp 479-485.
- [71] BIOLEK D., BIOLKOVA V., KOLKA Z., BAJER J., Single-Input Multi-Output Resistorless Current-Mode Biquad, *In proc. of the European Conference on Circuit Theory and Design ECCTD 2009*, 2009, Antalya, Turkey, pp. 225-228.
- [72] BIOLEK D., BIOLKOVA V., Current-Input Current-Output 2nd-Order All-Pass Filter Employing Two ZC-CITAs, *In Proc. of the 20th International Conference Radioelektronika (RADIOELEKTRONIKA)*, 2010, Brno, Czech Republic, pp. 1-4.
- [73] KESKIN A. Ü., HANCIOGLU E., Current mode multifunction filter using two CDBAs, *International Journal of Electronics and Communications (AEÜ)*, 2005, vol. 59, issue 8, pp. 495-498.
- [74] TSUKUTANI T., SUMI Y., YABUKI N., Electronically tunable current-mode universal biquadratic filter using CCCDBAs, *In Proc. International Symposium Intelligent Signal Processing and Communications Systems ISPACS*, 2008, Bangkok, Thailand, pp. 1-4.
- [75] TANGSRIRAT W., SURAKAMPONTORN W., Design of Electronically Tunable Ladder Filters Using Current-Controlled Current Differential Buffered Amplifiers, *In Proc. 2004 IEEE Region 10th Conference TENCN*, 2004, pp. 368-371 Vol. 4.
- [76] SIRIPRUCHYANUN M., JAIKLA W., Current-mode biquadratic filter using DO-CCCDBAs, *International Journal of Circuit Theory and Applications*, 2010, vol. 38, no. 3, pp. 321-330.
- [77] PAL R., TIWARI R. C., PANDEY R., Single CDBA Based Current Mode First Order Multifunctional Filter, *International Journal of Engineering Science and Technology (IJEST)*, 2014, vol. 6, no. 7, pp. 444-451.
- [78] SOTNER R., JERABEK J., HERENC SAR N., ZAK T., JAIKLA W., VRBA K., Modified Current Differencing Unit and its Application for Electronically Reconfigurable Simple First-order Transfer Function, *Advances in Electrical and Computer Engineering*, 2015, vol. 15, no. 1, pp. 3-10.
- [79] SOTNER R., JERABEK J., HERENC SAR N., PROKOP R., VRBA K., DOSTAL T., First-order Reconfigurable Reconnection- less Filters Using Modified Current Differencing Unit, *In Proc. of 25th*

- International Conference RADIOELEKTRONIKA*, 2015, Pardubice: University of Pardubice, Faculty of Electrical Engineering and Informatics, Czech Republic, pp. 46-50.
- [80] JERABEK J., VRBA K., Návrh kmitočtových filtrů pomocí integračních článků s proudovými aktivními prvky (The Proposal of Frequency Filters With Current Active Elements Based on Integrators), *Elektrorevue*, 2009, No. 9, pp. 9-1 - 9-7.
- [81] KOTON J., MINARCIK M., Využití grafů signálových toků pro analýzu obvodů s proudovými konvejory (Usage of Signal-Flow Graphs to Analyze Electrical Networks With Current Conveyors), *Elektrorevue* 2006, no. 10, pp. 1.
- [82] CHAICHANA A., KUMNGERN M., JAIKLA W., Electronically Tunable Versatile Current-Mode MISO Universal Filter Including Minimum Component Count Circuits, *In Proc. The 11th International Conference Electrical Engineering/Electronics, Computer, Telecommunications and Information Technology (ECTI-CON)*, 2014, Nakhon Ratchasima, Thailand, pp. 1-4.
- [83] ALZAHER H. A., A CMOS Digitally Programmable Universal Current-Mode Filter, *IEEE Transactions on circuits and systems—II: Express briefs*, 2008, vol. 55, no. 8, pp. 758-762.
- [84] JERABEK J., DVORAK J., SOTNER R., METIN B., VRBA K., Multifunctional current-mode filter with dual-parameter control of the pole frequency, *Advances in Electrical and Computer Engineering*, 2016, vol. 16, issue 3, pp. 31-36.
- [85] JERABEK J., SOTNER R., HERENC SAR N., POLAK J., DVORAK J., KOTON J., MISO Universal Frequency Filter with Dual-Parameter Control of the Pole Frequency, *In Proc. ELECO 2015 9th International Conference on Electrical and Electronics Engineering*, 2015, Bursa, Turkey, pp. 24-28.
- [86] TANGSRIRAT W., DUMAWIPATA T., SURAKAMPONTORN W., Multiple-input single-output current-mode multifunction filter using current differencing transconductance amplifiers, *International Journal of Electronics and Communications (AEÜ)*, 2007, vol. 61, issue 4, pp. 209-214.
- [87] MAHESHWARI S., Current-mode filters with high output impedance and employing only grounded components, *WSEAS transaction on electronics*, 2008, Vol. 5, Issue 6, pp. 238-243.
- [88] JERABEK J., VRBA K., Design of Fully-Differential Filters with nth-order Synthetic Elements and Comparison with Single-Ended Solution, *In Proc. IEEE The 3rd International Conference Communication Software and Networks (ICCSN)*, 2011, Xi'an, China, pp. 437-441.
- [89] BRANDSTETTER P., KLEIN L., Third Order Low-Pass Filter Using Synthetic Immittance Elements With Current Conveyors, *Advances in Electrical and Electronic Engineering*, 2012, vol. 10, no. 2, pp. 89-94.
- [90] INTAWICHAHAI K., TANGSRIRAT W., Signal Flow Graph Realization of nth-Order Current-Mode Allpass Filters Using CFTAs, *In Proc. Electrical Engineering/Electronics, Computer, Telecommunications and Information Technology (ECTI-CON)*, 2013, Krabi, Thailand, pp. 1-6.
- [91] JERABEK J., VRBA K., Comparison of the Fully-Differential and Single-Ended Solutions of the Frequency Filter with Current Followers and Adjustable Current Amplifier, *In Proc. ICN2012 The 11th International Conference on Networks*, 2012, Reunion, France: IARIA, pp. 50-54.
- [92] TOUMAZOU C., LIDGEY F. J., HAIGH D. G., *Analog IC design: the current-mode approach*, Institution of Electrical Engineers, London, 1996, 646 pages.
- [93] KOTON J., HERENC SAR N., SLADOK O., HORNG J., Pseudo-differential second-order band- reject filter using current conveyors. *International Journal of Electronics and Communications (AEÜ)*, 2016, vol. 70, no. 6, pp. 814-821.

- [94] IBRAHIM M. A., MINAEI S., KUNTMAN H., DVCC based differential-mode all-pass and notch filters with high CMRR, *Int J Electron*, 2006, vol. 93, pp. 231-240.
- [95] HORNG J., WU C., HERENC SAR N. Fully differential first-order allpass filters using a DDCC, *Indian J. Eng. Mater. Sci.*, 2014, vol. 21, pp. 345–350.
- [96] ANSARI M. S., SONI G. S., Digitally-programmable fully-differential current-mode first-order LP, HP and AP filter sections, *In Proc. of 2014 international conference on signal propagation and computer technology (ICSPCT)*, 2014, Ajmer, India, pp. 524–528.
- [97] JERABEK J., KOTON J., VRBA K., Zobecněná metoda návrhu multifunkčních kmitočtových filtrů (A Generalized Method of Multifunctional Frequency Filter Design), *Elektrorevue*, 2007, no. 41, pp. 41-1 - 41-10.
- [98] KOTON J., VRBA K., Návrh kmitočtových filtrů pomocí autonomního obvodu s úplnou sítí admitancí (Designing of Frequency Filters Using Autonomous Circuit With a Full Admittance Network), *Elektrorevue*, 2005, no. 33, pp. 1.
- [99] KOTON J., VRBA K., Zobecněné metody návrhu kmitočtových filtrů (Generalized Methods of Frequency Filter Design), *Elektrorevue*, 2008, no. 26, pp. 26-1 - 26-17.
- [100] HERENC SAR N., KOTON J., VRBA K., LATTENBERG I., MISUREC J., Generalized Design Method for Voltage-Controlled Current-Mode Multifunction Filters, *Telfor Journal*, 2009, vol. 1, no. 2, pp. 49-52.
- [101] BRANDSTETTER P., KLEIN L., Design of Frequency Filters by Method of Synthetic Immittance Elements with Current Conveyors, *In Proc. International Conference Applied Electronics (AE)*, 2012, Pilsen, Czech Republic, pp. 37-40.
- [102] JERABEK J., VRBA K., Návrh přeladitelného kmitočtového filtru s proudovými aktivními prvky za pomoci metody grafu signálových toků (The Proposal of Tunable Frequency Filter With Current Active Elements Using Signal-Flow Graphs Method), *Elektrorevue*, 2009, no. 42, pp. 42-1 - 42-7.
- [103] KUBANEK D., *Teoretický návrh ADSL Splitterů. Studijní zpráva pro STROM telecom*, (Theoretical Design of ADSL Splitters. Report for STROM telecom) Department of Telecommunication, FEKT, BUT, Brno, 2003. 119 pages.
- [104] MAUNDY B., ELWAKIL A., FREEBORN T., On the practical realization of higher-order filters with fractional stepping, *Signal Processing*, 2011, vol. 91, no. 3, pp. 484-491.
- [105] KRISHNA M. S., DAS S., BISWAS K., GOSWAMI B., Fabrication of a fractional order capacitor with desired specifications: A study on process identification and characterization, *IEEE Transactions on Electron Devices*, 2011, vol. 58, no.11, pp. 4067-4073.
- [106] FREEBORN T., A Survey of Fractional-Order Circuit Models for Biology and Biomedicine, *IEEE Circuits and Systems Magazine*, 2013, vol. 3, no. 3, pp. 416-424.
- [107] ELWAKIL A., Fractional-order circuits and systems: An emerging interdisciplinary research area, *IEEE Circuits and Systems Magazine*, 2010, vol. 10, no. 4, pp. 40-50.
- [108] ALI A. S., RADVAN A., SOLIMAN A. M., Fractional Order Butterworth Filter: Active and Passive Realizations, *IEEE Journal on Emerging and Selected Topics in Circuits and Systems*, 2013, vol. 3, no. 3, pp. 346-354.
- [109] FREEBORN T., MAUNDY B., ELWAKIL A., Approximated Fractional Order Chebyshev Lowpass Filters. *Mathematical Problems in Engineering*, 2015, vol. 2015, pp. 1-7.

- [110] RADWAN A., SALAMA K., Fractional-order RC and RL circuits, *Circuits Systems and Signal Processing*, 2012, vol. 31, no. 6, pp. 1901-1915.
- [111] TSIRIMOKOU G., LAOUDIAS C., PSYCHALINOS C., 0.5-V fractional-order companding filters, *International Journal of Circuit Theory and Applications*, 2015, vol. 43, no. 9, pp. 1105-1126.
- [112] TSIRIMOKOU G., PSYCHALINOS C., ELWAKIL A., Digitally Programmed Fractional-Order Chebyshev Filters Realizations Using Current-Mirrors, *In. Proc. of IEEE International Symposium on Circuits and Systems (ISCAS 2015)*, 2015, Lisbon, Portugal, pp. 2337-2340.
- [113] JERABEK J., SOTNER R., KUBANEK D., DVORAK J., LANGHAMMER L., HERENC SAR N., VRBA K., Fractional-Order Low-Pass Filter with Electronically Adjustable Parameters, *In Proc. of 2016 39th International Conference on Telecommunications and Signal Processing (TSP)*, 2016, Vienna, Austria, pp. 569-574.
- [114] FREEBORN T., Comparison of $(1+\alpha)$ Fractional-Order Transfer Functions to Approximate Lowpass Butterworth Magnitude Responses, *Circuits, Systems, and Signal Processing*, 2016, vol. 35, no. 6, pp. 1983-2002.
- [115] KHATEB F., KUBANEK D., TSIRIMOKOU G., PSYCHALINOS C., Fractional-order filters based on low-voltage DDCCs, *Microelectronics Journal*, 2016, vol. 50, no. 1, pp. 50-59.
- [116] TSIRIMOKOU G., PSYCHALINOS C., Ultra-low voltage fractional-order circuits using current mirrors, *International Journal of Circuit Theory and Applications*, 2016, vol. 44, no. 1, pp. 109-126.
- [117] FREEBORN T., MAUNDY B., ELWAKIL A., Field programmable analogue array implementation of fractional step filters, *IET Circuits Devices*, 2010, vol. 4, no. 9, pp. 514-524.
- [118] AHMADI P., MAUNDY B., ELWAKIL A., BELOSTOTSKI L., High-quality factor asymmetric-slope band-pass filters: a fractional-order capacitor approach, *IET Circuits, Devices and Systems*, 2012, vol. 6, no. 3, pp. 187-197.
- [119] JERABEK J., VRBA K., Diferenční převodníky U/I a I/ U pro měření obvodů v proudovém módu (Differential V/I I/V converters for measurement of current-mode circuits), *Elektrorevue*, 2011, vol. 2011, no. 40, pp. 1-5.
- [120] MATEJICEK L., VRBA K., Srovnání citlivostí aktivních kmitočtových filtrů s OZ, CC a OTA (A Comparison of the Sensitivity of Active Frequency Filters with OA, CC and OTA), *Elektrorevue*, 2002, no. 2, pp. 1-9.
- [121] CAJKA J., KVASIL J., *Teorie lineárních obvodů* (Theory of linear circuits), 1st ed. SNTL, 1979, 355 pages.
- [122] CHEN W., *The circuits and filters handbook*, 3rd ed. CRC Press, 2003, 3364 pages.
- [123] MASON S. J., Feedback Theory: Some Properties of Signal Flow Graphs, *In Proc. IRE*, 1953, vol 41, no. 9, pp. 1144-1156.
- [124] COATES C. L., Flow graph solutions of linear algebraic equations, *In Proc. IRE*, 1959, vol. 6, no. 2, pp. 170-187.
- [125] NISE N. S., *The Control Hand-book*, IEEE Press, 1996, 1566 pages.
- [126] VRBA K., JERABEK J., Filters Based on Active Elements with Current Mirrors and Inverters, *International Transactions Communication and Signal Processing*, 2006, vol. 1, issue 8, pp. 1-8.

- [127] CZARNIAK A., SZCZEPANSKI S., The convergence of Volterra series describing lowpass OTA-capacitor (OTA-C) filters, *In Proc. Circuit Theory and Design*, Brighton, England, 1989, pp. 661-664.
- [128] KOTON J., HERENC SAR N., JERABEK J., VRBA K., Fully Differential Current-Mode Band-Pass Filter: Two Design Solutions, *In Proc. 33rd International conference on Telecommun. and Signal Processing (TSP)*, 2010, Vienna, Austria, p. 1-4.
- [129] BIOLEK D., SENANI R., BIOLKOVA V., KOLKA Z., Active Elements for Analog Signal Processing: Classification, Review, and New Proposals, *Radioengineering*, 2008, vol. 17, no. 4, pp. 15-32.
- [130] Datasheet UCC-N1B, Universal current conveyor (UCC) and second-generation current conveyor (CCII+/-), rev. 1. Brno University of Technology, On Semiconductor Ltd., 2012.
- [131] SPONAR R., VRBA K., Measurements and Behavioral Modelling of Modern Conveyors, *International Journal of Computer Science and Network Security*, 2006, vol. 3A, issue 6, pp. 57-63.
- [132] JERABEK J., SOTNER R., VRBA K., Electronically Adjustable Triple-Input Single-Output Filter with Voltage Differencing Transconductance Amplifier, *Revue Roumaine des Sciences Techniques - Serie Électrotechnique et Énergétique*, 2015, vol. 59, no. 2, pp. 163-172.
- [133] SOTNER R., HERENC SAR N., JERABEK J., PROKOP R., KARTCI A., DOSTAL T., VRBA K., Z-Copy Controlled-Gain Voltage Differencing Current Conveyor: Advanced Possibilities in Direct Electronic Control of First-Order Filter, *Elektronika ir Elektrotechnika*, 2014, vol. 20, no. 6, pp. 77-83.
- [134] EL2082 Current Mode Amplifier, Intersil [online], 1996, [cited 22.8.2016], available online <<http://www.intersil.com/data/fn/fn7152.pdf>>.

Own Papers Relevant to Content of the Thesis

- [135] POLAK J., LANGHAMMER L., JERABEK J., Behavioral modeling of Digitally Adjustable Current Amplifier, *International Journal of Advances in Telecommunications, Electrotechnics, Signals and Systems*, 2015, vol. 4, no. 1, pp. 1-7.
- [136] LANGHAMMER L., JERABEK J., Fully Differential Universal Current-Mode Frequency Filters Based on Signal-Flow Graphs Method, *International Journal of Advances in Telecommunications, Electrotechnics, Signals and Systems*, 2014, vol. 3, no. 1, pp. 1-12.
- [137] LANGHAMMER L., JERABEK J., POLAK J., Tunable Fully-Differential Filters Designed Using Signal- Flow Graphs Method, *Elektrorevue*, 2015, vol. 6, no. 3, pp. 38-48.
- [138] LANGHAMMER L., JERABEK J., POLAK J., PANEK D., A Single-Ended and Fully-Differential Universal Current-Mode Frequency Filter with MO-CF and DACA Elements, *Advances in Electrical and Computer Engineering*, 2016, vol. 16, issue 3, pp. 43-48.
- [139] LANGHAMMER L., JERABEK J., POLAK J., SOTNER R., STORK P., Tunable fully-differential filter employing MOTA and DACA elements, *Indian Journal of Engineering and Materials Sciences*, 2016, paper accepted for publication on 25.04.2016.
- [140] LANGHAMMER L., JERABEK J., POLAK J., Single-Ended and Fully-Differential Multifunctional Current-Mode Frequency Filter Employing Operational Transconductance Amplifiers and Transresistance Amplifier, *Elektronika ir Elektrotechnika*, in review, paper submitted on 12.11.2015.

- [141] LANGHAMMER L., JERABEK J., POLAK J., CIKA P., Single-Ended and Fully-Differential Current-Input Current-Output, Universal Frequency Filter with Transconductance and Transresistance, Amplifiers, *WSEAS Transactions on Circuits*, 2015, vol. 14, no. 2015, pp. 56-67.
- [142] DVORAK J., LANGHAMMER L., JERABEK J., KOTON J., SOTNER R., POLAK J., Electronically Tunable Fractional-Order Low-Pass Filter with Current Followers, *In Proc. of 2016 39th International Conference on Telecommunications and Signal Processing (TSP)*, 2016, Vienna, Austria, pp. 587-592.
- [143] LANGHAMMER L., DVORAK J., JERABEK J., KOTON J., SOTNER R., Fractional-Order Low-Pass Filter with Electronic Tunability of Its Order and Cut-Off Frequency, *International Journal of Electronics and Communications (AEÜ)*, in review, paper submitted on 21.06.2016.

APPENDICES

A EQUATIONS OF THE SENSITIVITY ANALYSIS OF THE F- D FILTER FROM CHAPTER 6.2

$$\begin{aligned}
 b_2 = & -1 (4n_{23}n_{35}C_1G_1G_2C_2 - 2A_1n_{24}n_{32}n_{11}C_1G_1G_2C_2 + 4n_{26}n_{35}C_1G_1G_2C_2 + 16C_1G_1G_2C_2 - \\
 & -A_1n_{21}n_{13}C_1G_1C_2 + 4C_1G_2C_2 + 4C_1G_1C_2 + 2A_1n_{21}n_{35}n_{11}C_1G_1G_2C_2 + C_1C_2 + 2n_{23}C_1G_1C_2 + \\
 & + 8n_{35}C_1G_1G_2C_2 + 8n_{23}C_1G_1G_2C_2 - 2A_1n_{21}n_{35}n_{13}C_1G_1G_2C_2 + 2n_{26}C_1G_1C_2 + 2A_1n_{21}n_{32}n_{11}C_1G_1G_2C_2 \\
 & - \\
 & -4A_1n_{24}n_{11}C_1G_1G_2C_2 + 4A_1n_{21}n_{11}C_1G_1G_2C_2 - A_1n_{24}n_{11}C_1G_1C_2 + A_1n_{21}n_{11}C_1G_1C_2 + \\
 & + 4A_1n_{24}n_{13}C_1G_1G_2C_2 + 2n_{35}C_1G_2C_2 + A_1n_{24}n_{13}C_1G_1C_2 + 4n_{23}n_{32}C_1G_1G_2C_2 \\
 & + 2A_1n_{24}n_{32}n_{13}C_1G_1G_2C_2 - \\
 & -2A_1n_{21}n_{32}n_{13}C_1G_1G_2C_2 + 4n_{26}n_{32}C_1G_1G_2C_2 + 8n_{32}C_1G_1G_2C_2 + 8n_{26}C_1G_1G_2C_2 - \\
 & 4A_1n_{21}n_{13}C_1G_1G_2C_2 + 2n_{32}C_1G_2C_2 - 2A_1n_{24}n_{35}n_{11}C_1G_1G_2C_2 + 2A_1n_{24}n_{35}n_{13}C_1G_1G_2C_2),
 \end{aligned} \tag{A.1}$$

$$\begin{aligned}
 b_1 = & -1 (2A_1n_{24}n_{31}A_2n_{13}C_1G_1G_2^2 + 8n_{23}n_{35}C_1G_1G_2^2 + 4n_{23}n_{26}G_1^2C_2 + 2G_1C_2 + \\
 & + 2A_1n_{24}n_{31}n_{35}A_2n_{13}C_1G_1G_2^2 + 16n_{32}C_1G_1G_2^2 + 8n_{23}n_{32}G_1^2G_2C_2 + 4A_1n_{21}n_{35}n_{11}C_1G_1G_2^2 + 2C_1G_2 - \\
 & -4A_1n_{24}n_{11}C_1G_1G_2^2 + 2n_{32}C_1G_2 + 16n_{35}C_1G_1G_2^2 + 16n_{26}G_1^2G_2C_2 + 4C_1G_2^2 + 4n_{23}n_{35}G_1G_2C_2 - \\
 & -4A_1n_{24}n_{32}n_{11}C_1G_1G_2^2 + 8A_1n_{21}n_{11}G_1^2G_2C_2 + 4A_1n_{24}n_{32}n_{13}C_1G_1G_2^2 + 16C_1G_1G_2^2 + 8n_{23}G_1G_2C_2 + \\
 & + 2A_1n_{21}n_{11}G_1^2C_2 + 16n_{23}n_{26}G_1^2G_2C_2 + 2A_1n_{24}n_{13}C_1G_1G_2 + 4n_{32}C_1G_2^2 + 4A_1n_{21}n_{11}C_1G_1G_2^2 + \\
 & + 2A_1n_{21}n_{32}n_{11}C_1G_1G_2 + 8A_1n_{23}n_{24}n_{13}G_1^2G_2C_2 + 4A_1n_{24}n_{13}C_1G_1G_2^2 + 4A_1n_{24}n_{35}n_{13}G_1^2G_2C_2 + \\
 & + 8n_{32}G_1^2G_2C_2 + 4n_{23}C_1G_1G_2 + 4A_1n_{23}n_{24}n_{35}n_{13}G_1^2G_2C_2 - 2A_1n_{24}n_{32}n_{11}C_1G_1G_2 + 4n_{35}G_1G_2C_2 + \\
 & + 16n_{23}G_1^2G_2C_2 + 4n_{26}n_{32}C_1G_1G_2 + 4n_{23}n_{32}G_1G_2C_2 + 4n_{23}G_1^2C_2 + 2n_{23}G_1C_2 + 8n_{26}n_{32}n_{35}C_1G_1G_2^2 + \\
 & + 4G_1^2C_2 - 2A_1n_{24}n_{32}n_{34}A_2n_{11}C_1G_1G_2^2 + 4A_1n_{24}n_{32}n_{35}n_{13}C_1G_1G_2^2 + 8n_{23}n_{35}G_1^2G_2C_2 + 4n_{35}C_1G_2^2 + \\
 & + 2A_1n_{21}n_{32}n_{11}G_1G_2C_2 + A_1n_{24}n_{31}A_2n_{13}C_1G_1G_2 + 4n_{23}n_{32}C_1G_1G_2 + 8n_{35}G_1^2G_2C_2 - \\
 & -2A_1n_{24}n_{31}A_2n_{11}C_1G_1G_2^2 + 8G_1G_2C_2 - 2A_1n_{21}n_{32}n_{34}A_2n_{13}C_1G_1G_2^2 + 8n_{32}C_1G_1G_2 + \\
 & + 2A_1n_{24}n_{32}n_{34}A_2n_{13}C_1G_1G_2^2 + 8n_{23}n_{32}n_{35}C_1G_1G_2^2 + 4A_1n_{21}n_{32}n_{35}n_{11}C_1G_1G_2^2 + 8n_{23}C_1G_1G_2^2 + \\
 & + 8C_1G_1G_2 - 4A_1n_{21}n_{32}n_{35}n_{13}C_1G_1G_2^2 + 4n_{32}G_1G_2C_2 - A_1n_{21}n_{31}A_2n_{13}C_1G_1G_2 + 16n_{32}n_{35}C_1G_1G_2^2 + \\
 & + 4A_1n_{23}n_{24}n_{32}n_{13}G_1^2G_2C_2 + 4n_{32}n_{35}C_1G_2^2 - A_1n_{24}n_{31}A_2n_{11}C_1G_1G_2 + 16G_1^2G_2C_2 + \\
 & + 4A_1n_{24}n_{32}n_{13}G_1^2G_2C_2 - 2A_1n_{21}n_{31}n_{35}A_2n_{13}C_1G_1G_2^2 + 4n_{26}C_1G_1G_2 - 2A_1n_{21}n_{13}C_1G_1G_2 - \\
 & -2A_1n_{24}n_{11}C_1G_1G_2 + 2A_1n_{21}n_{11}C_1G_1G_2 + 8A_1n_{21}n_{26}n_{11}G_1^2G_2C_2 + 4n_{26}G_1^2C_2 + 8n_{26}n_{35}C_1G_1G_2^2 + \\
 & + 8n_{23}n_{32}C_1G_1G_2^2 + 8A_1n_{24}n_{13}G_1^2G_2C_2 + 8n_{26}n_{35}G_1^2G_2C_2 + 2A_1n_{24}n_{13}G_1^2C_2 + \\
 & + 4A_1n_{21}n_{26}n_{32}n_{11}G_1^2G_2C_2 + A_1n_{21}n_{11}G_1C_2 + 8n_{26}n_{32}G_1^2G_2C_2 - 2A_1n_{24}n_{34}A_2n_{11}C_1G_1G_2^2 + \\
 & + 4A_1n_{21}n_{32}n_{11}C_1G_1G_2^2 - 4A_1n_{24}n_{35}n_{11}C_1G_1G_2^2 - 2A_1n_{21}n_{34}A_2n_{13}C_1G_1G_2^2 \\
 & + 2A_1n_{21}n_{34}A_2n_{11}C_1G_1G_2^2 + 2A_1n_{23}n_{24}n_{13}G_1^2C_2 - 2A_1n_{21}n_{31}A_2n_{13}C_1G_1G_2^2 + 2A_1n_{21}n_{26}n_{11}G_1^2C_2 \\
 & + 2A_1n_{21}n_{31}A_2n_{11}C_1G_1G_2^2 + A_1n_{21}n_{31}A_2n_{11}C_1G_1G_2 + 8n_{23}n_{26}n_{35}G_1^2G_2C_2 + 2A_1n_{24}n_{32}n_{13}C_1G_1G_2 \\
 & + 2A_1n_{21}n_{35}n_{11}G_1G_2C_2 - \\
 & -4A_1n_{21}n_{35}n_{13}C_1G_1G_2^2 + 2A_1n_{21}n_{32}n_{34}A_2n_{11}C_1G_1G_2^2 - 2A_1n_{24}n_{31}n_{35}A_2n_{11}C_1G_1G_2^2 + \\
 & + 2A_1n_{21}n_{31}n_{35}A_2n_{11}C_1G_1G_2^2 - 4A_1n_{21}n_{32}n_{13}C_1G_1G_2^2 - 4A_1n_{24}n_{32}n_{35}n_{11}C_1G_1G_2^2 - \\
 & 2A_1n_{21}n_{32}n_{13}C_1G_1G_2^2 + 4A_1n_{21}n_{32}n_{11}G_1^2G_2C_2 + 8n_{26}C_1G_1G_2^2 - 4A_1n_{21}n_{13}C_1G_1G_2^2 \\
 & + 4A_1n_{21}n_{11}G_1G_2C_2 + 2A_1n_{24}n_{34}A_2n_{13}C_1G_1G_2^2 + 8n_{26}n_{32}C_1G_1G_2^2 + 4A_1n_{21}n_{35}n_{11}G_1^2G_2C_2 \\
 & + 4A_1n_{21}n_{26}n_{35}n_{11}G_1^2G_2C_2 + 8n_{23}n_{26}n_{32}G_1^2G_2C_2 + 4A_1n_{24}n_{35}n_{13}C_1G_1G_2^2),
 \end{aligned} \tag{A.2}$$

$$\begin{aligned}
 b_0 = & -4A_1n_{21}n_{26}n_{31}n_{35}A_2n_{11}G_1^2G_2^2 - 16n_{26}n_{32}n_{35}G_1^2G_2^2 - 8A_1n_{24}n_{35}n_{13}G_1^2G_2^2 - 4A_1n_{21}n_{34}A_2n_{11}G_1^2G_2^2 - \\
 & -2A_1n_{21}n_{34}A_2n_{11}G_1G_2^2 - 8n_{32}G_1^2G_2 - 16n_{23}G_1^2G_2^2 - 8n_{23}G_1G_2^2 - 16G_1^2G_2^2 - 8G_1G_2^2 - \\
 & -8A_1n_{24}n_{32}n_{13}G_1^2G_2^2 - 4n_{23}G_1G_2 - 8G_1^2G_2 - 4G_1G_2 - 4A_1n_{24}n_{32}n_{34}A_2n_{13}G_1^2G_2^2 - 16n_{26}G_1^2G_2^2 -
 \end{aligned} \tag{A.3}$$

$$\begin{aligned}
& -16n_{23}n_{35}G_1^2G_2^2 - 8n_{23}n_{35}G_1G_2^2 - 8A_1n_{24}n_{32}n_{35}n_{13}G_1^2G_2^2 - 4A_1n_{21}n_{11}G_1G_2^2 - 16n_{35}G_1^2G_2^2 - 8n_{35}G_1G_2^2 - \\
& -2A_1n_{24}n_{31}A_2n_{13}G_1^2G_2^2 - 16n_{23}n_{32}G_1^2G_2^2 - 8n_{23}n_{32}G_1G_2^2 - 4A_1n_{21}n_{26}n_{32}n_{11}G_1^2G_2^2 - \\
& -4A_1n_{24}n_{31}n_{35}A_2n_{13}G_1^2G_2^2 - 8n_{23}n_{32}G_1^2G_2^2 - 8A_1n_{23}n_{24}n_{13}G_1^2G_2^2 - 2A_1n_{21}n_{32}n_{34}A_2n_{11}G_1G_2^2 - \\
& -16n_{32}G_1^2G_2^2 - 8n_{32}G_1G_2^2 - 4A_1n_{23}n_{24}n_{34}A_2n_{13}G_1^2G_2^2 - 8A_1n_{23}n_{24}n_{35}n_{13}G_1^2G_2^2 - 8n_{23}n_{26}G_1^2G_2^2 - \\
& -4n_{32}G_1G_2^2 - 16n_{23}n_{26}n_{35}G_1^2G_2^2 - 4A_1n_{23}n_{24}n_{32}n_{13}G_1^2G_2^2 - 16n_{32}n_{35}G_1^2G_2^2 - 8n_{32}n_{35}G_1G_2^2 - \\
& -4A_1n_{23}n_{24}n_{31}A_2n_{13}G_1^2G_2^2 - 2A_1n_{23}n_{24}n_{31}A_2n_{13}G_1^2G_2^2 - 4A_1n_{23}n_{24}n_{31}n_{35}A_2n_{13}G_1^2G_2^2 - \\
& -4A_1n_{21}n_{31}n_{35}A_2n_{11}G_1^2G_2^2 - 2A_1n_{21}n_{31}n_{35}A_2n_{11}G_1G_2^2 - 8A_1n_{21}n_{26}n_{11}G_1^2G_2^2 - 8n_{26}G_1^2G_2^2 - \\
& -8A_1n_{21}n_{11}G_1^2G_2^2 - 4A_1n_{21}n_{32}n_{11}G_1G_2^2 - 4A_1n_{21}n_{26}n_{34}A_2n_{11}G_1^2G_2^2 - 16n_{26}n_{35}G_1^2G_2^2 - 4A_1n_{21}n_{11}G_1^2G_2^2 - \\
& -2A_1n_{21}n_{11}G_1G_2^2 - 8A_1n_{21}n_{26}n_{32}n_{11}G_1^2G_2^2 - 8n_{23}G_1^2G_2^2 - 16n_{26}n_{32}G_1^2G_2^2 - 8A_1n_{21}n_{26}n_{32}n_{35}n_{11}G_1^2G_2^2 - \\
& -8n_{26}n_{32}G_1^2G_2^2 - 2A_1n_{21}n_{26}n_{31}A_2n_{11}G_1^2G_2^2 - 16n_{23}n_{32}n_{35}G_1^2G_2^2 - 8n_{23}n_{32}n_{35}G_1G_2^2 - 16n_{23}n_{26}G_1^2G_2^2 - \\
& -4A_1n_{21}n_{32}n_{35}n_{11}G_1G_2^2 - 4A_1n_{21}n_{26}n_{11}G_1^2G_2^2 - 4A_1n_{21}n_{32}n_{11}G_1^2G_2^2 - 8A_1n_{23}n_{24}n_{32}n_{13}G_1^2G_2^2 - \\
& -4A_1n_{21}n_{35}n_{11}G_1G_2^2 - 16n_{23}n_{26}n_{32}G_1^2G_2^2 - 8A_1n_{21}n_{35}n_{11}G_1^2G_2^2 - 8n_{23}n_{26}n_{32}G_1^2G_2^2 - \\
& -16n_{23}n_{26}n_{32}n_{35}G_1^2G_2^2 - 4A_1n_{24}n_{32}n_{13}G_1^2G_2^2 - 4n_{23}n_{32}G_1G_2^2 - 4A_1n_{21}n_{26}n_{31}A_2n_{11}G_1^2G_2^2 - \\
& -4A_1n_{21}n_{32}n_{34}A_2n_{11}G_1^2G_2^2 - 8A_1n_{21}n_{32}n_{11}G_1^2G_2^2 - 8A_1n_{21}n_{32}n_{35}n_{11}G_1^2G_2^2 - 4A_1n_{24}n_{34}A_2n_{13}G_1^2G_2^2 - \\
& -4A_1n_{21}n_{26}n_{32}n_{34}A_2n_{11}G_1^2G_2^2 - 2A_1n_{21}n_{32}n_{11}G_1G_2^2 - 4A_1n_{24}n_{31}A_2n_{13}G_1^2G_2^2 - 4A_1n_{24}n_{13}G_1^2G_2^2 - \\
& -4A_1n_{23}n_{24}n_{13}G_1^2G_2^2 - 2A_1n_{21}n_{31}A_2n_{11}G_1^2G_2^2 - 8A_1n_{23}n_{24}n_{32}n_{35}n_{13}G_1^2G_2^2 - A_1n_{21}n_{31}A_2n_{11}G_1G_2^2 - \\
& -2A_1n_{21}n_{31}A_2n_{11}G_1G_2^2 - 8A_1n_{24}n_{13}G_1^2G_2^2 - 4A_1n_{21}n_{31}A_2n_{11}G_1^2G_2^2 - 8A_1n_{21}n_{26}n_{35}n_{11}G_1^2G_2^2 - \\
& -4A_1n_{23}n_{24}n_{32}n_{34}A_2n_{13}G_1^2G_2^2.
\end{aligned}$$

$$\begin{aligned}
I_{LP \text{ real}} = & s(2A_1n_{24}n_{33}n_{35}n_{11}C_1G_1G_2^2 - A_1n_{24}n_{33}n_{13}C_1G_1G_2^2 - 2A_1n_{21}n_{33}n_{11}C_1G_1G_2^2 - \\
& A_1n_{21}n_{33}n_{11}C_1G_1G_2^2 - 2A_1n_{24}n_{33}n_{13}C_1G_1G_2^2 + 2A_1n_{21}n_{33}n_{35}n_{13}C_1G_1G_2^2 - 2A_1n_{21}n_{33}n_{35}n_{11}C_1G_1G_2^2 - \\
& 2A_1n_{24}n_{33}n_{35}n_{13}C_1G_1G_2^2 + 2A_1n_{24}n_{33}n_{11}C_1G_1G_2^2 + A_1n_{24}n_{33}n_{11}C_1G_1G_2^2 + 2A_1n_{21}n_{33}n_{13}C_1G_1G_2^2 \\
& + A_1n_{21}n_{33}n_{13}C_1G_1G_2^2) - 4A_1n_{21}n_{26}n_{33}n_{35}n_{11}G_1^2G_2^2 - 4A_1n_{24}n_{33}n_{35}n_{13}G_1^2G_2^2 - 4A_1n_{24}n_{33}n_{13}G_1^2G_2^2 - \\
& 2A_1n_{24}n_{33}n_{13}G_1^2G_2^2 - 2A_1n_{21}n_{33}n_{11}G_1G_2^2 - 2A_1n_{21}n_{33}n_{11}G_1^2G_2^2 - A_1n_{21}n_{33}n_{11}G_1G_2^2 - \\
& 2A_1n_{23}n_{24}n_{33}n_{13}G_1^2G_2^2 - 4A_1n_{23}n_{24}n_{33}n_{35}n_{13}G_1^2G_2^2 - 4A_1n_{23}n_{24}n_{33}n_{13}G_1^2G_2^2 - 4A_1n_{21}n_{33}n_{11}G_1^2G_2^2 - \\
& 2A_1n_{21}n_{33}n_{35}n_{11}G_1G_2^2 - 2A_1n_{21}n_{26}n_{33}n_{11}G_1^2G_2^2 - 4A_1n_{21}n_{33}n_{35}n_{11}G_1^2G_2^2 - 4A_1n_{21}n_{26}n_{33}n_{11}G_1^2G_2^2,
\end{aligned} \tag{A.4}$$

$$\begin{aligned}
I_{BP \text{ real}} = & s^2(n_{22}n_{11}C_1G_1C_2 + 4n_{22}n_{11}C_1G_1G_2C_2 - 4n_{22}n_{13}C_1G_1G_2C_2 - n_{22}n_{13}C_1G_1C_2 + \\
& + 2n_{22}n_{32}n_{11}C_1G_1G_2C_2 + 2n_{22}n_{35}n_{11}C_1G_1G_2C_2 - 2n_{22}n_{35}n_{13}C_1G_1G_2C_2 - 2n_{22}n_{32}n_{13}C_1G_1G_2C_2) - s(\\
& 2n_{22}n_{32}n_{13}C_1G_1G_2 - 4n_{22}n_{35}n_{11}C_1G_1G_2^2 - 4n_{22}n_{32}n_{11}G_1^2G_2C_2 - 4n_{22}n_{32}n_{11}C_1G_1G_2^2 - 4n_{22}n_{11}C_1G_1G_2^2 \\
& - 4n_{22}n_{11}G_1G_2C_2 + 4n_{22}n_{13}C_1G_1G_2^2 - 4n_{22}n_{32}n_{35}n_{11}C_1G_1G_2^2 + 2n_{22}n_{13}C_1G_1G_2 - 2n_{22}n_{11}G_1^2C_2 + \\
& + 4n_{22}n_{35}n_{13}C_1G_1G_2^2 - 2n_{22}n_{32}n_{11}C_1G_1G_2 + 4n_{22}n_{32}n_{35}n_{13}C_1G_1G_2^2 - 2n_{22}n_{11}C_1G_1G_2 - \\
& 8n_{22}n_{11}G_1^2G_2C_2 - \\
& - 2n_{22}n_{32}n_{11}G_1G_2C_2 - n_{22}n_{11}G_1C_2 - 8n_{22}n_{26}n_{11}G_1^2G_2C_2 - 2n_{22}n_{35}n_{11}G_1G_2C_2 + 4n_{22}n_{32}n_{13}C_1G_1G_2^2 - \\
& - 4n_{22}n_{26}n_{32}n_{11}G_1^2G_2C_2 - 4n_{22}n_{26}n_{35}n_{11}G_1^2G_2C_2 - 4n_{22}n_{35}n_{11}G_1^2G_2C_2 - 2n_{22}n_{26}n_{11}G_1^2C_2) + \\
& + 4n_{22}n_{11}G_1^2G_2^2 + 2n_{22}n_{11}G_1G_2 + 4n_{22}n_{32}n_{35}n_{11}G_1G_2^2 + 8n_{22}n_{26}n_{11}G_1^2G_2^2 + 2n_{22}n_{32}n_{11}G_1G_2 + \\
& + 8n_{22}n_{32}n_{11}G_1^2G_2^2 + 4n_{22}n_{32}n_{11}G_1G_2^2 + 8n_{22}n_{26}n_{35}n_{11}G_1^2G_2^2 + 8n_{22}n_{11}G_1^2G_2^2 + 4n_{22}n_{11}G_1G_2^2 + \\
& + 4n_{22}n_{32}n_{11}G_1^2G_2^2 + 4n_{22}n_{26}n_{32}n_{11}G_1^2G_2^2 + 8n_{22}n_{26}n_{32}n_{35}n_{11}G_1^2G_2^2 + 8n_{22}n_{26}n_{32}n_{11}G_1^2G_2^2 + \\
& + 8n_{22}n_{32}n_{35}n_{11}G_1^2G_2^2 + 4n_{22}n_{35}n_{11}G_1G_2^2 + 4n_{22}n_{26}n_{11}G_1^2G_2^2 + 8n_{22}n_{35}n_{11}G_1^2G_2^2,
\end{aligned} \tag{A.5}$$

$$\begin{aligned}
I_{HP \text{ real}} = & -s^2(4n_{12}C_1G_1C_2 + 16n_{12}C_1G_1G_2C_2 + n_{12}C_1C_2 + 4n_{12}C_1G_2C_2 + 2n_{23}n_{12}C_1G_1C_2 + \\
& + 8n_{23}n_{12}C_1G_1G_2C_2 + 8n_{32}n_{12}C_1G_1G_2C_2 + 4n_{23}n_{32}n_{12}C_1G_1G_2C_2 + 8n_{35}n_{12}C_1G_1G_2C_2 \\
& + 2n_{26}n_{12}C_1G_1C_2 + 2n_{35}n_{12}C_1G_2C_2 + 4n_{26}n_{32}n_{12}C_1G_1G_2C_2 + n_{32}n_{12}C_1G_2C_2 + 8n_{26}n_{12}C_1G_1G_2C_2 \\
& + 4n_{23}n_{35}n_{12}C_1G_1G_2C_2 + 4n_{26}n_{35}n_{12}C_1G_1G_2C_2) - s(4n_{12}C_1G_2^2 + 8n_{12}G_1G_2C_2 \\
& + 8n_{26}n_{35}n_{12}G_1^2G_2C_2 + 8n_{23}n_{32}n_{12}C_1G_1G_2^2 + 16n_{35}n_{12}C_1G_1G_2^2 + 8n_{12}C_1G_1G_2 + 8n_{23}n_{12}G_1G_2C_2
\end{aligned} \tag{A.6}$$

$$\begin{aligned}
& +4n_{23}n_{26}n_{12}G_1^2C_2 + 8n_{32}n_{12}C_1G_1G_2 + 4n_{32}n_{12}G_1G_2C_2 + 8n_{35}n_{12}G_1^2G_2C_2 + 2n_{32}n_{12}C_1G_2 \\
& + 4n_{35}n_{12}G_1G_2C_2 + 4n_{32}n_{35}n_{12}C_1G_2^2 + 16n_{12}C_1G_1G_2^2 + 4n_{32}n_{12}C_1G_2^2 + 8n_{26}n_{32}n_{12}C_1G_1G_2^2 \\
& + 16n_{23}n_{26}n_{12}G_1^2G_2C_2 + 4n_{26}n_{32}n_{12}C_1G_1G_2 + 4n_{23}n_{32}n_{12}C_1G_1G_2 + 2n_{12}C_1G_2 + 16n_{26}n_{12}G_1^2G_2C_2 \\
& + 8n_{26}n_{32}n_{35}n_{12}C_1G_1G_2^2 + 2n_{12}G_1C_2 + 16n_{12}G_1^2G_2C_2 + 16n_{32}n_{35}n_{12}C_1G_1G_2^2 + 4n_{23}n_{12}C_1G_1G_2 \\
& + 8n_{23}n_{35}n_{12}G_1^2G_2C_2 + 4n_{23}n_{12}G_1^2C_2 + 4n_{23}n_{35}n_{12}G_1G_2C_2 + 16n_{23}n_{12}G_1^2G_2C_2 + 4n_{26}n_{12}C_1G_1G_2 \\
& + 4n_{35}n_{12}C_1G_2^2 + 8n_{32}n_{12}G_1^2G_2C_2 + 8n_{26}n_{35}n_{12}C_1G_1G_2^2 + 4n_{26}n_{12}G_1^2C_2 + 8n_{23}n_{35}n_{12}C_1G_1G_2^2 \\
& + 8n_{23}n_{12}C_1G_1G_2^2 + 16n_{32}n_{12}C_1G_1G_2^2 + 8n_{23}n_{32}n_{35}n_{12}C_1G_1G_2^2 + 8n_{23}n_{26}n_{32}n_{12}G_1^2G_2C_2 \\
& + 4n_{12}G_1^2C_2 + 8n_{26}n_{12}C_1G_1G_2^2 + 8n_{23}n_{32}n_{12}G_1^2G_2C_2 + 8n_{26}n_{32}n_{12}G_1^2G_2C_2 \\
& + 8n_{23}n_{26}n_{35}n_{12}G_1^2G_2C_2 + 4n_{23}n_{32}n_{12}G_1G_2C_2 + 2n_{23}n_{12}G_1C_2) - \\
& -16n_{26}n_{35}n_{12}G_1^2G_2^2 - 4n_{12}G_1G_2 - 16n_{23}n_{12}G_1^2G_2^2 - 8n_{23}n_{12}G_1G_2^2 - 16n_{23}n_{26}n_{12}G_1^2G_2^2 - \\
& -16n_{26}n_{32}n_{12}G_1^2G_2^2 - 8n_{32}n_{12}G_1G_2^2 - 8n_{26}n_{32}n_{12}G_1^2G_2 - 16n_{12}G_1^2G_2^2 - 8n_{12}G_1G_2^2 - 4n_{32}n_{12}G_1G_2 - \\
& -4n_{23}n_{32}n_{12}G_1G_2 - 8n_{12}G_1^2G_2 - 8n_{23}n_{35}n_{12}G_1G_2^2 - 16n_{32}n_{35}n_{12}G_1^2G_2^2 - 8n_{32}n_{35}n_{12}G_1G_2^2 - \\
& -8n_{23}n_{32}n_{35}n_{12}G_1G_2^2 - 8n_{23}n_{26}n_{12}G_1^2G_2 - 8n_{23}n_{12}G_1^2G_2 - 4n_{23}n_{12}G_1G_2 - 16n_{35}n_{12}G_1^2G_2^2 - \\
& 8n_{35}n_{12}G_1G_2^2 - \\
& -8n_{32}n_{12}G_1^2G_2 - 8n_{23}n_{26}n_{32}n_{12}G_1^2G_2 - 16n_{23}n_{35}n_{12}G_1^2G_2^2 - 16n_{23}n_{26}n_{32}n_{35}n_{12}G_1^2G_2^2 - \\
& 8n_{23}n_{32}n_{12}G_1G_2^2 - \\
& -16n_{23}n_{32}n_{35}n_{12}G_1^2G_2^2 - 8n_{26}n_{12}G_1^2G_2 - 8n_{23}n_{32}n_{12}G_1^2G_2 - 16n_{32}n_{12}G_1^2G_2^2 - 16n_{23}n_{32}n_{12}G_1^2G_2^2 - \\
& -16n_{26}n_{12}G_1^2G_2^2 - 16n_{23}n_{26}n_{35}n_{12}G_1^2G_2^2 - 16n_{26}n_{32}n_{35}n_{12}G_1^2G_2^2 - 16n_{23}n_{26}n_{32}n_{12}G_1^2G_2^2,
\end{aligned}$$

$$\begin{aligned}
I_{BS \text{ real}} = & -s^2(4n_{12}C_1G_1C_2 + 8n_{35}n_{12}C_1G_1G_2C_2 + 4n_{26}n_{35}n_{12}C_1G_1G_2C_2 + 4n_{12}C_1G_2C_2 + n_{12}C_1C_2 \\
& + 8n_{26}n_{12}C_1G_1G_2C_2 + 16n_{12}C_1G_1G_2C_2 + 4n_{23}n_{35}n_{12}C_1G_1G_2C_2 + 8n_{32}n_{12}C_1G_1G_2C_2 + 2n_{35}n_{12}C_1G_2C_2 \\
& + 2n_{26}n_{12}C_1G_1C_2 + 2n_{32}n_{12}C_1G_2C_2 + 4n_{26}n_{32}n_{12}C_1G_1G_2C_2 + 8n_{23}n_{12}C_1G_1G_2C_2 \\
& + 4n_{23}n_{32}n_{12}C_1G_1G_2C_2 + 2n_{23}n_{12}C_1G_1C_2) - s(16n_{23}n_{12}G_1^2G_2C_2 + 4n_{32}n_{35}n_{12}C_1G_2^2 \\
& + 2A_1n_{24}n_{33}n_{35}C_1G_1G_2^2n_{13} + 8n_{26}n_{35}n_{12}G_1^2G_2C_2 + 4n_{23}n_{32}n_{12}C_1G_1G_2 - 2A_1n_{21}n_{33}C_1G_1G_2^2n_{13} \\
& + 4n_{12}C_1G_2^2 + 8n_{26}n_{32}n_{35}n_{12}C_1G_1G_2^2 + 16n_{23}n_{26}n_{12}G_1^2G_2C_2 + 4n_{23}n_{12}G_1^2C_2 + 16n_{12}G_1^2G_2C_2 \\
& + 16n_{32}n_{12}C_1G_1G_2^2 + 8n_{32}n_{12}G_1^2G_2C_2 + 8n_{23}n_{26}n_{35}n_{12}G_1^2G_2C_2 + 8n_{12}C_1G_1G_2 \\
& + 8n_{23}n_{26}n_{32}n_{12}G_1^2G_2C_2 + 8n_{26}n_{32}n_{12}C_1G_1G_2^2 + 16n_{32}n_{35}n_{12}C_1G_1G_2^2 + 2n_{12}C_1G_2 \\
& + A_1n_{24}n_{33}C_1G_1G_2n_{13} - 2A_1n_{24}n_{33}n_{11}C_1G_1G_2^2 + 4n_{26}n_{12}C_1G_1G_2 + 8n_{26}n_{32}n_{12}G_1^2G_2C_2 + 8n_{12}G_1G_2C_2 \\
& + 4n_{12}G_1^2C_2 + 2n_{12}G_1C_2 + 4n_{23}n_{35}n_{12}G_1G_2C_2 + 16n_{35}n_{12}C_1G_1G_2^2 + 4n_{26}n_{12}G_1^2C_2 \\
& + 8n_{26}n_{35}n_{12}C_1G_1G_2^2 + 4n_{35}n_{12}C_1G_2^2 - A_1n_{21}n_{33}C_1G_1G_2n_{13} + 8n_{23}n_{32}n_{12}G_1^2G_2C_2 \\
& + 4n_{23}n_{32}n_{12}G_1G_2C_2 + 8n_{35}n_{12}G_1^2G_2C_2 + 4n_{35}n_{12}G_1G_2C_2 + 8n_{23}n_{35}n_{12}C_1G_1G_2^2 + 8n_{26}n_{12}C_1G_1G_2^2 \\
& + 8n_{32}n_{12}C_1G_1G_2 + 4n_{32}n_{12}C_1G_2^2 + 16n_{26}n_{12}G_1^2G_2C_2 + 2n_{32}n_{12}C_1G_2 + 4n_{23}n_{26}n_{12}G_1^2C_2 \\
& + 16n_{12}C_1G_1G_2^2 + 4n_{23}n_{12}C_1G_1G_2 + 4n_{32}n_{12}G_1G_2C_2 + 2A_1n_{24}n_{33}C_1G_1G_2^2n_{13} + 8n_{23}n_{12}G_1G_2C_2 \\
& + 2A_1n_{21}n_{33}n_{11}C_1G_1G_2^2 + 8n_{23}n_{32}n_{35}n_{12}C_1G_1G_2^2 - 2A_1n_{24}n_{33}n_{35}n_{11}C_1G_1G_2^2 + 2n_{23}n_{12}G_1C_2 \\
& + 2A_1n_{21}n_{33}n_{35}n_{11}C_1G_1G_2^2 + 8n_{23}n_{35}n_{12}G_1^2G_2C_2 - A_1n_{24}n_{33}n_{11}C_1G_1G_2 + 8n_{23}n_{32}n_{12}C_1G_1G_2^2 \\
& + 4n_{26}n_{32}n_{12}C_1G_1G_2 + A_1n_{21}n_{33}n_{11}C_1G_1G_2 - 2A_1n_{21}n_{33}n_{35}C_1G_1G_2^2n_{13} + 8n_{23}n_{12}C_1G_1G_2^2) - \\
& 4A_1n_{21}n_{26}n_{33}n_{35}n_{11}G_1^2G_2^2 - 16n_{23}n_{12}G_1^2G_2^2 - 8n_{23}n_{12}G_1G_2^2 - 8n_{32}n_{12}G_1^2G_2 - 4n_{32}n_{12}G_1G_2 - \\
& 8n_{23}n_{12}G_1^2G_2 - 4n_{23}n_{12}G_1G_2 - 16n_{32}n_{35}n_{12}G_1^2G_2^2 - 16n_{12}G_1^2G_2^2 - 8n_{12}G_1G_2^2 - 16n_{23}n_{32}n_{35}n_{12}G_1^2G_2^2 \\
& - 16n_{23}n_{35}n_{12}G_1^2G_2^2 - 8n_{12}G_1^2G_2 - 4n_{12}G_1G_2 - 4A_1n_{24}n_{33}n_{35}G_1^2G_2^2n_{13} - 8n_{26}n_{12}G_1^2G_2 - \\
& 2A_1n_{23}n_{24}n_{33}G_1^2G_2n_{13} - 4A_1N_{23}n_{24}n_{33}n_{35}G_1^2G_2^2n_{13} - 16n_{23}n_{32}n_{12}G_1^2G_2^2 - 8n_{23}n_{32}n_{12}G_1G_2^2 - \\
& 16n_{35}n_{12}G_1^2G_2^2 - 8n_{35}n_{12}G_1G_2^2 - 8n_{23}n_{32}n_{12}G_1^2G_2 - 4n_{23}n_{32}n_{12}G_1G_2 - 16n_{26}n_{32}n_{12}G_1^2G_2^2 - \\
& 2A_1n_{24}n_{33}G_1^2G_2n_{13} - 8n_{23}n_{32}n_{35}n_{12}G_1G_2^2 - 16n_{23}n_{26}n_{12}G_1^2G_2^2 - 16n_{26}n_{32}n_{35}n_{12}G_1^2G_2^2 - \\
& 8n_{23}n_{26}n_{12}G_1^2G_2 - 16n_{32}n_{12}G_1^2G_2^2 - 8n_{32}n_{12}G_1G_2^2 - 16n_{23}n_{26}n_{35}n_{12}G_1^2G_2^2 - 16n_{23}n_{26}n_{32}n_{12}G_1^2G_2^2 - \\
& A_1n_{21}n_{33}n_{11}G_1G_2 - 16n_{26}n_{35}n_{12}G_1^2G_2^2 - 16n_{23}n_{26}n_{32}n_{35}n_{12}G_1^2G_2^2 - 8n_{23}n_{26}n_{32}n_{12}G_1^2G_2 - \\
& 4A_1n_{21}n_{33}n_{11}G_1^2G_2^2 - 8n_{32}n_{35}n_{12}G_1G_2^2 - 4A_1n_{23}n_{24}n_{33}G_1^2G_2^2n_{13} - 2A_1n_{21}n_{26}n_{33}n_{11}G_1^2G_2 - \\
& 8n_{26}n_{32}n_{12}G_1^2G_2 - 2A_1n_{21}n_{33}n_{11}G_1^2G_2 - 16n_{26}n_{12}G_1^2G_2^2 - 2A_1n_{21}n_{33}n_{35}n_{11}G_1G_2^2 - \\
& 4A_1n_{21}n_{26}n_{33}n_{11}G_1^2G_2^2 - 2A_1n_{21}n_{33}n_{11}G_1G_2^2 - 4A_1n_{21}n_{33}n_{35}n_{11}G_1^2G_2^2 - 4A_1n_{24}n_{33}G_1^2G_2^2n_{13} - \\
& 8n_{23}n_{35}n_{12}G_1G_2^2.
\end{aligned} \tag{A.7}$$

B EQUATIONS OF THE SENSITIVITY ANALYSIS OF THE F- D FILTER FROM CHAPTER 6.5

$$b_2 = 2C_2C_1G_1n_{12} + 16G_2C_2C_1G_1 + C_2C_1 + 4C_2C_1G_1 + 4G_2C_2C_1G_1n_{15}n_{21} + 4G_2C_2C_1 + 2G_2C_2C_1n_{21} + 2C_2C_1G_1n_{15} + 8G_2C_2C_1G_1n_{28} + 4G_2C_2C_1G_1n_{12}n_{28} + 4G_2C_2C_1G_1n_{15}n_{28} + 2G_2C_2C_1n_{28} + 8G_2C_2C_1G_1n_{21} + 8G_2C_2C_1G_1n_{12} + 4G_2C_2C_1G_1n_{12}n_{21} + 8G_2C_2C_1G_1n_{15}, \quad (B.1)$$

$$b_1 = 8G_2^2C_1G_1n_{12}n_{21}n_{28} + 16G_2C_2G_1^2 + 16G_2^2C_1G_1n_{21}n_{28} + 8G_2^2C_1G_1n_{12}n_{21} + 8A_1G_2^2C_1G_1n_{21}n_{26} + 8A_1G_2^2C_1G_1n_{26} + 8G_2^2C_1G_1n_{12} + 8G_2^2C_1G_1n_{12}n_{28} + 4A_1G_2^2C_1G_1n_{15}n_{26} + 4G_2^2C_1G_1n_{21}n_{28} + 8G_2C_2G_1^2n_{21} + 4A_1G_2^2C_1G_1n_{12}n_{26} + 4A_1G_2^2C_1G_1n_{12}n_{21}n_{26} + 16G_2^2C_1G_1n_{21} + 16G_2^2C_1G_1n_{28} + 2A_1G_2^2C_1n_{23} + 2A_1G_2^2C_1n_{23}n_{28} + 16G_2^2C_1G_1 + 4G_2C_2G_1n_{28} + 4G_2C_2G_1n_{12}n_{28} + 2G_2C_1 + 2G_2C_1n_{21} + 16G_2C_2G_1^2n_{15} + 8G_2^2C_1G_1n_{15} + 8G_2^2C_1G_1n_{15}n_{28} + 8G_2^2C_1G_1n_{15}n_{21} + 8G_2^2C_1G_1n_{15}n_{21}n_{28} + 4G_2^2C_1 + 4G_2^2C_1n_{28} + 4G_2^2C_1n_{21} + 8A_1G_2^2C_1G_1n_{23} + 8A_1G_2^2C_1G_1n_{23}n_{28} + 4A_1G_2^2C_1G_1n_{12}n_{23} + 4A_1G_2^2C_1G_1n_{12}n_{23}n_{28} + 4A_1G_2^2C_1G_1n_{15}n_{23} + 4A_1G_2^2C_1G_1n_{15}n_{23}n_{28} + 8G_2C_1G_1n_{21} + 8G_2C_2G_1^2n_{28} + 8G_2C_2G_1^2n_{15}n_{28} + 8G_2C_2G_1^2n_{12}n_{28} + 8G_2C_2G_1^2n_{12}n_{15}n_{28} + 8G_2C_2G_1^2n_{12}n_{15}n_{21} + 8G_2C_2G_1 + 4A_1G_2^2C_1G_1n_{15}n_{21}n_{26} + 2A_1G_2^2C_1n_{26} + 4C_2G_1^2 + 4C_2G_1^2n_{15} + 4C_2G_1^2n_{12} + 4C_2G_1^2n_{12}n_{15} + 2C_2G_1 + 2C_2G_1n_{12} + 4G_2C_1G_1n_{15}n_{21} + 4A_1G_2C_1G_1n_{23} + 4G_2C_2G_1n_{21} + 8G_2C_2G_1n_{12} + 4G_2C_2G_1n_{12}n_{21} + 8G_2C_1G_1 + 2A_1G_2^2C_1n_{21}n_{26} + 4G_2C_1G_1n_{12} + 4G_2C_1G_1n_{12}n_{21} + 4G_2C_1G_1n_{15} + 16G_2C_2G_1^2n_{12}n_{15} + 2A_1G_2C_1G_1n_{15}n_{23} + 2A_1G_2C_1G_1n_{12}n_{23} + 8G_2C_2G_1^2n_{15}n_{21} + A_1G_2C_1n_{23} + 8G_2C_2G_1^2n_{12}n_{21} + 16G_2C_2G_1^2n_{12}, \quad (B.2)$$

$$b_0 = 4A_1G_2^2G_1^2A_2n_{12}n_{16}n_{21}n_{27} + 16G_2^2G_1^2n_{15}n_{21} + 16G_2^2G_1^2n_{15}n_{21}n_{28} + 16G_2^2G_1^2n_{12} + 16G_2^2G_1^2n_{12}n_{28} + 16G_2^2G_1^2n_{12}n_{21} + 16G_2^2G_1^2n_{12}n_{21}n_{28} + 16G_2^2G_1^2n_{12}n_{15} + 8A_1G_2^2G_1^2n_{26} + 8A_1G_2^2G_1^2n_{21}n_{26} + 8A_1G_2^2G_1^2n_{15}n_{26} + 8A_1G_2^2G_1^2n_{15}n_{21}n_{26} + 8A_1G_2^2G_1^2n_{12}n_{26} + 8A_1G_2^2G_1^2n_{12}n_{21}n_{26} + 8A_1G_2^2G_1^2n_{12}n_{15}n_{26} + 8A_1G_2^2G_1^2n_{12}n_{15}n_{21}n_{26} + 16G_2^2G_1^2 + 16G_2^2G_1^2n_{28} + 16G_2^2G_1^2n_{21} + 16G_2^2G_1^2n_{21}n_{28} + 16G_2^2G_1^2n_{15} + 16G_2^2G_1^2n_{15}n_{28} + 4A_1G_2^2G_1^2A_2n_{12}n_{16}n_{27} + 4A_1G_2^2G_1^2A_2n_{11}n_{15}n_{22} + 4A_1G_2^2G_1^2A_2n_{11}n_{15}n_{22}n_{28} + 2A_1G_2^2G_1A_2n_{11}n_{22} + 8G_2G_1^2 + 8G_2G_1^2n_{21} + 8G_2G_1^2n_{15} + 16G_2^2G_1^2n_{12}n_{15}n_{28} + 16G_2^2G_1^2n_{12}n_{15}n_{21} + 16G_2^2G_1^2n_{12}n_{15}n_{21}n_{28} + 8G_2^2G_1 + 8G_2^2G_1n_{28} + 8G_2^2G_1n_{21} + 8G_2^2G_1n_{21}n_{28} + 8G_2^2G_1n_{12} + 8G_2^2G_1n_{12}n_{28} + 8G_2^2G_1n_{12}n_{21} + 8G_2^2G_1n_{12}n_{21}n_{28} + 4A_1G_2G_1^2n_{12}n_{15}n_{23} + 2A_1G_2G_1n_{23} + 2A_1G_2G_1n_{12}n_{23} + 4A_1G_2^2G_1^2A_2n_{11}n_{22}n_{28} + 8G_2G_1^2n_{12}n_{15}n_{21} + 8A_1G_2^2G_1^2n_{23} + 8A_1G_2^2G_1^2n_{23}n_{28} + 8A_1G_2^2G_1^2n_{15}n_{23} + 8A_1G_2^2G_1^2n_{15}n_{23}n_{28} + 8A_1G_2^2G_1^2n_{12}n_{23} + 8G_2G_1^2n_{15}n_{21} + 8G_2G_1^2n_{12} + 8G_2G_1^2n_{12}n_{21} + 8G_2G_1^2n_{12}n_{15} + 4A_1G_2^2G_1^2A_2n_{16}n_{21}n_{27} + 4G_2G_1 + 4G_2G_1n_{21} + 4G_2G_1n_{12} + 4G_2G_1n_{12}n_{21} + 4A_1G_2^2G_1n_{26} + 4A_1G_2^2G_1n_{21}n_{26} + 4A_1G_2^2G_1n_{12}n_{26} + 4A_1G_2^2G_1n_{12}n_{21}n_{26} + 4A_1G_2^2G_1^2A_2n_{11}n_{22} + 4A_1G_2^2G_1n_{23} + 4A_1G_2^2G_1n_{23}n_{28} + 4A_1G_2^2G_1n_{12}n_{23} + 4A_1G_2^2G_1n_{12}n_{23}n_{28} + 2A_1G_2^2G_1A_2n_{11}n_{27} + 2A_1G_2^2G_1A_2n_{11}n_{21}n_{27} + 4A_1G_2^2G_1^2A_2n_{12}n_{16}n_{22} + 8A_1G_2^2G_1^2n_{12}n_{23}n_{28} + 8A_1G_2^2G_1^2n_{12}n_{15}n_{23} + 8A_1G_2^2G_1^2n_{12}n_{15}n_{23}n_{28} + 4A_1G_2^2G_1^2A_2n_{16}n_{27} + A_1G_2G_1A_2n_{11}n_{22} + 4A_1G_2^2G_1^2A_2n_{11}n_{27} + 4A_1G_2^2G_1^2A_2n_{11}n_{21}n_{27} + 4A_1G_2^2G_1^2A_2n_{11}n_{15}n_{27} + 4A_1G_2^2G_1^2A_2n_{11}n_{15}n_{21}n_{27} + 4A_1G_2G_1^2n_{12}n_{23} + 4A_1G_2^2G_1^2A_2n_{12}n_{16}n_{22}n_{28} + 2A_1G_2G_1^2A_2n_{16}n_{22} + 2A_1G_2G_1^2A_2n_{12}n_{16}n_{22} + 2A_1G_2G_1^2A_2n_{11}n_{15}n_{22} + 2A_1G_2^2G_1A_2n_{11}n_{22}n_{28} + 4A_1G_2^2G_1^2A_2n_{16}n_{22} + 4A_1G_2G_1^2n_{15}n_{23} + 2A_1G_2G_1^2A_2n_{11}n_{22} + 4A_1G_2G_1^2n_{23} + 4A_1G_2^2G_1^2A_2n_{16}n_{22}n_{28}. \quad (B.3)$$

$$I_{LP \text{ real}} = -4A_1G_2^2G_1^2A_2n_{13}n_{22} - 4A_1G_2^2G_1^2A_2n_{13}n_{22}n_{28} - 4A_1G_2^2G_1^2A_2n_{13}n_{15}n_{22} - 4A_1G_2^2G_1^2A_2n_{13}n_{15}n_{22}n_{28} - 2A_1G_2^2G_1A_2n_{13}n_{22} - 2A_1G_2^2G_1A_2n_{13}n_{22}n_{28} - 2A_1G_2G_1^2A_2n_{13}n_{22} - 2A_1G_2G_1^2A_2n_{13}n_{15}n_{22} - A_1G_2G_1A_2n_{13}n_{22} - 4A_1G_2^2G_1^2A_2n_{13}n_{27} - 4A_1G_2^2G_1^2A_2n_{13}n_{21}n_{27} - 4A_1G_2^2G_1^2A_2n_{13}n_{15}n_{27} - 4A_1G_2^2G_1^2A_2n_{13}n_{15}n_{21}n_{27} - 2A_1G_2^2G_1A_2n_{13}n_{27} - 2A_1G_2^2G_1A_2n_{13}n_{21}n_{27}, \quad (B.4)$$

$$\begin{aligned}
I_{\text{BP1 real}} = & -s(8A_1G_2^2C_1G_1n_{24}n_{28} + 4A_1G_2^2C_1G_1n_{15}n_{24}n_{28} + 2A_1G_2^2C_1n_{24} + 2A_1G_2^2C_1n_{24}n_{28} + \\
& + 8A_1G_2^2C_1G_1n_{24} + A_1G_2C_1n_{24} + 4A_1G_2^2C_1G_1n_{12}n_{24} + 4A_1G_2^2C_1G_1n_{12}n_{24}n_{28} + 4A_1G_2^2C_1G_1n_{15}n_{24} + \\
& + 4A_1G_2C_1G_1n_{24} + 2A_1G_2C_1G_1n_{12}n_{24} + 2A_1G_2C_1G_1n_{15}n_{24}) - 8A_1G_2^2G_1^2n_{12}n_{15}n_{24}n_{28} - 4A_1G_2^2G_1n_{24} - \\
& - 4A_1G_2^2G_1n_{24}n_{28} - 4A_1G_2^2G_1n_{12}n_{24} - 4A_1G_2^2G_1n_{12}n_{24}n_{28} - 8A_1G_2^2G_1^2n_{12}n_{24} - 8A_1G_2^2G_1^2n_{12}n_{24}n_{28} - \\
& - 8A_1G_2^2G_1^2n_{12}n_{15}n_{24} - 8A_1G_2^2G_1^2n_{24} - 8A_1G_2^2G_1^2n_{24}n_{28} - 8A_1G_2^2G_1^2n_{15}n_{24} - 8A_1G_2^2G_1^2n_{15}n_{24}n_{28} - \\
& - 4A_1G_2G_1^2n_{12}n_{24} - 4A_1G_2G_1^2n_{12}n_{15}n_{24} - 2A_1G_2G_1n_{24} - 2A_1G_2G_1n_{12}n_{24} - 4A_1G_2G_1^2n_{24} - \\
& 4A_1G_2G_1^2n_{15}n_{24},
\end{aligned} \tag{B.5}$$

$$\begin{aligned}
I_{\text{BP2 real}} = & s(2A_1G_2^2C_1A_2n_{22} + 2A_1G_2^2C_1A_2n_{22}n_{28} + 4A_1G_2^2C_1G_1A_2n_{15}n_{22}n_{28} + \\
& + 4A_1G_2^2C_1G_1A_2n_{12}n_{21}n_{27} + 4A_1G_2^2C_1G_1A_2n_{15}n_{27} + 4A_1G_2^2C_1G_1A_2n_{15}n_{21}n_{27} + 2A_1G_2^2C_1A_2n_{27} + \\
& + 8A_1G_2^2C_1G_1A_2n_{22} + 8A_1G_2^2C_1G_1A_2n_{22}n_{28} + 4A_1G_2^2C_1G_1A_2n_{12}n_{22} + 4A_1G_2^2C_1G_1A_2n_{12}n_{22}n_{28} + \\
& + 4A_1G_2^2C_1G_1A_2n_{15}n_{22} + 8A_1G_2^2C_1G_1A_2n_{27} + 8A_1G_2^2C_1G_1A_2n_{21}n_{27} + 4A_1G_2^2C_1G_1A_2n_{12}n_{27} + \\
& + 4A_1G_2C_1G_1A_2n_{22} + 2A_1G_2C_1G_1A_2n_{12}n_{22} + 2A_1G_2C_1G_1A_2n_{15}n_{22} + A_1G_2C_1A_2n_{22} + \\
& + 2A_1G_2^2C_1A_2n_{21}n_{27}) + 4A_1G_2G_1^2A_2n_{15}n_{22} + 4A_1G_2G_1^2A_2n_{12}n_{22} + 4A_1G_2G_1^2A_2n_{12}n_{15}n_{22} + \\
& + 2A_1G_2G_1A_2n_{22} + 2A_1G_2G_1A_2n_{12}n_{22} + 4A_1G_2^2G_1A_2n_{22}n_{28} + 4A_1G_2^2G_1A_2n_{12}n_{22} + \\
& + 4A_1G_2^2G_1A_2n_{12}n_{22}n_{28} + 8A_1G_2^2G_1^2A_2n_{22} + 8A_1G_2^2G_1^2A_2n_{22}n_{28} + 8A_1G_2^2G_1^2A_2n_{15}n_{22} + \\
& + 8A_1G_2^2G_1^2A_2n_{15}n_{22}n_{28} + 8A_1G_2^2G_1^2A_2n_{12}n_{22} + 8A_1G_2^2G_1^2A_2n_{12}n_{22}n_{28} + 8A_1G_2^2G_1^2A_2n_{12}n_{15}n_{22} + \\
& + 8A_1G_2^2G_1^2A_2n_{12}n_{15}n_{22}n_{28} + 4A_1G_2^2G_1A_2n_{22} + 8A_1G_2^2G_1^2A_2n_{15}n_{21}n_{27} + 8A_1G_2^2G_1^2A_2n_{12}n_{27} + \\
& + 8A_1G_2^2G_1^2A_2n_{12}n_{21}n_{27} + 8A_1G_2^2G_1^2A_2n_{12}n_{15}n_{21}n_{27} + 4A_1G_2^2G_1A_2n_{27} + 4A_1G_2^2G_1A_2n_{21}n_{27} + \\
& + 4A_1G_2^2G_1A_2n_{12}n_{27} + 4A_1G_2G_1^2A_2n_{22} + 4A_1G_2^2G_1A_2n_{12}n_{21}n_{27} + 8A_1G_2^2G_1^2A_2n_{27} + \\
& + 8A_1G_2^2G_1^2A_2n_{21}n_{27} + 8A_1G_2^2G_1^2A_2n_{15}n_{27} + 8A_1G_2^2G_1^2A_2n_{12}n_{15}n_{27},
\end{aligned} \tag{B.6}$$

$$\begin{aligned}
I_{\text{HP real}} = & s^2(2A_1G_2C_2C_1n_{28} + 8A_1G_2C_2C_1G_1n_{12} + 4A_1G_2C_2C_1G_1n_{12}n_{21} + 8A_1G_2C_2C_1G_1n_{21} + \\
& + 4A_1G_2C_2C_1G_1n_{15}n_{28} + 16A_1G_2C_2C_1G_1 + 4A_1C_2C_1G_1 + 2A_1C_2C_1G_1n_{12} + 8A_1G_2C_2C_1G_1n_{28} + \\
& + 4A_1G_2C_2C_1G_1n_{12}n_{28} + 8A_1G_2C_2C_1G_1n_{15} + 4A_1G_2C_2C_1G_1n_{15}n_{21} + 4A_1G_2C_2C_1 + 2A_1G_2C_2C_1n_{21} + \\
& + 2A_1C_2C_1G_1n_{15} + A_1C_2C_1) + s(4A_1G_2^2C_1n_{21}n_{28} + 8A_1G_2^2C_1G_1n_{12}n_{28} + 4A_1G_2^2C_1n_{28} + \\
& + 4A_1G_2^2C_1n_{21} + 4A_1G_2C_1G_1n_{15}n_{21} + 2A_1G_2C_1 + 2A_1G_2C_1n_{21} + 8A_1G_2^2C_1G_1n_{12}n_{21} + \\
& + 8A_1G_2^2C_1G_1n_{12}n_{21}n_{28} + 8A_1G_2^2C_1G_1n_{15} + 8A_1G_2^2C_1G_1n_{15}n_{28} + 8A_1G_2^2C_1G_1n_{15}n_{21} + \\
& + 8A_1G_2^2C_1G_1n_{15}n_{21}n_{28} + 4A_1G_2^2C_1 + 16A_1G_2^2C_1G_1 + 16A_1G_2^2C_1G_1n_{28} + 16A_1G_2^2C_1G_1n_{21} + \\
& + 16A_1G_2^2C_1G_1n_{21}n_{28} + 8A_1G_2^2C_1G_1n_{12} + 8A_1G_2C_2G_1^2n_{12}n_{15}n_{21} + 8A_1G_2C_2G_1 + 4A_1G_2C_2G_1n_{21} + \\
& + 8A_1G_2C_2G_1n_{12} + 4A_1G_2C_2G_1n_{12}n_{21} + 8A_1G_2C_1G_1 + 8A_1G_2C_1G_1n_{21} + 4A_1G_2C_1G_1n_{12} + \\
& + 4A_1G_2C_1G_1n_{12}n_{21} + 4A_1G_2C_1G_1n_{15} + 16A_1G_2C_2G_1^2n_{12} + 8A_1G_2C_2G_1^2n_{12}n_{21} + \\
& + 16A_1G_2C_2G_1^2n_{12}n_{15} + 8A_1G_2C_2G_1^2n_{21} + 4A_1C_2G_1^2 + 4A_1C_2G_1^2n_{15} + 4A_1C_2G_1^2n_{12} + \\
& + 4A_1C_2G_1^2n_{12}n_{15} + 16A_1G_2C_2G_1^2 + 8A_1G_2C_2G_1^2n_{12}n_{28} + 16A_1G_2C_2G_1^2n_{15} + 8A_1G_2C_2G_1^2n_{15}n_{21} + \\
& + 4A_1G_2C_2G_1n_{12}n_{28} + 8A_1G_2C_2G_1^2n_{28} + 8A_1G_2C_2G_1^2n_{15}n_{28} + 2A_1C_2G_1 + 8A_1G_2C_2G_1^2n_{12}n_{15}n_{28} + \\
& + 4A_1G_2C_2G_1n_{28} + 2A_1C_2G_1n_{12}) + 16A_1G_2^2G_1^2n_{12}n_{28} + 16A_1G_2^2G_1^2n_{12}n_{21} + 16A_1G_2^2G_1^2n_{12}n_{21}n_{28} + \\
& + 16A_1G_2^2G_1^2n_{12}n_{15} + 16A_1G_2^2G_1^2n_{12}n_{15}n_{28} + 16A_1G_2^2G_1^2n_{12}n_{15}n_{21} + 16A_1G_2^2G_1^2n_{12}n_{15}n_{21}n_{28} + \\
& + 8A_1G_2^2G_1 + 8A_1G_2^2G_1n_{28} + 8A_1G_2^2G_1n_{21} + 8A_1G_2^2G_1n_{21}n_{28} + 8A_1G_2^2G_1n_{12} + 8A_1G_2^2G_1n_{12}n_{28} + \\
& + 8A_1G_2^2G_1n_{12}n_{21} + 8A_1G_2^2G_1n_{12}n_{21}n_{28} + 4A_1G_2G_1n_{21} + 16A_1G_2^2G_1^2 + 16A_1G_2^2G_1^2n_{28} + \\
& + 16A_1G_2^2G_1^2n_{21} + 16A_1G_2^2G_1^2n_{21}n_{28} + \\
& + 16A_1G_2^2G_1^2n_{15} + 16A_1G_2^2G_1^2n_{15}n_{28} + 16A_1G_2^2G_1^2n_{15}n_{21} + 16A_1G_2^2G_1^2n_{15}n_{21}n_{28} + \\
& + 16A_1G_2^2G_1^2n_{12} + 8A_1G_2G_1^2N_{12}n_{15}n_{21} + 4A_1G_2G_1 + 8A_1G_2G_1^2n_{15} + 4A_1G_2G_1n_{12} + 4A_1G_2G_1n_{12}n_{21} + \\
& + 8A_1G_2G_1^2n_{12}n_{21} + 8A_1G_2G_1^2 + 8A_1G_2G_1^2n_{21} + 8A_1G_2G_1^2n_{15}n_{21} + 8A_1G_2G_1^2n_{12} + \\
& + 8A_1G_2G_1^2n_{12}n_{15},
\end{aligned} \tag{B.7}$$

$$\begin{aligned}
I_{\text{BS real}} = & s^2(4A_1C_2C_1G_1 + 16A_1G_2C_2C_1G_1 + 8A_1G_2C_2C_1G_1n_{15} + 4A_1G_2C_2C_1G_1n_{15}n_{21} \\
& + 4A_1G_2C_2C_1 + 2A_1G_2C_2C_1n_{21} + 2A_1C_2C_1G_1n_{12} + 2A_1C_2C_1G_1n_{15} + A_1C_2C_1 + 8A_1G_2C_2C_1G_1n_{28} + \\
& + 4A_1G_2C_2C_1G_1n_{12}n_{28} + 4A_1G_2C_2C_1G_1n_{15}n_{28} + 2A_1G_2C_2C_1n_{28} + 8A_1G_2C_2C_1G_1n_{21} \\
& + 8A_1G_2C_2C_1G_1n_{12} + 4A_1G_2C_2C_1G_1n_{12}n_{21}) + s(16A_1G_2^2C_1G_1n_{21} + 8A_1G_2^2C_1G_1n_{15}n_{21} \\
& + 16A_1G_2^2C_1G_1n_{28} + 4A_1C_2G_1^2n_{12}n_{15} + 2A_1C_2G_1 + 2A_1C_2G_1n_{12} + 16A_1G_2^2C_1G_1 + 8A_1G_2C_2G_1n_{12} \\
& + 16A_1G_2^2C_1G_1n_{21}n_{28} + 8A_1G_2^2C_1G_1n_{12} + 8A_1G_2^2C_1G_1n_{12}n_{28} + 8A_1G_2^2C_1G_1n_{12}n_{21} \\
& + 8A_1G_2^2C_1G_1n_{12}n_{21}n_{28} + \\
& + 8A_1G_2^2C_1G_1n_{15} + 8A_1G_2^2C_1G_1n_{15}n_{28} + 2A_1G_2C_1 + 2A_1G_2C_1n_{21} + 8A_1G_2^2C_1G_1n_{15}n_{21}n_{28} \\
& + 4A_1G_2^2C_1 + 4A_1G_2^2C_1n_{28} + 4A_1G_2^2C_1n_{21} + 4A_1G_2^2C_1n_{21}n_{28} + 4A_1G_2C_2G_1n_{12}n_{21} + 8A_1G_2C_1G_1 \\
& + 8A_1G_2C_1G_1n_{21} + 4A_1G_2C_1G_1n_{12} + 4A_1G_2C_1G_1n_{12}n_{21} + 4A_1G_2C_1G_1n_{15} + 4A_1G_2C_1G_1n_{15}n_{21} \\
& + 8A_1G_2C_2G_1^2n_{15}n_{21} + 16A_1G_2C_2G_1^2n_{12} + 8A_1G_2C_2G_1^2n_{12}n_{21} + 16A_1G_2C_2G_1^2n_{12}n_{15} \\
& + 8A_1G_2C_2G_1^2n_{28} + 8A_1G_2C_2G_1^2n_{15}n_{28} + 8A_1G_2C_2G_1^2n_{12}n_{28} + 8A_1G_2C_2G_1^2n_{12}n_{15}n_{28} \\
& + 4A_1G_2C_2G_1n_{28} + 4A_1G_2C_2G_1n_{12}n_{28} + 16A_1G_2C_2G_1^2n_{15} + 16A_1G_2C_2G_1^2 + 8A_1G_2C_2G_1^2n_{21} \\
& + 4A_1C_2G_1^2n_{12} + 4A_1C_2G_1^2 + 4A_1C_2G_1^2n_{15} + 8A_1G_2C_2G_1 + 4A_1G_2C_2G_1n_{21} + 8A_1G_2C_2G_1^2n_{12}n_{15}n_{21} \\
&) - A_1G_2G_1A_2n_{13}n_{22} + 16A_1G_2^2G_1^2n_{12}n_{15}n_{28} + 16A_1G_2^2G_1^2n_{12}n_{15}n_{21} + 16A_1G_2^2G_1^2n_{12}n_{15}n_{21}n_{28} \\
& + 8A_1G_2^2G_1 + 8A_1G_2^2G_1n_{28} + 8A_1G_2^2G_1n_{21} + 8A_1G_2^2G_1n_{21}n_{28} + 8A_1G_2^2G_1n_{12} + 8A_1G_2^2G_1n_{12}n_{28} \\
& + 8A_1G_2^2G_1n_{12}n_{21} + 8A_1G_2G_1^2 + 8A_1G_2G_1^2n_{21} + 8A_1G_2G_1^2n_{15} + 8A_1G_2G_1^2n_{15}n_{21} + 8A_1G_2G_1^2n_{12} \\
& + 16A_1G_2^2G_1^2 + 16A_1G_2^2G_1^2n_{28} + 16A_1G_2^2G_1^2n_{21} + 16A_1G_2^2G_1^2n_{21}n_{28} + 16A_1G_2^2G_1^2n_{15} \\
& + 16A_1G_2^2G_1^2n_{15}n_{28} + 16A_1G_2^2G_1^2n_{15}n_{21} + 16A_1G_2^2G_1^2n_{15}n_{21}n_{28} + 16A_1G_2^2G_1^2n_{12} \\
& + 16A_1G_2^2G_1^2n_{12}n_{28} + 16A_1G_2^2G_1^2n_{12}n_{21} + 16A_1G_2^2G_1^2n_{12}n_{21}n_{28} + 16A_1G_2^2G_1^2n_{12}n_{15} = - \\
& 4A_1G_2^2G_1^2A_2n_{13}n_{27} - 4A_1G_2^2G_1^2A_2n_{13}n_{21}n_{27} - \\
& - 4A_1G_2^2G_1^2A_2n_{13}n_{15}n_{27} - 4A_1G_2^2G_1^2A_2n_{13}n_{15}n_{21}n_{27} - 4A_1G_2^2G_1^2A_2n_{13}n_{22} - 4A_1G_2^2G_1^2A_2n_{13}n_{22}n_{28} - \\
& - 4A_1G_2^2G_1^2A_2n_{13}n_{15}n_{22} - 4A_1G_2^2G_1^2A_2n_{13}n_{15}n_{22}n_{28} - 2A_1G_2^2G_1A_2n_{13}n_{27} - 2A_1G_2^2G_1A_2n_{13}n_{21}n_{27} + \\
& + 8A_1G_2^2G_1n_{12}n_{21}n_{28} - 2A_1G_2^2G_1A_2n_{13}n_{22}n_{28} - 2A_1G_2G_1^2A_2n_{13}n_{22} - 2A_1G_2G_1^2A_2n_{13}n_{15}n_{22} + \\
& + 4A_1G_2G_1n_{12} + 4A_1G_2G_1n_{12}n_{21} + 8A_1G_2G_1^2n_{12}n_{21} + 8A_1G_2G_1^2n_{12}n_{15} + 8A_1G_2G_1^2n_{12}n_{15}n_{21} \\
& + 4A_1G_2G_1 + 4A_1G_2G_1n_{21} - 2A_1G_2^2G_1A_2n_{13}n_{22}.
\end{aligned} \tag{B.8}$$

Curriculum Vitae

Lukáš Langhammer

OSOBNÍ INFORMACE

Adresa: Pratecká 229, 66451 Kobylnice
Narozen: 10. 02. 1987, Brno
E-mail: langhammer.lukas@gmail.com
Jazykové znalosti: Angličtina (pokročilá znalost)

VZDĚLÁNÍ

2012 - 2016: Vysoké učení technické v Brně, Fakulta elektrotechniky a komunikačních technologií

- Doktorské studium - obor Teleinformatika

2010 - 2012: Vysoké učení technické v Brně, Fakulta elektrotechniky a komunikačních technologií

- Navazující magisterské studium - obor Telekomunikační a informační technika

2007 - 2010: Vysoké učení technické v Brně, Fakulta elektrotechniky a komunikačních technologií

- Bakalářské studium - obor Teleinformatika

2003 - 2007: ISS - COP Olomoucká

- střední vzdělání s maturitou - obor mechanik elektrotechnik (26-41-L/01)

PEDAGOGICKÁ PRAXE

- výuka laboratorních cvičení kurzu Komunikační technologie a Pokročilé komunikační techniky na ústavu teleinformatiky

- vedení 6 diplomových a 4 bakalářských prací

ÚČAST NA PROJEKTECH

Projekty podporované Grantovou Agenturou České Republiky:

- GA16-06175S Syntéza a analýza systémů fraktálního řádu využívající netradiční aktivní prvky

- GA102/09/1681 Počítačové automatizování metod syntézy lineárních funkčních bloků a výzkum nových aktivních prvků

Projekty Ministerstva školství, mládeže a tělovýchovy

- LO1401 Interdisciplinární výzkum bezdrátových technologií (INWITE)
- ED2.1.00/03.0072 Centrum senzorických, informačních a komunikačních systémů (SIX)

Projekty Evropské Unie

- CZ.1.07/2.2.00/28.0096 Příprava specialistů pro telekomunikace a informatiku - magisterské studium telekomunikační a informační technika
- CZ.1.07/2.2.00/28.0193 Komplexní inovace studijních programů a zvyšování kvality výuky na FEKT VUT v Brně
- CZ.1.07/2.2.00/28.0062 Společné aktivity VUT a VŠB - TUO při vytváření obsahu a náplně odborných akreditovaných kurzů ICT

Projekty Vysokého učení technického v Brně

- FEKT-S-14-2352 Výzkum elektronických komunikačních a informačních systémů
- FEKT-S-11-15 Výzkum elektronických komunikačních systémů

PUBLIKACE

Celkový počet publikací: 24

Počet publikovaných či přijatých příspěvků v časopisech s impaktním faktorem: 4

Počet prezentovaných či přijatých příspěvků na mezinárodních konferencích indexovaných databází Thomson Reuters (ISI WoS): 4